UNIVERSIDADE FEDERAL DO PARANÁ

CAROLINE ZARZZEKA

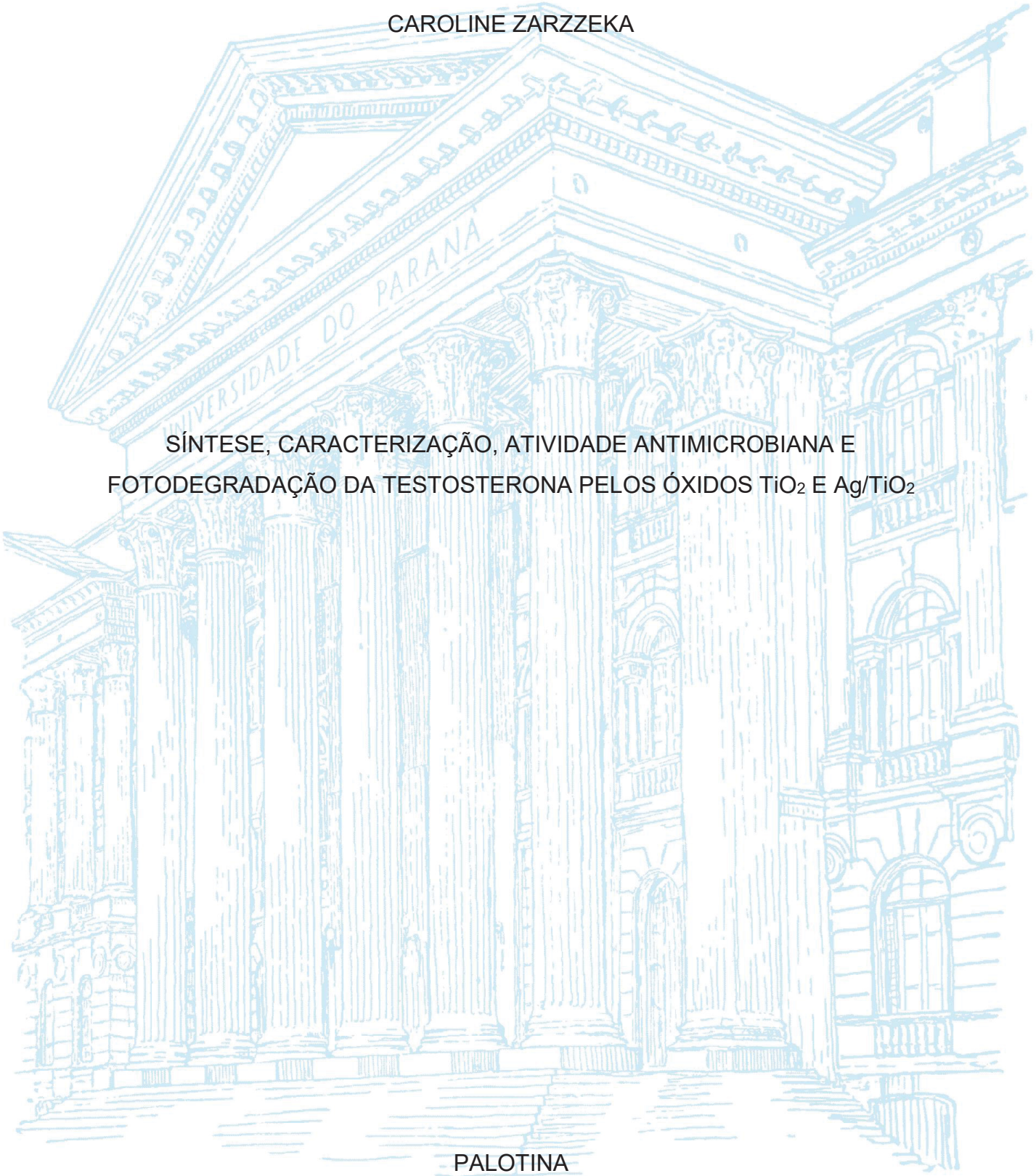


# SÍNTESE, CARACTERIZAÇÃO, ATIVIDADE ANTIMICROBIANA E FOTODEGRADAÇÃO DA TESTOSTERONA PELOS ÓXIDOS $TiO_2$ E $Ag/TiO_2$

PALOTINA

2025

CAROLINE ZARZZEKA

# SÍNTESE, CARACTERIZAÇÃO, ATIVIDADE ANTIMICROBIANA E FOTODEGRADAÇÃO DA TESTOSTERONA PELOS ÓXIDOS $TiO_2$ E $Ag/TiO_2$

Tese apresentada ao curso de Pós-Graduação em Engenharia e Tecnologia Ambiental, Setor Palotina - PR, Universidade Federal do Paraná como requisito parcial à obtenção do título de Doutora em Engenharia e Tecnologia Ambiental.

Orientadora: Prof.ª Dr.ª Leda Maria Saragiotto Colpini

Coorientadora: Prof.ª Dr.ª Margarete Dulce Bagatini

PALOTINA
2025

Universidade Federal do Paraná. Sistemas de Bibliotecas.
Biblioteca UFPR Palotina.

Z38 Zarzzeka, Caroline
Síntese, caracterização, atividade antimicrobiana e fotodegradação da testosterona pelos óxidos TiO2 e Ag/TiO2 / Caroline Zarzzeka. – Palotina, PR, 2025.

Tese (Doutorado) – Universidade Federal do Paraná, Setor Palotina, PR, Programa de Pós-Graduação em Engenharia e Tecnologia Ambiental.
Orientadora: Prof.a Dr.a Leda Maria Saragiotto Colpini.
Coorientadora: Prof.a Dr.a Margarete Dulce Bagatini.

1. Bactérias. 2. Fotoactivação. 3. Síntese Verde. I. Colpini, Leda Maria Saragiotto. II. Bagatini, Margarete Dulce. III. Universidade Federal do Paraná. IV. Título.

CDU 502

Bibliotecária: Aparecida Pereira dos Santos – CRB 9/1653

# TERMO DE APROVAÇÃO

Os membros da Banca Examinadora designada pelo Colegiado do Programa de Pós-Graduação ENGENHARIA E TECNOLOGIA AMBIENTAL da Universidade Federal do Paraná foram convocados para realizar a arguição da tese de Doutorado de **CAROLINE ZARZZEKA**, intitulada: **Síntese, Caracterização, Atividade Antimicrobiana e Fotodegradação da Testosterona pelos óxidos TiO2 e Ag/TiO2**, sob orientação da Profa. Dra. LEDA MARIA SARAGIOTTO COLPINI, que após terem inquirido a aluna e realizada a avaliação do trabalho, são de parecer pela sua APROVAÇÃO no rito de defesa.

A outorga do título de doutora está sujeita à homologação pelo colegiado, ao atendimento de todas as indicações e correções solicitadas pela banca e ao pleno atendimento das demandas regimentais do Programa de Pós-Graduação.

Palotina, 27 de Fevereiro de 2025.

Assinatura Eletrônica
27/02/2025 17:53:38.0
LEDA MARIA SARAGIOTTO COLPINI
Presidente da Banca Examinadora

Assinatura Eletrônica
27/02/2025 16:21:26.0
TÂNIA FORSTER CARNEIRO
Avaliador Externo (UNIVERSIDADE ESTADUAL DE CAMPINAS)

Assinatura Eletrônica
27/02/2025 19:42:16.0
DIRLEI DIEDRICH KIELING
Avaliador Externo (UNIVERSIDADE FEDERAL DO PARANÁ - CAMPUS JANDAIA DO SUL)

Assinatura Eletrônica
28/02/2025 13:49:34.0
CÁTIA TAVARES DOS PASSOS FRANCISCO
Avaliador Externo (UFFS - UNIVERSIDADE FEDERAL DA FRONTEIRA SUL)

Assinatura Eletrônica
27/02/2025 16:19:48.0
GIANE GONÇALVES LENZI
Avaliador Externo (UNIVERSIDADE TECNOLÓGICA FEDERAL DO PARANÁ)

Assinatura Eletrônica
28/02/2025 07:32:15.0
MARGARETE DULCE BAGATINI
Coorientador(a) (55002856)

AO MEU ESPOSO JONAS E FILHOS.

## AGRADECIMENTOS

Ao meu esposo pelo amor e apoio incondicionais durante todo esse percurso. Pelo carinho, paciência, dedicação, debates acadêmicos, alívio, felicidade, simplesmente por estar ao meu lado e por termos construído esta linda família. Te amo! A minha Isis, meu raio de sol, meu norte, minha alegria e vida. Como é gigantesco o meu amor por você, Isis! Te Amo imensamente! Nossa Família e nosso relacionamento são os mais especiais que poderia pedir, construir e ter, sem vocês não teria conseguido e nem seria possível, muito obrigado. A meus familiares pelos momentos de descontração.

Às minhas orientadoras, meu imenso agradecimento à Leda Colpini e à Margarete Bagatini por trazerem ensinamentos pessoais e profissionais, por terem me auxiliado na realização deste trabalho e suas respectivas contribuições. As palavras parecem pequenas diante da minha admiração por vocês. Suas orientações foram um presente inestimável em minha vida acadêmica. Vocês sempre foram solícitas e pacientes em suas orientações, sempre em ações conjuntas e ouvindo atentamente ideias e sugestões. Ser guiada por vocês foi um privilégio que tornou nosso vínculo de amizade ainda mais especial. Eu não seria a pesquisadora que me tornei hoje sem vocês. Obrigada!

Aos meus amigos que me ajudaram, de maneira especial Filomena Marafon por sua imensa participação e amizade. Aos meus colegas de trabalho da UFFS, por momentos de descontração, por ajudarem com debates, possibilidade de afastamento integral, apoio estrutural, técnico e pessoal para realização de todos os experimentos desse projeto. Ao programa de doutorado em Engenharia e Tecnologia Ambiental da UFPR pela oportunidade. A todos cujos nomes não foram citados, mas que contribuíram para o desenvolvimento deste trabalho, de forma direta ou indiretamente. Agradeço a Deus pela vida, sabedoria e ajuda. Obrigada!

## RESUMO

Materiais fotoativados pela luz emergem como uma alternativa promissora no processo de remoção de poluentes emergentes. A fotodegradação da testosterona utilizando o Ag/$TiO_2$ representa um campo de pesquisa relativamente novo, com número limitado de estudos, sendo promissor na busca por novas estratégias para identificar e desenvolver a futura geração de fármacos para controlar infecções bacterianas. Neste estudo, sintetizou-se catalisadores a base de prata (Ag) (2% e 10% m/m%) suportados em dióxido de titânio ($TiO_2$), via impregnação por excesso de solvente (2AgT/I e 10AgT/I), sol-gel modificada utilizando a tapioca como gelificante (2AgT/V e 10AgT/V) e sol-gel (2AgT/SG e 10AgT/SG). Buscou-se então, caracterizá-los e avaliá-los quanto a inativação bacteriana e na degradação da testosterona via fotólise e fotocatálise heterogênea. Os catalisadores Ag/$TiO_2$ caracterizados por espectros na região do infravermelho apresentaram bandas características de titânio, vibração assimétrica do Ti–Ag–O e ligação Ag-$TiO_2$, confirmando a deposição da prata sob o suporte. A Difração de raios X identificou para os catalisadores impregnados poucos picos representando fases cristalinas desorganizadas. Enquanto, os catalisadores AgT/V tiveram picos característicos de Ag metálica e anatase e os AgT/SG apresentaram picos anatase, representando fases cristalinas organizadas. Observa-se a partir da Calorimetria Exploratória Diferencial picos endotérmicos menores para os catalisadores AgT/SG, indicando ponto de fusão baixos. Nota-se, através da Análise Termogravimétrica, uma perda mínima de massa para os catalisadores. Assim, a Microscopia Eletrônica de Varredura identificou morfologias aglomeradas e irregulares a medida que a Ag era adicionada para os catalisadores AgT/I e AgT/V. Por outro lado, os catalisadores AgT/SG tiveram aspecto denso. Na determinação de fisissorção de $N_2$ verificou-se que o aumento da Ag diminui a área específica dos catalisadores AgT/I e AgT/V e o efeito inverso ocorre para o AgT/SG. O band gap dos catalisadores mesosporosos diminuiu em relação ao $TiO_2$. O método sol-gel destaca-se das outras vias de síntese, pois apresenta maior área especifica e volume de poros. Os catalisadores 10AgT/I, AgT/V e o 10AgT/SG tiveram ações bactericidas contra *Escherichia coli* sugerindo um efeito antimicrobiano intrínseco a concentração de Ag. A fotoativação dos catalisadores AgT/I, AgT/V e AgT/SG sob luz negra resultaram em uma significativa inativação bacteriana contra *Escherichia coli* (NEWP0022) e *Staphylococcus aureus* (NEWP0023). A produção de espécies reativas de oxigênio, comprovada no teste de detecção, foi induzida pela radiação ultravioleta e em conjunto com a ação antimicrobiana intrínseca da Ag. Esses resultados demonstram o potencial dos catalisadores AgT/I, AgT/V e AgT/SG para o desenvolvimento de revestimentos antimicrobianos para superfícies, contribuindo para a prevenção e controle de infecções em diversos ambientes. A eficiência do processo de fotólise (82%) foi similar à da fotocatálise heterogênea utilizando o catalisador 2AgT/SG (79,9%), na fotodegradação da testosterona. Os catalisadores AgT/SG e 10AgT/V apresentaram maior atividade fotocatalítica na fotodegradação da testosterona, com degradação maior que 72% (2AgT/SG>T/SG>10AgT/V>10AgT/SG). Esses catalisadores podem encontrar aplicações em diversos processos de tratamento de água, como a remoção de desreguladores endócrinos. A criação destes materiais

fotocatalíticos são essenciais para o desenvolvimento de tecnologias mais eficientes e sustentáveis para o tratamento de água.

Palavras-chave: Impregnação por Excesso de Solvente, Síntese Verde, Sol-Gel, Bactérias e Fotoactivação.

## ABSTRACT

Light-activated materials are emerging as a promising alternative in the process of removing emerging pollutants. The photodegradation of testosterone using Ag/$TiO_2$ represents a relatively new field of research, with a limited number of studies, and is promising in the search for new strategies to identify and develop the future generation of drugs to control bacterial infections. In this study, silver (Ag) catalysts (2% and 10% m/m%) supported on titanium dioxide ($TiO_2$) were synthesized via excess solvent impregnation (2AgT/I and 10AgT/I), modified sol-gel using tapioca as a gelling agent (2AgT/V and 10AgT/V) and sol-gel (2AgT/SG and 10AgT/SG). The aim was to characterize and evaluate them in terms of bacterial inactivation and testosterone degradation via photolysis and heterogeneous photocatalysis. The Ag/$TiO_2$ catalysts characterized by spectra in the infrared region showed characteristic titanium bands, asymmetric vibration of Ti-Ag-O and Ag-$TiO_2$ bonding, confirming the deposition of silver on the support. X-ray diffraction identified few peaks representing disorganized crystalline phases for the impregnated catalysts. Meanwhile, the AgT/V catalysts had peaks characteristic of metallic Ag and anatase and the AgT/SG catalysts had anatase peaks, representing organized crystalline phases. Differential Scanning Calorimetry shows smaller endothermic peaks for the catalysts. Thermogravimetric analysis showed minimal loss of mass for the catalysts. Scanning Electron Microscopy identified agglomerated and irregular morphologies as Ag was added to the AgT/I and AgT/V catalysts. The AgT/SG catalysts had a dense appearance. When determining $N_2$ physisorption, it was found that increasing Ag decreased the specific area of the AgT/I and AgT/V catalysts and the opposite effect occurred for AgT/SG. The band gap of the mesosporous catalysts decreased in relation to $TiO_2$. The sol-gel method stands out from other synthesis routes because it presents a larger specific area and pore volume. The 10AgT/I, AgT/V and 10AgT/SG catalysts had bactericidal actions against *Escherichia coli*, suggesting an intrinsic antimicrobial effect of the Ag concentration. The photoactivation of the AgT/I, AgT/V and AgT/SG catalysts under black light resulted in significant bacterial inactivation against *Escherichia coli* (NEWP0022) and *Staphylococcus aureus* (NEWP0023). The production of reactive oxygen species, proven in the detection test, was induced by ultraviolet radiation and in conjunction with the intrinsic antimicrobial action of Ag. These results demonstrate the potential of the AgT/I, AgT/V and AgT/SG catalysts for the development of antimicrobial coatings for surfaces, contributing to the prevention and control of infections in various environments. The efficiency of the photolysis process (82%) was similar to that of heterogeneous photocatalysis using the 2AgT/SG catalyst (79.9%) in the photodegradation of testosterone. The AgT/SG and 10AgT/V catalysts showed greater photocatalytic activity in the photodegradation of testosterone, with degradation greater than 72% (2AgT/SG>T/SG>10AgT/V>10AgT/SG). These catalysts can find applications in several water treatment processes, such as the removal of endocrine disruptors. The creation of these photocatalytic materials is essential for the development of more efficient and sustainable technologies for water treatment.



Keywords: Impregnation by Excess Solvent, Green Synthesis, Sol-Gel, Bacteria and Photoactivation.

## SUMÁRIO

# 1 STATE OF ART

The growing concern about environmental pollution, caused by a variety of emerging pollutants (EPs) such as microorganisms, organic compounds and heavy metals, represents a serious global challenge (AL SABER et al., 2021; AZAD et al., 2022). The prevalence of EPs in surface and groundwater is a serious problem, as it deteriorates water quality and can lead to health problems (MISHRA et al., 2023). Due to increased consumption and the complexity of industrial processes, these contaminants have been detected in aquatic and terrestrial environments. Originating from pharmaceuticals, personal care products, endocrine disruptors and insecticides, they pose significant environmental and health concerns, even in minute quantities. Exposure to EPs can be associated with various health problems, such as endocrine disorders, antimicrobial resistance and the development of chronic diseases (K.T; RAM ACHAR; SIRIGER, 2021). The primary source of aquatic contamination is the effluent discharged from sewage treatment plants. Although there are reliable methods for detecting EPs at low concentrations, there is a need for research into the toxicity and transformation pathways of these contaminants (LIU et al., 2012; THOMAIDIS NS, 2013).

Among EPs are steroid hormones, such as testosterone, belong to the group of endocrine disruptors. These chemical substances play a fundamental role in regulating various biological processes (KAVLOCK et al., 1996). These hormonal pollutants can cause reproductive disorders in humans and other aquatic and terrestrial animals (CAMPBELL et al., 2006). Exposure to steroid hormones is associated with a range of health problems, including reproductive alterations (decreased sperm production), cancer development (testicular, breast and others) and endocrine disorders (KAVLOCK et al., 1996). The persistence of these compounds in the environment and their bioaccumulation in the food chain represent a significant threat to public health and ecosystems. Testosterone concentrations between 0.3 and 0.8 ng $L^{-1}$ were measured in effluents from Nalgene municipal wastewater treatment plants (Rochester, NY, USA) (KOLODZIEJ; GRAY; SEDLAK, 2003). The Jordan River, in Israel, a maximum concentration of 5.6 ng $L^{-1}$ of testosterone was detected (SHORE et al., 2004) and in agricultural basins (animal husbandry and aquaculture) 16 ng $L^{-1}$ was found. An average concentration of 9 ng $L^{-1}$ was detected in hospital wastewater in

Taiwan (LIN; YU; LIN, 2008). Median values of 258 ng $L^{-1}$ were also found in wastewater treatment plants in South Africa (MANICKUM; JOHN, 2014). In groundwater, concentrations of 0.3 to 26.3 ng $L^{-1}$ have been detected and the lowest observable effect concentration was 0.89 mg $L^{-1}$ (VULLIET; CREN-OLIVÉ, 2011; ROSENMAI et al., 2013). In wastewater influent, testosterone concentrations can reach up to 290 ng/L (BACKE et al., 2011). Chronic exposure to testosterone at 0.31-2.48 mg/L reduces fecundity and fertility in Daphnia magna, though these levels exceed environmental concentrations (BARBOSA et al., 2008). Recent studies on Caenorhabditis elegans show that testosterone concentrations above 0.01 µg/L significantly reduce brood size and germ cell counts, with a proposed ecological risk assessment threshold (BMDL10) of 1.160 ng/L (MENG et al., 2024). Prevention and control of the production and use of hazardous chemicals are essential measures to minimize the impacts of these pollutants on the environment (WANG et al., 2022).

The combination of different pollutants in the environment makes the degradation of these contaminants a complex challenge, requiring the development of new technologies and materials to minimize environmental impacts (OJEA-JIMÉNEZ et al., 2012). The choice of the most suitable technology depends on several factors, such as the nature of the pollutants present in the effluent, the volume to be treated and the quality requirements of the effluent water. Nanotechnology, with its high surface area materials, is emerging as a promising tool for removing pollutants (BISWAS et al., 2021; RAHMAN et al., 2020), exploring their interaction in penetrating the cell membrane of pathogens and in biochemical actions (SINGH, 2017).

Water treatment is essential for the protection of water resources and public health. Over the years, various technologies have been developed to meet this demand, from conventional methods such as lagooning and activated sludge to more modern and efficient processes such as reverse osmosis and advanced oxidative processes (POAs) (CASTRO et al., 2020). Conventional biological processes, such as coagulation and flocculation, are widely used in wastewater treatment, but they have limitations that restrict their efficiency in removing certain pollutants. The formation of biofilms on the membranes, high energy consumption and the generation of large volumes of sludge are some of the challenges associated with these technologies (HOMEM; SANTOS, 2011; RAJAITHA et al.,

2022; VIENO et al., 2007). In view of these limitations, the use of new technologies, such as POAs, has intensified. Among the POAs is photolysis, which plays a significant role in the transformation of hormones in the environment. Steroid estrogens and synthetic growth promoters undergo direct photolysis in sunlit waters, with half-lives ranging from minutes to hours (NAG et al., 2021; WHIDBEY et al., 2012). In aqueous solutions, testosterone undergoes light-induced degradation, with varying quantum yields depending on the excitation wavelength (VULLIET et al., 2010). Heterogeneous photocatalysis also offers a promising approach for the complete degradation of pesticides, polychlorinated biphenyls, endocrine disruptors, dyes and pharmaceuticals. For example, the photocatalytic degradation of 17α-methyltestosterone using doped titanium dioxide ($TiO_2$) has shown promising results, with the efficiency depending on the concentration and type of dopant and heat treatment (ARÉVALO-PÉREZ et al., 2020). Thus, photocatalysis is based on irradiating semiconductors, such as $TiO_2$ (SHARMA et al., 2019; SONU et al., 2019) with ultraviolet (UV) light, generating charge carriers through electron excitation, producing reactive oxygen species (ROS) that oxidize and mineralize organic contaminants, transforming them into inert and less toxic substances (FUJISHIMA; HONDA, 1972; RAMESH; NEZAMZADEH-EJHIEH, 2023).

$TiO_2$ is a semiconductor material used for environmental remediation due to its photocatalytic properties (GOPINATH et al., 2020). When exposed to UV radiation above 385 nm, $TiO_2$ generates electron ($e^-$) and gap ($h^+$) pairs that react with water and molecular oxygen to form hydroxyl ($OH^\bullet$) and superoxide ($O_2^{-\bullet}$) radicals. These highly reactive radicals oxidize and mineralize a variety of organic pollutants, and inactivating microorganisms. The ROS produced on the surface of this oxide degrade the bacterial cell through lipid oxidation and membrane disruption (FOSTER et al., 2012), preventing the initial adhesion of bacteria to its surface (WEI et al., 2014). $TiO_2$'s high photostability, low cost, biocompatibility, high refractive index, low toxicity and good chemical stability make it a promising material for application in various water treatment processes (FERREIRA et al., 2021).

In order to optimize the photocatalytic activity of $TiO_2$, doping with metals and the formation of heterojunctions have been used (ANUCHA et al., 2022). Heterojunction involves the combination of two or more semiconductors with

different band structures. This interface between the materials allows efficient separation of the $e^-/h^+$ pairs generated by the light, increasing the efficiency of photocatalysis (ZARZZEKA et al., 2024). Doping consists of incorporating metal ions, such as silver (Ag), into the crystal structure of $TiO_2$. This modification can significantly improve the material's properties, such as antibacterial activity and self-cleaning capacity (KANAKARAJU et al., 2022; SHARMA et al., 2019). When used as a dopant, Ag is effective in improving the photocatalytic performance of $TiO_2$, as it can act as an $e^-$ capture center, reducing the recombination of $e^-/h^+$ pairs and, consequently, increasing the production of ROS, which are responsible for the degradation of pollutants and bacterial death. It also reduces the band gap and enhances light absorption due to the plasmon resonance of the Ag surface (KUMAR et al., 2019; SARAVANAN et al., 2018).

The $Ag/TiO_2$ photocatalyst is very promising in photocatalysis and has high efficiency in eliminating various pollutants compared to pure $TiO_2$ (CAO et al., 2014). The photodegradation of testosterone using $Ag/TiO_2$ represents a promising area in the search for solutions for the decontamination of water resources by hormones. Previous studies have demonstrated the effectiveness of photocatalysis with $Ag/TiO_2$ in the degradation of other sex hormones, such as estrogens and progesterone (DE LIZ et al., 2017; FRONTISTIS et al., 2012; LIMA et al., 2020; PADOVAN et al., 2021).

The presence of Ag in $TiO_2$ increases its photocatalytic activity and can promote the generation of more efficient ROS in the oxidation of testosterone. It also increases the antibacterial properties of this catalyst, expanding its applications. The choice of synthesis method is fundamental to obtaining materials with the desired properties. Each method has its own particularities, advantages and disadvantages. The choice of synthesis method will depend on the desired properties of the final material and the specific applications. Variables such as pH, temperature and aging time of the gel, among others, can affect the structure and properties of the materials (CHAKHTOUNA et al., 2021; ZARZZEKA et al., 2024).

The excess solvent impregnation method is a simple yet effective approach for preparing heterogeneous catalysts, including $Ag/TiO_2$. This technique involves impregnating $TiO_2$ with a solution containing the desired metal precursor, such as silver nitrate. The solvent is then removed, leaving the metal ions dispersed on the surface of the support. A simple method that is easy to scale up,

it allows good control of the metal load. By combining the simplicity of the impregnation method with the synthesis of $Ag/TiO_2$, efficient catalysts can be developed for a wide range of applications (CHAKHTOUNA et al., 2021; ZARZZEKA et al., 2024).

The sol-gel method is a versatile chemical synthesis technique for producing inorganic materials, particularly $Ag/TiO_2$. This process involves the hydrolysis and condensation of molecular precursors in water or alcohol to form a gel (BOKOV et al., 2021). The method offers advantages such as mild reaction conditions, control at the molecular level and the ability to produce nanoparticles with uniform morphology and high purity. The process parameters, such as precursor concentration, type of catalyst and drying method, significantly influence the properties of the final product. The addition of Ag to the oxide can increase photocatalytic activity and influence phase transitions (GOLIM et al., 2019).

The modified sol-gel method, which employs tapioca in a green synthesis approach as a complexing agent and gel structure modifier, is a promising technique for obtaining materials with unique properties. The inclusion of tapioca as a precursor in the modified sol-gel method adds an innovative and sustainable touch. Thus, the addition of activated cassava stem charcoal to $Ag/TiO_2$ further improved the photocatalytic efficiency, achieving 98.08% degradation of the bright green dye under sunlight. These nanoparticle showed excellent photocatalytic activity for degrading organic pollutants and dyes (SATHISHKUMAR et al., 2022). These green synthesis methods produce $Ag/TiO_2$ nanoparticle with particle sizes ranging from 12 to 40 nm, demonstrating improved photocatalytic efficiency and antibacterial activity and potential applications in water treatment (HERRERA-BARROS et al., 2018).

Thus, the synthesis of $Ag/TiO_2$ catalysts with high photocatalytic activity and selectivity for testosterone degradation is a new field of research. This study aims to contribute to the development of more efficient and selective photocatalytic materials, contributing to the protection of water resources and human health. The potential use of these catalysts for applications in clean technologies and their industrial use is promising, making it possible for them to be applied effectively in society. In this way, it is hoped to have a positive impact on the environment, so that future generations can use natural resources with a better environmental and

collective awareness in relation to conscious consumption, aimed at minimizing waste and greater environmental preservation.

## 2 AIMS

Synthesize and characterize $Ag/TiO_2$ mixed oxides for application with antimicrobial activity and in the photodegradation of testosterone.

### 2.1 SPECIFIC AIM

- Prepare and synthesize $Ag/TiO_2$ mixed oxides containing nominal proportions of silver (2% and 10%) using the excess solvent impregnation, modified sol-gel methods, and sol-gel;
- Characterize the morphology of the oxides obtained using infrared spectrometry, scanning electron microscopy with energy dispersive X-rays, $N_2$ physisorption, thermogravimetric analysis, differential scanning calorimetry, X-ray diffraction and photoacoustic spectroscopy;
- Evaluate the antimicrobial behavior of $Ag/TiO_2$ and $TiO_2$ mixed oxides against *Escherichia coli* and *Staphylococcus aureus* bacteria;
- Evaluate the intracellular generation of reactive oxygen species in *Escherichia coli* and *Staphylococcus aureus* subjected to $Ag/TiO_2$ and $TiO_2$ catalysts under black light.
- Evaluate the efficiency of $Ag/TiO_2$ mixed oxides synthesized and $TiO_2$ in the degradation of testosterone through photolysis and heterogeneous photocatalysis.

## REFERENCES


ANUCHA, C. B.; ALTIN, I.; BACAKSIZ, E.; STATHOPOULOS, V. N. Titanium dioxide ($TiO_2$)-based photocatalyst materials activity enhancement for contaminants of emerging concern (CECs) degradation: In the light of modification strategies. **Chemical Engineering Journal Advances**, v. 10, p. 100262, 2022.

AL SABER, M.; BISWAS, P.; DEY, D.; et al. A Comprehensive Review of Recent Advancements in Cancer Immunotherapy and Generation of CAR T Cell by CRISPR-Cas9. **Processes**, v. 10, n. 1, p. 16, 2021.

ARÉVALO-PÉREZ, J. C.; CRUZ-ROMERO, D. DE LA; CORDERO-GARCÍA, A.; et al. Photodegradation of 17 α-methyltestosterone using $TiO_2$ -$Gd^{3+}$ and $TiO_2$-$Sm^{3+}$ photocatalysts and simulated solar radiation as an activation source. **Chemosphere**, v. 249, p. 126497, 2020.

AZAD, S.; AHMED, S.; BISWAS, P.; et al. Quantitative analysis of the factors influencing IDA and TSH downregulation in correlation to the fluctuation of activated vitamin D3 in women. **Journal of Advanced Biotechnology and Experimental Therapeutics**, v. 5, n. 2, p. 320, 2022.

BACKE, W. J.; ORT, C.; BREWER, A. J.; et al. Analysis of androgenic steroids in environmental waters by large-volume injection liquid chromatography tandem mass spectrometry. **Analytical chemistry,** n. *83,* v. 7, p. 2622-2630, 2011.

BARBOSA, I. R.; NOGUEIRA, A. J. A; SOARES, A. M.V.M. Efeitos agudos e crônicos da testosterona e da 4-hidroxiandrostenediona no crustáceo *Daphnia magna*. **Ecotoxicologia e Segurança Ambiental**, v. 71, n. 3, pág. 757-764, 2008.

BISWAS, P.; HASAN, M. M.; DEY, D.; et al. Candidate antiviral drugs for COVID-19 and their environmental implications: a comprehensive analysis. **Environmental Science and Pollution Research**, v. 28, n. 42, p. 59570–59593, 2021.

BOKOV, D.; TURKI JALIL, A.; CHUPRADIT, S.; et al. Nanomaterial by Sol-Gel Method: Synthesis and Application. **Advances in Materials Science and Engineering**, v. 2021, n. 1, 2021.

CAMPBELL, C. G.; BORGLIN, S. E.; GREEN, F. B.; et al. Biologically directed environmental monitoring, fate, and transport of estrogenic endocrine disrupting compounds in water: A review. **Chemosphere**, v. 65, n. 8, p. 1265–1280, 2006.

CAO, Z.; ZHU, S.; QU, H.; et al. Preparation of visible-light nano-photocatalysts through decoration of $TiO_2$ by silver nanoparticles in inverse miniemulsions. **Journal of Colloid and Interface Science**, v. 435, p. 51–58, 2014.

CASTRO, L. E. N. DE; MEURER, E. C.; ALVES, H. J.; et al. Photocatalytic Degradation of Textile dye Orange-122 Via Electrospray Mass Spectrometry. **Brazilian Archives of Biology and Technology**, v. 63, 2020.

CHAKHTOUNA, H.; BENZEID, H.; ZARI, N.; QAISS, A. EL KACEM; BOUHFID, R. Recent progress on Ag/$TiO_2$ photocatalysts: photocatalytic and bactericidal behaviors. **Environmental Science and Pollution Research**, v. 28, n. 33, p. 44638–44666, 2021.

DE LIZ, M.; DE LIMA, R.; DO AMARAL, B.; et al. Suspended and Immobilized $TiO_2$ Photocatalytic Degradation of Estrogens: Potential for Application in Wastewater Treatment Processes. **Journal of the Brazilian Chemical Society**, 2017.

FERREIRA, V. R. A.; SANTOS, P. R. M.; SILVA, C. I. Q.; AZENHA, M. A. Latest developments on $TiO_2$-based photocatalysis: a special focus on selectivity and hollowness for enhanced photonic efficiency. **Applied Catalysis A: General**, v. 623, p. 118243, 2021.

FOSTER, H. A.; SHEEL, D. W.; EVANS, P.; et al. Antimicrobial Activity Against Hospital-related Pathogens of Dual Layer CuO/$TiO_2$ Coatings Prepared by CVD. **Chemical Vapor Deposition**, v. 18, n. 4–6, p. 140–146, 2012.

FRONTISTIS, Z.; DROSOU, C.; TYROVOLA, K.; et al. Experimental and Modeling Studies of the Degradation of Estrogen Hormones in Aqueous $TiO_2$ Suspensions under Simulated Solar Radiation. **Industrial & Engineering Chemistry Research**, v. 51, n. 51, p. 16552–16563, 2012.

FUJISHIMA, A.; HONDA, K. Electrochemical Photolysis of Water at a Semiconductor Electrode. **Nature**, v. 238, n. 5358, p. 37–38, 1972.

GOLIM, O. P.; DESIATI, R. D.; MUSLIMIN, A. N.; SUGIARTI, E. Morphological evolution of sol-gel synthesized Ag-$TiO_2$ nanocomposite. **Journal of Physics: Conference Series**, v. 1191, p. 012049, 2019.

GOPINATH, K. P.; MADHAV, N. V.; KRISHNAN, A.; MALOLAN, R.; RANGARAJAN, G. Present applications of titanium dioxide for the photocatalytic removal of pollutants from water: A review. **Journal of Environmental Management**, v. 270, p. 110906, 2020.

HERRERA-BARROS, A.; TEJADA-TOVAR, C.; VILLABONA-ORTIZ, A.; GONZALEZ-DELGADO, A.; REYES-RAMOS, A. Synthesis and characterization of cassava, yam and lemon peels modified with $TiO_2$ nanoparticles. **Contemporary Engineering Sciences**, v. 11, n. 38, p. 1863–1871, 2018.

HOMEM, V.; SANTOS, L. Degradation and removal methods of antibiotics from aqueous matrices – A review. **Journal of Environmental Management**, v. 92, n. 10, p. 2304–2347, 2011. Academic Press.

K.T, V.; RAM ACHAR, R.; SIRIGER, S. A review on emerging micropollutants: sources, environmental concentration and toxicity. **Bionatura**, v. 6, n. 4, p. 2305–2325, 2021.

KANAKARAJU, D.; ANAK KUTIANG, F. D.; LIM, Y. C.; GOH, P. S. Recent progress of Ag/$TiO_2$ photocatalyst for wastewater treatment: Doping, co-doping,

and green materials functionalization. **Applied Materials Today**, v. 27, p. 101500, 2022. Elsevier.

KAVLOCK, R. J.; DASTON, G. P.; DEROSA, C.; et al. Research needs for the risk assessment of health and environmental effects of endocrine disruptors: a report of the U.S. EPA-sponsored workshop. **Environmental Health Perspectives**, v. 104, n. suppl 4, p. 715–740, 1996.

KOLODZIEJ, E. P.; GRAY, J. L.; SEDLAK, D. L. Quantification of steroid hormones with pheromonal properties in municipal wastewater effluent. **Environmental Toxicology and Chemistry**, v. 22, n. 11, p. 2622–2629, 2003.

KUMAR, A.; SHARMA, G.; NAUSHAD, M.; et al. Highly visible active $Ag_2CrO_4$/Ag/$BiFeO_3$@RGO nano-junction for photoreduction of $CO_2$ and photocatalytic removal of ciprofloxacin and bromate ions: The triggering effect of Ag and RGO. **Chemical Engineering Journal**, v. 370, p. 148–165, 2019. Elsevier.

LIMA, K. V.; EMÍDIO, E. S.; PUPO NOGUEIRA, R. F.; VASCONCELOS, N. DO S. L.; ARAÚJO, A. B. Application of a stable Ag/$TiO_2$ film in the simultaneous photodegradation of hormones. **Journal of Chemical Technology & Biotechnology**, v. 95, n. 10, p. 2656–2663, 2020.

LIN, A. Y.-C.; YU, T.-H.; LIN, C.-F. Pharmaceutical contamination in residential, industrial, and agricultural waste streams: Risk to aqueous environments in Taiwan. **Chemosphere**, v. 74, n. 1, p. 131–141, 2008.

LIU, S.; YING, G.-G.; ZHAO, J.-L.; et al. Occurrence and fate of androgens, estrogens, glucocorticoids and progestagens in two different types of municipal wastewater treatment plants. **J. Environ. Monit.**, v. 14, n. 2, p. 482–491, 2012.

MANICKUM, T.; JOHN, W. Occurrence, fate and environmental risk assessment of endocrine disrupting compounds at the wastewater treatment works in Pietermaritzburg (South Africa). **Science of The Total Environment**, v. 468–469, p. 584–597, 2014.

MENG, K.; Shi, Y. C.; Li, W. X.; et al. Testosterone Mediates Reproductive Toxicity in *Caenorhabditis elegans* by Affecting Sex Determination in Germ Cells through nhr-69/mpk-1/fog-1/3. **Toxics**, v. 12, n. 7, p. 502, 2024.

MISHRA, R. K.; MENTHA, S. S.; MISRA, Y.; DWIVEDI, N. Emerging pollutants of severe environmental concern in water and wastewater: A comprehensive review on current developments and future research. **Water-Energy Nexus**, v. 6, p. 74–95, 2023.

NAG, R.; MONAHAN, C.; WHYTE, P.; et al. Risk assessment of *Escherichia coli* in bioaerosols generated following land application of farmyard slurry. **Science of The Total Environment**, v. 791, p. 148189, 2021. Elsevier.

OJEA-JIMÉNEZ, I.; LÓPEZ, X.; ARBIOL, J.; PUNTES, V. Citrate-Coated Gold Nanoparticles As Smart Scavengers for Mercury (II) Removal from Polluted

Waters. **ACS Nano**, v. 6, n. 3, p. 2253–2260, 2012.

PADOVAN, R. N.; DE CARVALHO, L. S.; DE SOUZA BERGO, P. L.; et al. Degradation of hormones in tap water by heterogeneous solar $TiO_2$-photocatalysis: Optimization, degradation products identification, and estrogenic activity removal. **Journal of Environmental Chemical Engineering**, v. 9, n. 6, p. 106442, 2021.

RAHMAN, M. A.; RAHMAN, MD. HASANUR; HOSSAIN, M. S.; et al. Molecular Insights into the Multifunctional Role of Natural Compounds: Autophagy Modulation and Cancer Prevention. **Biomedicines**, v. 8, n. 11, p. 517, 2020.

RAJAITHA, P. M.; HAJRA, S.; SAHU, M.; et al. Unraveling highly efficient nanomaterial photocatalyst for pollutant removal: a comprehensive review and future progress. **Materials Today Chemistry**, v. 23, p. 100692, 2022.

RAMESH, A.; NEZAMZADEH-EJHIEH, A. Photocatalytic activity of ZnO-PbS nanoscale toward Allura Red AC in an aqueous solution: Characterization and mechanism study. **Journal of Photochemistry and Photobiology A: Chemistry**, v. 434, p. 114254, 2023. Elsevier.

ROSENMAI, A. K.; NIELSEN, F. K.; PEDERSEN, M.; et al. Fluorochemicals used in food packaging inhibit male sex hormone synthesis. **Toxicology and Applied Pharmacology**, v. 266, n. 1, p. 132–142, 2013.

SARAVANAN, R.; MANOJ, D.; QIN, J.; et al. Mechanothermal synthesis of $Ag/TiO_2$ for photocatalytic methyl orange degradation and hydrogen production. **Process Safety and Environmental Protection**, v. 120, p. 339–347, 2018.

SATHISHKUMAR, K.; SOWMIYA, K.; ARUL PRAGASAN, L.; et al. Enhanced photocatalytic degradation of organic pollutants by $Ag–TiO_2$ loaded cassava stem activated carbon under sunlight irradiation. **Chemosphere**, v. 302, p. 134844, 2022.

SHARMA, K.; DUTTA, V.; SHARMA, S.; et al. Recent advances in enhanced photocatalytic activity of bismuth oxyhalides for efficient photocatalysis of organic pollutants in water: A review. **Journal of Industrial and Engineering Chemistry**, v. 78, p. 1–20, 2019.

SHORE, L. S.; REICHMANN, O.; SHEMESH, M.; WENZEL, A.; LITAOR, M. I. Washout of accumulated testosterone in a watershed. **Science of The Total Environment**, v. 332, n. 1–3, p. 193–202, 2004.

SINGH, N. A. Nanotechnology innovations, industrial applications and patents. **Environmental Chemistry Letters**, v. 15, n. 2, p. 185–191, 2017.

SONU; DUTTA, V.; SHARMA, S.; et al. Review on augmentation in photocatalytic activity of $CoFe_2O_4$ via heterojunction formation for photocatalysis of organic pollutants in water. **Journal of Saudi Chemical Society**, v. 23, n. 8, p. 1119–1136, 2019.

THOMAIDIS NS, A. A. E B. A. Emerging contaminants : a tutorial mini-review. **Global NEST Journal**, v. 14, n. 1, p. 72–79, 2013.

VIENO, N. M.; HÄRKKI, H.; TUHKANEN, T.; KRONBERG, L. Occurrence of Pharmaceuticals in River Water and Their Elimination in a Pilot-Scale Drinking Water Treatment Plant. **Environmental Science & Technology**, v. 41, n. 14, p. 5077–5084, 2007.

VULLIET, E.; CREN-OLIVÉ, C. Screening of pharmaceuticals and hormones at the regional scale, in surface and groundwaters intended to human consumption. **Environmental Pollution**, v. 159, n. 10, p. 2929–2934, 2011.

VULLIET, E.; FALLETTA, M.; MAROTE, P.; et al. Light induced degradation of testosterone in waters. **Science of The Total Environment**, v. 408, n. 17, p. 3554–3559, 2010.

WANG, J.; WANG, Z.; CHEN, J.; et al. Environmental systems engineering consideration on treatment of emerging pollutants and risk prevention and control of chemicals. **Chinese Science Bulletin**, v. 67, n. 3, p. 267–277, 2022.

WEI, X.; YANG, Z.; TAY, S. L.; GAO, W. Photocatalytic $TiO_2$ nanoparticles enhanced polymer antimicrobial coating. **Applied Surface Science**, v. 290, p. 274–279, 2014.

WHIDBEY, C. M.; DAUMIT, K. E.; NGUYEN, T.-H.; et al. Photochemical induced changes of in vitro estrogenic activity of steroid hormones. **Water Research**, v. 46, n. 16, p. 5287–5296, 2012.

ZARZZEKA, C.; GOLDONI, J.; DE PAULA DE OLIVEIRA, J. DO R.; et al. Photocatalytic action of $Ag/TiO_2$ nanoparticles to emerging pollutants degradation: A comprehensive review. **Sustainable Chemistry for the Environment**, v. 8, p. 100177, 2024.

# CHAPTER I

Article published in the journal *Biocatalysis and Agricultural Biotechnology,* Volume 50, July 2023, 102710. https://doi.org/10.1016/j.bcab.2023.102710

## Use of titanium dioxide nanoparticles for cancer treatment: A comprehensive review and bibliometric analysis


### ABSTRACT

Titanium dioxide nanoparticles have shown great therapeutic potential and are a promising strategy for cancer treatment when interacting with photodynamic, photothermal, sonodynamic, and near-infrared light therapies. Such interactions increase cancer cell deaths due to the formation and release of reactive oxygen species, acting as antioxidants in cells and interacting with macromolecules. These nanoparticles have been demonstrated as biocompatible, reactive and chemically stable, with potential application in biomedical areas, especially for cancer treatment. The systematic literature search revealed that 734 documents (603 articles and 131 reviews) were published in the research of titanium dioxide nanoparticles for cancer treatment between 2003 and 2022. The bibliometric analysis of the main keywords demonstrates that photocatalysis was one of the first methods applied to produce of titanium dioxide nanoparticles, and nowadays, the production these nanoparticles by green synthesis with biological extracts is an efficient method to produce non-toxic materials for cancer treatment. Despite the scientific expansion of research on the use these nanoparticles, the clinical applicability remains limited, requiring additional in vivo studies for further industrial production on a commercial scale.


**Keywords**: Nanomaterials, Nanotechnology, Green synthesis, Antitumor effect, Photocatalytic activity, Melanoma

## 1. Introduction

Cancer has been considered an obstacle to the world's aging population and is one of the most challenging pathologies for health (Bray et al., 2021; Sung et al., 2021; Uthaman et al., 2018). Although increased life expectancy is the main cause of the growing incremental burden of cancer, the estimates are not favorable for those diagnosed in the more advanced stages of this disease (Xia et al., 2022). Cancer is defined by an abnormal cell growth caused by epigenetic modifications and cell proliferation production to boost tissue invasion and differentiation (INCA. Instituto Nacional de Câncer José Alencar Gomes da Silva, 2022). The high complexity related to the early finding and diagnosis of the pathogenicity of cancer require effective treatment (Sandbhor Gaikwad and Banerjee, 2018; Fouad and Aanei, 2017).

Radiation therapy and chemotherapy can cause some side effects, such as vomiting, fever, fatigue, or diarrhea. Therefore, personalized treatments have been sought, such as photodynamic, photothermal, sonodynamic, near-infrared light therapies associated with nanoparticles or composite materials to reduce these undesirable effects (Chu et al., 2018; Ketabat et al., 2019). Nanoparticles (NPs) can be used as the carriers and therapeutics agents in nanomedicine due to their catalytic, biological, and physicochemical characteristics (Anjum et al., 2021; Chen et al., 2021; Chiang et al., 2021). The NPs are structures whose sizes range from 1 to 100 nm and can be classified in terms of their physical characteristics (such as electric charge), chemical composition (such as the composition of the NPs), shape (tubes, films), and natural (viral or volcanic NPs) or artificial (synthesized NPs) origin (Ajdary et al., 2018).

The metal, metal oxide, and semiconductor NPs have a high potential to generate reactive oxygen species (ROS) and regulate leukocyte chemotaxis and pro-inflammatory cytokines, thus enhancing the immune response of the body against cancer cells through various mechanisms such as damage to specific sites, demonstrating a high capacity for application in cancer treatment (Anjum et al., 2021; Chen et al., 2021; Chiang et al., 2021). Titanium dioxide ($TiO_2$) NPs have a variety of applications in photocatalysis, solar cells, catalysts, biomedicine, microbiology, and biofilms (Prakash et al., 2022; Roy, 2022; Zhang and Rhim, 2022). Among the photoactive materials used for phototherapy, $TiO_2$ NPs exhibit excellent electrical, optical, magnetic, photocatalytic, biocompatibility, also

excellent structural stability (Jafari et al., 2020; Meng et al., 2019; Roy et al., 2011), and low toxicity (Hidaka et al., 1997). The $TiO_2$ NPs can be used as anticancer agents because their high accumulation in cells can cause modifications in gene expression, DNA damage, metabolic processes, homeostasis, inflammatory responses, and oxidation of lipids, leading to necrosis or programmed cell death. Effects of this type have been observed in HepG2 tumor cells (Li and Zhang, 2020; Xia et al., 2018; Yang et al., 2018). The $TiO_2$ NPs can be used as a photosensitizer, transforming energy into hyperthermia due to its high absorption in the ultraviolet (UV) light range (Huilan et al., 2021; Yu et al., 2020). The effects of $TiO_2$ NPs have been investigated for the treatment of various cancers, especially melanoma, lung cancer and breast cancer (Mohammadinejad et al., 2019). Photodynamic, sonodynamic, photothermal, near-infrared light, and ultraviolet light therapies are some of the phototherapeutic treatments that can be associated with $TiO_2$ NPs. These act as anticancer agents when activated by light and ultrasound waves, promoting the generation of ROS or heat, thus causing the death of cancer cells (Caputo et al., 2015; Galata et al., 2019; Ikram et al., 2021; Kwon et al., 2019; Sargazi et al., 2022; Shi et al., 2022; Tong et al., 2017). These are promising treatments and interesting solutions to eliminate tumor growth through light irradiation, caused by the production of ROS or ablation by heating, achieving synergistic effects, promoting cancer regression, and even reaching immunological memory (Ng et al., 2018).

The bibliometric analysis of scientific data follows a quantitative perspective that helps to map the published documents, aggregating the data by metric resources (e.g., number of publications and citations) and evaluating the importance of the scientific area (Zupic and Cater, 2015). The main objectives of a bibliometric analysis are to assimilate trends and develop knowledge in some area of scientific exploration, measure the degree of cooperation among authors, evaluate citation and co-citation methods, analyze statistical factors of language, measure the development of some fields, and the emergence of recent themes (Vanti, 2002). However, there is a lack in the literature regarding the description of a bibliometric analysis of scientific research on the application of $TiO_2$ NPs for cancer treatment. Bibliometric analysis can contribute to establishing future research by offering novel perspectives, suggestions, and hot topics.

Therefore, this comprehensive review (1) proposes an analysis of the advantages and limitations of photodynamic, photothermal, sonodynamic, near-infrared light therapies associated with $TiO_2$ NPs as a potential anticancer agent. Moreover, (2) bibliometric analysis elucidates the association between therapy function and $TiO_2$ NPs, elucidating global research trends, gaps, important topics, and future perspectives. Finally, (3) this review aims to verify the application of nanotechnology for cancer treatment, focusing on the biological action of $TiO_2$ NPs obtained by different chemical and physical methods, discussed in different tumor cell lineages, but detailing its action in melanoma considering it is a cancer with high metastasis rates.

This review was structured in the description of cutaneous melanoma (Section 2), followed by an overview of nanotechnology for cancer treatment (Section 3). Then, the description of the main aspects associated with $TiO_2$ (Section 4), biological mechanism (Section 5), synthesis, and characteristics of $TiO_2$ NPs were described (Section 6). The application of $TiO_2$ NPs as an alternative phototherapy technique for cancer treatment was presented in Section 7. Section 8 presents the bibliometric overview of $TiO_2$ NPs for cancer treatment, highlighting the research trends, bibliometric analysis of keywords, most relevant authors, institutions, countries, journals, and the most cited articles. Finally, the conclusion, future prospect, and recommendations were described in Section 9.

## 2. Overview of cutaneous melanoma

Cancer incidence rates, such as colorectal cancer, lip and oral cavity cancer, breast cancer, cervical cancer, and others, tend to double and even triple in countries, such as some countries in Africa, India, and New Zealand, with a medium or low human development index compared to developed countries, such as Europe, North America, and high-income countries in Asia and Oceania that have effective interventions for prevention, early detection, and treatment (Bray et al., 2018).

In 2020, there were 19.3 million new cancer cases worldwide. Excluding non-melanoma skin cancer, this number drops to 18.1 million. It is estimated that one in five individuals will develop cancer during their lifetime. Breast cancer is the most common cancer in the world during this period, with 2.3 million new cases,

accounting for 11.7% of all new cases, followed by tracheal, bronchial, and lung cancer with 2.2 million cases, or 11.4%. The third most common cancer is colon, rectosigmoid junction, rectum, and anus cancer, with 1.9 million cases, accounting for 10%. It is estimated that by 2025, there could be 21.9 million new cancer cases worldwide (INCA. Instituto Nacional de Câncer José Alencar Gomes da Silva, 2023; IARC. International Agency for Research on Cancer, 2023). This review will detail melanoma skin cancer, a malignancy with low incidence, but extremely lethal (INCA. Instituto Nacional de Câncer José Alencar Gomes da Silva, 2023).

The skin, the largest organ in the body, consists of the epidermis and dermis. The epidermis has Langerhans cells that process antigens and melanocytes. The melanocytes are pigment dendritic cells that produce melanin pigment. The melanin is produced in organelles, known as melanosomes, from an enzymatic cascade that encompasses thyrokinase and its proteins (Junqueira et al., 2017). Melanin effectively protects against the deleterious effects of UV radiation, as it reduces DNA damage and genomic mutability (Callahan et al., 2016).

Melanoma is characterized as a malignant neoplasm, mainly cutaneous, with histopathological properties that are constituted by the multiplication and abnormal proliferation of melanocytes involving genetic and environmental factors (Azulay et al., 2017; Valko-Rokytovská et al., 2018). It is classified according to its clinical properties, anatomical position of the primary neoplasm, microscopic parameters of growth, and age group of the individual (Rastrelli et al., 2014).

Among the subtypes are superficial spreading melanoma, which is the most common and characterized by radial growth, asymptomatic, occurring more commonly on women's legs and men's trunk, and color varying from brown to light brown. Lentigo maligna melanoma is more prevalent in the elderly and associated with epidermal atrophy and solar elastosis. It appears as a beige or brown macule and occurs on the face or other areas of chronic sun exposure. Acral lentiginous melanoma has diverse histopathological properties and occurs on the plantar, palmar, and subungual regions, accounting for only 2–10% of melanomas. Finally, nodular melanoma demonstrates vertical growth with early metastases, asymptomatic, rapid growth, and color varying from pearly gray to black (American Cancer Society, 2023).

The worldwide estimate in 2020 was 325,000 cases, but for 2025, it is projected to be 350,000 new cases of skin melanoma, considering both sexes (IARC. International Agency for Research on Cancer, 2023). Melanoma is responsible for 3–5% of cases of cutaneous malignancies, the highest incidence rates are in Australia, New Zealand, and Western Europe (Cavarsan, 2014; Oliveira et al., 2020; Ferlay et al., 2021). The number of new cases in Brazil for non-melanoma skin cancer from 2023 to 2025 are 220.490 and for melanoma, the estimated number of new cases is 8,980, corresponding to a risk of 4.13 per 100,000 inhabitants (INCA. Instituto Nacional de Câncer José Alencar Gomes da Silva, 2023).

Almost one-sixth of people diagnosed, in the world, with melanoma have a small probability of survival (Paddock et al., 2016). Thus, melanoma is one of the most severe cutaneous tumors because it impairs consecutive dermis levels and has high proliferation capacity, angiogenesis incitement, and metastasis production through hematogenous or lymphatic processes (Wick, 2016). People identified in the primary stages of melanoma show a 5-year survival rate of approximately 98%, reducing to 63.8 and 15% for a regional and distant tumor detected (Paddock et al., 2016). For early-stage identification of melanoma, it is essential to investigate any lesion that changes in size, shape, color, or elevation. This skin cancer is commonly asymmetric, with color oscillation, with a diameter greater than 6.0 mm3, and irregular edges (Callahan et al., 2016).

The UV radiation is responsible for inflammation, immunosuppressive features this occurs through negative regulation of T cell-mediated immunity, DNA lesions, carcinogenesis and contributes to melanoma development (Volkovova et al., 2012). The main sources of risk for skin cancer are prolonged exposure to UV rays, especially in childhood and adolescence, family history, genetics, and even exposure to tanning beds (American Cancer Society, 2022; INCA. Instituto Nacional de Câncer José Alencar Gomes da Silva, 2019). The process of melanoma aggravation has not been completely elucidated. However, the etiology has a multifactorial character (Rastrelli et al., 2014). Most cases of cutaneous malignancy are random and are related to irregular, early, and intense sun exposure, especially among populations with more sensitive phototypes. The body disposition of the lesions varies

according to gender. It is more frequent in the trunk for men and lower limbs for women (Azulay et al., 2017).

Malignant melanoma therapy is challenging due to its propensity for therapeutic resistance (Chen et al., 2019). Several treatments were approved by the Food and Drug Administration European Union and U. S., for melanoma oscillate due to the neoplasm's location, stage, and genetic profile (Li et al., 2017; Silk et al., 2022). Depending on these characteristics of melanoma, therapeutic options can be chosen, including radiation therapy, chemotherapy, photodynamic therapy, surgical resection (varies according to clinical-pathological properties), immunotherapy (increases immune response by inducing lymphocyte action), or targeted therapy. Among the limitations of melanoma treatment are low efficacy due to resistance to immunological, chemo/targeted, and intralesional therapies. Additionally, serious adverse effects may lead to cutaneous and gastrointestinal toxicity, usually related to the lack of specificity for neoplastic cells and immune reactions (Domingues et al., 2018).

The increase in the number of melanoma cases may be related to the involvement of the purinergic system (Di Virgilio and Adinolfi, 2017). Other factors that may be related to the development and progression of melanoma include a strong inflammatory response that differs depending on the cause (environmental, mutagenic, and others); the mechanism and intensity (oncogenic mutations, genomic instability, early tumor development, and increased angiogenesis). Among the inflammatory responses are autoimmunity and dysregulation of the immune system. Inflammatory bowel disease, for example, increases the risk of colorectal cancer (Grivennikov et al., 2010; Cazes and Ronai, 2016). And oxidative stress is involved in all stages of advancement of this disease and the modulation of intracellular pathways associated with cell proliferation and death (Sanches et al., 2017). The oxidative damage arising from high intracellular levels of ROS can cause cell death through the oxidation of DNA, lipids, and proteins (Peiris-Pagès et al., 2015).

The homeostatic balance of melanocytes can be impaired by oxidative stress, as melanocytes become vulnerable to excessive ROS production, affecting their survival or leading to malignant modifications. This occurs due to the pro-oxidant state produced during melanin synthesis, which is excessively stimulated

by sun exposure during tanning and inflammation resulting in post-inflammatory hyperpigmentation (Denat et al., 2014). Stress imbalance can result in or worsen mutations in several melanoma-related genes (Jenkins et al., 2011). And high rates of oxidative stress increase melanoma aggressiveness (Hambright et al., 2015). Many reasons and risk factors for cancer, such as bacterial and viral infections, smoking, cellular senescence, obesity, and age, are related to some form of chronic inflammation, thus the inflammatory process is crucial in melanomagenesis. Up to 20% of cancers are related to chronic infections, 30% may be linked to smoking and pollutants such as silica and asbestos that are inhaled, and 35% to diabetes (Grivennikov et al., 2010).

Gold, magnetic, carbon, and $TiO_2$ NPs have great potential in the diagnosis and treatment of oncological pathological conditions (De Paula, 2019). Thus, the effect of $TiO_2$ NPs activated by different phototherapies as an anticancer agent has been explored for the treatment of cancer (Li and Zhang, 2020).

## 3. Nanotechnology for cancer treatment

Nanotechnology is a therapeutic resource for all types of cancer, delineating its system for releasing drugs for tumors. The NPs have a high surface area and absorption efficiency and allow binders on their surface, such as drugs, proteins, nucleic acids, and others (Halwani et al., 2016). The NPs have been developed and used as multifunctional carriers on the nanoscale for the delivery of drugs, which improve therapeutic efficiency and reduce the side effects of conventional treatments used in cancer therapy (Li et al., 2018). In conventional treatments, drugs have reduced action because angiogenesis increases vascular density, forming gaps between cells in tumor blood vessels. Thanks to these gaps, macromolecular drugs are retained and drugs that are not coated with NPs are released, having a shorter circulation time (Meng et al., 2020; Yang et al., 2021). Advances in nanoscale science can benefit human health through changes to improve the efficacy of NPs, the development of techniques, and the expansion of their applications. Thus, improving the areas of bioengineering and biomedical in cancer treatment. The nanometric dimensions of NPs improve their coupling and conduction properties to cells. Among the applications of NPs in the biomedical field are cell imaging, biosensors, drug release systems, and genetic engineering (Fei Yin et al., 2013). It is used to design, measure, assemble, and manufacture

materials on a scale of 1–100 nm, with high precision and controllability. For cancer nanotechnology, defining properties are included in its innovative potential to assist patients. This interdisciplinary branch of science has the ability to manipulate matter at the molecular or atomic level, which allows for various applications in the fields of solar energy, electronics, optics, and biomedical areas (Ferrari, 2005; Lagopati et al., 2021; Singh et al., 2020).

The NPs have chemical and physical characteristics, such as charge eletric positive or negative, crystallinity, size, solubility, specific surface area, aggregation state, and form, which play a significant role in toxicology (Ajdary et al., 2018). The NPs vary according to the active sites of the surface and may be lipophilic or lipophobic, active or passive, and hydrophilic or hydrophobic in terms of their catalytic activity (Yu et al., 2016). The uptake of NPs in all eukaryotic cells can be passive by free diffusion and active diffusion by endocytosis (Behzadi et al., 2017). The size of NPs is responsible for triggering active or passive diffusion, i.e., they can be eliminated by macrophages or found free in the cytoplasm of epithelial cells, endothelial cells, and fibroblasts (Geiser et al., 2008) or membrane-bound, in the case of larger NPs (Manke et al., 2013).

The NPs can penetrate cells via endocytosis and become enveloped by lysosomes, where they are then located in late endosomes that can induce signaling pathways that depend on ROS (Ajdary et al., 2018). They may also cause autophagy by other means, such as impaired lysosome-autophagosome aggregation, a relationship with autophagic proteins, positive regulation of autophagy-related genes, and oxidative stress (Azimee et al., 2020; Mohammadalipour et al., 2020). The most researched NPs against cancer cells include gold, zinc, silver, copper, cobalt, magnesium, iron, manganese, platinum and titanium (Chen et al., 2021).

## 4. Titanium dioxide ($TiO_2$)

The ninth most abundant chemical element on Earth, titanium (Ti), was discovered in 1791 by William Gregor and can be found in igneous rocks and sediments from the weathering of these rocks (Gázquez et al., 2014). This element has a low density and high mechanical strength. The $TiO_2$ is extracted from sedimentary deposits using the wet mining process, where mechanical blasting occurs, and then the ores undergo magnetic, gravimetric, and electrostatic

processes. The deposits are from iron titanate ($FeTiO_3$) and other silicates and oxides (Bertoni, 2014; Fernandes dos, 2015; Santos, 2010). Approximately 95% of this element generated worldwide is used in $TiO_2$ (Santos, 2010). The $TiO_2$ has a global production capacity of 4.7 million tons per year (Bertoni, 2014; Santos, 2010). The total estimated global reserves of $TiO_2$ amount to more than 2 billion tons, including anatase, ilmenite, and rutile (Gambogi, 2021). Ilmenite is a mineral composed of iron and $FeTiO_3$, with a black color and metallic to submetallic luster (Santos, 2010).

The $TiO_2$ has three polymorphic structures: anatase, rutile, brookite (**Fig. 1**). Anatase has a tetragonal arrangement, is metastable at low temperatures (below 450 °C), and has a bandgap of 3.2 eV (Di Paola et al., 2013; Ali et al., 2018). Rutile has a tetragonal arrangement, is the most thermodynamically stable form, is most common, and has a bandgap of 2.96 eV (Ali et al., 2018). Brookite has an orthorrombic arrangement, formed under hydrothermal conditions and has a bandgap of 3.02 eV (Ahmad et al., 2017; Ali et al., 2018; Bet-Moushoul et al., 2016; Di Paola et al., 2013; J. Liu et al., 2017).

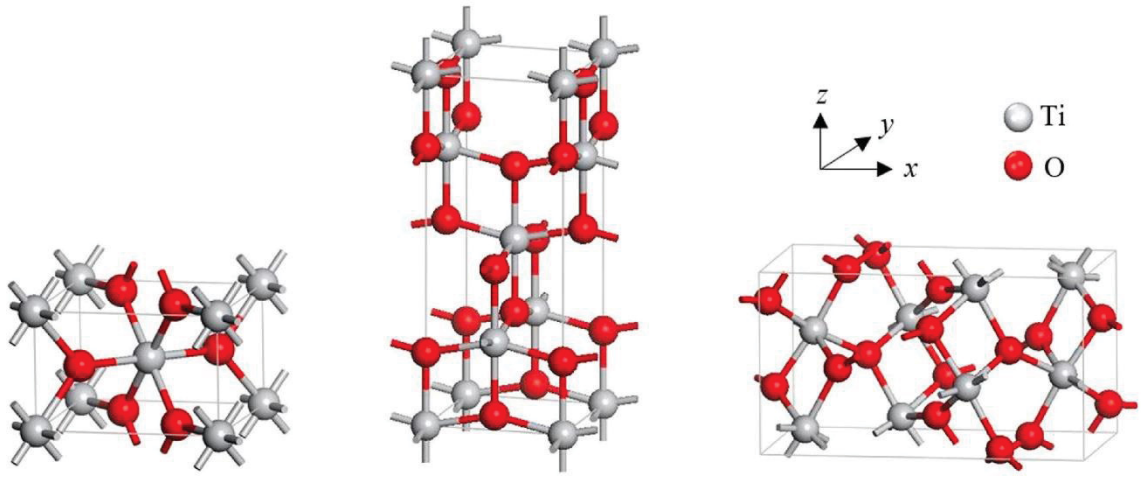


**Figure 1.** Illustrative representation of the polymorphic structures of $TiO_2$. (a) Rutile, (b) anatase and (c) brookite $TiO_2$. Reproduced from Samat et al. (2016), with permission from Elsevier.

The remarkable photocatalytic performance of $TiO_2$ was described in 1972 in a study on the oxidation of suspended water by this oxide, producing hydrogen and oxygen, according to reactions described from **Eq. 1** to **10** (Fujishima and Honda, 1972).

Photoactivation of the semiconductor particle:

$TiO_2 + hv \rightarrow e^-_{CB} + h^+_{VB}$ (1)

Reaction between the valence band gap and adsorbed water:

$H_2O + h^+_{VB} \rightarrow OH^\bullet + H^+$ (2)

Reaction between the valence band gap and the $OH^-$ groups on the $TiO_2$ particle surface:

$OH^- + h^+_{VB} \rightarrow OH^\bullet$ (3)

Formation of the superoxide radical ion:

$O_2 + e^-_{CB} \rightarrow O_2^{\bullet-}$ (4)

Formation of hydrogen peroxide:

$O_2^{\bullet-} + H^+ \rightarrow HO_2^\bullet$ (5)

$HO_2^\bullet + HO_2^\bullet \rightarrow H_2O_2 + O_2$ (6)

$O_2^{\bullet-} + HO_2^\bullet \rightarrow HO_2^- + O_2$ (7)

$HO_2^- + H^+ \rightarrow H_2O_2$ (8)

Generation of hydroxyl radicals by the breakdown of hydrogen peroxide:

$H_2O_2 + e^-_{CB} \rightarrow OH^\bullet + OH^-$ (9)

$H_2O_2 + O_2^{\bullet-} \rightarrow OH^\bullet + OH^- + O_2$ (10)

*where* VB is the valence band; CB is the conduction band; $h^+$ is the photogenerated hole; $e^-$ is the photogenerated electron; $O_2^{\bullet-}$ is the oxygen radical; $H_2O_2$ is the hydrogen peroxide; $OH^-$ is the hydroxyl radical; $H_2O$ is water; and $H^+$ is the hydrogen radical (Herrmann, 1999; Li et al., 2002).

The $TiO_2$ is a solid oxide, white, odorless, tasteless, and that has excellent properties such as high chemical stability, excellent corrosion and oxidation resistance, high thermal resistance, and high photoactivity. It is also a low-cost and non-flammable material. It is among the top ten most abundant elements in the Earth's crust, considering that $Ti^{4+}$ occurs in 45 mineral species (Grilli et al., 2016; Shiva Samhitha et al., 2022; Ziental et al., 2020). The $TiO_2$ is a semiconductor of

type n this occurs when impurities alter the semiconductor properties of materials by introducing an excess of electrons or electronic holes, can generate ROS when exposed to UV radiation and it can be used in photodynamic therapies due to its mutagenic capacity (Moosavi et al., 2016; Nogueira et al., 2018).

The $TiO_2$ NPs have been used in drug delivery and combined cancer treatments due to their ability to reach drug release in cancer cells, their autophagic, photodynamic characteristics, and their non-toxicity up to a concentration of 1 µg/ml for normal cells. They can be explored in the treatment of melanoma (Azimee et al., 2020; Mhammadinejad et al., 2019).

## 5. Biological mechanism of $TiO_2$ NPs

The use of iron-doped $TiO_2$ NPs has the potential to selectively target tumor cells and tissues. With the help of magnets, the doped $TiO_2$ NPs can deliver drugs such as doxorubicin, increasing their intracellular concentration and enhancing the anticancer efficiency of the chemotherapeutic agent. The delivered doped NPs, with the aid of magnets, are used as photosensitizers in photodynamic and photothermal therapies where they are irradiated with UV radiation. The irradiation activates the doped $TiO_2$ NPs, increasing their photosensitizing activity and further attacking cancer cells, potentially causing apoptosis of the tumor tissues. Damage to surrounding tissues is avoided due to the low penetration of UV, thus reducing side effects (Zhang et al., 2016; Davalli et al., 2016; Nita and Grzybowski, 2016).

The $TiO_2$ NPs can also detach intracellular anticancer substances, such as anthracyclines, antitumor antibiotics, topoisomerases, and others following the redox process release mechanism (Wachesk et al., 2021; Zheng et al., 2019), release ROS and oxidative products, attenuate antioxidants in cells and interact with DNA and other macromolecules (Egbuna et al., 2021; Nie et al., 2019; Oliveira et al., 2021; Rahmati M et al., 2020; Wachesk et al., 2021).

A moderate level of ROS favors tumorigenesis, due to its involvement in pro-oncogenic signaling pathways or by stimulating mutations in genomic DNA. For example, the activation of transcription factors, sensitive to ROS, to regulate the expression of proteins involved in proliferation, immortalization, and metastasis. Mitochondrial ROS amplifies the tumorigenic phenotype and stimulates the accumulation of mutations, thus facilitating metastasis. Therefore, a high production of ROS levels is needed through the activation of $TiO_2$ NPs,

surpassing the levels in cancer cells. Excess ROS can overload the cell's antioxidant capacity and trigger cell death (Yang et al., 2019).

The $TiO_2$ NPs produce considerable ROS, affecting the positive regulation of the caspase protein and mitochondrial depolarization and leading to hypothermia that causes apoptosis and necrosis of cancer cells (Gao et al., 2014). Apoptosis is a regulated form of cell death that aids in physiological events, extinguishing unnecessary or abnormal cells (Lagopati et al., 2021). On the other hand, necrosis is the most common mode of cell death from exogenous impulses, caused by physical agents (temperature, radiation, and others), toxic or non-toxic chemicals (alcohol, drugs, detergents, and others), biological agents (viral, bacterial, or fungal infections, parasites, and others), and circulatory insufficiencies (vasoconstrictions, infarctions, and others), such as cell disruption and organelle deterioration (Grecco et al., 2015).

Cellular signaling and biochemical events mediated by $TiO_2$ NPs are linked to DNA damage, induction of ROS, and cell death involving the breakdown of calcium homeostasis (Yu et al., 2015), disruption of mitochondrial membrane potential (Filippi et al., 2015). It is also related to the activation of nuclear factor kappa B (NF-κB), a protein complex that acts as a transcription factor and is involved in cellular response to stimuli such as stress, cytokines, free radicals, UV radiation, and antigens, as well as regulation of immune response to infection and autoimmunity (Setyawati et al., 2015). And also, stimulation of executioner caspases (Wang et al., 2015) and caspase 12 (Yu, et al., 2015) and the elimination of proinflammatory cytokines (De Angelis et al., 2013).

The Wnt signaling pathway is involved in carcinogenesis and tumor development, and is composed of 19 secreted glycoproteins that are grouped based on sequence similarity, including β-catenin. Mutations in the β-catenin gene are found in melanoma, pancreatic cancer, and ovarian cancer. The Wnt signaling pathway is also associated with the epithelial-mesenchymal transition characterized by cellular invasion and migration. This mesenchymal transition leads to metastasis, which is initiated by the dysregulation of E-cadherin. This dysregulation, combined with the negative regulation of E-cadherin, results in the loss of cell-cell adhesion, invasion, and migration, which are found in cancers such as melanoma. The expression of E-caderina and β-catenin did not change by $TiO_2$ NPs (Wright et al., 2017).

Near-infrared (NIR) activated nanoparticles can induce cancer cell death through an apoptotic pathway involving the mitochondria, which can occur through the upregulation of caspase 3 expression in the tumor tissue (Yang et al., 2019). Thus, one of the cleavage targets of caspase-3, belonging to the caspase family, during the apoptosis process is nuclear poly ADP-ribose polymerase (PARP). PARP is a nuclear poly(ADP-ribose) polymerase and is involved in DNA repair in response to environmental stress, and is a target of caspase-3 cleavage. The cleavage of this polymerase favors cellular dismantling, indicating the presence of cells undergoing apoptosis, and is increased in the presence of $TiO_2$ NPs (Lagopati et al., 2010).

The **Figure 2** schematically demonstrates $TiO_2$ NPs being engulfed by lysosomes, due to their nanometric size, into the cellular cytoplasm. These NPs are then irradiated by exogenous interventions such as UV (photothermal, photodynamic therapies or near-infrared light) or ultrasound (sonodynamic therapy), presented in the next section, which can cause cyto and genotoxicity. Induction of apoptosis and/or necrosis of cancer cells is accompanied by activation of biological cascades such as secretion of pro-inflammatory cytokines and recruitment of immune cells (Yang et al., 2019; Lagopati et al., 2021).

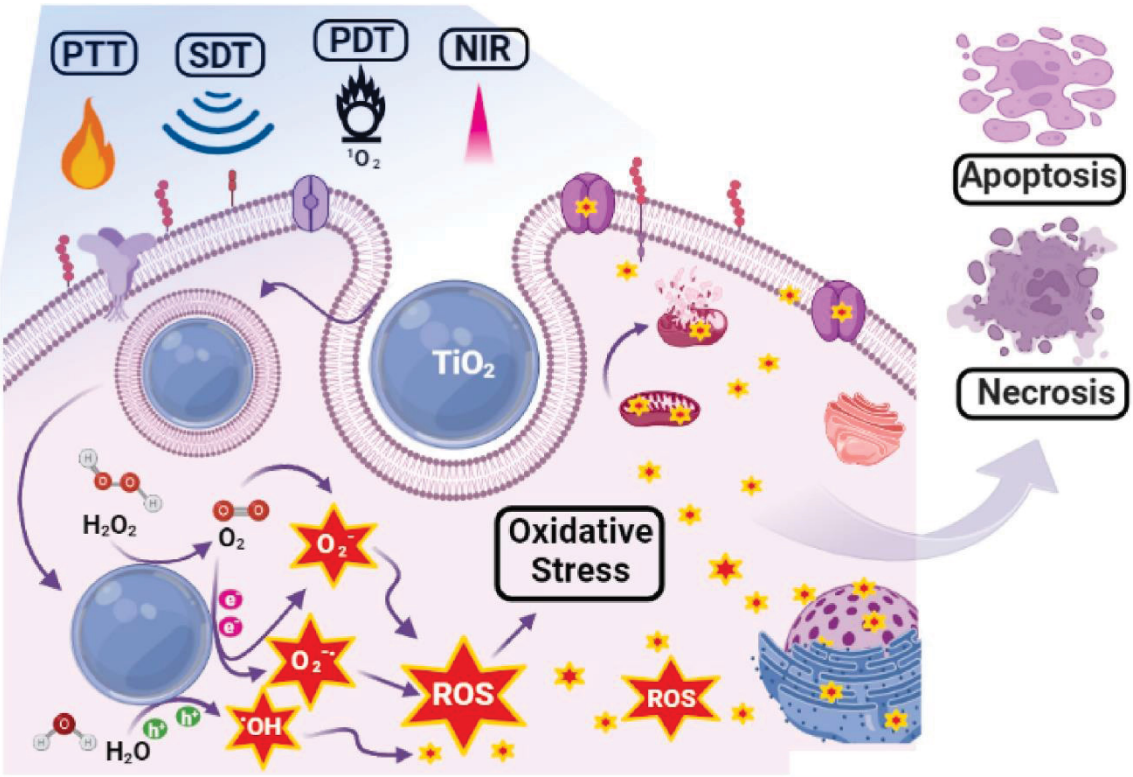

**Figure 2.** Illustrates the mechanism of action of $TiO_2$ NPs. Due to their nanosize, $TiO_2$ NPs are engulfed by lysosomes and enter the cytoplasm, where they are excited by an exogenous stimulus (light or sound) from Therapies: Photothermal (PTT), Photodynamic (PDT), Near Infrared (NIR), or Sonodynamic (SDT). Upon activation, there is a superproduction of intracellular ROS that overwhelms the cell's antioxidant capacity, triggering apoptosis or necrosis of the target cells, accompanied by the activation of biological cascades such as the secretion of pro-inflammatory cytokines and the recruitment of immune cells.

External photo or sono (ultrasound) excitation allows for efficient catalytic generation of ROS, such as superoxide anions, hydroxyl radicals, and singlet oxygen. They are highly reactive with cell membranes and the cell interior, including DNA, affecting cell stiffness and the chemical arrangement of surface structures with cytotoxic effects. These damages caused by ROS to cellular components and macromolecules, if produced in excess or not neutralized by innate antioxidant defense mechanisms, can cause cell death. The existence of molecular scavengers of hydroxyl radicals and $H_2O_2$, such as N-acetylcysteine and catalase, attenuates cell death (Lagopati et al., 2010; Yang et al., 2019).

## 6. Overview of the synthesis and characteristics of $TiO_2$ NPs

There are several chemical and physical methods to produce $TiO_2$ NPs, such as the grinding of ball mills (Malevu, 2021; Mariño-Gámez et al., 2022), microwave irradiation (Cheng et al., 2020; Qiang et al., 2022), sol-gel (Lukong et al., 2022; Solanki et al., 2021), hydrothermal (Mezzourh et al., 2022; Sukidpaneenid et al., 2023), coprecipitation (Chen et al., 2022; Liu et al., 2021), pyrolysis by flame spray (Boningari et al., 2018; Meng and Zhao, 2020), wet chemistry (Liao et al., 2022; Wadge et al., 2022), spreading and centrifugation (Timoumi et al., 2020; Trabelsi et al., 2020). These preparation methods of oxides have enabled the development of new materials with particular properties, such as appropriate porosity, surface area, dimension, structure, morphology, and crystallinity (Diamantopoulou et al., 2019; Takahashi, 2018).

The **Figure 3** illustrates these properties of $TiO_2$ NPs in the anatase phase, through the UV–Vis absorption spectrum, scanning electron microscopy (SEM)

micrograph, energydispersive X-ray analysis, transmission electron microscope (TEM) micrograph, size distribution; and X-ray diffraction pattern (Fátima et al., 2021). Effective control of porosity, surface area, dimension, structure, morphology, and crystallinity occurs because nanomorphology and dimensionality are essential properties that establish these NPs optoelectronic characteristics, structure, and photocatalytic performance (Diamantopoulou et al., 2019; Takahashi, 2018).

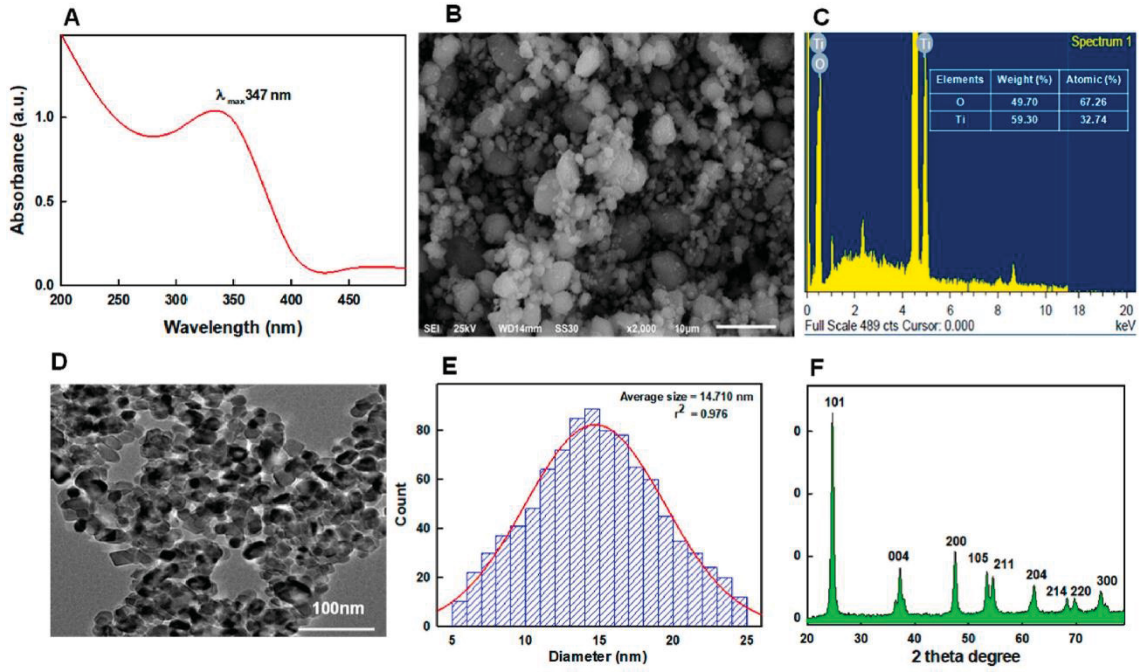


**Figure 3.** Characteristics of $TiO_2$NPs. (a) UV–Vis absorption spectrum; (b) SEM micrographs; (c) energy dispersive X-ray analysis; (d) TEM micrograph; (e) size distribution; and (f) X-ray diffraction pattern. Reproduced from Fatima et al. (2021).

The excitation of $TiO_2$ NPs (**Figure 4**) occurs because the photon's energy (hv) is greater than the energy gap of the compound. From this excitation, pairs of electrons ($e^-$) and gaps ($h^+$), which are located in the conduction band and in the valence band, respectively, are produced. The pairs of $e^-/h^+$ generated by light excitation react with existing molecules in biological systems, such as water and oxygen ($O_2$), generating hydroxyl radicals ($^{\bullet}OH$) and anionic oxygen ($O^{\bullet 2-}$). These species ($^{\bullet}OH$ e $O^{\bullet 2-}$) are short-lived and have high activity for redox reactions, thus degrading tumors (Xiong et al., 2013; Zhou et al., 2016). The $TiO_2$ NPs can be used to treat tumors due to high levels of ROS, which include •OH and $O_2^{\bullet 2-}$, under any source of irradiation, sunlight or artificial light (such as UV) (Li and Zhang,

2020; Wang et al., 2019; Yang et al., 2019; Ziental et al., 2020). The $TiO_2$ NPs are biocompatible molecules that are very reactive, chemically stable, and safe for humans, as the absorption of $TiO_2$ NPs administered orally has insignificant effects on human intestinal microbiota, and the biodisponibility may be independent of particle size according to the Food and Drug Administration (Piccinno et al., 2012; Li et al., 2017).

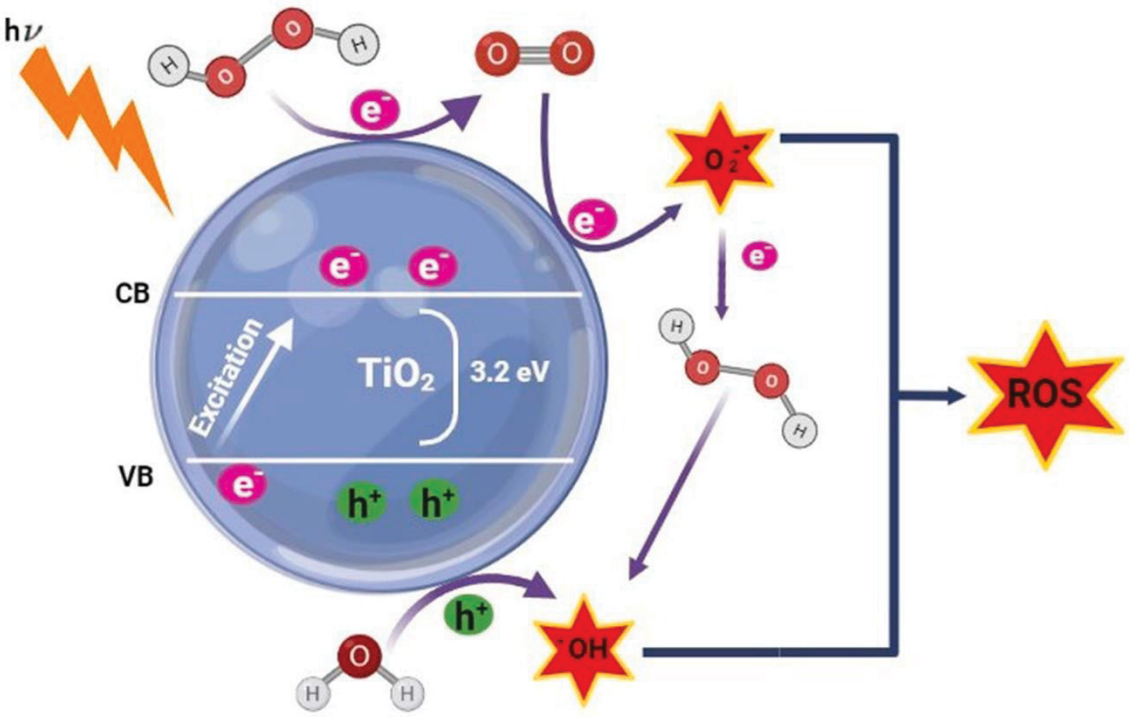


**Figure 4**: The excitation of $TiO_2$ NPs occurs because the photon's energy (hv) is greater than the energy gap of the compound. From this excitation, pairs of electrons ($e^-$) and gaps ($h^+$), which are located in the conduction band and in the valence band, respectively, are produced. Os pares de $e^-/h^+$ fotogerados react with existing molecules in biological systems, such as water and oxygen ($O_2$), generating hydroxyl radicals ($^{\bullet}OH$) and anionic oxygen ($O^{\bullet 2-}$). These species ($^{\bullet}OH$ e $O^{\bullet 2-}$) are short-lived and have high activity for redox reactions, thus degrading tumors.

## 7. Alternative phototherapy techniques for cancer treatment with $TiO_2$ NPs

Phototherapy is a rising therapeutic method to improve for all types of cancer therapy, with high therapeutic efficiency, minimal cell invasion, and irrelevant side effects (Meng and Zhao, 2020; Yang et al., 2021). Phototherapy and synergistic treatments based on $TiO_2$ have received extensive attention and

numerous advances (Gao et al., 2019). Photothermal, near-infrared light, and UV radiation, being a safe and selective method that uses a laser-oriented procedure to eliminate malignant cells (Gao et al., 2020; Veeranarayanan et al., 2019; Xie et al., 2020). Light irradiation is more efficient and less invasive against tumors when compared to conventional methods such as radiotherapy, hormone replacement therapy, and chemotherapy, and it can be used in combination with these methods for cancer treatment (Baneshi et al., 2019; Irajirad et al., 2019; Xie et al., 2020; Shirvalilou et al., 2021).

Photosensitizing agents, for example, drugs, dyes, and $TiO_2$ NPs, with high optical absorption, present in photodynamics and photothermal therapy, are applied to the production of cytotoxic ROS in the tumor region or transport the energy of laser light to hyperthermia to combat cancer effectively (Wei et al., 2020; Zheng et al., 2019). The ROS are responsible for a latent situation that can damage and oxidize cellular constituents of tumor cells, such as lipids, DNA, and proteins (Li et al., 2021; Shields et al., 2021).

Photothermal therapy uses cyclic or continuous-wave lasers to impair electromagnetic wave carcinoma, causing an abrupt temperature increase in which the energy of the incident light is modified in heat, leading to apoptosis by various paths (Hu et al., 2018). Photothermal therapy requires photothermal agents such photosensitive drugs, non-toxic dyes, and $TiO_2$ NPs that can transform light into hyperthermia in specific cancer places and is independent of oxygen concentration within tumor cells (Zhi et al., 2020; Zhu et al., 2018). The induction of NPs, which act as absorbing sources of exogenous energy with a specific wavelength is absorbed and dispersed through a non-radioactive decay process, causing a local temperature increase, protein and DNA denaturation, and tissue coagulation (Fei Yin et al., 2013; Melamed et al., 2015). Photothermal therapy is a therapy that presents high efficiency, high specificity, minimal invasiveness, tenuous tissue effects, and low toxicity (Xie et al., 2020; Yougbaré et al., 2020).

Tumor tissues are more affected than normal tissues by hyperthermia due to the unstructured and uneven vasculature of tumors, thus making the pH and the oxygen port within the tumor environment smaller (De Paula, 2019). The mortality rate of tumor cells in photothermal therapy is proportional to the treatment time, depending on the type of tissue and cell lineage. Thus, with one hour of therapy at

temperatures of 40 to 45 °C, there is enough energy to denature proteins, mitochondrial swelling and membrane rupture (De Paula, 2019; Weng et al., 2020). The $TiO_2$ NPs have been considered great photothermal agents due to their low toxicity, optimal optical absorption, good conductivity, and thermal stability (Fei Yin et al., 2013).

Photodynamic requires a photosensitive molecule called a photosensitizer. It is activated when irradiated with visible light and in the presence of oxygen, inactive and nontoxic in the dark, and acts as an energy transducer (Castano et al., 2005; Wang et al., 2021). Photosensitizer conduct energy to molecular $O_2$, thus deteriorating the target cancer cells (Liu et al., 2019). Photodynamic kill cancer cells in three routes: *i)* by producing ROS during light irradiation, *ii)* through irreversible lesions to tumor vasculature, and *iii)* through stimulation of the immune response directed against cancerous tissues (Castano et al., 2006). The success of this therapy is influenced by the properties of photosensitizer, such as photochemical and pharmacokinetics (Lucky et al., 2015). The light source depends on the category of photosensitizer involved (organic and inorganic), the amount of light required to penetrate cancer cells (UV or near-infrared), and the tumor region (deep sites with hypoxia and nutrient imbalance or superficial sites) (Yang et al., 2019).

The reaction between ROS and oxygen produces the superoxide anion ($O_2^-$). When photosensitizer react with triplet oxygen ($^3O_2$), they generate cytotoxic singlet oxygen ($^1O_2$), it is a ROS. The $^1O_2$ and the $O_2^-$ anion cause cell death via two mechanisms. The first covers apoptosis and necrosis, and the second comprise an indirect mechanism that causes antitumor immunity (Cengel et al., 2007) and microvascular disorders (Azaïs et al., 2017). Normal cells are minimally affected by ROS, as only malignant cells absorb and accumulate the correct amount of photosensitizer dosage (Aishwarya and Sanjay, 2018; Lee et al., 2018). Thus, photodynamic is effective in treating cancer compared with other available methods such as radiofrequency, radiotherapy, and chemotherapy (Wang et al., 2019) because it acts in a localized manner, with spatial direction and local specificity (Gangopadhyay et al., 2015).

Autophagy is a possible path of death of cancer cells in photodynamics, which acts on the displacement of proteins and cellular organelles through lysosomal degradation and is linked to development, cell differentiation, and

survival (Moosavi et al., 2016). When proteins receive irreversible damage from ROS, they generate toxic oxidized proteins that stimulate autophagy to remove them. Failure to remove the oxidized proteins results in an accumulation of macromolecules beyond the cell's ability to degrade them, thus compromising vital functions and leading to cell death (Mehraban and Freeman, 2015). Recently, drugs (He et al., 2018), drugs in association with dopers (Yu et al., 2017), antibodies (Wang et al., 2018), $TiO_2$ NPs (Safavipour et al., 2020), and dyes (Basit et al., 2022) were tested as photosensitizers. Silane agents such as 3-aminopropiltriethoxysilane have also been used as photosensitizers, which, through the condensation reaction, produce amine functional groups on the surface of $TiO_2$ NPs (Youssef et al., 2017). Anticancer substances, such as doxorubicin, camptothecin, and daunorubicin, join the surface of altered $TiO_2$ NPs functional groups and, through intramolecular bonds, are used in the delivery of medicinal products (Abdurahman et al., 2016).

Metals such as Fe, V, W, Au, Ni, Cr, Co, Cu, and Ag are also added to the crystal structure of $TiO_2$ to decrease the band gap energy, increase the photocatalytic reactivity, and broaden the light absorption capacity from the UV range to the visible range of $TiO_2$ (Anju et al., 2018). The $TiO_2$ NPs were loaded with the drugs vorinostat and erlotinib to treat human cancer amniotic cells - WISH and breast cancer cells - MDA-MB-231 and MCF-7 (Abdel-Ghany et al., 2020). The $TiO_2$ NPs present a magnetic center that can aggregate a vast set of teranotic resources, comprising a therapeutic delivery organization guided by magnetism and magnetic stimuli (Kafshgari and Goldmann, 2020; Peng et al., 2017).

The therapeutic action of phototherapy and photodynamic therapy is lower when applied individually, but when these two therapies are combined, their action against cancer cells is increased (Yang et al., 2018; Zeng et al., 2018). The synchronous and synergistic photodynamic/photothermal action under a single laser irradiation has been investigated in studies using $TiO_2$ NPs as photosensitizers in cancer therapy with a single wavelength (Mou et al., 2017, 2016; Wang et al., 2019).

Near-infrared light is another therapeutic resource that presents two absorption regions (750-1000 nm and 1000-1350 nm). Near-infrared light has an excellent depth of penetration in tumor tissues and has a maximum exposure time allowed for medical uses (Gao et al., 2019; Zhang et al., 2020). Near-infrared light

has a therapeutic window corresponding to a region between 700 - 900 nm that is minimally absorbed by water, blood, and soft tissues. And demonstrates greater tissue penetration, minimal damage to healthy tissues, high therapeutic purpose, and low autofluorescence in living systems (Li and Zhang, 2020; Shi et al., 2020).

The UV light can cause cellular or tissue damage from the production of ROS due to its potential to excite electrons to create gaps, which can react with hydroxyl groups to form oxidative radicals (Wang et al., 2017; Sun et al., 2017). These tumor microenvironments have high levels of low hydrogen peroxide and pH (i.e., acidic environments) (Chen et al., 2017). Due to the rapid metabolism of tumors and the scarce blood supply, hydrogen peroxide rates tend to be overexpressed (Lin et al., 2018; Liu et al., 2017). Wavelengths below 385 nm have insufficient penetration depth of UV light in deep tissues and can cause damage to biological samples, thus limiting their therapeutic action (Wu and Butt, 2016).

Sonodynamic therapy applies ultrasound in medicine and is non-invasive and was derived from photodynamic methods with a similar purpose, modifying the energy source, i.e., light by ultrasound (Wu et al., 2019). The penetration of sound into deep cancerous tissues is efficient, minimally invasive, and low cost (He et al., 2018; Lin et al., 2019; Wu et al., 2019). The sound penetration into the tissue occurs rapidly through acoustic cavitation, which raises the temperature, acting in the generation of ROS to scare the suppression of tumor development or cause the death of the tumor (Kwon et al., 2019; Wu et al., 2019). The term cavitation refers to the creation, development, and breakdown of vapor-filled cavities within the liquid structure of tissue. Cavitation occurs from the non-thermal interaction of ultrasound waves, resulting in the modification of permeability in the cell membrane (Gorgizadeh et al., 2019).

Sonodynamic is essential in clinical imaging diagnosis and tumor ablation resulting from sonosensitizer activation to produce sonosensitizers, causing apoptosis and/or cellular necrosis (Yue et al., 2019). Sonodynamic depends on the efficiency of sonosensitizers, divided into organic sonosensitizer activation and inorganic nanonosonossensitizers. This therapy also depends on oxygen content, as solid tumors have hypoxic properties (Deepagan et al., 2016; Teranishi et al., 2019). The hypoxic tumor microenvironment limits the production of ROS, which, attributed to the decrease in $O_2$ due to sonochemical reactions during

sonodynamic therapy, aggravates the local hypoxic microenvironment. The hypoxic tumor microenvironment can be a favorable factor to activate sonodynamic therapy through prodrugs (such as tirapazamine) that are activated by hypoxia and generate cytotoxic metabolites, obtaining a synergistic treatment (Ning et al., 2022).

White $TiO_2$ NPs are not good sonosensitizers due to their low efficiency in producing ROS. Instead, there is a rapid rearrangement of electrons and holes in the bands, limiting their interactions with $H_2O$ and $O_2$, resulting in a low sonodynamic therapeutic effect (Dai et al., 2017). The efficiency of ROS production can be enhanced by associating $TiO_2$ NPs with noble metals such as Ag, Au, and Pt. When $TiO_2$ is excited by ultrasound irradiation, its electrons and holes are transferred from its band to the band of metals, which act as a capture network for electrons and holes. The noble metals then transport the electrons and holes to react with $H_2O$ and $O_2$, thus producing ROS (Ismail and Bahnemann, 2011; Deepagan et al., 2016; Han et al., 2018; Liang et al., 2020). Therefore, this therapy uses $TiO_2$ NPs as a sonosensitizer activator and presents promising results in cancer treatment (He et al., 2018; Wu et al., 2019).

Studies against different types of cancer, such as human cervical adenocarcinoma, melanoma, breast cancer, and others, have shown the applications of $TiO_2$ NPs associated with photodynamic, photothermal, sonodynamic, near-infrared light therapies with significant effects for cancer treatment, which are further detailed in **Table 1.**

**Table 1.** Application of $TiO_2$ NPs for cancer treatment.

| Catalyst | Cell Type/ Animal | Method/ Synthesis | Findings | Reference |
|---|---|---|---|---|
| NPs PEG-$TiO_2$ | Metastatic murine melanoma cells/ Consanguineous mice | Photothermal (808 nm) / ultrasound Overview | - The average tumor size in mice that received NPs of PEG-$TiO_2$ + photothermal decreased by 40.6 $mm^3$/day;<br>- 70% necrosis;<br>- Low cytotoxicity and high optical absorbance. | Behnam et al., 2018 |

| | | | | |
|---|---|---|---|---|
| Nanorods of $TiO_2$ and 2,2,6,6, tetramethylpiperidine -N-oxil | Human breast cancer cells / - | Photodynamics under light UV (340 nm)/ Sun-gel synthesis | - Loss of cell viability ~ 80%;<br>- Nanorods indicate a synergistic response of the photodynamic effect. | Fakhar-and-Alam et al., 2020 |
| $TiO_2$/ $Fe_3O_4$ | 4T1 cancer cells; murganho colon cancer cells, and human umbilical vein endothelial cells/<br>Balb/c mice | Reaction photo Fenton/ Sonication synthesis | - $TiO_2$/$Fe_3O_4$ adsorbed more $H_2O_2$ and amplified the efficiency of the Fenton reaction;<br>- High biocompatibility;<br>- The rate of suppression, *in vivo*, of the tumor volume of 79%;<br>- Loss of cell viability above 80% for 4T1 cells *in vitro*. | Wang et al., 2021 |
| HPT and HPT-HPT-DOX | Normal murine fibroblast cells, HeLa and 4T1 cells/ Balb/c mice | Sonodynamics Chemotherapy /Vacuum metal spray deposition synthesis | - HPT-DOX + Sonodynamics had an extraordinary effect of tumor inhibition *in vivo* (tumour volume below 200 $mm^3$);<br>- Drastic reduction of tumor weight *in vivo*;<br>- HPT-DOX + Sonodynamics had cellular viability below 15% *in vitro* for 4T1 cells. | Liang et al., 2020 |
| BT-CTS Hydrogel | Metastatic murine melanoma cells/ Mice | Photothermal/ Photodynamic and Near Infrared Light (808 nm) | - Injectable hydrogel;<br>- Cell viability of 11.4% *in vitro*;<br>- Photothermal area (> 45 °C) of 72.2 $mm^2$ *in vivo*;<br>- Tumor growth was suppressed after 4 days (BT-CTS + Near Infrared Light;<br>- Regeneration of skin tissue in a murine model of the chronic wound;<br>- Excellent thermostability. | Wang et al., 2019 |

| | | | | |
|---|---|---|---|---|
| Nanoreactor $TiO_2/MnO_2$-GOx/C | B16/F10 cells and 4T1/ Mice cells | Enhanced Radiotherapy (346 nm) | - GOx oxidizes glucose and produces gluconic acid and $H_2O_2$;<br>- $MnO_2$ converts $H_2O_2$ at $O_2$ and relieves tumor hypoxia;<br>- Loss of *in vitro* viability of tumor cells was greater than 85%;<br>- May prevent the formation of lung metastasis;<br>- The metastatic lung tumor has disappeared with $TiO_2/MnO_2$-GOx/C + rays X. | Pan et al., 2020 |
| NPs of $Ag/TiO_2$ | Murine cutaneous melanoma cells/ Mice C57BL/6J | Photothermal and Near Infrared Light (808 nm) /Sun-gel synthesis | - Photothermal conversion efficiency of 60%;<br>- The tumors shrank after 1 min of irradiation;<br>- Cancer almost disappeared, *in vivo*, after 16 days for the group $Ag/TiO_2$ + Photothermal and Near Infrared Light;<br>- *In vivo* and *in vitro* biocompatibility;<br>- The cell survival rate was less than 4% *in vitro*. | Nie et al., 2020 |
| $TiO_2$ and Au-$TiO_2$ /DOX | Breast Cancer Cells / Dawley Prague Rats | Photodynamics (500 nm)/ hydrothermal synthesis | - The Au-$TiO_2$/DOX spreads easily in the vicinity of the tumor;<br>- Loss of viability of cancer cells up to 82% (Au-$TiO_2$/DOX + Photodynamics). | Akram et al., 2019 |
| NTs of TNT–Qu | B16/F10 / C57BL/6 mice and chicken corioalantoic membrane | Two-stage chemical carcinogenesis/ alkaline hydrothermal synthesis and sonication | - Reduced the number of tumors (6 to 1);<br>- Reduced tumor size from 13 mm to 5.9 mm *in vivo*;<br>- Inhibited tumor growth by regulating fopho-TAT3 levels; | Gulla et al., 2022 |

| | | | | |
|---|---|---|---|---|
| | | | - The NTs do not affect the color of the skin;<br>- Increased cell population T γδ to 1.27%, normal skin level. | |
| NCs of Au/$TiO_2$ | Cancer cells C540 (B16/F10) | Photothermal (808 and 650 nm), sonodynamics and hydrothermal synthesis | - Promising stability and excellent efficiency of photothermal conversion and biocompatibility;<br>- Simultaneous irradiation photothermal + sonodynamics/NCs cell viability was <1%;<br>- C540 cells were obliterated. | Perota et al., 2022 |
| TNT electrodeposited with Ag;<br>TNT coated with Ag;<br>TNT doped with Ag. | MCF-7 cells | Exposed to light UV (360–400 nm) | - The negative charge on the surface of TNTs reclaims MCF-7 cells and interferes with growth and proliferation;<br>- Cell cytotoxicity was 97% for Ag-coated TNT;<br>- The reduction of viable cells was 6.5 times more pronounced in Ag-coated TNTs;<br>- Cell viability was <10% nos TNTs coated with Ag. | Zandvakili et al., 2022 |
| NPs of $TiO_2$/PAA-CaP and $TiO_2$/PAA-CaP(DOX) | MCF-7 cells and BEAS-2B cells | Irradiation UV-A (365 nm)/ hydrothermal synthesis | - Increased cellular uptake of NPs $TiO_2$/PAA-CaP(DOX);<br>- Fast cumulative release of DOX on pH= 5,2;<br>- 7% of MCF-7 and 15% of cells BEAS-2B survive at NPs $TiO_2$/PAA-CaP;<br>- The NPs $TiO_2$/PAA-CaP(DOX) exhibited cytotoxicity of ~ 10%;<br>- The viability of MCF-7 cells treated with NPs $TiO_2$/PAA-CaP(DOX) + UV-A was ~ 15%. | Han et al., 2022 |

| | | | | |
|---|---|---|---|---|
| NPs of D-$TiO_2$ | 4T1 / Mice BALB/c | Photodynamics and UV (365 nm) / hydrothermal synthesis | - Reduced cellular viability 54% (200 µCi) *in vitro*;<br>- Excellent biocompatibility;<br>- Cell viability decreased, according to the concentration of D-$TiO_2$;<br>- Exhibited DNA damage;<br>- Tumor volumes, *in vivo*, were significantly inhibited (under 100 $mm^3$). | Duan et al., 2018 |
| Au/$TiO_2$-RBC | MCF-7 | Photothermal (808 nm) and UV (310 nm)/ sonodynamics synthesis and centrifugation | - Viability of the cells was 21% (Au/$TiO_2$-RBC + UV and Near Infrared Light);<br>- Higher levels of ROS;<br>- Au/$TiO_2$-RBC have good stability;<br>- The coating of RBC has reduced the cytotoxicity of the Au/$TiO_2$. | Li and Zhang, 2020 |
| NPs of nitreto $TiO_2$ (2-ethylhexanoic acid and acetonitrile + titanium isopropoxide) and $SiO_2$ | HeLa Cells | Photothermal (808 nm e 785 nm) and UV / Nitrate synthesis | - Kills almost 99% of cells HeLa (50 µg $mL^{-1}$/ temperatures above 60 °C);<br>- Photothermal efficiency coefficient of 58%;<br>- Mass extinction coefficient of 31.6 L $g^{-1}$ $cm^{-1}$;<br>- NPs exhibited increased plasmonic performance and reduced coupling effects. | Gschwend et al., 2019 |
| NTs of $TiO_2$ and zeolytic imidazolate carrying DOX | Neuroblastoma cells | UV (365 nm)/ Anoding overview | - Without DOX, cell viability was 75%, but with DOX decreased to zero (*in vivo*);<br>- UV + NPs (without DOX) had a cell reduction of ~ 25%. | Sharsheeva et al., 2019 |

| | | | | |
|---|---|---|---|---|
| NCs graphene doped with N and $TiO_2$ | MDA-MB-231 and fibroblast singof human foreskin. | Photodynamics and Near Infrare (700–900 nm) / Microwave and hydrothermal | - Increased concentrations of NCs trigger mitochondrial-associated apoptosis in cells MDA-MB-231;<br>- Reduction in cell viability of 29% in MDA-MB-231.<br>- Bandgap energy of the NCs of 1.53 eV. | Ramachandran al., 2022 |
| NPs of $TiO_2$/Ru/siRNA | HN6, HSC-6, and HSC-3 and DOK/ Mice BALB/c-COE and Male Sprague-Dawley Rats | Photodynamics (525 nm) / Microwave synthesis | - It causes photodynamic effects by raising the level of cellular AIS through the pathways dependent on $O_2$ and independent, inducing pyptosis;<br>- Remodels the microenvironment by the negative regulation of immunosuppressants;<br>- Positive regulation of immune cytokines and lymphocyte activation T CD4+ e CD8+;<br>- Tumor weight decreases 10 times in COE;<br>- HN6 is the most sensitive lineage to photodynamics;<br>- Cytotoxicity ($IC_{50}$) of NPs in cells HN6: 0.18 μg $mL^{-1}$ (normoxia) and 0.22 μg $mL^{-1}$ (hypoxia). | Zhou et al., 2022 |
| NPs of $TiO_2$ with collagenase and H-$TiO_2$. | Pancreatic cancer cells/ Mice BALB/C (pancreatic ductal adenocarcinoma xenograft) | Sonodynamics, Dissolution synthesis and network position | - Degrades stromal barriers;<br>- Collagenase released by sonodynamics irradiation degrades the fibers of the tumor matrix, decreases the interstitial fluid, and improves the sign of intratumoral sonodynamics;<br>- Loss of cell viability ~ 50%; | Luo et al., 2022 |

| | | | | |
|---|---|---|---|---|
| | | | - Cellular apoptosis ~ 41%. | |
| NCs of rGO-$CeO_2$/$TiO_2$ and rGO-$TiO_2$/$CeO_2$ | MCF-7 | Treatment with different concentrations /Synthesis core-shell and hydrothermal | - rGO-$CeO_2$/$TiO_2$ had the highest photocatalytic activity;<br>- 92% toxicity in the concentration of 17.5 mg $mL^{-1}$ of rGO-$CeO_2$/$TiO_2$;<br>- Cellular cytotoxicity with $IC_{50}$ of 1.0 mg $mL^{-1}$ (rGO-$CeO_2$/$TiO_2$) and bandgap: 2.03 eV (rGO-$CeO_2$/$TiO_2$). | Malekkiani et al., 2022 |
| NTs CNTs and NPs of de $TiO_2$ | B16/F10 / Female mice consanguineous | Photothermal (808 nm) / Sonication synthesis | - B16/F10 cell destruction *in vivo* was 85% for CNTs and 45% of NPs of $TiO_2$. | Asrar et al., 2022 |
| $TiO_2$ nanowires and Au NPs | HeLa and MCF7 cancer cells | Treatment with different concentrations/ Synthesis pulsed laser ablation | - Cell viability ~ 41% for HeLa and MCF7. | Elsayed et al., 2022 |
| NCs of $TiO_2$ and carbon | Panc02 Cells /Naked Mice BALB/B | Sonodynamics / hydrothermal Synthesis | - Good biocompatibility and no toxicity *in vitro* and *in vivo*;<br>- Loss of cell viability < 50% (10 µg/mL de Ti), *in vitro*;<br>- NCs of $TiO_2$ and carbon + sonodynamics induced apoptosis and necrosis;<br>- Antitumor activity of NCs both *in vitro* and *in vivo*. | Cao et al., 2021 |

List of abbreviations: 4T1 - Murine breast carcinoma cells PEG-$TiO_2$ - Nanoparticles of polyethylene glycol and titanium dioxide UV - Ultraviolet $Fe_3O_4$ - Iron oxide III $H_2O_2$ - Hydrogen peroxide HPT - Hydrogen, platinum and titanium dioxide HPT-DOX - Hydrogen, platinum, titanium dioxide and Doxorubicin DOX - Doxorubicin BT-CTS - Magnesium, B-$TiO_{2x}$ and Chitosan GOx - Glucose oxidase $TiO_2$/$MnO_2$-GOx/C - Glucose oxidase with $TiO_2$, $MnO_2$ and carbon B16/F10 - Metastatic murine melanoma cells $O_2$ - Oxygen Ag/$TiO_2$ - Silver and titanium dioxide Au-$TiO_2$/DOX - Gold, titanium dioxide and Doxorubicin NTs - Nanotubes TNT-Qu - Titanium dioxide with quercetin C540 - Mouse malignant melanoma cell line NCs - Nanocomposites Au/$TiO_2$ - Gold and titanium dioxide Human MCF-7 - Human breast carcinoma cells TNT - Nanotubes of titanium dioxide $TiO_2$/PAA-CaP and $TiO_2$/PAA-CaP(DOX) - Titanium dioxide with poly(acrylic acid)-calcium phosphate and Doxorubicin BEAS-2B - Human non-tumorigenic lung epithelial cells D-$TiO_2$ - Titanium dioxide modified with dextran Au/$TiO_2$-RBC - Red

blood cells encapsulating gold and titanium dioxide $TiO_2$/Ru/siRNA - Titanium dioxide and ruthenium loaded with siRNA (ribonucleic acid) $SiO_2$ - Silicon dioxide HeLa - Human cervical adenocarcinoma cells MDA-MB-231 - Epithelial cells of human breast cancer HN6, HSC-6, and HSC-3 - Human tongue squamous cell carcinoma cells DOK - Oral keratinocyte cells of dysplasia COE - Oral squamous cell carcinoma xenograft H-$TiO_2$ - Hydrogen and titanium dioxide rGO-$CeO_2$/$TiO_2$ and rGO-$TiO_2$/$CeO_2$ - Titanium dioxide, cerium dioxide and graphene oxide IC50 - Half maximal inhibitory concentration Pd/H-$TiO_2$-PEG - Palladium, hydrogen, titanium dioxide and polyethylene glycol C6 - Glioma cells CNTs - Carbon nanotubes.

## 8. Bibliometric overview of $TiO_2$ NPs for cancer treatment

### *8.1. Methodology for literature search and bibliometric analysis*

The bibliometric analysis was conducted based on the methodology described in previous studies (Oliveira et al., 2022; Rosa et al., 2022; Sganzerla et al., 2021; Sganzerla and da Silva, 2022) The systematic literature search and bibliometric analysis were conducted based on the scientific publications indexed in the Science Citation Index Expanded (SCI-E) of Clarivate Analytics' Institute for Scientific Information (ISI). The research in the Web of Science© core collection was conducted in the section “advanced search”. For this, the following logic operation was applied: ("titanium dioxide nanoparticle" OR "$TiO_2$ nanoparticle" OR "titanium dioxide nanoparticles" OR "$TiO_2$ nanoparticles") AND ("cancer" OR "antitumor activity " OR "anticancer activity"). The dataset obtained was exported for VosViewer© software (version 1.6.14) (Van Eck and Waltman, 2010) and Bibliometrix (R language) (Aria and Cuccurullo, 2017) to conduct the bibliometric analysis. The adoption of VOSviewer© and Bibliometrix to perform the bibliometric analysis was chosen based on the advantages generated with the interpretation of the results in both software. For this, maps based on the main keywords and the connections among them were generated by both software. The thematic map was plotted in the Bibliometrix with the most relevant keywords, which were grouped into four quadrants: i) motor, ii) basic, iii) emerging or declining, and iv) niche. Additionally, the number of publications over the years, the research fields category, most important affiliations, countries, authors, and journals were analyzed in the bibliometric study.

### *8.2. Research trends of $TiO_2$ NPs for cancer treatment over 2003 and 2022*

From the systematic search, a total of 734 documents (603 articles and 131 reviews) were obtained between 2003 and 2022. The evolution of the research on $TiO_2$ NPs for cancer treatment can be observed in **Figure 5**. The first study in the

field was published in 2003 (Xian-Ying et al., 2003), where the authors described for the first time that $TiO_2$ NPs inhibited the proliferation of hepatoma cells (Bel-7402) and hepatocytes (L-02). In 2007, water-soluble and biocompatible $TiO_2$ NPs were fabricated by high-temperature nonhydrolytic method and applied as carriers and anticancer medicines (Seo et al., 2007). The hepatoma cells could take within by the process of endocytosis (e.g., the cellular process in which substances are brought into the cell) with the presence of $TiO_2$ NPs (Sheng et al., 2005). In addition, Xu et al. (2007) reported that the combination of electroporation and conjugation of $TiO_2$ NPs with a monoclonal antibody could improve the photokilling selectivity and efficiency of cancer cells in photodynamic therapy. The synthesis and *in vitro* application of $TiO_2$ NPs for cancer treatment was extensively studied until 2012, with a peak in the number of publications in 2011 (Chen et al., 2014; Jiao et al., 2011; Li et al., 2011; Thurn et al., 2011). In 2013, the *in vivo* anticancer activity of $TiO_2$ NPs started to be studied (Venkatasubbu et al., 2013). Chu et al. (2019) explored the effect of $TiO_2$ NPs-induced radical therapy (termed microdynamic therapy). The $TiO_2$ NPs exhibited higher cytotoxicity on osteosarcoma UMR-106 cells than on mouse fibroblast L929 cells, demonstrating their potential for cancer treatment. In addition, Zhao et al. (2018) described that the activation of the immune response induced by $TiO_2$ NPs was correlated with their ability to inhibit cancer metastasis. In the last three years (2020 to 2022), the therapeutic potential of $TiO_2$ NPs has been confirmed (Ikram et al., 2021). A robust adverse outcome pathway with exposure to $TiO_2$ NPs was proposed in the oral and gastrointestinal tract, where colorectal cancer, liver injury, reproductive toxicity, cardiac and kidney damage, and hematological effects stand out as possible adverse outcomes (Rolo et al., 2022).

In addition, the focus of recent years (up to 2022) has been the production of biogenic $TiO_2$ NPs by green synthesis (Sagadevan et al., 2022; Xiaoshang et al., 2021). The application of green synthesis is an environmentally friendly, less expensive and harmless approach to produce $TiO_2$ NPs (Verma et al., 2022). The biological production of $TiO_2$ NPs occurs through the oxidation and reduction process, involving the presence of organic acids, proteins, vitamins, and secondary metabolites for the formation of NPs (Aravind et al., 2021). For this, several plant species were used to produce $TiO_2$ NPs, such as Nyctanthes arbor-tristis (Oelaceae), Psidium guajava (Myrtaceae), Trigonellafoenum – graceum

(Fabaceae), Mentha arvensis (Lamiaceae), Allium eriophyllum (Alliaceae), Eclipta prostrata (Asteraceae), Sesbania grandiflora (Fabaceae), Strychnos spinosa (Loganiaceae), and Blighia sapida (Sapindaceae) (Jassal et al.,2022). Plant-mediated synthesis has been described as the most effective method to produce stable and biocompatible $TiO_2$ NPs for cancer treatment (Chahardoli et al., 2022; Irshad et al., 2020). However, there is a demand for research to synthesize $TiO_2$ NPs by employing green methods, as well as a deep investigation focused on analyzing metabolites present in biological extracts to determine their usefulness toward the synthesis of $TiO_2$ NPs (Irshad et al., 2021).

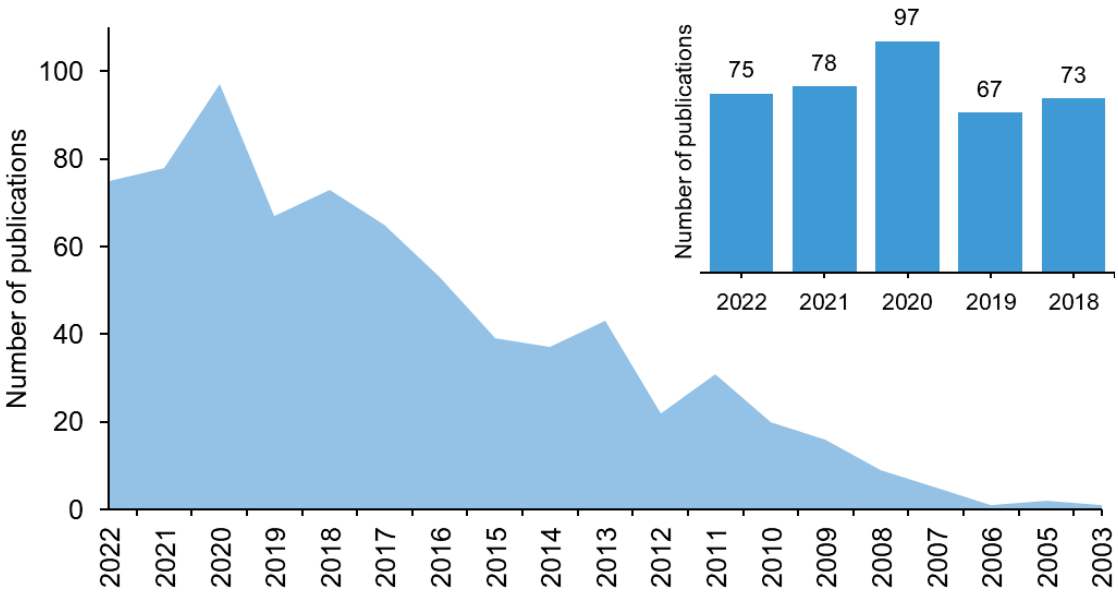


**Figure 5.** Evolution of publications during the period from 2003 to 2022 regarding the application of $TiO_2$NPs for cancer treatment.

### *8.3. Bibliometric analysis of the main keywords*

The bibliometric analysis of the main keywords associated with the studies published on $TiO_2$ NPs for cancer treatment was summarized in **Figure 6**. The main keywords used were *nanoparticles* (91 occurrences), *titanium dioxide* (82 occurrences), *cytotoxicity* (82 occurrences), *titanium dioxide nanoparticles* (42 occurrences), *$TiO_2$ nanoparticles* (41 occurrences), *photodynamic therapy* (39 occurrences), *apoptosis* (37 occurrences), *reactive oxygen species* (33 occurrences), *oxidative stress* (32 occurrences), *sonodynamic therapy* (32 occurrences), and *cancer* (30 occurrences). The high frequencies can indicate the relevance of the keywords in the research field of $TiO_2$ NPs for cancer treatment.

The 50 most frequently used keywords from the 734 documents were selected for the co-occurrence analysis (**Figure 6a**). The keywords were grouped into different clusters, represented in different colors in **Figure 6a**. Blue cluster represents the general aspects in the research field, including studies on nanotechnology and other metals (silver, zinc, and titanium). Green cluster is associated with the oxidative stress, genotoxicity, and DNA damage. Yellow cluster shows the studies on photocatalysis, photodynamic, and sonodynamic therapy. Purple cluster is associated with the inflammation response with the application of $TiO_2$ NPs. Red cluster is associated with the novel aspects of $TiO_2$ NPs, including toxicity, green synthesis, and nanocomposites. As indicated in the network analysis (**Figure 6a** and **6b**), there is an association between the clusters, mainly with the keywords *nanoparticles*, *titanium dioxide*, *$TiO_2$ nanoparticles*, and *photodynamic activity*, demonstrating a significant application of nanotechnology for cancer treatment. The red cluster color focuses on the production and application of nanoparticles, focusing on the toxicity and toxicology of $TiO_2$ NPs. The main research field of red clusters was the green synthesis of $TiO_2$ NPs and nanocomposites for anticancer activity. In addition, the yellow cluster describes the application of $TiO_2$ NPs produced by photocatalysis for photodynamic and sonodynamic therapy. Finally, the green cluster was constituted by specific keywords associating $TiO_2$ NPs with cancer treatment, such as genotoxicity, DNA damage, and oxidative stress.

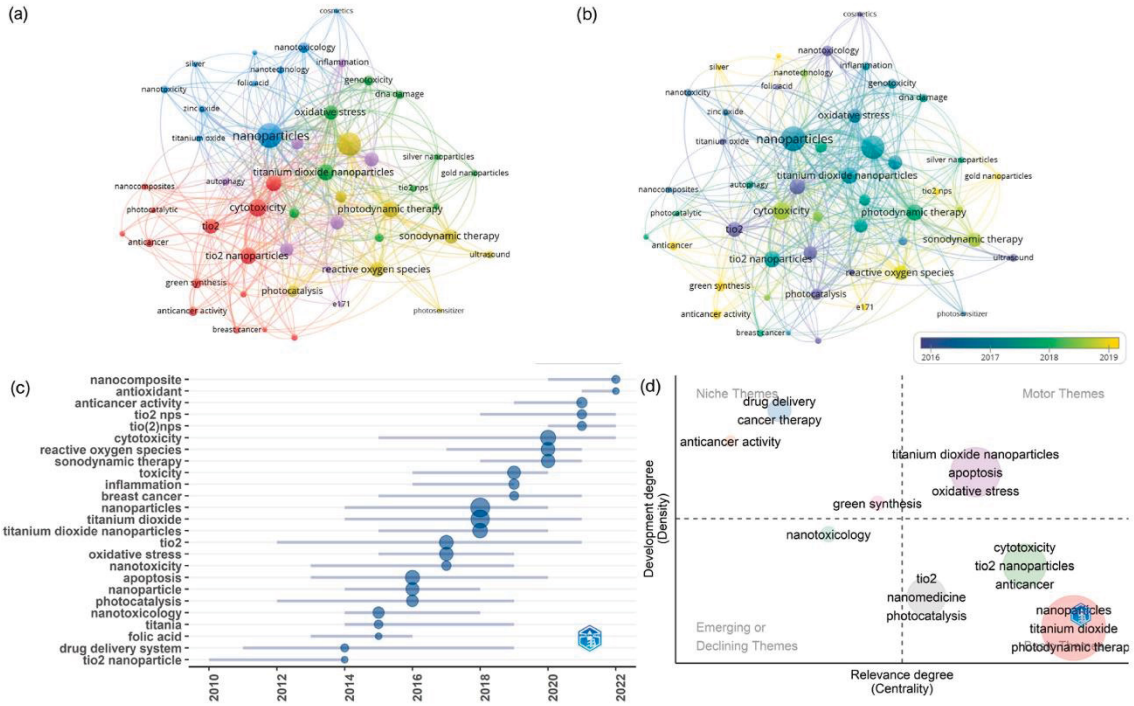


**Figure 6.** Bibliometric analysis of the main keywords. (a) Co-occurrence analysis based on clusters; (b) co-occurrence analysis based on year; (c) trend topics; and (d) thematic map.

Furthermore, the co-occurrence analysis of keywords was plotted over the years (**Figure 6b**). The colors ranging from blue and yellow indicate publications in approximately 2016 and 2019, respectively. The selected timespan (2016 and 2019) was automatically selected by the VOSviewer© software for the analysis of co-occurrence analysis over the years. From this analysis, it can be observed that photocatalysis is one of the first methods applied to produce $TiO_2$ NPs. Between 2017 and 2018, photodynamic therapy started to be applied as a technique for cancer treatment with $TiO_2$ NPs. Since 2019, there has been a trend in the study of anticancer $TiO_2$ NPs by green synthesis, as well as the cytotoxicity of the nanoparticles. This fact demonstrates that further studies should be conducted to elucidate the production of non-toxic nanoparticles as an efficient method for cancer treatment. This fact corroborated the analysis of the trend topics (**Figure 6c**), where the keywords *toxicity*, *cytotoxicity*, *sonodynamic therapy*, *reactive oxygen species*, and *anticancer activity* were the most expressive between 2019 and 2021.

The trend topics presented in **Figure 6c** show the evolution of the main keywords over the years. In 2014, there was a trend in the study of $TiO_2$ NPs and its delivery system. The study of $TiO_2$ NPs evolves to the determination of oxidative stress and toxicity in 2017 and sonodynamic therapy and breast cancer in 2019. Moreover, the production of nanocomposites based on $TiO_2$ NPs has been highlighted as the most trend topic in the field. The production of $TiO_2$ nanocomposites has been elucidated in a few studies (Khan et al., 2022; Roufegarinejad, 2022; Xie et al., 2022); however, the literature about the application of this material for cancer treatment is scarce (Elsayed et al., 2022), demanding further investigation.

The thematic map was plotted to understand better research themes (**Figure 6d**). The motor themes (*$TiO_2$ nanoparticles*, *apoptosis*, and *oxidative stress*) represent well-developed and important keywords. The basic themes are important keywords for basic research, such as *photocatalysis*, *photodynamic therapy*, and *nanomedicine*. The niche theme was highlighted by a cluster composed of the keywords *drug delivery*, *cancer therapy*, and *anticancer activity*, demonstrating that this very specialized theme should be deeply investigated in association with the emerging themes associated with *green synthesis* and *nanotoxicology*.

### *8.4. Bibliometric analysis of the most relevant authors, institutions, countries, and journals*

The most relevant authors, journals, institutions, and countries dedicated to research on $TiO_2$ NPs for cancer treatment between 2003 and 2022 are shown in **Figure 7**. The top 5 most important authors with the respective number of articles published were Wu AG from Chinese Academy of Sciences, China (19 articles), Paunesku T from Northwestern University, Denmark (13 articles), Ogino C from Kobe University, Japan (12 articles), Woloschak GE from Northwestern University, Denmark (12 articles) and Ren WZ from Jilin University, China (9 articles) (**Figure 7a**). The journals most dedicated to publishing $TiO_2$ nanoparticles for cancer treatment were *RSC Advances* (19 documents), *Nanomaterials* (16 documents), *Scientific Reports* (14 documents), *Journal of Materials Chemistry B* (12 documents), and *International Journal of Nanomedicine* (11 documents) (**Figure 7b**). The affiliations with the most number of published articles were the *Chinese*

*Academy of Sciences* (41 documents), *Egyptian Knowledge Bank* (21 documents), *King Saud University* (19 documents), *Fudan University* (18 documents), and *Islamic Azad University* (10 documents) (**Figure 7c**). In addition, China (216 documents), the United States of America (143 documents), India (94 documents), Iran (55 documents), and Japan (47 documents) were the most expressive countries publishing documents in the research field (**Figure 7d**). The **Figure 8** presents a three-field plot (Sankey diagram) relating the authors, authors' keywords, and journals. Based on this visualization, the flow from one set of values to another parameter can be associated with the connection between the items, showing that the keyword *titanium dioxide* was used by all the authors and published mainly in *Nanomaterials*, one of the most expressive journals since presents the highest score and association with the studied keywords. The analysis of the most relevant authors, institutions, countries, and journals contribute to disseminating scientific information regarding the production and application of $TiO_2$ NPs, guiding future international collaboration and scientific impact for publishing future research

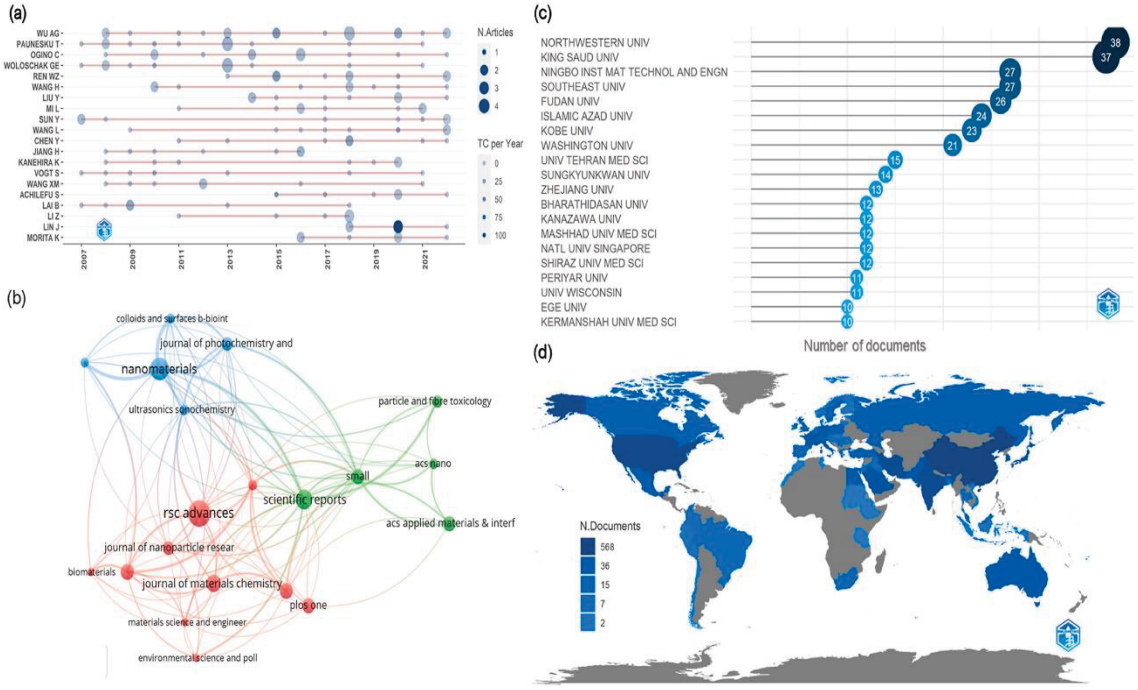


**Figure 7.** Bibliometric analysis of the relevant authors (a), journals (b), institutions (c), and countries (d) dedicated to research on $TiO_2$ NPs for cancer treatment.

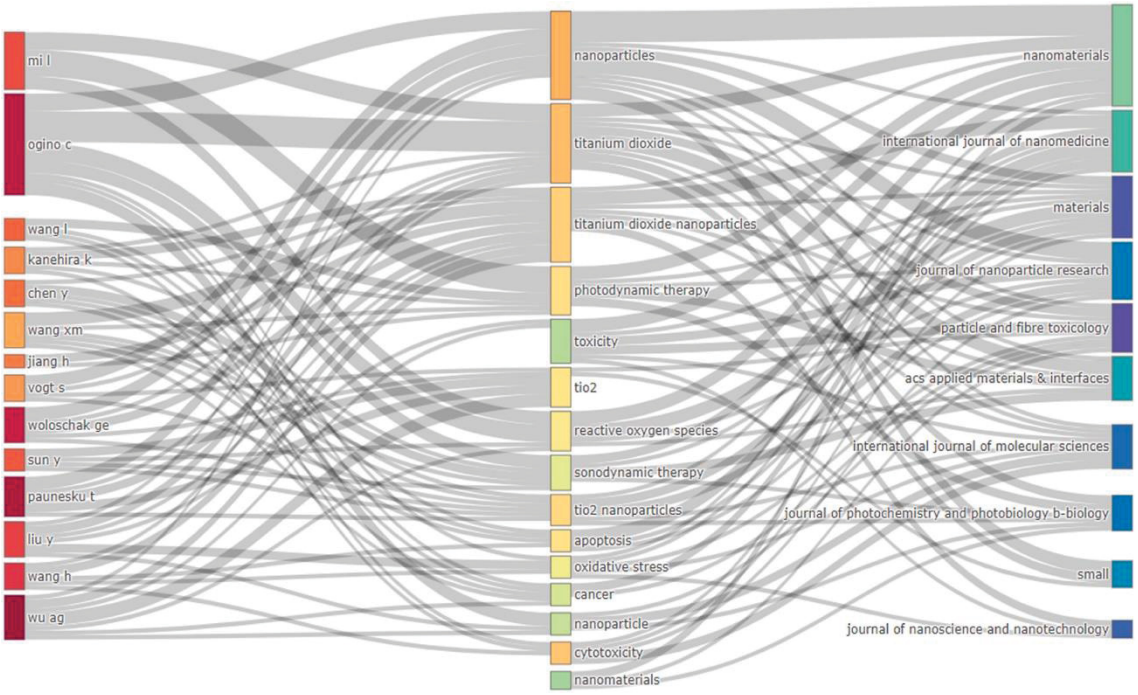


**Figure 8.** Three-field plot of the most important authors, keywords, and journals.

### *8.5. Summary of the most cited articles*

The analysis of the most cited documents is used to better understand knowledge development. The ten most cited documents over the 734 documents published in the field of $TiO_2$ NPs for cancer treatment between 2003 and 2022 were analyzed and discussed. The most cited document, "Titanium dioxide nanoparticles induce DNA damage and genetic instability *in vivo* in mice", was published in *Cancer Research* in 2009. The conclusion was that $TiO_2$ NPs induced genotoxicity *in vivo* in mice was possibly caused by a secondary genotoxic mechanism associated with inflammation and/or oxidative stress (Trouiller et al., 2009). Other highly cited papers studied the production of $TiO_2$ nanoparticles, nanotubes, and composites, such as the second (Zhu et al., 2010) and fifth (Deepagan et al., 2016) most cited papers. Experimental studies related to the application of $TiO_2$ NPs for cancer treatment were ranked in the list of highly cited papers. For instance, the sixth most cited paper (237 citations) described that infrared-irradiated H-$TiO_2$-PEG nanoparticles exhibited low toxicity and high efficiency as photothermal agents for cancer therapy and are promising for further biomedical applications. In addition, studies have focused on the toxicity of $TiO_2$ nanoparticles. The eighth most cited paper (231 citations) showed that low levels of ultraviolet light could induce toxicity of $TiO_2$ NPs to marine phytoplankton.

However, no effect of $TiO_2$ NPs on phytoplankton was obtained in treatments where ultraviolet light was blocked (Miller et al., 2012). Moreover, a one-week intake of $TiO_2$ NPs did not initiate intestinal inflammation. At the same time, a 100-day treatment promoted colon microinflammation and initiated preneoplastic lesions, fostering the growth of aberrant crypt foci in a chemically induced carcinogenesis model (Bettini et al., 2017).

Notwithstanding, several reviews were ranked in the list of the most cited documents. For instance, Fei Yin et al. (2013) reviewed the biomedical applications of $TiO_2$, such as photodynamic therapy for cancer treatment, drug delivery systems, cell imaging, biosensors, and genetic engineering. In addition, Skocaj et al. (2011) reviewed that $TiO_2$ is permitted as an additive in food and pharmaceutical products; however, there are no reliable data on $TiO_2$ NPs absorption, distribution, excretion, and toxicity upon oral exposure. The review "Nanoparticles in biomedical applications" investigated the use of nanosystems, including titanium dioxide, and how their physicochemical properties allow their use in biomedical applications (McNamara and Tofail, 2017). Finally, the progress of biological and biomedical applications of $TiO_2$ in molecular medicine was reviewed (Rajh et al., 2014).

## 9. Conclusion and outlook

Current studies leveraging photothermal, photodynamic, sonodynamic, and near-infrared therapies associated with $TiO_2$ NPs demonstrate significant antitumor efficacy in various cancer cell lines, such as melanoma. The combination of synchronous and synergistic therapies applied to $TiO_2$ NPs further increases their antitumor efficacy. The $TiO_2$ NPs hold promise in how they interact with tumors due to their nanosize and wide light absorption region, reducing side effects on healthy tissues. The addition of metals such as Ag, Au, Pt, and others, the diversification of their structures, and the preparation of distinct morphologies of $TiO_2$ NPs can increase light conversion efficiency and light penetration. The $TiO_2$ NPs have a high surface area that allows for the loading of chemotherapeutic drugs, biomolecules, and other nanomaterials, enabling specific targeting of cancer cells and minimizing the side effects of drugs. This increases the sensitivity, selectivity, and precision of tumor biomarker detection for prevention and treatment. The bibliometric analysis of the main keywords demonstrates that

photocatalysis was one of the first methods applied to produce $TiO_2$ NPs, and nowadays, the production of $TiO_2$ NPs by green synthesis with biological extracts is an efficient method to produce non-toxic materials for cancer treatment. However, despite the expansion of laboratory research on the use of $TiO_2$ NPs, their clinical applicability remains limited, requiring additional research on in vivo response. Industrial production faces obstacles in the manufacturing of $TiO_2$ NPs on a commercial scale, due to reproducibility and stability issues for clinical use, requiring further studies that provide feasible methodologies.

## References


Abdel-Ghany, S., Raslan, S., Tombuloglu, H., Shamseddin, A., Cevik, E., Said, O.A., Madyan, E.F., Senel, M., Bozkurt, A., Rehman, S., Sabit, H., 2020. Vorinostat-loaded titanium oxide nanoparticles (anatase) induce G2/M cell cycle arrest in breast cancer cells via PALB2 upregulation. 3 Biotech 10, 407. https://doi.org/10.1007/s13205-020-02391-2

Abdurahman, R., Yang, C.-X., Yan, X.-P., 2016. Conjugation of a photosensitizer to near infrared light renewable persistent luminescence nanoparticles for photodynamic therapy. Chem commun 52, 13303–13306. https://doi.org/10.1039/C6CC07616E

Ahmad, W., Noor, T., Zeeshan, M., 2017. Effect of synthesis route on catalytic properties and performance of $Co_3O_4/TiO_2$ for carbon monoxide and hydrocarbon oxidation under real engine operating conditions. Catal Commun 89, 19–24. https://doi.org/10.1016/j.catcom.2016.10.012

Aishwarya, S., Sanjay, K.R., 2018. Conjugation study of 5-aminolevulinic acid with microbial synthesized gold nanoparticles to evaluate its effect on skin melanoma and epidermoid carcinoma cell lines using photodynamic cancer therapy. Gold Bull 51, 11–19. https://doi.org/10.1007/s13404-017-0224-x

Ajdary, M., Moosavi, M., Rahmati, M., Falahati, M., Mahboubi, M., Mandegary, A., Jangjoo, S., Mohammadinejad, R., Varma, R., 2018. Health Concerns of Various Nanoparticles: A Review of Their *in Vitro* and *in Vivo* Toxicity. Nanomaterials 8, 634. https://doi.org/10.3390/nano8090634

Akram, M.W., Raziq, F., Fakhar-e-Alam, M., Aziz, M.H., Alimgeer, K.S., Atif, M., Amir, M., Hanif, A., Aslam Farooq, W., 2019. Tailoring of Au-$TiO_2$ nanoparticles conjugated with doxorubicin for their synergistic response and photodynamic therapy applications. J Photochem Photobiol A Chem 384, 112040. https://doi.org/10.1016/j.jphotochem.2019.112040

Ali, I., Suhail, M., Alothman, Z.A., Alwarthan, A., 2018. Recent advances in syntheses, properties and applications of $TiO_2$ nanostructures. RSC Adv 8, 30125–30147. https://doi.org/10.1039/C8RA06517A

American Cancer Society., 2022. Cancer facts and figures 2022. American cancer society. 80.

American Cancer Society: Cancer Facts & Figures 2023. Atlanta, American Cancer Society, 84.

Anju, K.R., Thankapan, R., Rajabathar, J.R., Al-Lohedan, H.A., 2018. Hydrothermal synthesis of nanosized (Fe, Co, Ni)-$TiO_2$ for enhanced visible

light photosensitive applications. Optik (Stuttg) 165, 408–415. https://doi.org/10.1016/j.ijleo.2018.03.091

Anjum, S., Ishaque, S., Fatima, H., Farooq, W., Hano, C., Abbasi, B.H., Anjum, I., 2021. Emerging Applications of Nanotechnology in Healthcare Systems: Grand Challenges and Perspectives. Pharmaceuticals 14, 707. https://doi.org/10.3390/ph14080707

Aravind, M., Amalanathan, M., Mary, M. S. M., 2021. Synthesis of $TiO_2$ nanoparticles by chemical and green synthesis methods and their multifaceted properties. SN Applied Sciences, 3, 1-10. https://doi.org/10.1007/s42452-021-04281-5

Aria, M., Cuccurullo, C., 2017. Bibliometrix: An R-tool for comprehensive science mapping analysis. J Informetr 11, 959–975. https://doi.org/10.1016/J.JOI.2017.08.007

Asrar, A., Sobhani, Z., Behnam, M.A., 2022. Melanoma Cancer Therapy Using PEGylated Nanoparticles and Semiconductor Laser. Adv Pharm Bull 12, 524–530. https://doi.org/10.34172/apb.2022.055

Azaïs, H., Mordon, S., Collinet, P., 2017. Traitement des métastases péritonéales des cancers épithéliaux de l'ovaire par thérapie photodynamique. Limites et perspectives. Gynecol Obstet Fertil Senol 45, 249–256. https://doi.org/10.1016/j.gofs.2017.02.005

Azimee, S., Rahmati, M., Fahimi, H., Moosavi, M.A., 2020. $TiO_2$ nanoparticles enhance the chemotherapeutic effects of 5-fluorouracil in human AGS gastric cancer cells via autophagy blockade. Life Sci 248, 117466. https://doi.org/10.1016/j.lfs.2020.117466

Azulay, R.D., Azulay, D.R., Azulay-Abulafia, L., 2017. Dermatologia, 7. ed. Guanabara Koogan, Rio de Janeiro.

Baneshi, M., Dadfarnia, S., Shabani, A.M.H., Sabbagh, S.K., Haghgoo, S., Bardania, H., 2019. A novel theranostic system of AS1411 aptamer-functionalized albumin nanoparticles loaded on iron oxide and gold nanoparticles for doxorubicin delivery. Int J Pharm 564, 145–152. https://doi.org/10.1016/J.IJPHARM.2019.04.025

Basit, M.A., Raza, F., Ali, G., Parveen, A., Khan, M., Park, T.J., 2022. Nanoscale modification of carbon fibers with CdS quantum-dot sensitized $TiO_2$: Photocatalytic and photothermal evaluation under visible irradiation. Mater Sci Semicond Process 142, 106485. https://doi.org/10.1016/J.MSSP.2022.106485

Behnam, M.A., Emami, F., Sobhani, Z., Dehghanian, A.R., 2018. The application of titanium dioxide ($TiO_2$) nanoparticles in the photo-thermal therapy of melanoma cancer model. Iran J Basic Med Sci 21, 1133–1139. https://doi.org/10.22038/ijbms.2018.30284.7304

Behzadi, S., Serpooshan, V., Tao, W., Hamaly, M.A., Alkawareek, M.Y., Dreaden, E.C., Brown, D., Alkilany, A.M., Farokhzad, O.C., Mahmoudi, M., 2017. Cellular uptake of nanoparticles: journey inside the cell. Chem Soc Rev 46, 4218–4244. https://doi.org/10.1039/C6CS00636A

Bertoni, P. M. V., 2014. Obtainment of porous ceramic objects of $TiO_2$ for usage as biomaterials. Dissertation (Master in Materials Science and Engineering) – Institute of Science and Technology, Federal University of Alfenas, Poços de Caldas/MG. https://bdtd.unifal-mg.edu.br:8443/handle/tede/638 (accessed 15 august 22)

Bet-Moushoul, E., Mansourpanah, Y., Farhadi, K., Tabatabaei, M., 2016. $TiO_2$ nanocomposite based polymeric membranes: A review on performance improvement for various applications in chemical engineering processes. Chem Eng J 283, 29–46. https://doi.org/10.1016/J.CEJ.2015.06.124

Bettini, S., Boutet-Robinet, E., Cartier, C., Coméra, C., Gaultier, E., Dupuy, J., Naud, N., Taché, S., Grysan, P., Reguer, S., Thieriet, N., Réfrégiers, M., Thiaudière, D., Cravedi, J.-P., Carrière, M., Audinot, J.-N., Pierre, F.H., Guzylack-Piriou, L., Houdeau, E., 2017. Food-grade $TiO_2$ impairs intestinal and systemic immune homeostasis, initiates preneoplastic lesions and promotes aberrant crypt development in the rat colon. Sci Rep 7, 40373. https://doi.org/10.1038/srep40373

Boningari, T., Inturi, S.N.R., Suidan, M., Smirniotis, P.G., 2018. Novel continuous single-step synthesis of nitrogen-modified $TiO_2$ by flame spray pyrolysis for photocatalytic degradation of phenol in visible light. J Mater Sci Technol 34, 1494–1502. https://doi.org/10.1016/J.JMST.2018.04.014

Bray, F., Ferlay, J., Soerjomataram, I., Siegel, R.L., Torre, L.A., Jemal, A., 2018. Global cancer statistics 2018: GLOBOCAN estimates of incidence and mortality worldwide for 36 cancers in 185 countries. CA Cancer J Clin 68, 394–424. https://doi.org/10.3322/caac.21492

Bray, F., Laversanne, M., Weiderpass, E., Soerjomataram, I., 2021. The ever-increasing importance of cancer as a leading cause of premature death worldwide. Cancer 127, 3029–3030. https://doi.org/10.1002/cncr.33587

Callahan, M.K., Flaherty, C.R., Postow, M.A., 2016. Checkpoint Blockade for the Treatment of Advanced Melanoma. pp. 231–250. https://doi.org/10.1007/978-3-319-22539-5_9

Cao, J., Sun, Y., Zhang, C., Wang, X., Zeng, Y., Zhang, T., Huang, P., 2021. Tablet-like $TiO_2$/C nanocomposites for repeated type I sonodynamic therapy of pancreatic cancer. Acta Biomater 129, 269–279. https://doi.org/10.1016/J.ACTBIO.2021.05.029

Caputo, F., de Nicola, M., Sienkiewicz, A., Giovanetti, A., Bejarano, I., Licoccia, S., Traversa, E., Ghibelli, L., 2015. Cerium oxide nanoparticles, combining antioxidant and UV shielding properties, prevent UV-induced cell damage and mutagenesis. Nanoscale 7, 15643–15656. https://doi.org/10.1039/C5NR03767K

Castano, A.P., Demidova, T.N., Hamblin, M.R., 2005. Mechanisms in photodynamic therapy: part two—cellular signaling, cell metabolism and modes of cell death. Photodiagnosis Photodyn Ther 2, 1–23. https://doi.org/10.1016/S1572-1000(05)00030-X

Castano, A.P., Mroz, P., Hamblin, M.R., 2006. Photodynamic therapy and anti-tumour immunity. Nat Rev Cancer 6, 535–545. https://doi.org/10.1038/nrc1894

Cavarsan, F., 2014. Epidemiologia do melanoma no Brasil., in: Wainstein A, B.F. (Ed.), Melanoma: Prevenção, Diagnóstico, Tratamento e Acompanhamento. Atheneu, São Paulo, pp. 11–22.

Cazes, A., Ronai, Z.A., 2016. Metabolism in melanoma metastasis. Pigment Cell Melanoma Res 29, 118–119. https://doi.org/10.1111/pcmr.12440

Cengel, K.A., Glatstein, E., Hahn, S.M., 2007. Intraperitoneal Photodynamic Therapy, in: Peritoneal Carcinomatosis. Springer US, Boston, MA, pp. 493–514. https://doi.org/10.1007/978-0-387-48993-3_34

Chahardoli, A., Hosseinzadeh, L., Shokoohinia, Y., Fattahi, A., 2022. Production of rutile titanium dioxide nanoparticles by trans-ferulic acid and their biomedical applications. Mater Today Commun 33, 104305. https://doi.org/10.1016/j.mtcomm.2022.104305

Chen, C., Xie, H., He, P., Liu, X., Yang, C., Wang, N., Ge, C., 2022. Comparison of low-temperature catalytic activity and $H_2O/SO_2$ resistance of the Ce-Mn/$TiO_2$ $NH_3$-SCR catalysts prepared by the reverse co-precipitation, co-precipitation and impregnation method. Appl Surf Sci 571, 151285. https://doi.org/10.1016/J.APSUSC.2021.151285

Chen, F., Liu, Q., Xiong, Y., Xu, L., 2021. Current Strategies and Potential Prospects of Nanomedicine-Mediated Therapy in Inflammatory Bowel Disease. Int J Nanomedicine Volume 16, 4225–4237. https://doi.org/10.2147/IJN.S310952

Chen, Q., Liang, C., Sun, X., Chen, J., Yang, Z., Zhao, H., Feng, L., Liu, Z., 2017. $H_2O_2$-responsive liposomal nanoprobe for photoacoustic inflammation imaging and tumor theranostics via *in vivo* chromogenic assay. Proc Natl Acad Sci U S A 114. https://doi.org/10.1073/pnas.1701976114

Chen, T., Yan, J., Li, Y., 2014. Genotoxicity of titanium dioxide nanoparticles. J Food Drug Anal 22, 95–104. https://doi.org/10.1016/j.jfda.2014.01.008

Chen, Y.S., Huang, T.H., Liu, C.L., Chen, H.S., Lee, M.H., Chen, H.W., Shen, C.R., 2019. Locally targeting the IL-17/IL-17RA axis reduced tumor growth in a Murine B16F10 melanoma model. Hum Gene Ther 30. https://doi.org/10.1089/hum.2018.104

Cheng, J., Song, L., Wu, R., Li, S., Sun, Y., Zhu, H., Qiu, W., He, H., 2020. Promoting effect of microwave irradiation on $CeO_2$-$TiO_2$ catalyst for selective catalytic reduction of NO by $NH_3$. J Rare Earths 38, 59–69. https://doi.org/10.1016/J.JRE.2019.04.014

Chiang, C.-L., Cheng, M.-H., Lin, C.-H., 2021. From Nanoparticles to Cancer Nanomedicine: Old Problems with New Solutions. Nanomaterials 11, 1727. https://doi.org/10.3390/nano11071727

Chu, D., Dong, X., Shi, X., Zhang, C., Wang, Z., 2018. Neutrophil-Based Drug Delivery Systems. Adv Mater 30, 1706245. https://doi.org/10.1002/adma.201706245

Chu, X., Mao, L., Johnson, O., Li, K., Phan, J., Yin, Q., Li, L., Zhang, J., Chen, W., Zhang, Y., 2019. Exploration of $TiO_2$ nanoparticle mediated microdynamic therapy on cancer treatment. Nanomedicine 18, 272–281. https://doi.org/10.1016/j.nano.2019.02.016

Dai, C., Zhang, S., Liu, Z., Wu, R., Chen, Y., 2017. Two-Dimensional Graphene Augments Nanosonosensitized Sonocatalytic Tumor Eradication. ACS Nano 11, 9467–9480. https://doi.org/10.1021/acsnano.7b05215

Davalli, P., Mitic, T., Caporali, A., Lauriola, A., D'Arca, D., 2016. ROS, Cell Senescence, and Novel Molecular Mechanisms in Aging and Age-Related Diseases. Oxid Med Cell Longev 2016, 1–18. https://doi.org/10.1155/2016/3565127

De Angelis, I., Barone, F., Zijno, A., Bizzarri, L., Russo, M.T., Pozzi, R., Franchini, F., Giudetti, G., Uboldi, C., Ponti, J., Rossi, F., de Berardis, B., 2013. Comparative study of ZnO and $TiO_2$ nanoparticles: physicochemical characterisation and toxicological effects on human colon carcinoma cells. Nanotoxicology 7, 1361–1372. https://doi.org/10.3109/17435390.2012.741724

De Paula, R. F. D. O., 2019. Study on the effect of phototermic therapy associated with nanoparticles on the development of melanoma murine. Thesis (Doctorate in Genetics and Molecular Biology) - Institute of Biology, State University of Campinas, Campinas.

Deepagan, V.G., You, D.G., Um, W., Ko, H., Kwon, S., Choi, K.Y., Yi, G.-R., Lee, J.Y., Lee, D.S., Kim, K., Kwon, I.C., Park, J.H., 2016. Long-Circulating Au-$TiO_2$ Nanocomposite as a Sonosensitizer for ROS-Mediated Eradication of Cancer. Nano Lett 16, 6257–6264. https://doi.org/10.1021/acs.nanolett.6b02547

Denat, L., Kadekaro, A.L., Marrot, L., Leachman, S.A., Abdel-Malek, Z.A., 2014. Melanocytes as Instigators and Victims of Oxidative Stress. J Invest Dermatol 134, 1512–1518. https://doi.org/10.1038/JID.2014.65

Di Paola, A., Bellardita, M., Palmisano, L., 2013. Brookite, the Least Known $TiO_2$ Photocatalyst. Catalysts 3, 36–73. https://doi.org/10.3390/catal3010036

Di Virgilio, F., Adinolfi, E., 2017. Extracellular purines, purinergic receptors and tumor growth. Oncogene 36, 293–303. https://doi.org/10.1038/onc.2016.206

Diamantopoulou, A., Sakellis, E., Romanos, G.E., Gardelis, S., Ioannidis, N., Boukos, N., Falaras, P., Likodimos, V., 2019. Titania photonic crystal photocatalysts functionalized by graphene oxide nanocolloids. Appl Catal B 240, 277–290. https://doi.org/10.1016/J.APCATB.2018.08.080

Domingues, B., Lopes, J., Soares, P., Populo, H., 2018. Melanoma treatment in review. Immunotargets Ther Volume 7, 35–49. https://doi.org/10.2147/ITT.S134842

Duan, D., Liu, H., Xu, Y., Han, Y., Xu, M., Zhang, Z., Liu, Z., 2018. Activating $TiO_2$ Nanoparticles: Gallium-68 Serves as a High-Yield Photon Emitter for Cerenkov-Induced Photodynamic Therapy. ACS Appl Mater Interfaces 10, 5278–5286. https://doi.org/10.1021/acsami.7b17902

Egbuna, C., Parmar, V.K., Jeevanandam, J., Ezzat, S.M., Patrick-Iwuanyanwu, K.C., Adetunji, C.O., Khan, J., Onyeike, E.N., Uche, C.Z., Akram, M., Ibrahim, M.S., el Mahdy, N.M., Awuchi, C.G., Saravanan, K., Tijjani, H., Odoh, U.E., Messaoudi, M., Ifemeje, J.C., Olisah, M.C., Ezeofor, N.J., Chikwendu, C.J., Ibeabuchi, C.G., 2021. Toxicity of Nanoparticles in Biomedical Application: Nanotoxicology. J Toxicol 2021, 1–21. https://doi.org/10.1155/2021/9954443

Elsayed, K.A., Alomari, M., Drmosh, Q.A., Manda, A.A., Haladu, S.A., Olanrewaju Alade, I., 2022. Anticancer Activity of $TiO_2$/Au Nanocomposite Prepared by Laser Ablation Technique on Breast and Cervical Cancers. Opt Laser Technol 149, 107828. https://doi.org/10.1016/J.OPTLASTEC.2021.107828

Fakhar-e-Alam, M., Aqrab-ul-Ahmad, Atif, M., Alimgeer, K.S., Suleman Rana, M., Yaqub, N., Aslam Farooq, W., Ahmad, H., 2020. Synergistic effect of TEMPO-coated $TiO_2$ nanorods for PDT applications in MCF-7 cell line model. Saudi J Biol Sci 27, 3199–3207. https://doi.org/10.1016/J.SJBS.2020.09.027

Fatima, S., Ali, K., Ahmed, B., al Kheraif, A.A., Syed, A., Elgorban, A.M., Musarrat, J., Lee, J., 2021. Titanium Dioxide Nanoparticles Induce Inhibitory Effects against Planktonic Cells and Biofilms of Human Oral Cavity Isolates of Rothia mucilaginosa, Georgenia sp. and Staphylococcus saprophyticus. Pharmaceutics 13, 1564. https://doi.org/10.3390/pharmaceutics13101564

Fei Yin, Z., Wu, L., Gui Yang, H., Hua Su, Y., 2013. Recent progress in biomedical applications of titanium dioxide. Phys Chem Chem Phys 15, 4844. https://doi.org/10.1039/c3cp43938k

Ferlay, J., Colombet, M., Soerjomataram, I., Parkin, D. M., Piñeros, M., Znaor, A., Bray, F., 2021. Cancer statistics for the year 2020: an overview. Int J Cancer, New York *149*, 778-789. https://doi.org/10.1002/ijc.33588

Fernandes, M.C. dos S., 2015. Titanium dioxide and biosilicate scaffolds prepared with organic particles for medical and dental applications. (Doctorate in Materials Science and Engineering). Federal University of São Carlos, São Carlos. https://repositorio.ufscar.br/handle/ufscar/7568 (Accessed 17 august 22)

Ferrari, M. 2005. Cancer nanotechnology: opportunities and challenges. Nature Rev Cancer 5, 161-171. https://doi.org/10.1038/nrc1566

Filippi, C., Pryde, A., Cowan, P., Lee, T., Hayes, P., Donaldson, K., Plevris, J., Stone, V., 2015. Toxicology of ZnO and $TiO_2$ nanoparticles on hepatocytes: Impact on metabolism and bioenergetics. Nanotoxicology 9, 126–134. https://doi.org/10.3109/17435390.2014.895437

Fouad, Y. A., Aanei, C., 2017. Revisiting the hallmarks of cancer. Am J Cancer Res 7, 1016–1036. https://pubmed.ncbi.nlm.nih.gov/28560055/ (Accessed 18 august 22)

Fujishima, A., Honda, K., 1972. Electrochemical Photolysis of Water at a Semiconductor Electrode. Nature 238, 37–38. https://doi.org/10.1038/238037a0

Galata, E., Georgakopoulou, E.A., Kassalia, M.-E., Papadopoulou-Fermeli, N., Pavlatou, E.A., 2019. Development of Smart Composites Based on Doped-$TiO_2$ Nanoparticles with Visible Light Anticancer Properties. Materials 12, 2589. https://doi.org/10.3390/ma12162589

Gambogi, J., 2021. Titanium mineral concentrates [WWW Document]. U.S. Geological Survey, Mineral Commodity Summaries. URL https://pubs.usgs.gov/periodicals/mcs2021/mcs2021-titanium-minerals.pdf (accessed 12 august 22).

Gangopadhyay, M., Mukhopadhyay, S.K., Karthik, S., Barman, S., Pradeep Singh, N.D., 2015. Targeted photoresponsive $TiO_2$–coumarin nanoconjugate for efficient combination therapy in MDA-MB-231 breast cancer cells: synergic effect of photodynamic therapy (PDT) and anticancer drug chlorambucil. Medchemcomm 6, 769–777. https://doi.org/10.1039/C4MD00481G

Gao, F., He, G., Yin, H., Chen, J., Liu, Y., Lan, C., Zhang, S., Yang, B., 2019. Titania-coated 2D gold nanoplates as nanoagents for synergistic photothermal/sonodynamic therapy in the second near-infrared window. Nanoscale 11, 2374–2384. https://doi.org/10.1039/C8NR07188H

Gao, K., Tu, W., Yu, X., Ahmad, F., Zhang, X., Wu, W., An, X., Chen, X., Li, W., 2019. W-doped $TiO_2$ nanoparticles with strong absorption in the NIR-II window for photoacoustic/CT dual-modal imaging and synergistic thermoradiotherapy of tumors. Theranostics 9, 5214–5226. https://doi.org/10.7150/thno.33574

Gao, L., Liu, R., Gao, F., Wang, Y., Jiang, X., Gao, X., 2014. Plasmon-Mediated Generation of Reactive Oxygen Species from Near-Infrared Light Excited Gold Nanocages for Photodynamic Therapy *in Vitro*. ACS Nano 8, 7260–7271. https://doi.org/10.1021/nn502325j

Gao, Y., Zhang, Luyun, Liu, Y., Sun, S., Yin, Z., Zhang, Lili, Li, A., Lu, G., Wu, A., Zeng, L., 2020. $Ce_6/Mn^{2+}$-chelated polydopamine@black-$TiO_2$ nanoprobes for enhanced synergistic phototherapy and magnetic resonance imaging in 4T1 breast cancer. Nanoscale 12, 1801–1810. https://doi.org/10.1039/C9NR09236F

Gázquez, M.J., Bolívar, J.P., Garcia-Tenorio, R., Vaca, F., 2014. A Review of the Production Cycle of Titanium Dioxide Pigment. Materials Sciences and Applications 05, 441–458. https://doi.org/10.4236/msa.2014.57048

Geiser, M., Casaulta, M., Kupferschmid, B., Schulz, H., Semmler-Behnke, M., Kreyling, W., 2008. The Role of Macrophages in the Clearance of Inhaled Ultrafine Titanium Dioxide Particles. Am J Respir Cell Mol Biol 38, 371–376. https://doi.org/10.1165/rcmb.2007-0138OC

Gorgizadeh, M., Azarpira, N., Lotfi, M., Daneshvar, F., Salehi, F., Sattarahmady, N., 2019. Sonodynamic cancer therapy by a nickel ferrite/carbon nanocomposite on melanoma tumor: *In vitro* and *in vivo* studies. Photodiagnosis Photodyn Ther 27, 27–33. https://doi.org/10.1016/J.PDPDT.2019.05.023

Grecco, C., Vollet-Filho, J.D., Carvalho, M.T., Bagnato, V.S., 2015. Physics of lasers and LEDs, in: Lasers in Dentistry. John Wiley & Sons, Inc, Hoboken, NJ, pp. 1–10. https://doi.org/10.1002/9781118987742.ch1

Grilli, M.L., Sytchkova, A., Mancini, M.R., Zurlo, F., Hu, G., di Bartolomeo, E., Piegari, A., 2016. Optical and Electrical Properties of $TiO_2$ Based Transparent Conductive Films and Multilayer Systems Fabricated by Radio Frequency Sputtering and E-Beam Evaporation, in: 18th Italian National Conference on Photonic Technologies (Fotonica 2016). Institution of Engineering and Technology, pp. 95 (4.)-95 (4.). https://doi.org/10.1049/cp.2016.0955

Grivennikov, S.I., Greten, F.R., Karin, M., 2010. Immunity, Inflammation, and Cancer. Cell 140, 883–899. https://doi.org/10.1016/J.CELL.2010.01.025

Gschwend, P.M., Conti, S., Kaech, A., Maake, C., Pratsinis, S.E., 2019. Silica-Coated TiN Particles for Killing Cancer Cells. ACS Appl Mater Interfaces 11, 22550–22560. https://doi.org/10.1021/acsami.9b07239

Gulla, S., Reddy, V.C., Araveti, P.B., Lomada, D., Srivastava, A., Reddy, M.C., Reddy, K.R., 2022. Synthesis of titanium dioxide nanotubes (TNT) conjugated with quercetin and its *in vivo* antitumor activity against skin cancer. J Mol Struct 1249, 131556. https://doi.org/10.1016/J.MOLSTRUC.2021.131556

Halwani, R., Sultana Shaik, A., Ratemi, E., Afzal, S., Kenana, R., Al-Muhsen, S., al Faraj, A., 2016. A novel anti-IL4Rα nanoparticle efficiently controls lung inflammation during asthma. Exp Mol Med 48, e262–e262. https://doi.org/10.1038/emm.2016.89

Hambright, H.G., Meng, P., Kumar, A.P., Ghosh, R., 2015. Inhibition of PI3K/AKT/mTOR axis disrupts oxidative stress-mediated survival of melanoma cells. Oncotarget 6, 7195–7208. https://doi.org/10.18632/oncotarget.3131

Han, J., Jang, E.K., Ki, M.R., Son, R.G., Kim, S., Choe, Y., Pack, S.P., Chung, S., 2022. pH-responsive phototherapeutic poly(acrylic acid)-calcium phosphate passivated $TiO_2$ nanoparticle-based drug delivery system for cancer treatment applications. J Ind Eng Chem 112, 258–270. https://doi.org/10.1016/J.JIEC.2022.05.019

Han, X., Huang, J., Jing, X., Yang, D., Lin, H., Wang, Z., Li, P., Chen, Y., 2018. Oxygen-Deficient Black Titania for Synergistic/Enhanced Sonodynamic and Photoinduced Cancer Therapy at Near Infrared-II Biowindow. ACS Nano 12, 4545–4555. https://doi.org/10.1021/acsnano.8b00899

He, L., Mao, C., Brasino, M., Harguindey, A., Park, W., Goodwin, A.P., Cha, J.N., 2018. $TiO_2$ - Capped Gold Nanorods for Plasmon-Enhanced Production of Reactive Oxygen Species and Photothermal Delivery of Chemotherapeutic

Agents. ACS Appl Mater Interfaces 10, 27965–27971. https://doi.org/10.1021/acsami.8b08868

Herrmann, J. M., 1999. Heterogeneous photocatalysis: fundamentals and applications to the removal of various types of aqueous pollutants. Catal Today, 53, 115-129. https://doi.org/10.1016/S0920-5861(99)00107-8

Hidaka, H., Horikoshi, S., Serpone, N., Knowland, J., 1997. *In vitro* photochemical damage to DNA, RNA and their bases by an inorganic sunscreen agent on exposure to UVA and UVB radiation. J Photochem Photobiol A Chem 111, 205–213. https://doi.org/10.1016/S1010-6030(97)00229-3

Hu, J.-J., Cheng, Y.-J., Zhang, X.-Z., 2018. Recent advances in nanomaterials for enhanced photothermal therapy of tumors. Nanoscale 10, 22657–22672. https://doi.org/10.1039/C8NR07627H

Huilan, Z., Juan, W., Wen, Z., Dong, H., Aiping, Z., 2021. $TiO_2$/$SiO_2$-NHOC-FA Nanocomposite as a Photosensitizer with Targeting Ability for Photocatalytic Killing MCF-7 Cells *in Vitro* and its Mechanism Exploration. Photochem Photobiol 97. https://doi.org/10.1111/php.13336

Ikram, M., Javed, B., Hassan, S.W.U., Satti, S.H., Sarwer, A., Raja, N.I., Mashwani, Z.-R., 2021. Therapeutic potential of biogenic titanium dioxide nanoparticles: a review on mechanistic approaches. Nanomedicine 16, 1429–1446. https://doi.org/10.2217/nnm-2021-0020

INCA. Instituto Nacional de Câncer José Alencar Gomes da Silva, 2019. Tipos de câncer. [WWW Document]. Inca. URL https://www.inca.gov.br/tipos-de-cancer. (accessed 13 march 22).

INCA. Instituto Nacional de Câncer José Alencar Gomes da Silva, 2022. O que é câncer?. [WWW Document]. Inca. URL https://www.gov.br/inca/pt-br/assuntos/cancer/o-que-e-cancer (accessed 25 march 23).

INCA. Instituto Nacional de Câncer José Alencar Gomes da Silva, 2023. Cancer Incidence in Brazil [WWW Document]. Inca. URL https://www.inca.gov.br/sites/ufu.sti.inca.local/files//media/document//estimativa-2023.pdf (accessed 25 march 23).

IARC. International Agency for Research on Cancer, 2023. Global Cancer Observatory. Cancer Tomorrow [WWW Document]. IARC. URLhttps://gco.iarc.fr/tomorrow/en (accessed 25 march 23).

Irajirad, R., Ahmadi, A., Najafabad, B.K., Abed, Z., Sheervalilou, R., Khoei, S., Shiran, M.B., Ghaznavi, H., Shakeri-Zadeh, A., 2019. Combined thermo-chemotherapy of cancer using 1 MHz ultrasound waves and a cisplatin-loaded sonosensitizing nanoplatform: an *in vivo* study. Cancer Chemother Pharmacol 84, 1315–1321. https://doi.org/10.1007/s00280-019-03961-9

Irshad, M.A., Nawaz, R., Rehman, M.Z. ur, Adrees, M., Rizwan, M., Ali, S., Ahmad, S., Tasleem, S., 2021. Synthesis, characterization and advanced sustainable applications of titanium dioxide nanoparticles: A review. Ecotoxicol Environ Saf 212, 111978. https://doi.org/10.1016/J.ECOENV.2021.111978

Irshad, M.A., Nawaz, R., Zia ur Rehman, M., Imran, M., Ahmad, J., Ahmad, S., Inam, A., Razzaq, A., Rizwan, M., Ali, S., 2020. Synthesis and characterization of titanium dioxide nanoparticles by chemical and green methods and their antifungal activities against wheat rust. Chemosphere 258, 127352. https://doi.org/10.1016/j.chemosphere.2020.127352

Ismail, A.A., Bahnemann, D.W., 2011. Mesostructured Pt/$TiO_2$ Nanocomposites as Highly Active Photocatalysts for the Photooxidation of Dichloroacetic Acid. J Phys Chem C 115, 5784–5791. https://doi.org/10.1021/jp110959b

Jafari, S., Mahyad, B., Hashemzadeh, H., Janfaza, S., Gholikhani, T., Tayebi, L., 2020. Biomedical Applications of $TiO_2$ Nanostructures: Recent Advances. Int J Nanomedicine 15, 3447–3470. https://doi.org/10.2147/IJN.S249441

Jassal, P. S., Kaur, D., Prasad, R., Singh, J., 2022. Green synthesis of titanium dioxide nanoparticles: Development and applications. J of Agriculture and Food Research, 100361. https://doi.org/10.1016/j.jafr.2022.100361

Jenkins, N.C., Liu, T., Cassidy, P., Leachman, S.A., Boucher, K.M., Goodson, A.G., Samadashwily, G., Grossman, D., 2011. The p16INK4A tumor suppressor regulates cellular oxidative stress. Oncogene 30, 265–274. https://doi.org/10.1038/onc.2010.419

Jiao, Z., Chen, Y., Wan, Y., Zhang, H., 2011. Anticancer efficacy enhancement and attenuation of side effects of doxorubicin with titanium dioxide nanoparticles. Int J Nanomedicine 2321. https://doi.org/10.2147/IJN.S25460

Junqueira, L.C.; Carneiro, J.; Abrahamsohn, P., 2017. Histologia básica: texto e atlas., 13ª Ed. ed. Guanabara Koogan, Rio de Janeiro.

Kafshgari, M. H., Goldmann, W.H., 2020. Insights into Theranostic Properties of Titanium Dioxide for Nanomedicine. Nanomicro Lett 12, 22. https://doi.org/10.1007/s40820-019-0362-1

Ketabat, P., Mohabatpour, L., Koutsopoulos, H., Chen, Papagerakis, P., 2019. Controlled Drug Delivery Systems for Oral Cancer Treatment—Current Status and Future Perspectives. Pharmaceutics 11, 302. https://doi.org/10.3390/pharmaceutics11070302

Khan, S., Sadiq, M., Muhammad, N., 2022. Enhanced photocatalytic potential of $TiO_2$ nanoparticles in coupled $CdTiO_2$ and $ZnCdTiO_2$ nanocomposites. Environ. Sci. and Pollut. Res. 29, 54745–54755. https://doi.org/10.1007/s11356-022-19807-6

Kwon, S., Ko, H., You, D.G., Kataoka, K., Park, J.H., 2019. Nanomedicines for Reactive Oxygen Species Mediated Approach: An Emerging Paradigm for Cancer Treatment. Acc Chem Res 52, 1771–1782. https://doi.org/10.1021/acs.accounts.9b00136

Lagopati, N., Evangelou, K., Falaras, P., Tsilibary, E.P.C., Vasileiou, P.V.S., Havaki, S., Angelopoulou, A., Pavlatou, E.A., Gorgoulis, V.G., 2021. Nanomedicine: Photo-activated nanostructured titanium dioxide, as a promising anticancer agent. Pharmacol Ther 222, 107795. https://doi.org/10.1016/J.PHARMTHERA.2020.107795

Lagopati, N., Kitsiou, P.V., Kontos, A.I., Venieratos, P., Kotsopoulou, E., Kontos, A.G., Dionysiou, D.D., Pispas, S., Tsilibary, E.C., Falaras, P., 2010. Photo-induced treatment of breast epithelial cancer cells using nanostructured titanium dioxide solution. J Photochem Photobiol A Chem 214, 215–223. https://doi.org/10.1016/j.jphotochem.2010.06.031

Lee, H., Han, J., Shin, H., Han, H., Na, K., Kim, H., 2018. Combination of chemotherapy and photodynamic therapy for cancer treatment with sonoporation effects. J Control Release 283, 190–199. https://doi.org/10.1016/J.JCONREL.2018.06.008

Li, J., Chen, C., Zhao, J., Zhu, H., Orthman, J., 2002. Photodegradation of dye pollutants on $TiO_2$ nanoparticles dispersed in silicate under UV–VIS irradiation. Appl Catal B, 37(4), 331-338. https://doi.org/10.1016/S0926-3373(02)00011-5

Li, J., Ma, Y.J., Wang, Y., Chen, B.Z., Guo, X.D., Zhang, C.Y., 2018. Dual redox/pH-responsive hybrid polymer-lipid composites: Synthesis, preparation,

characterization and application in drug delivery with enhanced therapeutic efficacy. Chem Eng J 341, 450–461. https://doi.org/10.1016/J.CEJ.2018.02.055

Li, M., Chong, Y., Fu, P. P., Xia, Q., Croley, T. R., Lo, Y. M., Yin, J. J., 2017. Effects of P25 $TiO_2$ nanoparticles on the free radical-scavenging ability of antioxidants upon their exposure to simulated sunlight. J Agric Food Chem, 65, 9893-9901.https://doi.org/10.1021/acs.jafc.7b03407

Li, S., Zhang, L., 2020. Erythrocyte membrane nano-capsules: biomimetic delivery and controlled release of photothermal–photochemical coupling agents for cancer cell therapy. Dalton Trans 49, 2645–2651. https://doi.org/10.1039/C9DT04335G

Li, W.-P., Yen, C.-J., Wu, B.-S., Wong, T.-W., 2021. Recent Advances in Photodynamic Therapy for Deep-Seated Tumors with the Aid of Nanomedicine. Biomedicines 9, 69. https://doi.org/10.3390/biomedicines9010069

Li, Z., Mi, L., Wang, P.-N., Chen, J.-Y., 2011. Study on the visible-light-induced photokilling effect of nitrogen-doped $TiO_2$ nanoparticles on cancer cells. Nanoscale Res Lett 6, 356. https://doi.org/10.1186/1556-276X-6-356

Liang, S., Deng, X., Xu, G., Xiao, X., Wang, M., Guo, X., Ma, P., Cheng, Z., Zhang, D., Lin, J., 2020. A Novel Pt–$TiO_2$ Heterostructure with Oxygen-Deficient Layer as Bilaterally Enhanced Sonosensitizer for Synergistic Chemo-Sonodynamic Cancer Therapy. Adv Funct Mater 30, 1908598. https://doi.org/10.1002/adfm.201908598

Liao, G., Tao, X., Fang, B., 2022. An innovative synthesis strategy for high-efficiency and defects-switchable-hydrogenated $TiO_2$ photocatalysts. Matter 5, 377–379. https://doi.org/10.1016/J.MATT.2022.01.006

Lin, H., Chen, Y., Shi, J., 2018. Nanoparticle-triggered *in situ* catalytic chemical reactions for tumour-specific therapy. Chem Soc Rev 47, 1938–1958. https://doi.org/10.1039/C7CS00471K

Lin, X., Qiu, Y., Song, L., Chen, S., Chen, Xiaofeng, Huang, G., Song, J., Chen, Xiaoyuan, Yang, H., 2019. Ultrasound activation of liposomes for enhanced ultrasound imaging and synergistic gas and sonodynamic cancer therapy. Nanoscale Horiz 4, 747–756. https://doi.org/10.1039/C8NH00340H

Liu, J., Bu, W., Shi, J., 2017. Chemical Design and Synthesis of Functionalized Probes for Imaging and Treating Tumor Hypoxia. Chem Rev 117, 6160–6224. https://doi.org/10.1021/acs.chemrev.6b00525

Liu, L., Liu, Y., Wang, X., Hu, N., Li, Y., Li, C., Meng, Y., An, Y., 2021. Synergistic effect of B-$TiO_2$ and MIL-100 (Fe) for high-efficiency photocatalysis in methylene blue degradation. Appl Surf Sci 561, 149969. https://doi.org/10.1016/J.APSUSC.2021.149969

Liu, P., Yang, W., Shi, L., Zhang, H., Xu, Y., Wang, P., Zhang, G., Chen, W.R., Zhang, B., Wang, X., 2019. Concurrent photothermal therapy and photodynamic therapy for cutaneous squamous cell carcinoma by gold nanoclusters under a single NIR laser irradiation. J Mater Chem B 7, 6924–6933. https://doi.org/10.1039/C9TB01573F

Liu, Y., Tian, L., Tan, X., Li, X., Chen, X., 2017. Synthesis, properties, and applications of black titanium dioxide nanomaterials. Sci Bull (Beijing) 62, 431–441. https://doi.org/10.1016/J.SCIB.2017.01.034

Lucky, S.S., Soo, K.C., Zhang, Y., 2015. Nanoparticles in Photodynamic Therapy. Chem Rev 115, 1990–2042. https://doi.org/10.1021/cr5004198

Lukong, V.T., Ukoba, K.O., Jen, T.C., 2022. Heat-assisted sol–gel synthesis of $TiO_2$ nanoparticles structural, morphological and optical analysis for self-cleaning application. J King Saud Univ Sci 34, 101746. https://doi.org/10.1016/J.JKSUS.2021.101746

Luo, J., Cao, J., Ma, G., Wang, X., Sun, Y., Zhang, C., Shi, Z., Zeng, Y., Zhang, T., Huang, P., 2022. Collagenase-Loaded H-$TiO_2$ Nanoparticles Enhance Ultrasound Imaging-Guided Sonodynamic Therapy in a Pancreatic Carcinoma Xenograft Model via Digesting Stromal Barriers. ACS Appl Mater Interfaces 14, 40535–40545. https://doi.org/10.1021/acsami.2c08951

Malekkiani, M., Ravari, F., Heshmati, J. M., A., Dadmehr, M., Groiss, H., Hosseini, H.A., Sharif, R., 2022. Fabrication of Graphene-Based $TiO_2$ @$CeO_2$ and $CeO_2$@$TiO_2$ Core–Shell Heterostructures for Enhanced Photocatalytic Activity and Cytotoxicity. ACS Omega 7, 30601–30621. https://doi.org/10.1021/acsomega.2c04338

Malevu, T.D., 2021. Ball Milling synthesis and characterization of highly crystalline $TiO_2$-ZnO hybrids for photovoltaic applications. Physica B Condens Matter 621, 413291. https://doi.org/10.1016/J.PHYSB.2021.413291

Manke, A., Wang, L., Rojanasakul, Y., 2013. Mechanisms of Nanoparticle-Induced Oxidative Stress and Toxicity. Biomed Res Int 2013, 1–15. https://doi.org/10.1155/2013/942916

Mariño-Gámez, A.E., Acosta-González, G.E., Pech-Canul, M.I., Hernández, M.B., García-Villarreal, S., Zambrano-Robledo, P., Vera Barrios, B.S., Aguilar-Martínez, J.A., 2022. Influence of high energy ball milling on structural, microstructural and optical properties of $TiO_2$ nanoparticles. Ceram Int 48, 3362–3367. https://doi.org/10.1016/J.CERAMINT.2021.10.111

McNamara, K., Tofail, S.A.M., 2017. Nanoparticles in biomedical applications. Adv Phys X 2, 54–88. https://doi.org/10.1080/23746149.2016.1254570

Mehraban, N., Freeman, H., 2015. Developments in PDT Sensitizers for Increased Selectivity and Singlet Oxygen Production. Materials 8, 4421–4456. https://doi.org/10.3390/ma8074421

Melamed, J.R., Edelstein, R.S., Day, E.S., 2015. Elucidating the Fundamental Mechanisms of Cell Death Triggered by Photothermal Therapy. ACS Nano 9, 6–11. https://doi.org/10.1021/acsnano.5b00021

Meng, A., Zhang, L., Cheng, B., Yu, J., 2019. Dual Cocatalysts in $TiO_2$ Photocatalysis. Advanced Materials 1807660. https://doi.org/10.1002/adma.201807660

Meng, L., Zhao, H., 2020. Low-temperature complete removal of toluene over highly active nanoparticles CuO-$TiO_2$ synthesized via flame spray pyrolysis. Appl Catal B 264, 118427. https://doi.org/10.1016/J.APCATB.2019.118427

Meng, X., Zhang, B., Yi, Y., Cheng, H., Wang, B., Liu, Y., Gong, T., Yang, W., Yao, Y., Wang, H., Bu, W., 2020. Accurate and Real-Time Temperature Monitoring during MR Imaging Guided PTT. Nano Lett 20. https://doi.org/10.1021/acs.nanolett.9b05267

Mezzourh, H., ben Moumen, S., Amjoud, M., Mezzane, D., el Amraoui, Y., Marbati, B., Lahmar, A., Jouiad, M., el Marssi, M., 2022. Effect of growth time on structural and surface properties of $TiO_2$ nanostructures deposited by single-step hydrothermal method. Mater Today Proc 51, 2053–2058. https://doi.org/10.1016/J.MATPR.2021.08.004

Miller, R.J., Bennett, S., Keller, A.A., Pease, S., Lenihan, H.S., 2012. $TiO_2$ Nanoparticles Are Phototoxic to Marine Phytoplankton. PLoS One 7, e30321. https://doi.org/10.1371/journal.pone.0030321

Mohammadalipour, Z., Rahmati, M., Khataee, A., Moosavi, M.A., 2020. Differential effects of N-$TiO_2$ nanoparticle and its photo-activated form on autophagy and necroptosis in human melanoma A375 cells. J Cell Physiol 235, 8246–8259. https://doi.org/10.1002/jcp.29479

Mohammadinejad, R., Moosavi, M.A., Tavakol, S., Vardar, D.Ö., Hosseini, A., Rahmati, M., Dini, L., Hussain, S., Mandegary, A., Klionsky, D.J., 2019. Necrotic, apoptotic and autophagic cell fates triggered by nanoparticles. Autophagy 15, 4–33. https://doi.org/10.1080/15548627.2018.1509171

Moosavi, M.A., Sharifi, M., Ghafary, S.M., Mohammadalipour, Z., Khataee, A., Rahmati, M., Hajjaran, S., Łos, M.J., Klonisch, T., Ghavami, S., 2016. Photodynamic N-$TiO_2$ Nanoparticle Treatment Induces Controlled ROS-mediated Autophagy and Terminal Differentiation of Leukemia Cells. Sci Rep 6, 34413. https://doi.org/10.1038/srep34413

Mou, J., Lin, T., Huang, F., Chen, H., Shi, J., 2016. Black titania-based theranostic nanoplatform for single NIR laser induced dual-modal imaging-guided PTT/PDT. Biomaterials 84, 13–24. https://doi.org/10.1016/J.BIOMATERIALS.2016.01.009

Mou, J., Lin, T., Huang, F., Shi, J., Chen, H., 2017. A New Green Titania with Enhanced NIR Absorption for Mitochondria-Targeted Cancer Therapy. Theranostics 7, 1531–1542. https://doi.org/10.7150/thno.17247

Ng, C.W., Li, J., Pu, K., 2018. Recent Progresses in Phototherapy-Synergized Cancer Immunotherapy. Adv Funct Mater 28, 1804688. https://doi.org/10.1002/adfm.201804688

Nie, C., Du, P., Zhao, H., Xie, H., Li, Y., Yao, L., Shi, Y., Hu, L., Si, S., Zhang, M., Gu, J., Luo, L., Sun, Z., 2020. Ag@$TiO_2$ Nanoprisms with Highly Efficient Near-Infrared Photothermal Conversion for Melanoma Therapy. Chem Asian J 15, 148–155. https://doi.org/10.1002/asia.201901394

Nie, Z., Ke, X., Li, D., Zhao, Y., Zhu, L., Qiao, R., Zhang, X.L., 2019. $NaYF_4$:Yb,Er,Nd@$NaYF_4$:Nd Upconversion Nanocrystals Capped with Mn:$TiO_2$ for 808 nm NIR-Triggered Photocatalytic Applications. J Phys Chem C 123, 22959–22970. https://doi.org/10.1021/acs.jpcc.9b05234

Ning, S., Dai, X., Tang, W., Guo, Q., Lyu, M., Zhu, D., Wang, X., 2022. Cancer cell membrane-coated C-$TiO_2$ hollow nanoshells for combined sonodynamic and hypoxia-activated chemotherapy. Acta Biomater, *152*, 562-574.https://doi.org/10.1016/j.actbio.2022.08.067

Nita, M., Grzybowski, A., 2016. The Role of the Reactive Oxygen Species and Oxidative Stress in the Pathomechanism of the Age-Related Ocular Diseases and Other Pathologies of the Anterior and Posterior Eye Segments in Adults. Oxid Med Cell Longev 2016, 1–23. https://doi.org/10.1155/2016/3164734

Nogueira, A.E., Ribeiro, L.S., Gorup, L.F., Silva, G.T.S.T., Silva, F.F.B., Ribeiro, C., Camargo, E.R., 2018. New Approach of the Oxidant Peroxo Method (OPM) Route to Obtain $Ti(OH)_4$ Nanoparticles with High Photocatalytic Activity under Visible Radiation. Int J Photoenergy 2018, 1–10. https://doi.org/10.1155/2018/6098302

Oliveira, L.A.A. de, Pádua, A.F. de, Medeiros e Melo, M.A., Galvão, E.R. de C.G.N., Vieira, M.C., Ibiapina, J.O., Fontinele, D.R. da S., Vieira, S.C., 2020.

Radiation-induced angiosarcoma: case report. Einstein (São Paulo) 18. https://doi.org/10.31744/einstein_journal/2020RC5439

Oliveira, H.A., Azevedo, A., Rubio, J., 2021. Removal of flocculated $TiO_2$ nanoparticles by settling or dissolved air flotation. Environ Technol 42, 1001–1012. https://doi.org/10.1080/09593330.2019.1650123

Oliveira, T.C.G., Sganzerla, W.G., Ampese, L.C., Sforça, B.P., Goldbeck, R., Forster-Carneiro, T., 2022. Sustainable valorization of apple waste in a biorefinery: a bibliometric analysis. Biofuels Bioprod Biorefining 16, 891–919. https://doi.org/10.1002/bbb.2343

Paddock, L.E., Lu, S.E., Bandera, E. V., Rhoads, G.G., Fine, J., Paine, S., Barnhill, R., Berwick, M., 2016. Skin self-examination and long-term melanoma survival. Melanoma Res 26, 401–408. https://doi.org/10.1097/CMR.0000000000000255

Pan, W., Cui, B., Gao, P., Ge, Y., Li, N., Tang, B., 2020. A cancer cell membrane-camouflaged nanoreactor for enhanced radiotherapy against cancer metastasis. Chem commun 56, 547–550. https://doi.org/10.1039/C9CC07878A

Peiris-Pagès, M., Martinez-Outschoorn, U.E., Sotgia, F., Lisanti, M.P., 2015. Metastasis and Oxidative Stress: Are Antioxidants a Metabolic Driver of Progression? Cell Metab 22, 956–958. https://doi.org/10.1016/J.CMET.2015.11.008

Peng, H., Hu, J., Hu, C., Wu, T., Tian, X., 2017. Microwave Absorbing $Fe_3O_4$@m$TiO_2$ Nanoparticles as an Intelligent Drug Carrier for Microwave-Triggered Synergistic Cancer Therapy. J Nanosci Nanotechnol 17, 5139–5146. https://doi.org/10.1166/jnn.2017.13809

Perota, G., Zahraie, N., Vais, R.D., Zare, M.H., Sattarahmady, N., 2022. Au/$TiO_2$ nanocomposite as a triple-sensitizer for 808 and 650 nm phototherapy and sonotherapy: Synergistic therapy of melanoma cancer *in vitro*. J Drug Deliv Sci Technol 76, 103787. https://doi.org/10.1016/J.JDDST.2022.103787

Piccinno, F., Gottschalk, F., Seeger, S., Nowack, B., 2012. Industrial production quantities and uses of ten engineered nanomaterials in Europe and the world. Journal of Nanoparticle Research. https://doi.org/10.1007/s11051-012-1109-9

Prakash, J., Cho, J., Mishra, Y.K., 2022. Photocatalytic $TiO_2$ nanomaterials as potential antimicrobial and antiviral agents: Scope against blocking the SARS-COV-2 spread. Micro and Nano Engineering 14, 100100. https://doi.org/10.1016/J.MNE.2021.100100

Qiao, X., Xue, L., Huang, H., Dai, X., Chen, Y., Ding, H., 2022. Engineering defected 2D Pd/H-$TiO_2$ nanosonosensitizers for hypoxia alleviation and enhanced sono-chemodynamic cancer nanotherapy. J Nanobiotechnology 20, 186. https://doi.org/10.1186/s12951-022-01398-6

Qiang, C., Li, N., Zuo, S., Guo, Z., Zhan, W., Li, Z., Ma, J., 2022. Microwave-assisted synthesis of $RuTe_2$/black $TiO_2$ photocatalyst for enhanced diclofenac degradation: Performance, mechanistic investigation and intermediates analysis. Sep Purif Technol 283, 120214. https://doi.org/10.1016/J.SEPPUR.2021.120214

Rahmati M, Amanpour S, Mohammadpour H., 2020. The role of nanoparticles in cancer therapy through apoptosis induction. nanoparticle drug deliv syst cancer treat. Jenny Stanford Publishing;, Nanoparticle Drug Delivery Systems for Cancer Treatment. https://doi.org/10.1201/9780429341250

Rajh, T., Dimitrijevic, N.M., Bissonnette, M., Koritarov, T., Konda, V., 2014. Titanium Dioxide in the Service of the Biomedical Revolution. Chem Rev 114, 10177–10216. https://doi.org/10.1021/cr500029g

Ramachandran, P., Khor, B.K., Lee, C.Y., Doong, R.A., Oon, C.E., Thanh, N.T.K., Lee, H.L., 2022. N-Doped Graphene Quantum Dots/Titanium Dioxide Nanocomposites: A Study of ROS-Forming Mechanisms, Cytotoxicity and Photodynamic Therapy. Biomedicines 10. https://doi.org/10.3390/biomedicines10020421

Rastrelli, M., Tropea, S., Rossi, C.R., Alaibac, M., 2014. Melanoma: Epidemiology, risk factors, pathogenesis, diagnosis and classification. *In Vivo* (Brooklyn). https://pubmed.ncbi.nlm.nih.gov/25398793/ (Accesed 18 august 22)

Ren, W., Yan, Y., Zeng, L., Shi, Z., Gong, A., Schaaf, P., Wang, D., Zhao, J., Zou, B., Yu, H., Chen, G., Brown, E.M.B., Wu, A., 2015. A Near Infrared Light Triggered Hydrogenated Black $TiO_2$ for Cancer Photothermal Therapy. Adv Healthc Mater 4, 1526–1536. https://doi.org/10.1002/adhm.201500273

Rolo, D., Assunção, R., Ventura, C., Alvito, P., Gonçalves, L., Martins, C., Bettencourt, A., Jordan, P., Vital, N., Pereira, J., Pinto, F., Matos, P., Silva, M.J., Louro, H., 2022. Adverse Outcome Pathways Associated with the Ingestion of Titanium Dioxide Nanoparticles—A Systematic Review. Nanomaterials 12, 3275. https://doi.org/10.3390/nano12193275

Rosa, R.G. da, Sganzerla, W.G., Barroso, T.L.C.T., Buller, L.S., Berni, M.D., Forster-Carneiro, T., 2022. Sustainable production of bioactive compounds from jabuticaba (Myrciaria cauliflora): A bibliometric analysis of scientific research over the last 21 years. Sustain Chem Pharm 27, 100656. https://doi.org/10.1016/j.scp.2022.100656

Roufegarinejad, L., 2022. Development and Characterization of the Reinforced Soy Protein Isolate-Based Nanocomposite Film with CuO and $TiO_2$ Nanoparticles. J Polym Environ 30, 2507–2515. https://doi.org/10.1007/s10924-022-02374-9

Roy, J., 2022. The synthesis and applications of $TiO_2$ nanoparticles derived from phytochemical sources. J Ind Eng Chem 106, 1–19. https://doi.org/10.1016/J.JIEC.2021.10.024

Roy, P., Berger, S., Schmuki, P., 2011. $TiO_2$ Nanotubes: Synthesis and Applications. Angew Chem Int Ed 50, 2904–2939. https://doi.org/10.1002/anie.201001374

Safavipour, M., Kharaziha, M., Amjadi, E., Karimzadeh, F., Allafchian, A., 2020. $TiO_2$ nanotubes/reduced GO nanoparticles for sensitive detection of breast cancer cells and photothermal performance. Talanta 208. https://doi.org/10.1016/j.talanta.2019.120369

Sagadevan, S., Imteyaz, S., Murugan, B., Anita Lett, J., Sridewi, N., Weldegebrieal, G.K., Fatimah, I., Oh, W.-C., 2022. A comprehensive review on green synthesis of titanium dioxide nanoparticles and their diverse biomedical applications. Green Process Synth 11, 44–63. https://doi.org/10.1515/gps-2022-0005

Samat, M.H., Ali, A.M.M., Taib, M.F.M., Hassan, O.H., Yahya, M.Z.A., 2016. Hubbard U calculations on optical properties of 3d transition metal oxide $TiO_2$. Results Phys 6, 891–896. https://doi.org/10.1016/j.rinp.2016.11.006

Sanches, L.J., Marinello, P.C., Panis, C., Fagundes, T.R., Morgado-Díaz, J.A., de-Freitas-Junior, J.C.M., Cecchini, R., Cecchini, A.L., Luiz, R.C., 2017.

Cytotoxicity of citral against melanoma cells: The involvement of oxidative stress generation and cell growth protein reduction. Tumor Biol 39. https://doi.org/10.1177/1010428317695914

Sandbhor Gaikwad, P., Banerjee, R., 2018. Advances in point-of-care diagnostic devices in cancers. Analyst. https://doi.org/10.1039/c7an01771e

Santos, J.F., 2010. Perfil do Titânio. Ministério Minas e Energia. [WWW Document]. URL http://www.mme.gov.br/portalmme/opencms/sgm/galerias/arquivos/plano_duo_ decenal/a_mineracao_brasileira/P16_RT36Perfil_do_Titxnio.pdf (accessed 16 august 22).

Sargazi, S., ER, S., Sacide Gelen, S., Rahdar, A., Bilal, M., Arshad, R., Ajalli, N., Farhan Ali Khan, M., Pandey, S., 2022. Application of titanium dioxide nanoparticles in photothermal and photodynamic therapy of cancer: An updated and comprehensive review. J Drug Deliv Sci Technol 75, 103605. https://doi.org/10.1016/J.JDDST.2022.103605

Seo, J., Chung, H., Kim, M., Lee, J., Choi, I., Cheon, J., 2007. Development of Water-Soluble Single-Crystalline $TiO_2$ Nanoparticles for Photocatalytic Cancer-Cell Treatment. Small 3, 850–853. https://doi.org/10.1002/smll.200600488

Setyawati, M.I., Tay, C.Y., Leong, D.T., 2015. Mechanistic Investigation of the Biological Effects of $SiO_2$, $TiO_2$, and ZnO Nanoparticles on Intestinal Cells. Small 11, 3458–3468. https://doi.org/10.1002/smll.201403232

Sganzerla, W.G., Ampese, L.C., Mussatto, S.I., Forster-Carneiro, T., 2021. A bibliometric analysis on potential uses of brewer's spent grains in a biorefinery for the circular economy transition of the beer industry. Biofuels Bioprod Biorefining 15, 1965–1988. https://doi.org/10.1002/bbb.2290

Sganzerla, W.G., da Silva, A.P.G., 2022. Uvaia (Eugenia pyriformis Cambess – Myrtaceae): An overview from the origin to recent developments in the food industry – A bibliometric analysis. J Agric Food Res 10, 100369. https://doi.org/10.1016/j.jafr.2022.100369

Sharsheeva, A., Iglin, V.A., Nesterov, P. v., Kuchur, O.A., Garifullina, E., Hey-Hawkins, E., Ulasevich, S.A., Skorb, E. v., Vinogradov, A. v., Morozov, M.I., 2019. Light-controllable systems based on $TiO_2$-ZIF-8 composites for targeted drug release: Communicating with tumour cells. J Mater Chem B 7. https://doi.org/10.1039/c9tb01377f

Sheng, H., Yuhua, Y., Youfa, W., Xianying, C., Shipu, L., 2005. Titanium dioxide nanoparticle absorbed by hepatoma cells *in vitro*. J Wuhan Univ Technol Mater Sci Ed 20, 31–34. https://doi.org/10.1007/BF02835021

Shi, J., Li, J., Wang, Y., Cheng, J., Zhang, C.Y., 2020. Recent advances in $MoS_2$ -based photothermal therapy for cancer and infectious disease treatment. J Mater Chem B 8, 5793–5807. https://doi.org/10.1039/D0TB01018A

Shi, J., Li, J., Wang, Y., Zhang, C.Y., 2022. $TiO_2$-based nanosystem for cancer therapy and antimicrobial treatment: A review. Chem Eng J. https://doi.org/10.1016/j.cej.2021.133714

Shields, H.J., Traa, A., van Raamsdonk, J.M., 2021. Beneficial and Detrimental Effects of Reactive Oxygen Species on Lifespan: A Comprehensive Review of Comparative and Experimental Studies. Front Cell Dev Biol. https://doi.org/10.3389/fcell.2021.628157

Shirvalilou, S., Khoei, S., Esfahani, A.J., Kamali, M., Shirvaliloo, M., Sheervalilou, R., Mirzaghavami, P., 2021. Magnetic Hyperthermia as an adjuvant cancer

therapy in combination with radiotherapy versus radiotherapy alone for recurrent/progressive glioblastoma: a systematic review. J Neurooncol. https://doi.org/10.1007/s11060-021-03729-3

Shiva Samhitha, S., Raghavendra, G., Quezada, C., Hima Bindu, P., 2022. Green synthesized $TiO_2$ nanoparticles for anticancer applications: Mini review. Mater Today Proc 54, 765–770. https://doi.org/10.1016/J.MATPR.2021.11.073

Silk, A.W., Barker, C.A., Bhatia, S., Bollin, K.B., Chandra, S., Eroglu, Z., Gastman, B.R., Kendra, K.L., Kluger, H., Lipson, E.J., Madden, K., Miller, D.M., Nghiem, P., Pavlick, A.C., Puzanov, I., Rabinowits, G., Ruiz, E.S., Sondak, V.K., Tavss, E.A., Tetzlaff, M.T., Brownell, I., 2022. Society for Immunotherapy of Cancer (SITC) clinical practice guideline on immunotherapy for the treatment of nonmelanoma skin cancer. J Immunother Cancer 10, e004434. https://doi.org/10.1136/jitc-2021-004434

Singh, T., Singh, A., Wang, W., Yadav, D., Kumar, A., Singh, P.K., 2020. Biosynthesized Nanoparticles and Its Implications in Agriculture, in: Biological Synthesis of Nanoparticles and Their Applications. https://doi.org/10.1201/9780429265235-19

Skocaj, M., Filipic, M., Petkovic, J., Novak, S., 2011. Titanium dioxide in our everyday life; is it safe? Radiol Oncol 45. https://doi.org/10.2478/v10019-011-0037-0

Solanki, K., Parmar, D., Savaliya, C., Kumar, S., Jethva, S., 2021. Surface morphology and optical properties of sol-gel synthesized $TiO_2$ nanoparticles: Effect of Co, Pd and Ni-doping, in: Materials Today: Proceedings. https://doi.org/10.1016/j.matpr.2021.10.182

Sukidpaneenid, S., Chawengkijwanich, C., Pokhum, C., Isobe, T., Opaprakasit, P., Sreearunothai, P., 2023. Multi-function adsorbent-photocatalyst MXene-$TiO_2$ composites for removal of enrofloxacin antibiotic from water. J Environ Sci (China) 124. https://doi.org/10.1016/j.jes.2021.09.042

Sun, L.; Li, Z.; Li, Z.; Hu, Y.; Chen, C.; Yang, C.; Du, B.; Sun, Y.; Besenbacher, F.; Yu, M., 2017. Design and mechanism of core-shell $TiO_2$ nanoparticles as a high-performance photothermal Agent. Nanoscale, 9, 16183-16192. http://dx.doi.org/10.1039/C7NR02848B

Sung, H., Ferlay, J., Siegel, R.L., Laversanne, M., Soerjomataram, I., Jemal, A., Bray, F., 2021. Global Cancer Statistics 2020: GLOBOCAN Estimates of Incidence and Mortality Worldwide for 36 Cancers in 185 Countries. CA Cancer J Clin 71. https://doi.org/10.3322/caac.21660

Takahashi, M., 2018. Oxide ($TiO_2$) Nanotubes Obtained Through Sol-Gel Method, in: Handbook of Sol-Gel Science and Technology. Springer International Publishing, Cham, pp. 737–764. https://doi.org/10.1007/978-3-319-32101-1_105

Teranishi, R., Matsuda, T., Yuba, E., Kono, K., Harada, A., 2019. Sonodynamic Therapeutic Effects of Sonosensitizers with Different Intracellular Distribution Delivered by Hollow Nanocapsules Exhibiting Cytosol Specific Release. Macromol Biosci 19. https://doi.org/10.1002/mabi.201800365

Thurn, K.T., Arora, H., Paunesku, T., Wu, A., Brown, E.M.B., Doty, C., Kremer, J., Woloschak, G., 2011. Endocytosis of titanium dioxide nanoparticles in prostate cancer PC-3M cells. Nanomedicine 7, 123–130. https://doi.org/10.1016/j.nano.2010.09.004

Timoumi, A., Albetran, H.M., Alamri, H.R., Alamri, S.N., Low, I.M., 2020. Impact of annealing temperature on structural, morphological and optical properties of

GO-$TiO_2$ thin films prepared by spin coating technique. Superlattices Microstruct 139. https://doi.org/10.1016/j.spmi.2020.106423
Tong, R., Lin, H., Chen, Y., An, N., Wang, G., Pan, X., Qu, F., 2017. Near-infrared mediated chemo/photodynamic synergistic therapy with DOX-UCNPs@m$SiO_2$/$TiO_2$-TC nanocomposite. Mater Sci Eng C 78, 998–1005. https://doi.org/10.1016/J.MSEC.2017.04.112
Trabelsi, F., Mercier, F., Blanquet, E., Crisci, A., Salhi, R., 2020. Synthesis of upconversion $TiO_2$:$Er^{3+}$-$Yb^{3+}$ nanoparticles and deposition of thin films by spin coating technique. Ceram Int 46. https://doi.org/10.1016/j.ceramint.2020.07.317
Trouiller, B., Reliene, R., Westbrook, A., Solaimani, P., Schiestl, R.H., 2009. Titanium Dioxide Nanoparticles Induce DNA Damage and Genetic Instability *In vivo* in Mice. Cancer Res 69, 8784–8789. https://doi.org/10.1158/0008-5472.CAN-09-2496
Uthaman, S., Huh, K.M., Park, I.K., 2018. Tumor microenvironment-responsive nanoparticles for cancer theragnostic applications. Biomater Res. https://doi.org/10.1186/s40824-018-0132-z
Valko-Rokytovská, M., Šimková, J., Milkovičová, M., Kostecká, Z., 2018. Possibilities for the Therapy of Melanoma: Current Knowledge and Future Directions, in: Human Skin Cancers - Pathways, Mechanisms, Targets and Treatments. InTech. https://doi.org/10.5772/intechopen.70368
Van Eck, N.J., Waltman, L., 2010. Software survey: VOSviewer, a computer program for bibliometric mapping. Scientometrics 84, 523–538. https://doi.org/10.1007/s11192-009-0146-3
Vanti, N. A. P., 2002. From bibliometry to webometry: a conceptual exploration of several forms of measuring information and knowledge. Ci. Inf. 31, 369-379. doi: https://doi.org/10.1590/S0100-19652002000200016
Veeranarayanan, M.S.M., S., Maekawa, T., D., S.K., 2019. External stimulus responsive inorganic nanomaterials for cancer theranostics. Adv Drug Deliv Rev 138, 18–40. https://doi.org/10.1016/j.addr.2018.10.007
Venkatasubbu, G.D., Ramasamy, S., Reddy, G.P., Kumar, J., 2013. *In vitro* and *In vivo* anticancer activity of surface modified paclitaxel attached hydroxyapatite and titanium dioxide nanoparticles. Biomed Microdevices 15, 711–726. https://doi.org/10.1007/s10544-013-9767-7
Verma, V., Al-Dossari, M., Singh, J., Rawat, M., Kordy, M. G., Shaban, M., 2022. A review on green synthesis of $TiO_2$ NPs: photocatalysis and antimicrobial applications. Polymers, 14, 1444. https://doi.org/10.3390/polym14071444
Volkovova, K., Bilanicova, D., Bartonova, A., Letaiová, S., Dusinska, M., 2012. Associations between environmental factors and incidence of cutaneous melanoma. Review. Environ Health. https://doi.org/10.1186/1476-069X-11-S1-S12
Wachesk, C.C., Seabra, S.H., dos Santos, T.A.T., Trava-Airoldi, V.J., Lobo, A.O., Marciano, F.R., 2021. *In vivo* biocompatibility of diamond-like carbon films containing $TiO_2$ nanoparticles for biomedical applications. J Mater Sci Mater Med 32, 117. https://doi.org/10.1007/s10856-021-06596-6
Wadge, M.D., Carrington, M.J., Constantin, H., Orange, K., Greaves, J., Islam, M.T., Zakir Hossain, K.M., Cooper, T.P., Kudrynskyi, Z.R., Felfel, R.M., Ahmed, I., Grant, D.M., 2022. Characterization of potential nanoporous sodium titanate film formation on $Ti_6Al_4V$ and $TiO_2$ microspherical substrates

via wet-chemical alkaline conversion. Mater Charact 185. https://doi.org/10.1016/j.matchar.2022.111760
Wang, P., Sun, L., Xu, M., Sun, S., Zhang, L., Zhang, J., Wang, S., Liang, X., 2021. Titania/iron oxide nanoplatform operates as hydrogen peroxide enriched vector for amplification of fenton catalytic efficiency in cancer theranostics. Chem Eng J 418. https://doi.org/10.1016/j.cej.2021.129381
Wang, S., Ren, W., Wang, J., Jiang, Z., Saeed, M., Zhang, L., Li, A., Wu, A., 2018. Black $TiO_2$-based nanoprobes for: T1-weighted MRI-guided photothermal therapy in CD133 high expressed pancreatic cancer stem-like cells. Biomater Sci 6. https://doi.org/10.1039/c8bm00454d
Wang, S., Yu, G., Wang, Z., Jacobson, O., Lin, L. sen, Yang, W., Deng, H., He, Z., Liu, Y., Chen, Z.Y., Chen, X., 2019. Enhanced Antitumor Efficacy by a Cascade of Reactive Oxygen Species Generation and Drug Release. Angew Chem Int Ed 58. https://doi.org/10.1002/anie.201908997
Wang, X., Luo, D., Basilion, J.P., 2021. Photodynamic therapy: Targeting cancer biomarkers for the treatment of cancers. Cancers (Basel). https://doi.org/10.3390/cancers13122992
Wang, X., Ma, B., Xue, J., Wu, J., Chang, J., Wu, C., 2019. Defective Black Nano-Titania Thermogels for Cutaneous Tumor-Induced Therapy and Healing. Nano Lett 19. https://doi.org/10.1021/acs.nanolett.9b00367
Wang, X., Wang, W., Yu, L., Tang, Y., Cao, J., Chen, Y., 2017. Site-specific sonocatalytic tumor suppression by chemically engineered single-crystalline mesoporous titanium dioxide sonosensitizers. J Mater Chem B 5, 4579–4586. https://doi.org/10.1039/C7TB00938K
Wang, Y., Santos, A., Evdokiou, A., Losic, D., 2015. An overview of nanotoxicity and nanomedicine research: principles, progress and implications for cancer therapy. J Mater Chem B 3, 7153–7172. https://doi.org/10.1039/C5TB00956A
Wei, B., Dong, F., Yang, W., Luo, C., Dong, Q., Zhou, Z., Yang, Z., Sheng, L., 2020. Synthesis of carbon-dots@$SiO_2$@$TiO_2$ nanoplatform for photothermal imaging induced multimodal synergistic antitumor. J Adv Res 23, 13–23. https://doi.org/10.1016/J.JARE.2020.01.011
Weng, Y., Guan, S., Wang, L., Lu, H., Meng, X., Waterhouse, G.I.N., Zhou, S., 2020. Defective Porous Carbon Polyhedra Decorated with Copper Nanoparticles for Enhanced NIR-Driven Photothermal Cancer Therapy. Small 16. https://doi.org/10.1002/smll.201905184
Wick, M.R., 2016. Cutaneous melanoma: A current overview. Semin Diagn Pathol 33, 225–241. https://doi.org/10.1053/J.SEMDP.2016.04.007
Wright, C., Iyer, A.K. v., Wang, L., Wu, N., Yakisich, J.S., Rojanasakul, Y., Azad, N., 2017. Effects of titanium dioxide nanoparticles on human keratinocytes. Drug Chem Toxicol 40, 90–100. https://doi.org/10.1080/01480545.2016.1185111
Wu, M., Ding, Y., Li, L., 2019. Recent progress in the augmentation of reactive species with nanoplatforms for cancer therapy. Nanoscale 11, 19658–19683. https://doi.org/10.1039/C9NR06651A
Wu, S., Butt, H.J., 2016. Near-Infrared-Sensitive Materials Based on Upconverting Nanoparticles. Adv Mater. https://doi.org/10.1002/adma.201502843
Xia, C., Dong, X., Li, H., Cao, M., Sun, D., He, S., Yang, F., Yan, X., Zhang, S., Li, N., Chen, W., 2022. Cancer statistics in China and United States, 2022: Profiles, trends, and determinants. Chin Med J (Engl) 135. https://doi.org/10.1097/CM9.0000000000002108

Xia, Z., He, J., Li, B., He, K., Yang, W., Chen, X., Zhang, J., Xiang, G., 2018. Titanium dioxide nanoparticles induce mitochondria-associated apoptosis in HepG2 cells. RSC Adv 8. https://doi.org/10.1039/c8ra05132a

Xian-Ying, C., Hong-Lian, D., Yu-Hua, Y., Shi-Pu, L., 2003. Selective anti-hepatoma treated with titanium oxide nanoparticles *in vitro*. Journal of Wuhan University of Technology-Mater. Sci. Ed. 18, 52–54. https://doi.org/10.1007/BF02835089

Xiaoshang, G., Murakonda, G.K., Jarubula, R., Zhao, S., 2021. Biosynthesized $TiO_2$ nanoparticles and their applications for the treatment of pediatric acute leukemia. Mater Res Express 8, 015022. https://doi.org/10.1088/2053-1591/abd89f

Xie, H., Luo, H., Pei, Z., Chen, S., Zhang, D., 2022. Improved discharge energy density and efficiency of polypropylene-based dielectric nanocomposites utilizing $BaTiO_3$@$TiO_2$ nanoparticles. Mater Today Energy 30, 101160. https://doi.org/10.1016/j.mtener.2022.101160

Xie, Z., Fan, T., An, J., Choi, W., Duo, Y., Ge, Y., Zhang, B., Nie, G., Xie, N., Zheng, T., Chen, Y., Zhang, H., Kim, J.S., 2020. Emerging combination strategies with phototherapy in cancer nanomedicine. Chem Soc Rev. https://doi.org/10.1039/d0cs00215a

Xiong, S., George, S., Ji, Z., Lin, S., Yu, H., Damoiseaux, R., France, B., Ng, K.W., Loo, S.C.J., 2013. Size of $TiO_2$ nanoparticles influences their phototoxicity: An *in vitro* investigation. Arch Toxicol 87. https://doi.org/10.1007/s00204-012-0912-5

Xu, J., Sun, Y., Huang, J., Chen, C., Liu, G., Jiang, Y., Zhao, Y., Jiang, Z., 2007. Photokilling cancer cells using highly cell-specific antibody–$TiO_2$ bioconjugates and electroporation. Bioelectrochemistry 71, 217–222. https://doi.org/10.1016/j.bioelechem.2007.06.001

Yang, B., Chen, Y., Shi, J., 2019. Reactive Oxygen Species (ROS)-Based Nanomedicine. Chem Rev 119, 4881–4985. https://doi.org/10.1021/acs.chemrev.8b00626

Yang, C., Chen, Y., Guo, W., Gao, Y., Song, C., Zhang, Q., Zheng, N., Han, X., Guo, C., 2018. Bismuth Ferrite-Based Nanoplatform Design: An Ablation Mechanism Study of Solid Tumor and NIR-Triggered Photothermal/Photodynamic Combination Cancer Therapy. Adv Funct Mater 28. https://doi.org/10.1002/adfm.201706827

Yang, M., Deng, J., Su, H., Gu, S., Zhang, J., Zhong, A., Wu, F., 2021. Small organic molecule-based nanoparticles with red/near-infrared aggregation-induced emission for bioimaging and PDT/PTT synergistic therapy. Mater Chem Front 5, 406–417. https://doi.org/10.1039/D0QM00536C

Yougbaré, S., Mutalik, C., Krisnawati, D.I., Kristanto, H., Jazidie, A., Nuh, M., Cheng, T.M., Kuo, T.R., 2020. Nanomaterials for the photothermal killing of bacteria. Nanomaterials. https://doi.org/10.3390/nano10061123

Youssef, Z., Vanderesse, R., Colombeau, L., Baros, F., Roques-Carmes, T., Frochot, C., Wahab, H., Toufaily, J., Hamieh, T., Acherar, S., Gazzali, A.M., 2017. The application of titanium dioxide, zinc oxide, fullerene, and graphene nanoparticles in photodynamic therapy. Cancer Nanotechnol. https://doi.org/10.1186/s12645-017-0032-2

Yu, F., Wang, C., Li, Y., Ma, H., Wang, R., Liu, Y., Suzuki, N., Terashima, C., Ohtani, B., Ochiai, T., Fujishima, A., Zhang, X., 2020. Enhanced Solar

Photothermal Catalysis over Solution Plasma Activated $TiO_2$. Adv Sci 7, 2000204. https://doi.org/10.1002/advs.202000204
Yu, K.N., Sung, J.H., Lee, S., Kim, J.E., Kim, S., Cho, W.Y., Lee, A.Y., Park, S.J., Lim, J., Park, C., Chae, C., Lee, J.K., Lee, J., Kim, J.S., Cho, M.H., 2015. Inhalation of titanium dioxide induces endoplasmic reticulum stress-mediated autophagy and inflammation in mice. Food and Chem. Toxicol. 85, 106–113. https://doi.org/10.1016/J.FCT.2015.08.001
Yu, N., Hu, Y., Wang, X., Liu, G., Wang, Z., Liu, Z., Tian, Q., Zhu, M., Shi, X., Chen, Z., 2017. Dynamically tuning near-infrared-induced photothermal performances of $TiO_2$ nanocrystals by Nb doping for imaging-guided photothermal therapy of tumors. Nanoscale 9. https://doi.org/10.1039/c7nr02180a
Yu, X., Trase, I., Ren, M., Duval, K., Guo, X., Chen, Z., 2016. Design of Nanoparticle-Based Carriers for Targeted Drug Delivery. J Nanomater. https://doi.org/10.1155/2016/1087250
Yue, W., Chen, L., Yu, L., Zhou, B., Yin, H., Ren, W., Liu, C., Guo, L., Zhang, Y., Sun, L., Zhang, K., Xu, H., Chen, Y., 2019. Checkpoint blockade and nanosonosensitizer-augmented noninvasive sonodynamic therapy combination reduces tumour growth and metastases in mice. Nat Commun 10. https://doi.org/10.1038/s41467-019-09760-3
Zandvakili, A., Moradi, M., Ashoo, P., Pournejati, R., Yosefi, R., Karbalaei-Heidari, H.R., Behaein, S., 2022. Investigating cytotoxicity effect of Ag-deposited, doped and coated titanium dioxide nanotubes on breast cancer cells. Mater Today Commun 32, 103915. https://doi.org/10.1016/J.MTCOMM.2022.103915
Zeng, J.Y., Zhang, M.K., Peng, M.Y., Gong, D., Zhang, X.Z., 2018. Porphyrinic Metal–Organic Frameworks Coated Gold Nanorods as a Versatile Nanoplatform for Combined Photodynamic/Photothermal/Chemotherapy of Tumor. Adv Funct Mater 28. https://doi.org/10.1002/adfm.201705451
Zhang, G., Zhang, Xingyu, Yang, Y., Chi, R., Shi, J., Hang, R., Huang, X., Yao, X., Chu, P.K., Zhang, Xiangyu, 2020. Dual light-induced in situ antibacterial activities of biocompatible$TiO_2$/$MoS_2$/PDA/RGD nanorod arrays on titanium. Biomater Sci 8. https://doi.org/10.1039/c9bm01507h
Zhang, H., Guo, L., Ding, S., Xiong, J., Chen, B., 2016. Targeted photo-chemo therapy of malignancy on the chest wall while cardiopulmonary avoidance based on $Fe_3O_4$@ZnO nanocomposites. Oncotarget 7, 36602–36613. https://doi.org/10.18632/oncotarget.9123
Zhang, W., Rhim, J.W., 2022. Titanium dioxide ($TiO_2$) for the manufacture of multifunctional active food packaging films. Food Packag Shelf Life 31, 100806. https://doi.org/10.1016/J.FPSL.2021.100806
Zhao, F., Wang, C., Yang, Q., Han, S., Hu, Q., Fu, Z., 2018. Titanium dioxide nanoparticle stimulating pro-inflammatory responses *in vitro* and *in vivo* for inhibited cancer metastasis. Life Sci 202, 44–51. https://doi.org/10.1016/j.lfs.2018.03.058
Zheng, T., Wang, W., Wu, F., Zhang, M., Shen, J., Sun, Y., 2019. Zwitterionic Polymer-Gated Au@$TiO_2$ Core-Shell Nanoparticles for Imaging-Guided Combined Cancer Therapy. Theranostics 9, 5035–5048. https://doi.org/10.7150/thno.35418
Zheng, Z., Zhu, S., Lv, M., Gu, Z., Hu, H., 2022. Harnessing nanotechnology for cardiovascular disease applications - a comprehensive review based on

bibliometric analysis. Nano Today 44, 101453. https://doi.org/10.1016/j.nantod.2022.101453

Zhi, D., Yang, T., O'Hagan, J., Zhang, S., Donnelly, R.F., 2020. Photothermal therapy. J Control Release 325, 52–71. https://doi.org/10.1016/J.JCONREL.2020.06.032

Zhou, J.-Y., Wang, W.-J., Zhang, C.-Y., Ling, Y.-Y., Hong, X.-J., Su, Q., Li, W.-G., Mao, Z.-W., Cheng, B., Tan, C.-P., Wu, T., 2022. Ru (II)-modified $TiO_2$ nanoparticles for hypoxia-adaptive photo-immunotherapy of oral squamous cell carcinoma. Biomaterials 289, 121757. https://doi.org/10.1016/j.biomaterials.2022.121757

Zhou, Z., Song, J., Nie, L., Chen, X., 2016. Reactive oxygen species generating systems meeting challenges of photodynamic cancer therapy. Chem Soc Rev. https://doi.org/10.1039/c6cs00271d

Zhu, C.-L., Zhang, M.-L., Qiao, Y.-J., Xiao, G., Zhang, F., Chen, Y.-J., 2010. $Fe_3O_4/TiO_2$ Core/Shell Nanotubes: Synthesis and Magnetic and Electromagnetic Wave Absorption Characteristics. J Phys Chem C 114, 16229–16235. https://doi.org/10.1021/jp104445m

Zhu, H., Li, J., Qi, X., Chen, P., Pu, K., 2018. Oxygenic Hybrid Semiconducting Nanoparticles for Enhanced Photodynamic Therapy. Nano Lett 18, 586–594. https://doi.org/10.1021/acs.nanolett.7b04759

Ziental, D., Czarczynska-Goslinska, B., Mlynarczyk, D.T., Glowacka-Sobotta, A., Stanisz, B., Goslinski, T., Sobotta, L., 2020. Titanium dioxide nanoparticles: Prospects and applications in medicine. Nanomaterials. https://doi.org/10.3390/nano10020387

Zupic, I., Cater, T., 2015. Bibliometric methods in management and organization. *Organ Res Methods,* 18, 3, 429-472. https://doi.org/10.1177/1094428114562629

# CHAPTER II

Article published in the journal *Sustainable Chemistry for the Environment*, Volume 8, December 2024, 100177, https://doi.org/10.1016/j.scenv.2024.100177

## Photocatalytic action of $Ag/TiO_2$ nanoparticles to emerging pollutants degradation: A comprehensive review


### ABSTRACT

Silver (Ag) doped titanium dioxide ($TiO_2$) nanoparticles are promising photocatalysts for the degradation of emerging pollutants. These nanocomposites enhance the photocatalytic activity of $TiO_2$ in visible light, suppress the $e^-/h^+$ rearrangement, and enhance their bactericidal properties. This review proposes a bibliometric analysis that elucidates research trends, and important topics on contaminant degradation, analyzes the advantages and limitations of different synthesis techniques (solvothermal, photochemical reduction, sol-gel, and others), their properties to produce $Ag/TiO_2$, and their potential for pollutant degradation. Thus, depending on the technique chosen, Ag doping of $TiO_2$ can offer high stability, recyclability for more than 3 cycles, customized morphologies and sizes, among others. Applications of $Ag/TiO_2$ include wastewater treatment, antibacterial surfaces, food packaging, implants, and others. Advances in the synthesis of $Ag/TiO_2$ photocatalysts offer excellent photocatalytic degradation, between 80-100%, for organic dyes, hormones, pharmaceuticals, pesticides and other emerging pollutants. $Ag/TiO_2$ photocatalysts show superior degradation rates compared to pure $TiO_2$, with some achieving up to 99% pollutant removal. The bibliometric analysis performed by Methodi Ordinatio, classifying 267 articles, reveals a foundation of relevant articles, around 35% of articles published on these topics were published between 2019 and 2021. A complete cost analysis of $Ag/TiO_2$ is considered to determine the feasibility for pilot and large-scale experimentation. These nanocomposites offer a promising solution to address the growing concern about emerging pollutants, disinfection of water, and in the inactivation of pathogenic microorganisms.


**Keywords:** Bibliometric analysis, Nanotechnology, Visible light, Photocatalysis, Water treatment.

## 1. Introduction

Environmental pollutants, including fungi, bacteria, herbicides, pesticides, drains and heavy metals, represent a complex challenge to manage [1, 2]. The complex combination of pollutants makes their degradation difficult, so employing a large set of techniques and materials is necessary to achieve this [3]. Nanotechnology, a key technology, helps in the production of nanomaterials, which have a high surface area, assisting in various industries (biochemical, biotechnological, medical, agribusiness, personal hygiene, food industry, agriculture) [4, 5].

Methods such as coagulation, flocculation, sedimentation and filtration are commonly applied in wastewater treatment plants, but have limited efficiency in degrading emerging pollutants [6, 7]. Among the limitations presented by biological techniques, physical process, membrane filtration, and chemical precipitation are: membrane fouling, high cost, higher energy consumption, secondary waste generation, mass displacement restrictions, and extensive procedural period [8].

Adsorption, photocatalysis, and microwave catalysis are also promising techniques for water treatment. Adsorption separates various pollutants from water, while photocatalysis converts toxic contaminants into harmless forms [9]. Microwave-assisted catalysis offers fast reaction rates and simple operation [10, 11]. However, there are still challenges in scaling up these technologies for industrial use [12].

Improved processes are needed to efficiently and economically degrade or extract pollutants from aquatic environments [13]. One process that combines photochemistry and catalysis is photocatalysis, which has gained significant attention for environmental applications such as water treatment and air purification [14]. Advanced oxidation processes (AOPs), such as heterogeneous photocatalysis, can effectively remove pesticides, polychlorinated biphenyls, endocrine disruptors, dyes, and pharmaceuticals [13]. This process uses light activation of heterogeneous photocatalysts, such as titanium dioxide ($TiO_2$), generating electron-hole ($e^-/h^+$) pairs and reactive oxygen species (ROS) that drive oxidation and reduction processes to degrade pollutants [15, 16]. The degradation of organic pollutants can occur through several pathways, such as reductive dehalogenation of compounds such as tetrachloromethane and oxidative

degradation of substances such as 4-chlorophenol and naphthalene [17]. Photocatalysis is a more efficient method to reduce pollutants in wastewater providing high efficiency and minimal harmful production compared to other methods such as ozonation, Fenton, sonolysis and chemical oxidation [18].

$TiO_2$ is a highly effective photocatalyst due to its action under the ultraviolet (UV) spectrum, changing the excitation state without decomposing. Its properties include high refractive index, high photostability, low cost, biocompatibility, low toxicity and easy synthesis. $TiO_2$ nanomaterials have high chemical stability and reduce or nullify the harmful effects of pollutants [19]. $TiO_2$ has antimicrobial action activated by UV (above 385 nm), which results in the production of $OH^{\bullet}$ and $O_2^{-\bullet}$ promoting the degradation of cells by lipid oxidation and disrupting the membrane of microorganisms [20].

To optimize the photocatalytic action of the $TiO_2$ can be dopped with metallic oxide or semiconductor (such as CdS, ZnO, CuO, and $SnO_2$) and changes by heterojunction [21]. The heterojunction occurs when combining two sections of different semiconductors with differentiated band conforming, producing an interfacial band arrangement. The heterojunction can be constructed with semiconductors, carbon nanostructures and metallic nanoparticles (NPs), to ensure efficient photocatalytic energy transfer [22, 23].

Silver (Ag) is a monovalent noble metal with higher electrical and thermal conductivity than other metals, high ductility and malleability [24]. Ag has been used as a doping agent for $TiO_2$ since 1984 [25] and it improves the physical chemistry characteristics of this pure oxide and can be applied in antibacterials, self-cleaning agents and water and air purification [26]. The combination of the characteristics of compounds such as $TiO_2$ and Ag has attracted interest, since this combination causes some changes in the ceramic and semiconductor matrix of $TiO_2$ [27, 28]. The doping of Ag in $TiO_2$ increases the photocatalytic action being attributed to the formation of a Schottky barrier at the $Ag/TiO_2$ interface, thus reducing the $e^-/h^+$ recombination. Furthermore, Ag acts as an electron trap and extends the light capture of $TiO_2$ to visible light due to the surface plasmon resonance of Ag and improves the bactericidal performance of $TiO_2$. The addition of Ag results in smaller particle sizes, larger surface areas, and an increase in oxygen vacancies in the $TiO_2$ matrix [21 - 23]. The $Ag/TiO_2$ photocatalyst is

promising and has upper photocatalytic performance in the degradation of various pollutants compared to pure $TiO_2$ [29 – 36].

The Methodi Ordinatio bibliometric analysis is a new systematic review methodology that facilitates research work by classifying articles using their publication year, number of citations, and impact factor. It uses bibliographic databases, for example Scopus and Web of Science, along with reference management, citing as examples Mendeley and JabRef [37]. However, there is a gap in the literature regarding a comprehensive bibliographic review that, based on relevant articles throughout history, describes the use of $Ag/TiO_2$ NPs to degrade emerging pollutants by photocatalysis [38]. A substantial body of research has been conducted to elucidate the influence of Ag doping on the photoactivity of $TiO_2$; however, there has been a paucity of studies examining the impact of the synthesis route or method on the photocatalytic activity of the $Ag/TiO_2$ catalyst [39]. Methodi Ordinatio is effective in identifying the most relevant literature in their respective fields, making it possible to build broad research portfolios and gain insights into current trends and developments [38].

Therefore, this review proposes a bibliometric analysis that elucidates global research trends, gaps, and hot topics on contaminant degradation using $Ag/TiO_2$ NPs and their efficiency in treating emerging pollutants. Furthermore, it seeks to analyze the advantages and limitations of different synthesis techniques and their properties to produce $Ag/TiO_2$ NPs. Finally, this review aims to verify the application of $Ag/TiO_2$ NPs, obtained via doping by different methods, in contaminant degradation, focusing on their efficiency in photodegradation of emerging pollutants.

The article's schematic summary, presented in **Figure 1**, outlines the synthesis methods of Ag/$TiO_2$ and the associated reaction parameters, as well as the photodegradation mechanism of emerging pollutants.

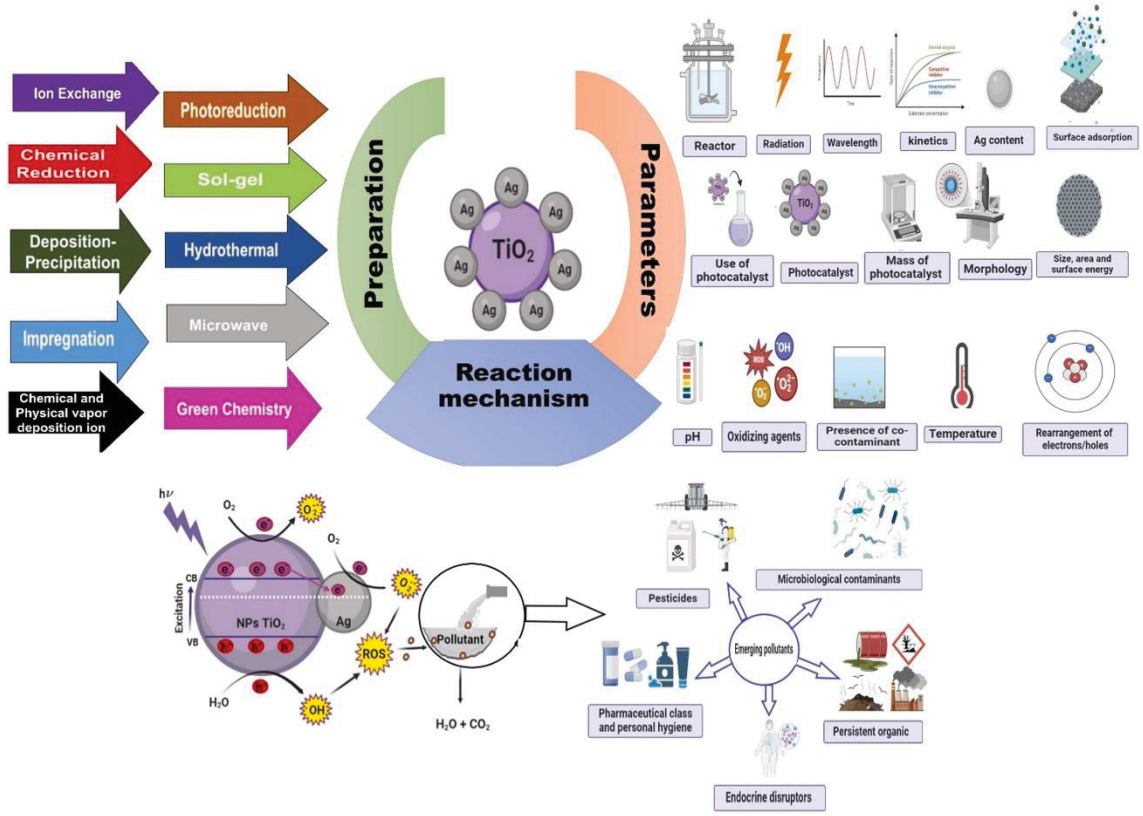


**Fig. 1.** Schematic summary of the Ag/$TiO_2$ synthesis methods, the reaction parameters and the photodegradation mechanism of emerging pollutants.

## 2. Bibliometric analysis

A bibliometric analysis was performed using the Methodi Ordinatio [37] to assess the relevance of the articles used in this review. The importance of the article was determined by the InOrdinatio equation, which considers the number of citations of the published article, year of research, and impact factor of the journal where it was published, according to equation (1):

$$InOrdinatio = \left\{(\Delta * IF) - \left[\lambda * \left(\frac{ResearchYear - PubYear}{HalfLife}\right)\right] + \Omega * \frac{\sum Ci}{[(ResearchYear + 1) - PubYear]}\right\} \quad (1)$$

Where, according Pagani *et. al.* (2022): IF mean Impact factor and is the journal metrics selected (JCR, CiteScore, SNIP, or SJR SCImago); $\Delta$ is a value

between 1 to 10 attributed by researcher, the closer to 10, the higher is the importance of the impact factor; $\lambda$ is the value between 0 and 10 that the researcher assigns to the relevance of the year of publication; Ω is the value between 0 and 10 that the researcher assigns to the importance of the publication's annual average of citations *ResearchYear* is the year the research is being done; *PublishYear* is the year the paper was published; $\sum Ci$ is the total number of citations found in Google scholar; and *HalfLife* is median cited Half-Life of journals with JCR 2020.

Methodi Ordinatio classified 267 articles, and the InOrdinatio value ranged from -4.55 to 7493.99, when we used 10, 5, and 8 for $\Delta$, $\lambda$, and Ω values, respectively. It was chosen to use 150 first articles, with InOrdinatio 149.45 as a cutoff score, up to its maximum value.

The most relevant keywords were: $TiO_2$, photocatalytic, visible light, $Ag/TiO_2$, photocatalyst, photocatalytic degradation, photocatalytic activity, photocatalysis, water, and green (**Figure 2**).

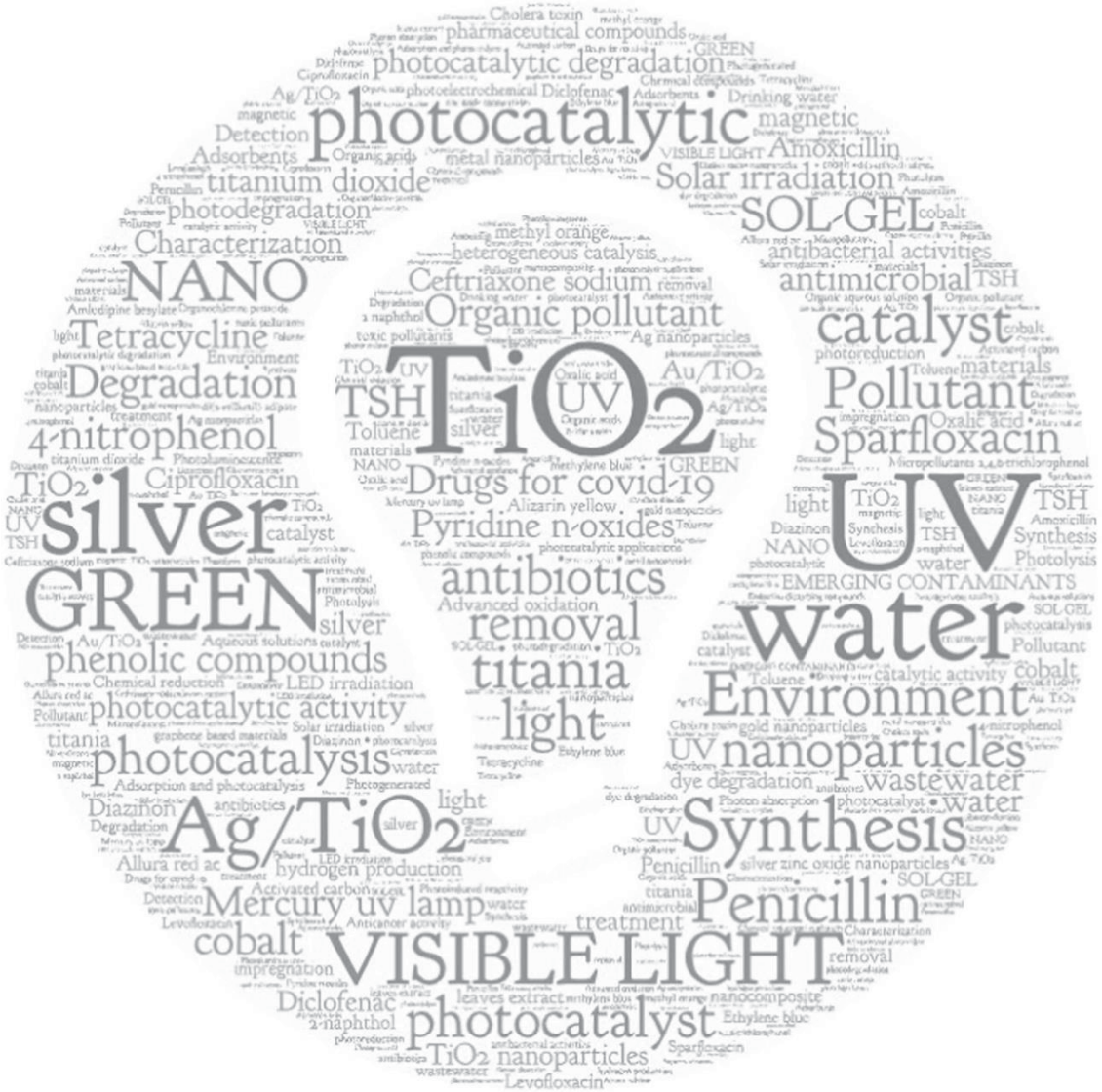


**Fig. 2.** Search's word cloud.

The journal that most published articles of relevance was the Chemical Engineering Journal, which contains 11 of the 126 publications; in second place is Chemosphere with 6 articles, and in third place are the newspapers with five articles each: Journal of Colloid and Interface Science, Chemical Reviews, and Applied Catalysis B: Environmental. In the **Figure 3**, it is possible to see which newspapers had more than two relevant publications. However, 53 of the 150 articles were published in 53 different journals.

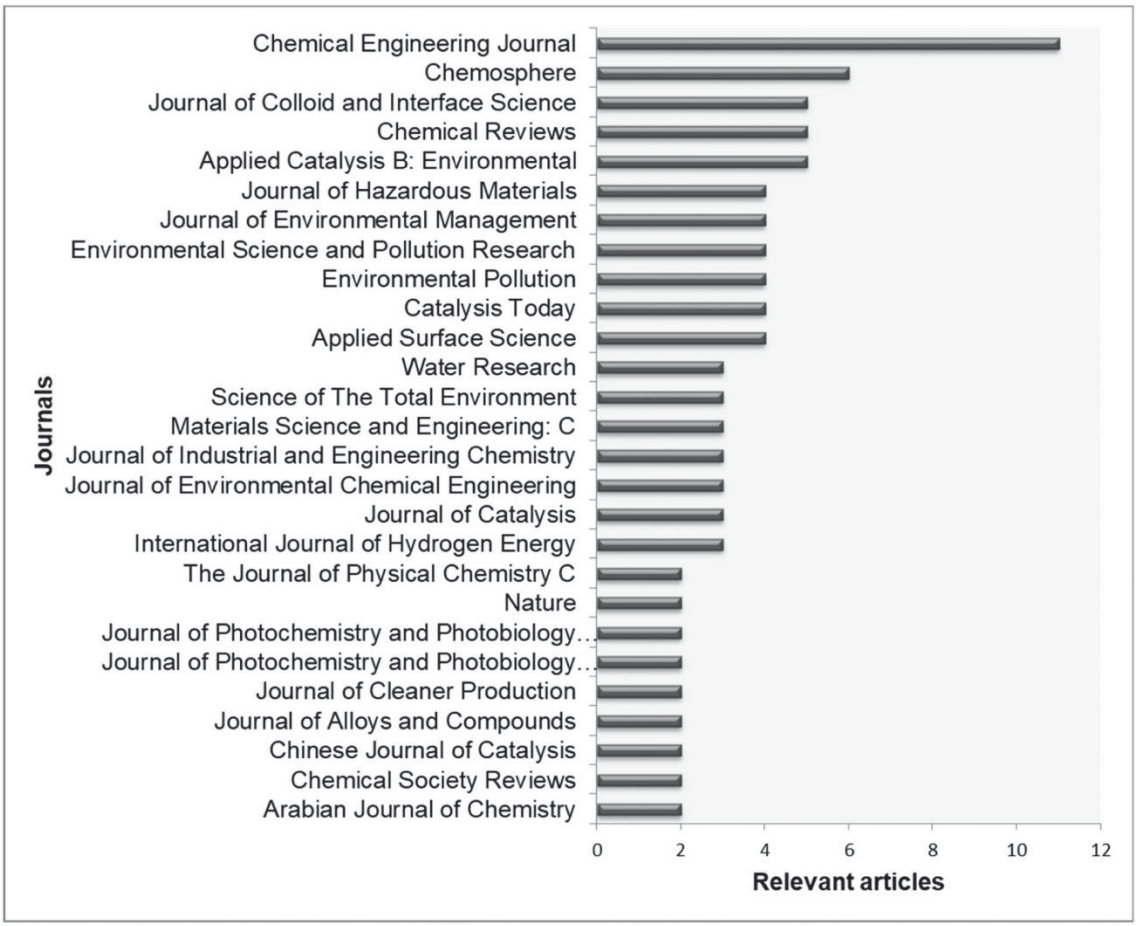


**Fig. 3.** Relevant publications X journals.

Another relevant bibliometric analysis is about the years of publication of the more significant in Methodi Ordinatio articles, 35% of the publications are concentrated between 2019 and 2021 (**Figure 4**). Furthermore, pioneering publications such as Fujishima and Honda (1972) and Lee and Aris (1985) remain traditional and highly cited [15, 39].

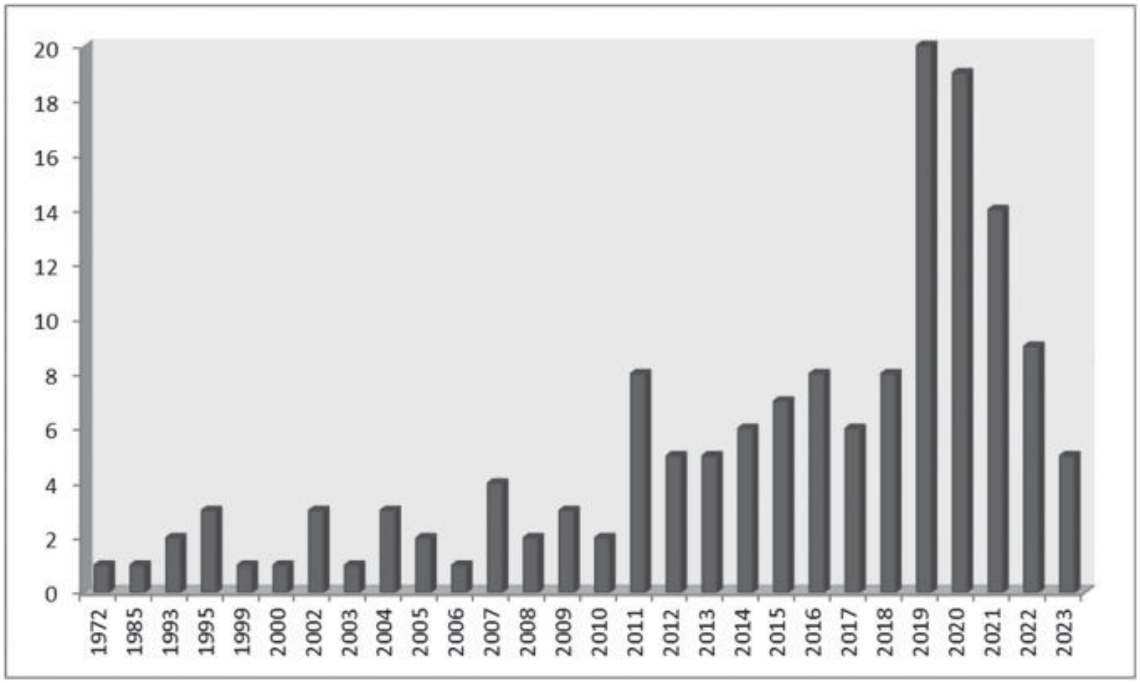


**Fig. 4.** Relevant publications X Published Year.

Bibliometric analysis of a subject is critical in research and academia, as it offers valuable insights into the relevance and impact of a particular area of study. By performing this analysis, it is possible to obtain quantitative information about the scientific production related to the topic, such as the number of publications, most cited authors, relevant journals, and trends over time. The Methodi Ordinatio is an efficient method of evaluating the articles found attractive to the chosen topic, as it classifies them in a ranking of relevance.

With this bibliometric analysis, it was possible to identify trends and research advances about the degradation of contaminants using Ag/$TiO_2$ NPs and their efficiency in degrading emerging pollutants. In addition, it was possible to identify a gap: a comprehensive bibliographic review that, based on relevant articles throughout history, described the use of these nanomaterials to degrade emerging pollutants by photocatalysis.

## 3. Emerging pollutants

Emerging pollutants can be defined as chemical products that have unknown environmental impacts, are not controlled, can reach diverse aquatic environmental niches on a global scale, are found in concentrations of the order of µg/L and ng/L, and there is a lack of studies on their toxic impacts [40, 41].

Emerging pollutants have harmful effects on aquatic species, and humans are resistant, complex, unstable and/or lipophilic micropollutants [42 - 44]. It is indicated that there are more than 60 million inorganic and organic compounds, 49 million of which are commercially available, and less than 1% are related or regulated. In fact, 12,000 new combinations are generated daily [45].

The sources of pollutants can be caused by the release of effluents, urban and industrial, without proper treatment in aquatic environments [46]. The contamination sources are subdivided into punctual, characterized by the easy identification of the origin of the release points (for example, wastewater and mining) and in non-specific, identified by the lack of specification of topics (such as rainwater and agricultural applications) [35]. Wastewater treatment plants can be the primary source of emerging pollutants, it happens in places where treatment is not carried out correctly, and waste removal is not practical [47].

Among the main sources of water pollution are: anionic and cationic dyes, organic substances, metal ions and bacteria, pharmaceuticals, and personal care products [48]. Emerging pollutants include persistent organic contaminants, pharmaceutical and personal care products, class of endocrine disruptors, and class of agricultural chemicals (**Figure 5**). They are delimited according to their intended purpose and origin, accelerating the verification of their existence and the techniques for their removal [49].

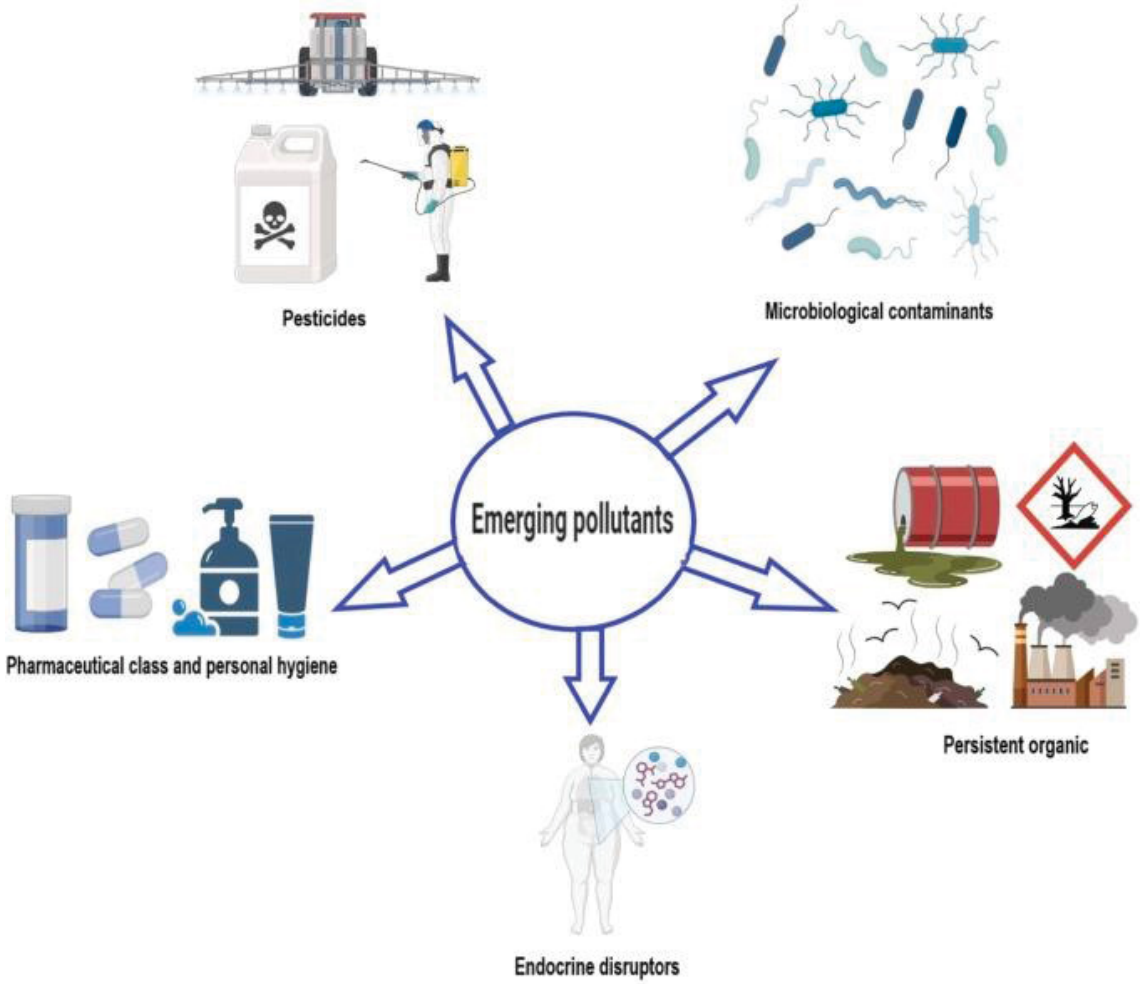


**Fig. 5.** The term "Emerging pollutants" encompasses a diverse range of chemical substances, including persistent organic contaminants, pharmaceutical and personal care products, endocrine disruptors, and agricultural chemicals.

Persistent organic contaminants are difficult to degrade and remove, comprising a vast portion of organic substances, such as polychlorinated benzenes, aromatic hydrocarbons, fuel oils, gasoline, and others, used in power transformers and in the manufacture of paints [49]. Organic dyes are toxic, carcinogenic to humans and aquatic species and are not naturally decomposed [49 - 51]. Industries and pharmaceutical companies use dyes, and the high concentrations present in their effluents end up in bodies of water [52].

Due to the lack of proper observation and regulation, the pharmaceutical class and personal hygiene are widespread in almost all aquatic ecosystems [53]. Pharmaceutical substances can cause overdoses and endocrine disruption from exposure to a synergistic combination of these substances, which is harmful to human health [50]. Most of these contaminants are used in an uncontrolled way

on a daily basis; for example, the antibiotics used against bacterial infections are not completely metabolized by the human body, are excreted via urine, and end up in the water in an unmodified form in 95% of consumption. An increase of 67% in the consumption of antibiotics across the planet is estimated by 2030 [54]. It is estimated that around 250 different antibiotics are used as human and veterinary drugs [55].

The endocrine disruptors influence the human endocrine system, formed by a set of glands. These secrete essential hormones that act as chemical signals, whose purpose is to regulate various organs. This class uses mechanisms to influence the endocrine system, such as the mimicry that some chemical compounds have simulating the hormonal structure. Therefore, they are noticed as hormones by the receptor regions of the human body; among them are the androgen, aryl hydrocarbons, and estrogen receptors. Furthermore, they interact with binding proteins and may modify hormonal metabolism [49]. The connection between exposure to endocrine disruptors, the reduced number of spermatozoa, and the increase in infertility occur due to the action of androgens within the transduced cells [56].

Microbiological contaminants, involving bacteria, protozoa, fungi, viruses, and others, are found in untreated domestic water that include fecal material and various biodegradable compounds. Their proliferation is facilitated thanks to access to food and the environment for growth, causing the spread of a variety of diseases. The bacteria *Escherichia coli* is the most commonly observed in water containing fecal material, causing diarrhea and kidney failure, and some strains are related to colitis [57] Salmonella causes typhoid fever and salmonellosis [58], while *Vibrio cholera* causes cholera [59].

Organochlorine pesticides can be found in aquatic environments and sediments, having severe health impacts. It is pointed out that cancer risk indices indicate danger for the consumption of fish from various surface water [60].

Heavy metals (cadmium, lead, mercury, and others) have a high atomic mass and a density more than water's and are used in various industries, electroplating, steel manufacturing, and metal processing due to their lower reactivity and strength [60, 61]. Toxic metals can accumulate in ecosystems and crops, their degradation by biological methods is difficult, and they can harm various human organs, causing mutations and diseases [62 - 64]. They affect

plants grown on land whose constitution contains heavy metals, as they hinder the assimilation of nutrients, causing a decline in productivity [65].

Some of the main and most established methods for detecting and quantifying emerging pollutants are based on chromatography (gas or liquid) coupled with sequential mass spectrometry. These methods have shown excellent results in detecting trace concentrations (below μg $L^{-1}$) of these products in water samples, as they have high sensitivity, specificity, and selectivity [66]. Other analytical methods have been used, such as capillary electrophoresis, fluoroimmunoassay, electroanalytical and microbiological tests [67].

## 4. Photocatalysis and the degradation of emerging pollutants

Conventional wastewater treatment techniques are not efficient in degrading emerging contaminants such as pharmaceuticals and heavy metals from water bodies. Therefore, developing an effective and economical process to degrade these contaminants is relevant [68]. In this situation, the AOPs, which involves the oxidation of substances from their interaction with free radicals, causes the degradation of pollutants [69].

AOPs, there are photocatalytic processes that are widely used in the degradation of contaminants thanks to their low investment, ecological character, and high efficiency [69 - 71]. $TiO_2$ based photocatalysis has shown promise in the degradation of pharmaceutical pollutants, with one study achieving 87.95% removal of ciprofloxacin at an operational cost of 786.56 INR (the Indian rupee)/Kg [72]. Green production method for $TiO_2$ NPs via anodic dissolution was estimated to have an operating cost of 30.5 USD/Kg [73]. Comparing the photocatalytic efficiency of commercial $TiO_2$ Anjatox with Degussa P-25, similar degradation efficiencies but significantly lower costs were found for Anjatox (110 INR/Kg vs. 1000 INR/Kg) [74]. A techno-economic evaluation of various AOPs for textile wastewater treatment concluded that UV/$TiO_2$ photocatalysis is the most promising and cost-effective method, requiring 10.79 kWh/$m^3$/application for COD removal at a cost of 0.77 USD/$m^3$ [75].

Heterogeneous AOPs using transition metal-based catalysts have shown higher kinetics and less sludge generation compared to homogeneous AOPs [76]. However, other studies report different findings, with Fenton-based AOPs being

the most energy efficient, with a median electrical energy per order of 0.98 kWh/$m^3$/application, followed by ozonation with 3.34 kWh/$m^3$/application and photocatalysis 91 kWh/$m^3$/application [77]. The studies collectively emphasize the importance of considering multiple factors, including energy efficiency, cost, and treatment effectiveness, when selecting an AOPs for wastewater treatment.

Photocatalysis is an efficient and low-impact method to remove organic contaminants and non-biodegradable substances from bodies of water, such as pesticides, halophenols, drugs, humic acid, and herbicides [77 - 79]. Other pollutants, such as polychlorinated bisphenols, phenol, organophosphates, and organochlorine substances, are effectively degraded using metal-doped $TiO_2$ photocatalysts in photocatalysis [80].

Photocatalysis is subdivided into heterogeneous, which encompasses reactions where the catalyst is in a different phase from the reaction solution, and homogeneous, which occurs when both are in the same phase. It is an environmentally correct, sustainable, economical technique and can be established in any location [80, 81].

It is used in the generation of hydrogen from the fractionation of water, treatment of bodies of water and in non-fouling parts used in filtration membranes [82, 83]. And yet, in lignin rupture [84], nullify harmful impacts of environmental contaminants [85] self-cleaning areas [34], pathogen inactivation [86] and water and air purification set and water and air purification set [87].

The principle of heterogeneous photocatalysis is based on the absorption of a photon by a semiconductor, such as $TiO_2$, which causes the excitation of the electron from the valence band to the conduction band, that is, the electron jumps from the ground state to the excited one, producing the pair $e^-/h^+$. Then, separate migration of the $e^-/h^+$ pairs to the $TiO_2$ surface occurs, and they engage in a cascade of oxidation/reduction reactions with adsorbed agents, such as $H_2O$ and $O_2$, to ROS [87, 88]. These then react with adsorbed organic substances or existing microorganisms on the surface of the semiconductor, thus causing its degradation into completely mineralized compounds, such as $H_2O$ and $CO_2$ [89].

The photo-produced electrons and holes have a reduced lifetime, which allows for a rapid rearrangement of them on the $TiO_2$ surface, causing a decrease in their photocatalytic activities [90]. Thus, noble metals can stop the newly produced electrons and provide other reactions generating peroxide and hydroxyl

radicals ($^{\bullet}OH$). In the conduction band, peroxide radicals are formed from the interaction of free electrons and $O_2^{\bullet}$ in the presence of $H_2O$. In the valence band, from the interaction of $H_2O$ and $O_2$, the $^{\bullet}OH$ are formed. Hydroxyl and peroxide radicals react with pollutants and micropollutants, thus causing their degradation [91, 92].

The reaction mechanisms of photocatalytic processes are described in detail in Equation (2) Photoexcitation; (3) $e^-/h^+$ recombination; (4) Reaction between the valence band gap and adsorbed water; (5) Reaction between the valence band gap and the $OH^-$ groups on the $TiO_2$ particle surface; (6) Production of superoxide anion radical; (7) – (10) Generation of hydrogen peroxide; (11) and (12) Generation of hydroxyl radicals by the breakdown of hydrogen peroxide; (13) - (15) Enhancer Ag and (16) Degradation processes.

$$TiO_2 + h\nu \rightarrow e^-_{CB} + h^+_{VB} \quad (2)$$

$$e^-_{CB} + h^+_{VB} \rightarrow \text{Energy} \quad (3)$$

$$h^+_{VB} + H_2O \rightarrow {}^{\bullet}OH + H^+ \quad (4)$$

$$OH^- + h^+_{VB} \rightarrow OH^{\bullet} \quad (5)$$

$$e^-_{CB} + O_2 \rightarrow {}^{\bullet}O_2^- \quad (6)$$

$$O_2^{\bullet-} + H^+ \rightarrow HO_2^{\bullet} \quad (7)$$

$$2\ HO_2^{\bullet} \rightarrow O_2 + H_2O_2 \quad (8)$$

$$O_2^{\bullet-} + HO_2^{\bullet} \rightarrow HO_2^- + O_2 \quad (9)$$

$$HO_2^- + H^+ \rightarrow H_2O_2 \quad (10)$$

$$H_2O_2 + e^-_{CB} \rightarrow OH^{\bullet} + OH^- \quad (11)$$

$$H_2O_2 + O_2^{\bullet-} \rightarrow OH^{\bullet} + OH^- + O_2 \quad (12)$$

$$Ag^+ + e^-_{CB}\ (TiO_2) \rightarrow Ag^- + TiO_2 \quad (13)$$

$$Ag^- + O_2 \rightarrow Ag + O^{2-} \quad (14)$$

$$O^{2-} + e^-_{CB}\ (TiO_2) + H^+ \rightarrow TiO_2 + H_2O_2 \quad (15)$$

$$EP + O_2^{\bullet-}/h^+/\ OH^{\bullet} \rightarrow \text{Intermediaries} \rightarrow CO_2 + H_2O \quad (16)$$

*where* EP: emerging pollutants; VB: valence band; CB: conduction band; $h^+$: photogenerated hole; $e^-$: photogenerated electron; $O_2^-$: oxygen radical; $H_2O_2$: hydrogen peroxide; $OH^-$: hydroxyl radical; $H_2O$: water; and $H^+$: hydrogen radical [93, 94]. The photoactivation of Ag/$TiO_2$ NPs are illustrated in **Figure 6**.

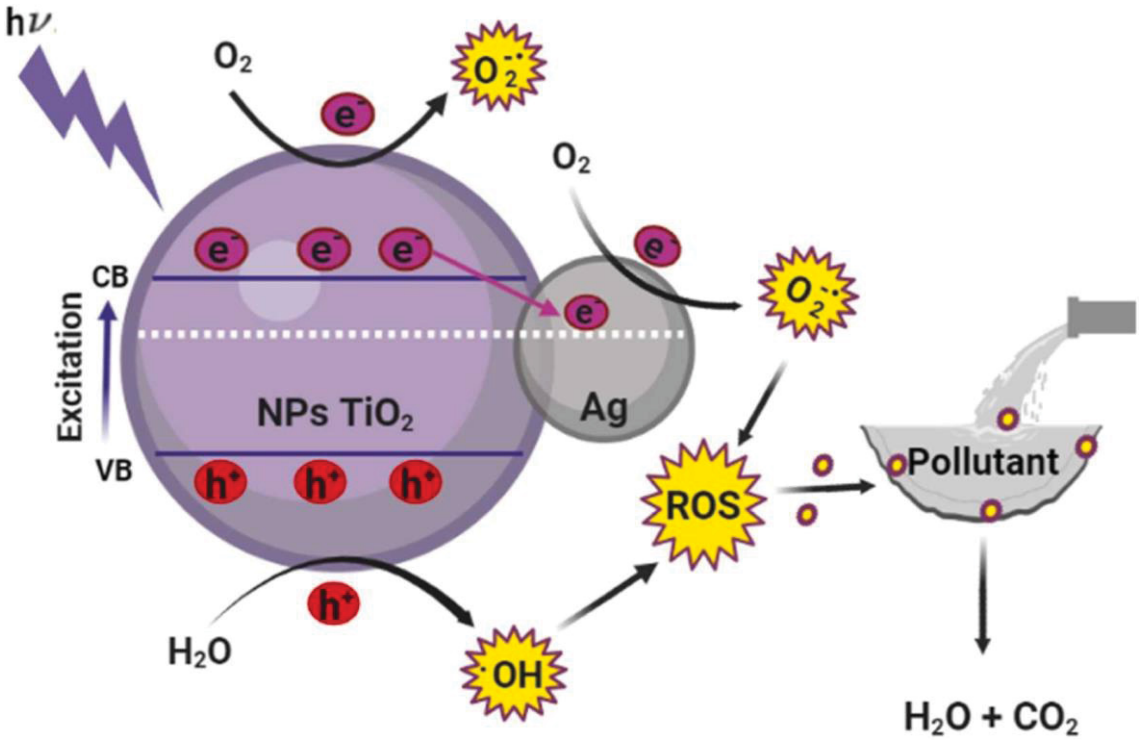


**Fig. 6.** The photoactivation of $TiO_2$ nanoparticles (NPs) excites the electron from the valence band (BV) to the conduction band (CB), producing $e^-/h^+$ pairs. Then, separate migration of the $e^-/h^+$ pairs to the $TiO_2$ surface occurs, which induces a cascade of oxidation/reduction reactions with $H_2O$ and $O_2$, producing ROS. These react with emerging pollutants that degrade them into $H_2O$ and $CO_2$. Ag captures moving electrons from $TiO_2$ CB and transports them to $O_2$, transforming them into superoxide radicals.

The EPs, which are present in Equation 16, represent five subclasses, among which are the dyes. Therefore, Equations 17 - 19 present the reactions on the $TiO_2$ surface that result in the degradation of this subclass [95]:

$$\text{Dye} + OH^{\bullet} \rightarrow \text{Degradation product} \quad (17)$$

$$\text{Dye} + h^+_{VB} \rightarrow \text{Oxidation product} \quad (18)$$

$$Dye + e^-_{CB} \rightarrow \text{Reduction product} \quad (19)$$

The $OH^\bullet$ radical, which is produced as a result of this process, is a highly potent oxidant that is capable of oxidizing a multitude of dyes. Consequently, photosensitized oxidation can occur as a result of the excitation of the dye by visible light (in contrast to UV radiation) and its subsequent interaction with the semiconductor. The process of photosensitized oxidation can be initiated by the oxidation of the dye, which then interacts with the semiconductor (Equations 20-26).

$$Dye + h\nu \rightarrow Dye^\bullet \quad (20)$$

$$Dye^\bullet + TiO_2 \rightarrow Dye^{+\bullet} + TiO_2^{-\bullet} \quad (21)$$

$$TiO_2^{-\bullet} + O_2 \rightarrow TiO_2 + O_2^{-\bullet} \quad (22)$$

$$O_2^{-\bullet} + 2H^+ \rightarrow H_2O_2 \quad (23)$$

$$H_2O_2 + TiO_2^{-\bullet} \rightarrow TiO_2 + OH^\bullet + OH^- \quad (24)$$

$$Dye^{+\bullet} + O_2\,(O_2^{-\bullet} \text{ or } OH^\bullet) \rightarrow \text{Peroxylated or intermediates} \quad (25)$$

$$\text{Hydroxylated} \rightarrow \text{degraded or mineralized products} \quad (26)$$

Regarding the subclass of drugs, antibiotics were used to exemplify the decomposition mechanism, such as ciprofloxacin (CIP) and norfloxacin (NFX), belonging to the fluoroquinolone family, to investigate, under visible light irradiation, the commercial $TiO_2$ P25 and $Ag/TiO_2$ catalysts. The concentration of CIP and NFX did not undergo a notable change significantly under visible light in the absence of the photocatalyst, indicating that photolysis was an insignificant factor. The degradation of CIP and NFX occurred for both catalysts, but was more rapid in the presence of $Ag/TiO_2$, with a reduction of 92% and 94% after 240 min of irradiation, respectively. This catalyst presented a degradation rate constant for CIP and NFX of 2.1 times and 1.7 times higher than for $TiO_2$ P25. This high photocatalytic activity under visible light may be due to the optical characteristics induced by Ag NPs distributed on the $TiO_2$ surface. CIP was selected as a model for the photocatalytic mechanism of $Ag/TiO_2$ under visible light irradiation. Scavenger experiments were performed to determine which ROS were involved in the photocatalytic degradation process. EDTA, a scavenger for $h^+$, and

isopropanol, a scavenger for $OH^{\bullet}$, significantly inhibited the degradation of CIP. Conversely, the addition of $AgNO_3$, a scavenger for $e^-$, resulted in a negligible change in the photocatalytic degradation of CIP. It was thus determined that $H^+$ and $OH^{\bullet}$ are the primary reactive oxygen species (ROS) generated by $Ag/TiO_2$ under visible light. The incorporation of Ag NPs into $TiO_2$ P25 enhances the photocatalytic activity under visible light, which can be attributed to the improved separation of $e^-/h^+$ pairs. Therefore, when $Ag/TiO_2$ is irradiated, the rutile phase of $TiO_2$ activates the $e^-$ that can be transferred to Ag NPs and to the anatase phase. The Ag clusters present on the $TiO_2$ surface serve as electron traps, thereby preventing the recombination of $e^-/h^+$ pairs (**Figure 7**) [96].

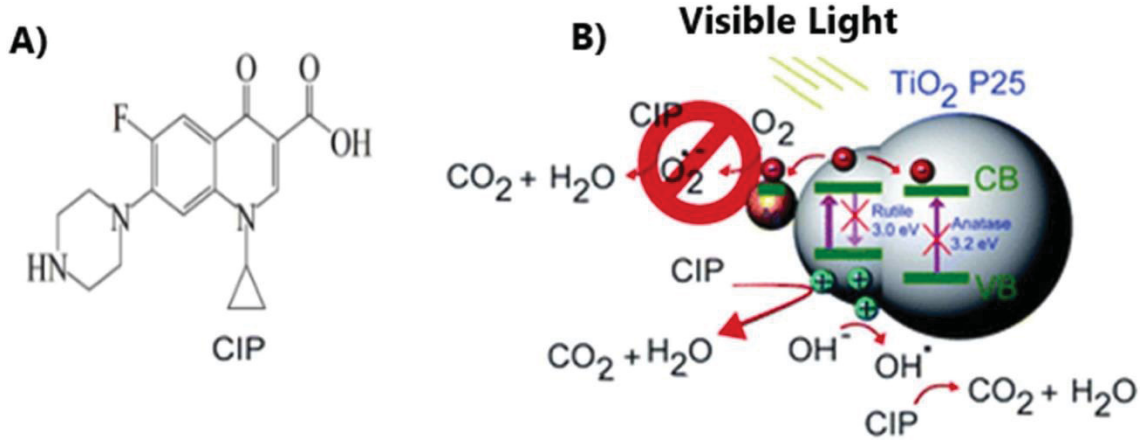


**Fig. 7.** (A) The chemical structure of CIP; (B) A schematic of the photodegradation mechanism of $Ag/TiO_2$ under visible light for CIP [96].

It is noted that $OH^{\bullet}$ radicals are the main active species in the degradation of dyes instead of holes and superoxide radicals. The degradation of CIP due to $O_2^{-\bullet}$ radicals was negligible. The importance of investigating the photocatalytic mechanism for each pollutant and catalyst used under specific conditions, as observed in reference [96].

The polluting compounds adsorbed on the surface of the photocatalyst are spontaneously attacked by ROS and cause their mineralization. Also, repeated operating phases contribute to increasing the photocatalyst's efficiency. Several methods are used to identify the by-products and their reaction media, thus comprising the photocatalytic method at a molecular level. Mention is made of absorption spectra that assess the degradation process, total chemical oxygen demand, and total or partial organic carbon that monitor the complete mineralization of contaminants [97].

Thus, photocatalysis has the benefits of using low-energy UV light, semiconductors that act as photocatalysts, and the total degradation of organic compounds into environmentally safe substances. Photocatalytic methods allow thermodynamically disadvantageous interactions to occur, thus leading to the degradation of resistant contaminants [98].

Therefore, when comparing the varying energy efficiencies and costs between AOPs and electrocoagulation for industrial wastewater treatment, it was observed that electrocoagulation was found to be more energy efficient, at >100 kWh/m³, than photocatalysis at <0.01 kWh/m³ for dye removal [99]. The efficiency of photocatalytic degradation of $TiO_2$ NPs depends on the pollutant composition, so more stable substances are more difficult to remove and consume more energy, for example 4-nitrophenol with 72.27 kWh/m³ [100]. Photocatalytic treatment combining UV light, $TiO_2$ and $H_2O_2$ showed promising results for several phenolic compounds, with energy consumption ranging from 52-248 kWh/m³/order [101]. Among various AOPs, electro-Fenton was identified as the most economical (108 – 125 €/m³) for phenol removal, regardless of the mineralization target. The cumulative oxygen equivalent chemical oxidation dose was proposed as a new classifier for systematic comparison of AOPs [102]. In the treatment of hospital wastewater, UV irradiation with $H_2O_2$ as an AOP effectively removes persistent pharmaceuticals, with low-pressure UV lamps proving more cost-effective [103].

Photocatalytic reactors containing $TiO_2$ supported on granular activated carbon removed 100% of total volatile solids (TVS) in 6 min, with a total operating cost of USD 0.68 per kg of TVS removal. The continuous process (at 60 mL/min) removed 63% of TVS in a hydraulic retention time of 240 min and cost USD 62.16 per kg of TVS removal. Economic analyses showed that the cost reduction was due to the optimal time spent for maximum removal efficiency. Therefore, photocatalysis can be economically applied to wastewater treatment [104].

Integrated systems combining electrocoagulation with AOPs show promise, with electrocoagulation/ozonation achieving complete decolorization and 99.7% chemical oxygen demand (COD) removal, while electrocoagulation/photo-Fenton resulted in 95.6% COD and 97% color removal [105]. For landfill leachate, a sono-ozone-electrocoagulation process achieved 100% color removal and 97.5% COD removal [106]. Ozonation and Fenton reactions are commonly evaluated for their economic viability in the treatment of various pollutants, including phenols, glycols,

and humic acids [107]. When evaluating commercial $TiO_2$ photocatalysts for air purification, both activity and cost should be considered using cost-effectiveness analysis [108]. These findings highlight the importance of considering multiple factors when evaluating pollutant removal technologies. Integrated systems offer the potential for efficient wastewater treatment. It is important to consider both treatment efficiency and energy consumption when selecting optimal technologies for specific applications.

The constitution of photocatalysts ranges from metallic oxides, organic polymers, and hybrid elements [109]. Metallic oxides, such as $TiO_2$, $SiO_2$, ZnO, $MoS_2$, $Fe_2O_3$, $WO_3$, especially in nanometric proportions, are the most used in heterogeneous photocatalysis [105, 106]. The proportion of these NPs has improved physical-chemical properties, such as nanometer size, high surface/mass/volume fraction, and superior chemical reactivity, which can generate more significant antimicrobial inhibition, greater mass transfer speed, and excellent mechanical and thermal stability [107, 108].

Of the various semiconductors used in photocatalytic techniques, for the degradation of several chemical species of environmental relevance is $TiO_2$. This oxide is constituted by titanium (Ti), the ninth most abundant chemical element in the earth's crust, found in minerals such as rutile ($TiO_2$) or ilmenite ($FeTiO_3$). Its first mention occurred in 1791 by William Gregor (1761-1817) [27, 109 - 111].

It has three crystalline phases (**Figure 8**): anatase (tetragonal arrangement), rutile (tetragonal arrangement), and brookite (orthorhombic arrangement) [112 - 115]. Rutile has high stability at high temperatures and pressures due to its slow phase conversion at room temperature. On the other hand, Anatase is stable under environmental conditions and under light radiation, enabling high applicability, which is also linked to its cost, chemical and biological inertia, photocatalytic efficiency, and toxicity [116]. Thus, anatase is the one that has the highest active photocatalytic activity compared to rutile and brookite [117].

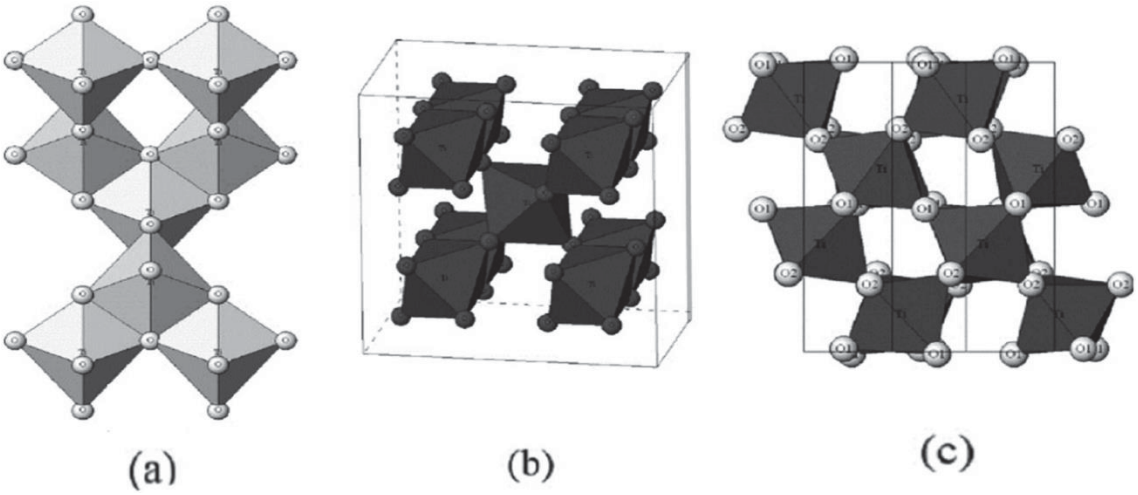


**Fig. 8.** Crystalline structures of titanium dioxide (a) anatase, (b) rutile, (c) brookite [118].

It is essential in photocatalysis to choose and design the best process, considering environmental impacts and easy recovery. There are products arising from photocatalytic degradation, such as dehalogenation (slow technique), hydroxylation, oxidation of the alkaline chain, isomerization and cyclization, opening of an aromatic ring, and decarboxylation [118].

## *5.* Factors that affect performance in the degradation of emerging pollutants

Some experimental factors govern the heterogeneous photocatalysis system and interfere decisively with the degradation efficiency of the pollutants. Among the system parameters that affect the efficiency of photocatalysis are: (1) use of photocatalyst, (2) photocatalyst (3) mass of photocatalyst used, (4) morphology, (5) reactor and its operational factors, (6) radiation applied to excite the photocatalyst, (7) wavelength, (8) kinetics, (9) pH, (10) presence of oxidizing agents, (11) presence of co-contaminant, (12) temperature, (13) surface adsorption, (14) rearrangement of electrons/holes, (15) size, area and surface energy, and (16) Ag content [119]. The factors affecting the performance in the degradation of emerging pollutants, are represented in **Figure 9**.

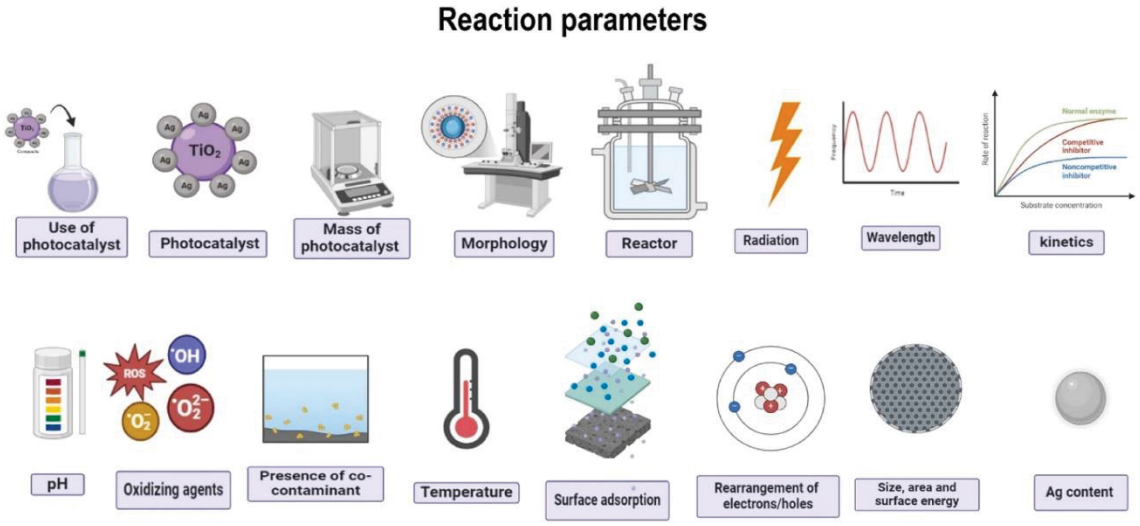


**Fig. 9.** The factors affecting the performance in the degradation of emerging pollutants.

It is necessary to determine (1) how the photocatalyst will be used, that is, in aqueous suspension or stabilized on a substrate. The suspension allows higher levels of degradation. However, it requires a separation phase, such as filtration, increasing the complexity and rates of the process [120].

Another important factor in the heterogeneous photocatalysis technique are the (2) photocatalysts since they are responsible for the performance of the reaction processes of this technique [121]. Therefore, an excellent performance of the photocatalyst is linked to an excellent absorption of light, with appropriate photoproduction of charge carriers, with low rearrangement and adequate levels of valence bands. It is also pointed out, high physical, biological, and chemical stability, being non-toxic and economical [122].

The effect of the photocatalyst (3) mass on the photocatalytic degradation influences the initial rate of the reaction, as it increases proportionally with the increase in the photocatalyst mass up to a certain limit, corresponding to the entire absorption of photons [118, 119]. However, above a certain amount of photocatalyst mass, the efficiency of the system will be independent this limit depends on the geometry and operational variables of the reactor. That is, a saturated amount of photocatalyst allows the particles present on the surface to be completely irradiated. When the quantity is supersaturated, there is a filtering or scattering effect of radiation due to the excess of particles [123, 124].

$TiO_2$ morphologies (4) play an essential role in photocatalytic activity. The adaptation of the facets is a strategy used to modify the photocatalyst, which can increase the photocatalytic action and the selectivity to remove emerging pollutants. Thus, numerous factors can be adjusted due to facet change to optimize the removal of contaminants, such as band structure, reagent adsorption, and desorption, surface free energy, redox point and charge change segregation. Several conformations of crystalline facets of $TiO_2$ influence the absorption of light and the redox potential of separation of excited $e^-/h^+$ pairs, thus modifying the photocatalytic action [125].

The heterogeneous photocatalysis technique takes place in a set formed by a light source and (5) reactor, where the photocatalyst is placed in polluted wate [126]. The reactor is used at room temperature and atmospheric pressure, under continuous irradiation and agitation, thus expanding the area of interaction between photocatalyst, substrate and light [127]. (5) Operational factors such as solvent, light power, temperature, substrate profile, concentration, and pH are essential for the technique. Oscillations of these factors influence the reaction dynamics of the photocatalyst and substrate, thus affecting the photocatalytic action [123, 124].

Thus, the amount of $TiO_2$ photocatalyst strongly influences the photocatalytic action, interfering with the depth of light penetration and grouping of NPs, limiting photocatalysis (6) [128 - 130]. A high amount of $TiO_2$ photocatalyst provides a more agile surface area to react with target contaminants. However, supersaturation of the photocatalyst, above 1 g/L, can cause an agglomeration of $TiO_2$ particles, making it difficult for light to penetrate and reducing the photocatalytic action [131]. The reaction rate can be increased by the amount of catalyst, thanks to the enlargement of the area $Ag/TiO_2$ surface exposed to light, however, if the amount of the photo catalyst is supersaturated the reaction may be impaired due to non-permeation of radiation [132].

The degree of degradation of a photocatalytic system that has a photocatalyst is proportional to the amount of radiation (6) incident on the surface. However, radiation transfer needs some factors, such as the reactor properties (geometry and composition), that influence the interaction of photons with the photocatalyst. Another factor is the reaction turbidity that can reduce the arrival of photons to the photocatalytic surface. The type of fixed bed employed is a factor

that can reduce radiation permeation. The period of exposure of the photocatalyst to radiation is linked to its residence time in suspension in the reaction medium. And yet, the applied lamp influences the degradation process, as it interferes with the effective amount of photons irradiated with the wavelength of interest [133].

Photocatalysis depends on the wavelength used, which is correlated with the absorbance range (7) of the photocatalyst. To electronically excite a semiconductor, radiation with a wavelength close to 384 nm (UV-UVA) is required. For maximum efficiency of this factor, it is important that other species present do not absorb radiation, which is directed to the photoactivation of the catalyst [129, 130]. For the degradation of emerging contaminants, UV light irradiation, between 10 and 400 nm, is more effective than visible light [134 - 136]. Thus, the photocatalytic action is linearly related to the light intensity. When the light intensity is higher, the formation of high-energy photons occurs, which can generate more photoexcited $e^-/h^+$ pairs and consequently more ROS in the system [137].

Photocatalytic degradation of pollutants follows Langmuir–Hinshelwood kinetics (8), with reaction rates influenced by light intensity and pollutant concentration. This equation models a reaction mechanism in which two parameters coexist, an adsorption pre-equilibrium and a slow surface reaction. However, in practice it is demonstrated that other mechanisms can interfere and that they are important in modeling the system [138]. The manipulation reactions are clearly dependent on light intensity. In many kinetic studies of photocatalytic reactions, it is found that the oxidation rate increases with increasing light intensity in a non-linear relationship. Furthermore, depending on the kinetics of the event, increasing light intensity may increase the rate of the event rapidly or slowly, or not at all, in which case the substrate can no longer generate $e^-/h^+$ pairs [134, 135].

Kinetic parameters, including rate constant (Kr) and apparent adsorption constant (Ks), are dependent on light intensity, with Kr typically increasing and Ks decreasing as intensity increases [139]. At low concentrations, process efficiency is high, but it decreases as pollutant levels increase due to saturation of the catalyst surface. Just to give an example of this issue, and taking into account only the power of the lamp used, this parameter can vary from 8 W to 4 kW. Therefore, the decrease in the concentration of a compound as a function of the irradiation time is not an argument for such a process to be applied in practice. To this end, one must also take into account whether or not it is economically viable, and knowledge

of energy consumption can help in this assessment. To this day, it is difficult to define its real performance, since there is a lack of standardization in the experimental parameters to be evaluated [140, 141]. The relationship between reaction rate and light intensity can vary from first order to half order, depending on the pollutant concentration. Understanding these relationships is crucial to optimizing photocatalytic processes, since the kinetic order in intensity and process economy can depend on the concentration [142].

Another important factor in photocatalysis is pH (9), as photooxidation is followed by proton release, and surface-convertible protonation can modify the effectiveness of the system [143]. The pH of the solution plays a critical role in the removal of emerging pollutants in a photocatalysis system, as it influences the surface charge of contaminants and photocatalysts [138, 139]. The segregation of the $e^-/h^+$ pair and the production of ROS can influence the pH [144, 145].

The effect of the presence of other oxidizing agents (10), such as $H_2O_2$ and $KBrO_3$, in suspensions with the photocatalyst is a factor that increases the reactional level of photooxidation. These agents can interact with photoproduced electrons in the conduction band, acting as an electron acceptor [145]. Furthermore, the existence of cations and anions can affect the degradation activity of emerging pollutants [21]. Thus, a high concentration of multivalent ions is related to high salinity, which may cause synergistic impacts on photocatalytic interactions [146]. It can delay the degradation activity of emerging pollutants by competing with the ROS adsorbed on the surface of the photocatalyst [147].

The presence of co-contaminants (11) can significantly affect $Ag/TiO_2$ composites are effective in treating water contaminated with certain metals and organic compounds, particularly those with standard reduction potentials more positive than 0.3 V. The photocatalytic process demonstrates synergy between the oxidation of organic compounds and the reduction of metals, leading to efficient decontamination of water with appropriate mixtures of pollutants [148]. However, the presence of organic matter and other contaminants in water bodies can impact the photocatalytic efficiency of $TiO_2$-based materials [19]. Dissolved organic matter, particularly humic substances, plays a crucial role in inhibiting the photocatalytic removal of pollutants and estrogenic activity. Inorganic ions such as $H_2PO_4^-$, $NH_4^+$, and $HCO_3^-$ also negatively affect $TiO_2$ photocatalysis due to their strong adsorption on the catalyst surface [149]. Complex mixtures in aqueous

matrices can lead to fouling and inactivation of $TiO_2$ photocatalytic systems, requiring prevention and regeneration methods [150].

Photocatalysis is an endothermic process it is not sensitive to minimal temperature fluctuations, it can take place at room temperature (12), without the need for heating, thanks to the activation of photons, but heat can influence the photochemical reaction. However, the temperature of the reaction set can increase the release of energy during the rearrangement of the $e^-/h^+$ pairs. Above 80 ºC, it approaches the boiling point of water, thus disfavoring the exothermic adsorption of the reagents, becoming limited due to the increase in the rearrangement of $e^-/h^+$. However, between 20 and 80 ºC, the degradation percentage is little influenced by temperature, making it ideal, and the adsorption energy is minimal [146, 147]. It is also noted that in solutions with higher concentrations, the reaction of the target substance with radiation becomes a limiting factor. Degradation usually occurs on the photocatalyst's surface that interacts with the particles to be degraded. So, the system's kinetics (13) depends on the reactant particles' adsorption on the photocatalyst's surface. The surface adsorption of the particles is associated with the hydrophilic or hydrophobic characteristic of the photocatalyst and pollutant. The bed used and the parameters applied to the support are relevant conditions that affect how the adsorption of the contaminant to the photocatalyst occurs. Therefore, the acceleration of degradation oscillates according to the level of semiconductor coating up to a concentration similar to or greater than the number of surface sites, thus reaching saturation. It is also noted that in solutions with higher concentrations, the reaction of the target substance with radiation becomes a limiting factor [151].

Considering that the rearrangement of photoproduced electrons and vacancies (14) is fast, the interfacial electron transition is kinetically concurrent only when the donor or acceptor is adsorbed before photolysis. The rearrangement system of the $e^-/h^+$ pair and the interfacial charge transition are competitors, and the predominance of one or the other will prevent or not the photocatalytic action of semiconductor [152, 153]. Adsorption is relevant to understand surface reactivity since the existence of $H^+$ and $OH^-$ induce properties of Bronsted acidity or basicity [154 - 156].

The efficiency of $TiO_2$ in environmental remediation stems from its polymorphic form, as well as its size, area, and surface energy (15) [150, 151].

Regarding the $TiO_2$ particle size, it needs to be small, and have a high surface area and energy, the energy being capable of providing high ionic exchanges and agile electronic transition [152, 153]. Thus, the small size and high surface area increases the surface-to-volume, number, and surface area of active points for the reaction to occur, increasing the removal of emerging pollutants. The crystallite area can improve the surface-to-volume ratio and increase the availability $e^-/h^+$ on the surface, making oxidation and reduction more efficient [157 - 159].

Ag content (16) significantly influences the structural and functional characteristics of $Ag/TiO_2$. Low Ag concentrations (0.75 – 1%) result in thermally stable anatase phase, smaller particle size, and larger surface area [160]. As the Ag content increases, phase transformation and inhibition of anatase crystallite growth occur. The Ag content for photocatalytic activity would be between 1–5% mol, where it effectively inhibits electron-hole recombination and introduces impurity bands and surface states [161]. However, excessive Ag content (above 5% mol) can lead to agglomeration and reduced photocatalytic activity [162].

From the limiting factors pointed out about photocatalysis, consequently $Ag/TiO_2$, numerous challenges are noted in the application of photocatalysis in water treatment systems, such as thermodynamic limitations, treatment time, kinetic disadvantages and engineering problems inherent to the heterogeneous nature of the process [163]. Additional obstacles include concerns about nanoparticle toxicity, poor performance under real-world conditions, mass transfer limitations, and durability issues, which hinder large-scale implementation. Flow rate considerations are also important, as optimization of contact time is necessary for efficient photocatalysis. However, it is important to explore strategies such as designing reactors that retain the photocatalyst, studying the degradation of micropollutants in various water matrices, and developing gas-phase reactors with optimized parameters [164].

## 6. $TiO_2$ Synthesis

Pure $TiO_2$ NPs, even with an effective percentage of degradation, have shown limits, such as limited photocatalytic action on visible radiation and a high rearrangement of $e^-/h^+$ pairs [165]. Thus, several approaches have sought to avoid

these limitations, such as bonding with metals nobles, doping and the elaboration of mixed products [166].

Doping encompasses adding compounds to a pure photocatalyst to modify its optical, electrical, and structural characteristics [167]. Thus, changing the activation energy level and structural metastability in fine crystalline elements, impacting the amount and arrangement of regions for nucleation on the catalyst surface and thickening index [168].

$TiO_2$ surface change via doping can be performed with metals [169], non-metals and co-doping [126, 165]. $TiO_2$ presents a wide light absorption region, which increases the quantum efficiency and hinders the rearrangement $e^-/h^+$ photoproduced in the conduction and valence bands, respectively. Furthermore, it expands the reduction potential of photogenerated radicals [170, 171]. The doping of $TiO_2$ with metals alters the surface characteristics of the photocatalyst, facilitating the production of hydroxyl radicals by the reaction of hydrogen peroxide ($H_2O_2$) and $O_2$ [172].

Transition, noble, and rare earth metals are involved in $TiO_2$ doping. Introducing transition metals in the oxide optimizes its results, decreasing the rearrangement index of the photoproduced $e^-/h^+$ pairs and the band gap. Also, by reducing the band gap energy by creating another conductive level between the valence band and the conduction band, they can still have partially occupied d orbitals [173, 174]. The doping of noble metals, such as Au and Ag, optimizes the photocatalytic action of $TiO_2$ on irradiation of visible and UV light [175]. Rare earth metals, consisting of scandium, yttrium, and 15 elements of the lanthanide family, can be incorporated into the $TiO_2$, as they have incomplete (4f) and vacant (5d) orbitals [164, 171].

The doping of $TiO_2$ with metals can occur by several synthesis processes such as impregnation, chemical reduction, sol-gel, green chemistry, encapsulation, hydrothermal/solvothermal, photo deposition, photoreduction, physical vapor deposition, sputtering, precipitation deposition, and exchange ionic [176, 177]. **Table 1** and **Figure 10 (a) and (b)** provides a summary of the precursors, reaction conditions, equipment and temperatures used in the $Ag/TiO_2$ synthesis methods.

**Table 1**. Summary of precursors, reaction conditions, equipment and temperature used in $Ag/TiO_2$ synthesis methods

| Method | Precursors | Reaction Conditions/ Equipament | Temperature |
|---|---|---|---|
| Sol-gel | Ti alkoxide, titanium tetraisopropoxide and titanium oxysulfate and precursor Ag | Hydrolysis and condensation. Carried out in an alcoholic medium, under acidic or basic conditions/Reaction vessel, stirring apparatus and inert atmosphere. | Calcination |
| Hydrothermal | $TiO_2$ and silver nitrate ($AgNO_3$) | Use of high-pressure/ Autoclave. | 100 °C - 180 °C |
| Photodeposition | $TiO_2$ and Ag salt | Aqueous solution/ UV light source and a reaction vessel. | low temperature |
| Chemical Vapor Deposition | Ti precursor and Ag precursor | Deposition/Chemical vapor deposition reactor. | low temperature |
| Microwave-Assisted | Ti precursor and $AgNO_3$ | Rapid heating using microwave radiation/ Microwave reactor. | 100 - 200 °C for short durations |
| Precipitation | $TiO_2$ and $AgNO_3$ | Involves the precipitation/ Reaction vessel and stirring apparatus. | 65 °C - 80 °C and calcination |
| Chemical Reduction | Ag salt and $TiO_2$ | Reduction of Ag ions using a reducing agent such as sodium borohydride/ Reaction vessel and stirring apparatus. | Room temperature |
| Green Chemistry | Natural extracts (e.g., plant extracts) as reducing agents and $TiO_2$ | Utilizes environmentally friendly processes and materials/ Reaction vessel and stirring apparatus. | Mild temperatures |
| Deposition/ Precipitation | Ag salt and $TiO_2$ | Deposition and precipitation/ Reaction vessel and stirring apparatus. | Involves heating |
| Photoreduction | Ag salt and $TiO_2$ | Reduction under light irradiation/ Light source and reaction vessel. | Often performed in an aqueous solution and high temperature |
| Ion Exchange | Ag ions and $TiO_2$ | Exchange of ions between Ag and $TiO_2$/ Reaction vessel and stirring apparatus. | Room temperature |

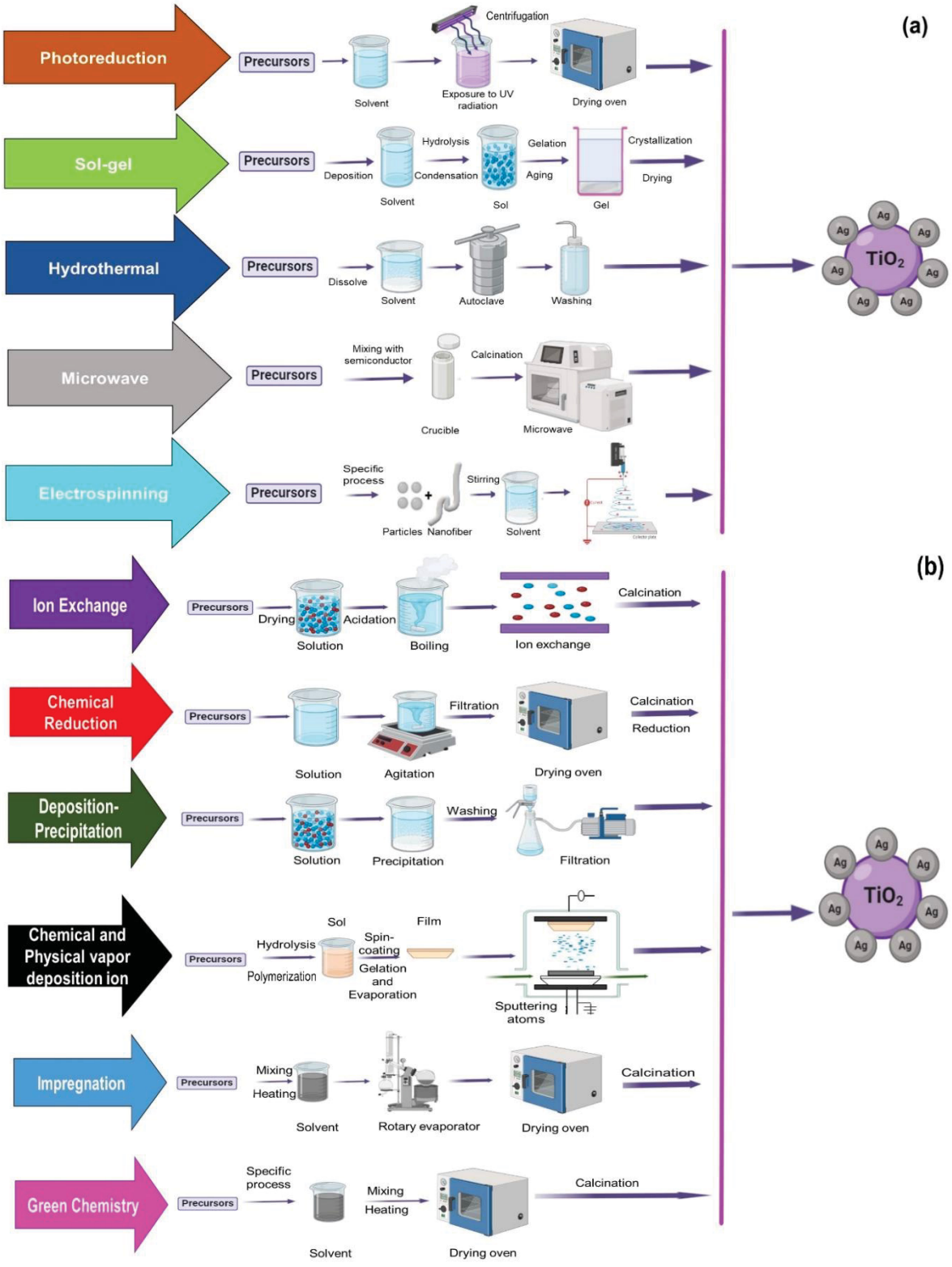


**Fig. 10.** Summary of the synthesis methods (a) and (b) of Ag/$TiO_2$ containing precursors, reaction conditions, equipment used.

Each preparation process has particular characteristics, benefits, and disadvantages regarding synthesis and performance. The purpose of these

processes is to synthesize Ag/$TiO_2$ NPs with high efficiency, homogeneity, and purity, optimize the absorption of pollutants, produce a narrow band gap, and prevent rearrangement of the $e^-/h^+$ pair [164, 173].

Recent studies have explored the impact of different synthesis techniques on the photocatalytic properties of Ag/$TiO_2$ composites, each offering unique advantages. Sol–gel and hydrothermal methods produce different crystal structures, with hydrothermal synthesis yielding superior photocatalytic activity for methylene blue degradation [178, 179]. Photodeposition and microwave-assisted synthesis of Ag/$TiO_2$ improve photocatalytic performance compared to bulk $TiO_2$, with photodeposition showing better results for rhodamine B, pharmaceutical, and pesticide degradation [39]. $Ag_2O$ impregnation loading on $TiO_2$ nanowires demonstrated optimal catalytic performance in the reduction of 4-nitrophenol [180]. Plasma-enhanced chemical and physical vapor deposition can produce well-dispersed Ag NPs on $TiO_2$, with 2.2 wt% Ag producing the highest photocatalytic activity [181 - 183]. All methods demonstrated enhanced photocatalytic activity of Ag/$TiO_2$ compared to pure $TiO_2$. The choice of synthesis method depends on specific requirements for Ag loading, particle size, and target pollutants.

Among the differences in the photoactivity of Ag/$TiO_2$ catalysts obtained by different methods are the level of oxidation of Ag on the support surface, particle diameter, final concentration rate of Ag in Ag/$TiO_2$, and thermal procedure during the synthesis processes [178]. The section below reviews and provides further details of various processes used in Ag/$TiO_2$ synthesis.

### *6.1. Impregnation*

This technique involves a surface area of the support impregnated with a metal precursor solution; subsequently evaporation at high temperature occurs, and finally, the reduction of the metal precursor obtaining the catalysts. Therefore, the impregnation consists of a liquid, which has dissolved metals and enters the pores of the substrates. These metallic ions are adsorbed inside the pores through the evaporation of the liquid [40]. Thus, this simple technique is used in the manufacture of Ag/$TiO_2$ photocatalyst, occurring from the mixture of the $AgNO_3$ solutions with the $TiO_2$ suspension, using water or organic solvents in an

established time. The solvent is extracted by drying and then calcination [182]. This method is carried out under wet and dry conditions [179, 180].

You can modify the synthesis variables, for example, the proportion of Ag or $TiO_2$, the addition of additives, the contact period, and the calcination temperature [184, 185]. It is an easy, accessible process to synthesize supported photocatalysts [40]. As disadvantages, the weak interaction between the metal particles and the support, moderately larger particle diameter, and the generation of high impurities [182].

### *6.2. Chemical Reduction*

Chemical reduction is one of the methods used in the synthesis of $Ag/TiO_2$, controlling the NPs diameter, shape, and dispersion [186]. The beginning of this technique includes the adsorption of precursors on the surface of the support before reducing agents, such as sodium borohydride and sodium citrate, accompanied by chemical reduction [187, 188]. It is a promising method thanks to its versatility and accessibility, at the same time, the use of appropriate reducing agents for the production of Ag NPs is an efficient tool to reduce the size of Ag nanostructures [184, 185]. There are several important factors in the preparation of nanometric Ag, such as the molar concentration ratio, the amount of dispersant, and the reagent addition rate [189, 190].

### *6.3. Sol-gel*

This method usually involves changing a part with a liquid/colloidal constitution, called a sol, to a solid part known as a gel. This process favors the production of ultrafine powders or thin films [191]. This technique comprises three phases, hydrolysis that transforms alkoxides into metallic hydroxides, condensation that produces gels, and drying. The hydrolysis is carried out at a temperature below 100 °C and controlled pH, thus ensuring the uniformity of the characteristics [115 -117].

Calcination is carried out at elevated temperatures for additional crystallization. The sol-gel synthesis is promising, well disseminated, and being used in the production of $Ag/TiO_2$ photocatalysts at room temperature or low

temperatures. Titanium IV tetrabutoxide, titanium tetrachloride ($TiCl_4$), or titanium IV isopropoxide can be used as precursors for $TiO_2$, which are added to an Ag precursor, such as $AgNO_3$. It is a method that provides control of homogeneity, purity of the final catalyst, its development, and the diameter of the particles [188-190]. Furthermore, it has the versatility to add high concentrations of dopants, producing catalysts with a high surface area and maintaining the purity of the chemical reagents. It is also pointed out that it is an easy-to-control synthesis, is reliable, reproducible, allows the production of thin films on substrates, uses basic apparatus, as well as has high chemical homogeneity in sets with dopants, high crystallinity, and allows control of functionalities [188, 191].

This process's disadvantages are slow deposition, time-consuming synthesis, relatively high precursor cost, and the substrate may not support high calcination temperatures and complex agglomeration capacity [189, 192 - 194].

### *6.4. Green Chemistry*

In 1991, the terminology “green chemistry” was inserted, whose purpose is related to minimizing or extinguishing the use of harmful products, thus reducing the detrimental effect on ecosystems and humans [195 - 197]. Green materials can be from plants, such as chitosan and cellulose, support based on ceramics, such as kaolin and clay, which contribute to the stability and recycling of $Ag/TiO_2$, biomass, biopolymers, animals and microorganisms [198].

Among the benefits of applying this technique are the prevention and reduction in the generation of superfluous waste. Since the solvents used can be reused, the absence of hazardous waste, chemical interactions with minimal risk, low cost, and products that do not remain in the ecosystem [193, 195]. They also present reduced polar surface characteristics, high surface area, ease of characterization, and great potential for adsorption of non-polar organic contaminants, being excellent support for $TiO_2$ [199].

### *6.5. Hydrothermal/Solvothermal*

The hydrothermal method takes place in an aqueous medium for crystal growth, where the $TiO_2$ precursor is added to an aqueous solution and then placed

in an autoclave coated with Teflon under pressurized conditions. Then, titania's precipitation occurs from the hydrothermal set's heating, at a high temperature and for a specific reaction period. The development of crystals requires their nucleation and growth. The higher temperature and pressure boost the interaction of the precursors during the fabrication of $Ag/TiO_2$ crystals with excellent qualities. Finally, the catalysts are washed and dried [200]. The hydrothermal process is well used to manufacture $Ag/TiO_2$, especially when mixed nanomorphologies are desired [32].

The hydrothermal process has a simple, easy, and time-efficient operation and produces high-quality crystals without impacting the chemical characteristics. It is environmentally friendly and has flexibility in manufacturing $Ag/TiO_2$ with narrow size distribution and dissemination [124-126]. However, the synthesis needs the autoclave making it expensive, and the development of crystals in situ occurs [197, 198]. It can also control the size of $Ag/TiO_2$ from different reaction conditions, such as pressure, temperature, and pH [199, 200 - 202].

The solvothermal process is very similar to hydrothermal, differing in the solvent used. Thus, this process uses an organic solvent that manages the morphology, structure, dissemination, and crystallinity of the $Ag/TiO_2$ format [112].

Another way of synthesizing photocatalysts supported on $TiO_2$ is thermal evaporation, characterized by the metal evaporating at high temperatures and subsequently being supported on the surface of a semiconductor [203 - 205].

### *6.6. Deposition-Precipitation*

This method is widely used to produce photocatalysts containing metals such as Au, Pd, Ag, Pt, supported on $TiO_2$, so precipitation by deposition requires washing followed by reduction [206]. This synthesis presents a minimum impurity rate, a high dispersion of metals, produces a matrix of narrow dimensions in support materials, and a smaller diameter of metallic particles. However, this method requires a lot of precipitating agent, as well as the size and shape of the nanomaterials are uneven [41, 203]. Oscillations in the reactional pH and the calcination temperature modify the particle diameter and the equivalent portion of the metals' charge [42]. The deposition-precipitation process synthesizes hybrid materials using halides and silver nitrate as precursors [207, 208].

*6.7. Photoreduction*

Photoreduction or photodeposition can be used with other processes, such as impregnation [209], deposition-precipitation [33] and ion exchange [210]. It is used in the synthesis of metal NPs, for example, Ag and Au, supported on various substrates, such as $TiO_2$. Photoreduction involves the reduction of metal ions that are adsorbed on the surface of $TiO_2$ [192].

The unique electronic arrangement of semiconductors such as $WO_3$, $TiO_2$, $Bi_2WO_4$, ZnO e CdS, consists of a completely filled valence band and an empty conduction band. When a photon with energy greater than that of the semiconductor gap radiates over it, the valence band electrons are excited to the conduction band, generating holes in the valence band. The skipped electrons then react with the precursors of their respective ionic metals, generating metal NPs that are supported in semiconductors [211].

It is an attractive technique for synthesizing $Ag/TiO_2$ whose simple principle involves lighting a mixed solution of $TiO_2$ and the Ag precursor for a particular time. It is necessary to reduce the $Ag^+$ ion to a $Ag^0$, thus ensuring its deposition on the surface of the semiconductor [212]. This method provides an effective coupling of Ag NPs on $TiO_2$ obtaining a photocatalyst with multifunctional nature [213].

Alcohol is used to prevent the development of positive charges during the photodeposition technique. Another critical variable is light intensity, as the average particle size is closely linked to light intensity. Another parameter is the concentration of the Ag precursor. When the Ag concentration decreases proportionally, the average particle size decreases [31].

This method takes place at room temperature, needs few reagents, no additional calcination, and presents good recovery and a relatively high deposition percentage of metals. Several metals are deposited on the support by consecutive or synchronous reduction reactions, the particles have smaller diameters, dispersing uniformly on the support, and the doping NPs are not clustered. However, the efficiency of this method increases with time and reproducibility [210, 211].

*6.8. Ion Exchange*

Ion exchange occurs when ions held by electrostatic forces to functional groups on a solid surface (resin) are exchanged for like-charged ions in solution [214 - 216]. It employs ion exchange resins, which are porous polymers with exchangeable functional groups, to remove unwanted ions from wastewater [217]. This process is used to manufacture photocatalysts, since the solubility of the reactant is greater than that of the products. To manufacture metallic materials, ion exchange is associated with the process of reduction, photoreduction, followed by calcination. Ion exchange is a highly efficient process where a mixed-part heterojunction photocatalyst with good interconnection can be acquired [218].

This method offers advantages such as wide applicability, reliability, cost-effectiveness, high separation selectivity, simple handling, and reusability, making it economical and sustainable for water treatment [217]. Ion exchange is widely used in industrial processes such as the removal of specific ions such as nitrate, chromate, and heavy metals, dissolved organic matter, and generates concentrated brine during resin regeneration [213, 215]. Some disadvantages are the separation speed, high detection limit, expensive method, and minimal applications [213, 216]. Ion exchange was used to synthesize Ag/$TiO_2$ with improved properties. As Ag ion exchanged zeolite/$TiO_2$ nanocomposites showed improved antibacterial performance and photocatalytic degradation of antibiotics [219 - 221]. Ag/$TiO_2$ spheres with core-shell structures produced by ion exchange exhibited excellent antibacterial activities [222].

*6. 9. Chemical and Physical vapor deposition*

Chemical vapor deposition unites the synthesis of the catalyst and its coating with appropriate NPs in an accessible and unique method, using titanium isopropoxide as a precursor. In the chemical deposition process, uniform thin films are obtained, reproducible yield, compatibility with excellent adherence, coatings with numerous constituents can be purchased, their format is adapted according to the support, and pure, durable, and uniform NPs are manufactured. Furthermore, the coated photocatalysts show higher catalytic activity than the

uncoated catalyst [223]. The disadvantages of the process are the cost of the necessary reagents, which have high purity, use corrosive gases, and high temperatures [224].

Physical vapor deposition replicates a variety of vacuum deposition processes that are employed to manufacture thin film wraps. It encompasses changes from a condensed state to a vapor state and back to the thin-film condensed state [225]. This technique encompasses the sputtering/evaporation of several constituents to produce a vapor state, the supersaturation of the vapor state in an inert environment to increase the condensation of metal NPs and the thermal procedure for solidification of the nanocomposite [226]. It isn't easy, and the temperature used is moderate. However, vacuum systems are used, making the method costly, and due to the different evaporation periods, the deposition of precursors from different origins is complex [225].

### *6.10. Microwave*

The method supported by microwaves in the synthesis of NPs has become popular thanks to its ease, high reaction rate, and efficiency. The reagents are heated by irradiation, not by a thermal source, which is usually used in conventional techniques. Microwave irradiation interacts with the polar substance generating a dipole moment in the reaction solution, which can affect the rotation of molecules [227]. This orientation increases the possibility of molecular collisions. However, it minimizes the activation energy and heat generation, causing a reactional displacement that favors the manufacture of NPs [228].

## 7. Ag-doped $TiO_2$ photocatalysts (Ag/$TiO_2$)

The high band energy of $TiO_2$ causes a high level of $e^-/h^+$ rearrangement and prevents the use of visible light and sunlight, thus reducing the photocatalytic action and high energy cost [225, 226]. The small size makes $TiO_2$ recovery difficult, thus making it costly and generating secondary contamination as particles remain in the effluents [229 - 231]. One way to overcome this problem is to immobilize the photocatalyst on a support such as silica, glass, stainless steel, fiberglass, fabrics, alumina, activated carbon, and others [232].

Thus, due to these restrictions on the use of $TiO_2$ on a large scale, innovations in the synthesis and structure of the oxide have been improved, both in its photocatalytic characteristics, as in the expansion of the optical spectrum to the visible range and in optimizing its segregation of reagents [229, 230].

Photocatalysts doped with Ag can be used in the degradation of pollutants. This metal is stable, has low investment, and has high electrical and thermal conductivity [29, 51]. Furthermore, it has excellent photocatalytic action, high surface area, excellent stability, and conductivity, which favors selective organic interactions and high efficiency [233 - 235]. Ag has an antibacterial characteristic with or without activation by light and synergistically stimulates the antipathogenic action of $TiO_2$, thus extending its application in the biomedical field [236].

Ag, in the $Ag/TiO_2$ photocatalyst, has a lower Fermi level than $TiO_2$, thermally favoring the excitation of electrons in the oxide conduction band [237]. The photon energy is similar or greater than the bandgap, in the case of $TiO_2$, it is 3.2 eV, activated by UV radiation. This radiation corresponds to 5% of the solar spectrum, compared to 45% of visible light [234, 235]. The rearrangement of the $e^-/h^+$ pairs can be delayed, and well's light absorption spectrum of $TiO_2$ is modified to visible light by doping the oxide with Ag [236 - 238].

Ag acts as a network to capture electrons that are moved from the $TiO_2$ conduction band and transport them to $O_2^{\bullet -}$, transforming them into superoxide radicals. They also help produce hydroxyl radicals that are generated from the reaction of $H_2O$ with the remaining photoproduced gaps present in the $TiO_2$ valence band. The free radicals produced are used to inhibit bacterial growth and for the photocatalytic oxidation of pollutants [239 - 242].

Studies on $TiO_2$-based photocatalysts reveal that $^{\bullet}OH$ is often the dominant oxidative species, while $O_2^{\bullet -}$ contributes less directly to degradation. $^{\bullet}OH$ radicals are identified as the main reactive species responsible for pollutant degradation regardless of the catalyst used [243–245]. While $^{\bullet}OH$ radicals are identified as the main reactive species responsible for dichloroacetic acid degradation, $O_2^{\bullet -}$ radicals contribute indirectly by transforming into $^{\bullet}OH$ radicals in noble metal-doped $TiO_2$ catalysts [243]. In $Ag/TiO_2$ heterojunctions, $O_2^{\bullet -}$ becomes the dominant reactive species, unlike in pure $TiO_2$ where $^{\bullet}OH$ is primary [246].

This change is attributed to changes in electron transfer pathways and improved charge carrier separation in the heterojunction. The addition of noble

metals such as Ag and Pt to $TiO_2$ enhances photocatalytic properties by promoting efficient electron-hole separation [243]. However, the relative importance of different ROS can vary depending on the target pollutant and catalyst composition. For example, in the degradation of pentachlorophenol, $^{\bullet}OH$ is primary for the starting compound, while $O_2^{\bullet-}$ and $H_2O_2$ become more significant for intermediates [244]. $TiO_2$ doped with noble metals, such as $Ag/TiO_2$, showed enhanced photocatalytic activity, with pre-illuminated $Ag/TiO_2$ capable of activating $H_2O_2$ to produce $^{\bullet}OH$ even in dark conditions [247]. Noble metal doping of $TiO_2$ can alter ROS generation pathways, potentially increasing photocatalytic efficiency [243].

Ag can extend the light absorption range of $TiO_2$ to visible light, thus increasing its photocatalytic efficiency due to the creation of the surface plasmon resonance effect in the range of 320–450 nm, which allows the absorption of photons at lower energies [248]. The plasmonic range of Ag is close to the absorption energy of the $TiO_2$ hole (388 nm) [237].

The plasmon effect creates a layer of spatial charge between the semiconductor and the metals (Schottky junction), and through this layer the electrons are excited from the $TiO_2$ conduction band to the metals; that is, there is an oscillation between the energy level of the metal and the conduction band of the semiconductor [249]. The incidence of light radiation on metals excites electrons to higher energy levels, thus causing a slight collective variation of electronic density in metals, thus causing a plasmon resonance located on the surface [246, 247]. This produces an electromagnetic area close to the NPs of metal [250 - 252].

Plasmonic materials, particularly Ag, Au, and Pt NPs, exhibit localized surface plasmon resonance (LSPR) properties that are highly tunable and dependent on size, shape, and composition [253]. Ag NPs exhibit strong SPR peaks and light scattering effects [254] and Au and Ag NPs produce strong extinction and scattering spectra [255]. Ag doping creates oxygen vacancies and increases the disorder of the system, further enhancing visible light absorption [256]. The size and concentration of Ag NPs influence the LSPR resonance band intensity and peak position, enabling tunable optical properties [257]. Ag acts as an electron donor under visible light and an electron acceptor under UV light. This enhancement leads to improved photocatalytic activity and photoelectrochemical performance under visible light [254, 255]. The interconversion between Ag (0) and

Ag (I) during alternating visible and UV irradiation contributes to the photocatalytic process [258 - 260]. The LSPR effect creates a local electric field near the $TiO_2$ surface, extending the light absorption band and promoting efficient charge separation [258]. The synergistic effects of Schottky barrier formation, doping, and mixed crystal phases (anatase + brookite) contribute to the enhanced photocatalytic performance [261] Compared with other dopants, Ag NPs offer advantages such as enhanced light scattering and electron–hole separation [253, 258].

The change in $TiO_2$ morphology caused by Ag doping increases its affinity for dissolved $O_2$, expands its adsorption surface and causes an increase in ROS production [262–265].

There are some limitations in the $Ag/TiO_2$ photocatalyst, such as the loss of photoactivity during prolonged storage and reuse [266] and the leaching of this metal [267]. The $Ag/TiO_2$ stability can be maximized with the addition of ionic liquids, which can impact the crystallinity, action, and morphology of the particles of this photocatalyst [268].

Recent research has focused on improving the recovery and reuse of $Ag/TiO_2$. Membrane separation, ultrafiltration, centrifugation, and sedimentation have emerged as effective methods for catalyst recovery. A cross-flow ultrafiltration system achieved over 99% recovery of $TiO_2$ and $Pt/TiO_2$ [269]. The recovery efficiencies of $TiO_2$ between a centrifuge, a sedimentation tank, and a microfilter membrane were evaluated, and centrifugation recovered 99.5% and was economically viable ($10–$15/1,000 gallons) among several technologies tested [270]. $AgTiO_2$ can be easily separated from water by sedimentation due to their one-dimensional structure due to its large length-to-diameter ratio, allowing simple recovery and reuse without decreasing photocatalytic activity [271]. Magnetic separation offers an efficient solution, such as the creation of magnetically separable composites of $Ag/TiO_2$ with high recyclability [272]. Another method uses magnetic flocculants to aggregate non-magnetic NPs, including Ag and $TiO_2$, allowing their separation and reuse [273]. $SiO_2$-$Ag/TiO_2$ hollow spheres have shown excellent recyclability, maintaining photocatalytic efficiency after five consecutive runs [274]. Ag NPs exhibit higher stability and mobility compared to $TiO_2$ NPs in the environment [275]. Furthermore, $Ag/TiO_2$ NPs retain significant degradation efficiency over three cycles [276].

Conventional treatments, including lime softening and alum coagulation, can achieve more than 93% removal of Ti-containing particles and dissolved Ti [277]. Enhanced coagulation achieved more than 99% removal of Ag, CuO, and $TiO_2$ NPs, although some ionic Ag may pass through the membranes due to dissolution [278]. Current methods for recovering Ag/$TiO_2$ NPs in water treatment systems remove 91-99.97%, showing variable effectiveness [279]. These modifications aim to increase photocatalytic efficiency, stability, and ease of separation, addressing the limitations of conventional Ag/$TiO_2$ systems in wastewater treatment applications.

Under visible light irradiation, Ag/$TiO_2$ photocatalysts oxidize various organic dyes and pollutants, such as phenol, methyl orange, tetracycline and 4-chlorophenol [280]. It was used in the elimination of pharmaceutical substances from wastewater, considering that their structures and harmful impacts on human health and the environment [281]. Phenolic substances are one of the most polluted organic contaminants in the environment, which generate odor and taste in drinking water [282]. Ag/$TiO_2$ has a high photocatalytic efficiency in the degradation of phenolic substances, thanks to its characteristics and structures. This photocatalyst has also demonstrated the same photocatalytic effect with regard to artificial and real wastewater [279, 280], further studies are arranged in **Table 2.**

Recent studies have compared the photocatalytic efficiency of Ag-modified $TiO_2$ and ZnO for degrading various pollutants. Ag/$TiO_2$ showed superior performance in degrading 2-chlorophenol compared to Ag/ZnO and ZnS [283 - 285]. Highly crystalline $TiO_2$ NPs achieved more than 90% degradation of levofloxacin in 120 min under UV light, surpassing commercial $TiO_2$ catalysts [286]. For organic dyes, Ag-modified ZnO and $TiO_2$ demonstrated enhanced photocatalytic activity, with higher Ag concentrations leading to increased degradation rates [287] . In the case of emerging contaminants like bisphenols, Ag/$TiO_2$ achieved 100% degradation within 10 - 60 min, outperforming unmodified $TiO_2$ and ZnO. However, fluconazole proved more resistant, with degradation not exceeding 70% in 60 min [288].

Ag/$TiO_2$ is an effective biocide to eliminate Gram negative and Gram positive bacteria [173, 285] (**Figure 11**). However, the morphology, shape, and gram of the bacteria modify the behavior of the photocatalyst [289 - 291]. It is

known that the thickness of the peptidoglycan layer of Gram-negative bacteria is thinner, and their cell wall structure is different from that of Gram-positive bacteria, which facilitates the entry of ROS into the cytoplasmic membrane of the bacterium, thus causing its death. The antibacterial action mechanisms of $Ag/TiO_2$ are multitarget, multidirectional and multifactorial and can occur by attacking the bacterial cell layer caused by $OH^{\bullet}$ and $Ag^{+}$, by the production of active hydroxyls, by irradiation of the photocatalyst and the interfacial charge transfer between Ag and $Ag_2O$ [286, 287].

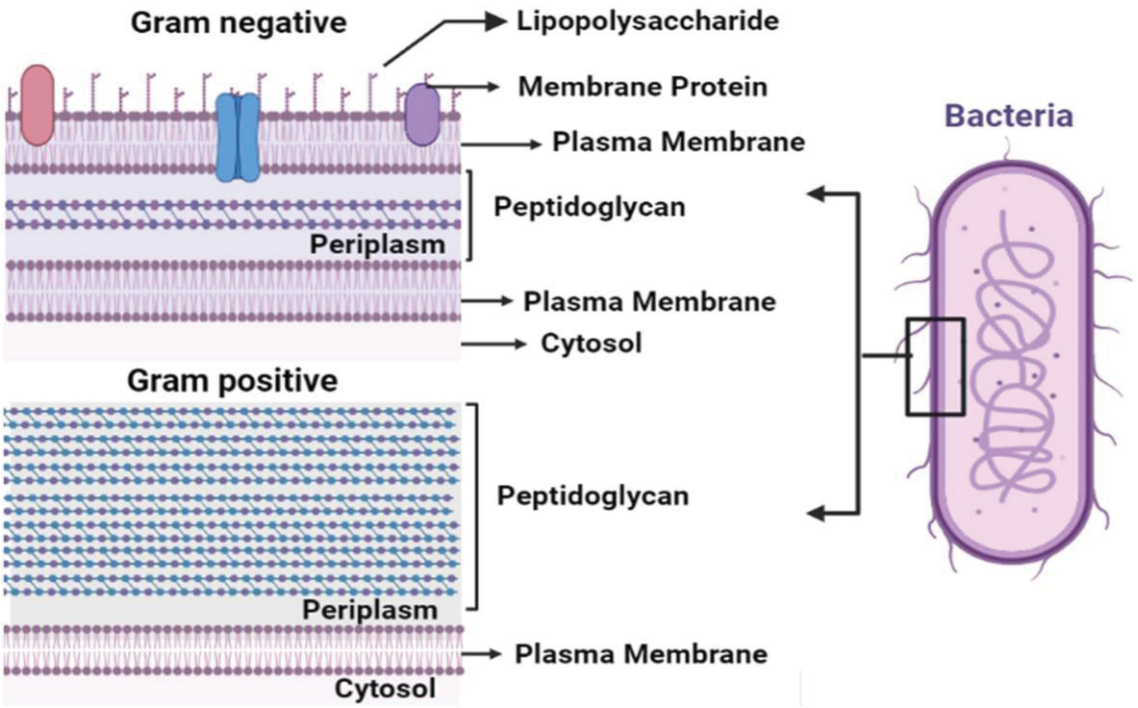


**Fig. 11.** Cell wall structure of gram-negative and gram-positive bacteria.

$Ag/TiO_2$ NPs were synthesized via the photochemical reduction method. The morphology and structure of the material were identified through the use of high-resolution transmission electron microscopy (HR-TEM). The findings revealed that the average diameter of the Ag NPs was 23.9 ± 18.3 nm, exhibiting a fine and homogeneous distribution on the $TiO_2$ surface. The photoresponse of $Ag/TiO_2$ NPs under 365 nm LED irradiation exhibited a higher intensity in the visible light region relative to $TiO_2$ P25. The $Ag/TiO_2$ system can be reused after five consecutive CIP photodegradation reactions, with a slight decrease in efficiency (8%). The presence of Ag (blue bars) in $Ag/TiO_2$ NPs was confirmed through X-ray diffraction (XRD) analysis (**Figure** 12 (f)). Furthermore, the composite

demonstrated antibacterial activity against *E. coli* (Fig. 12 (g) and (h)), indicating its potential for use in the treatment of hospital wastewater. As previously mentioned in reference [96], the results regarding the photodegradation of CIP and norfloxacin are as follows:

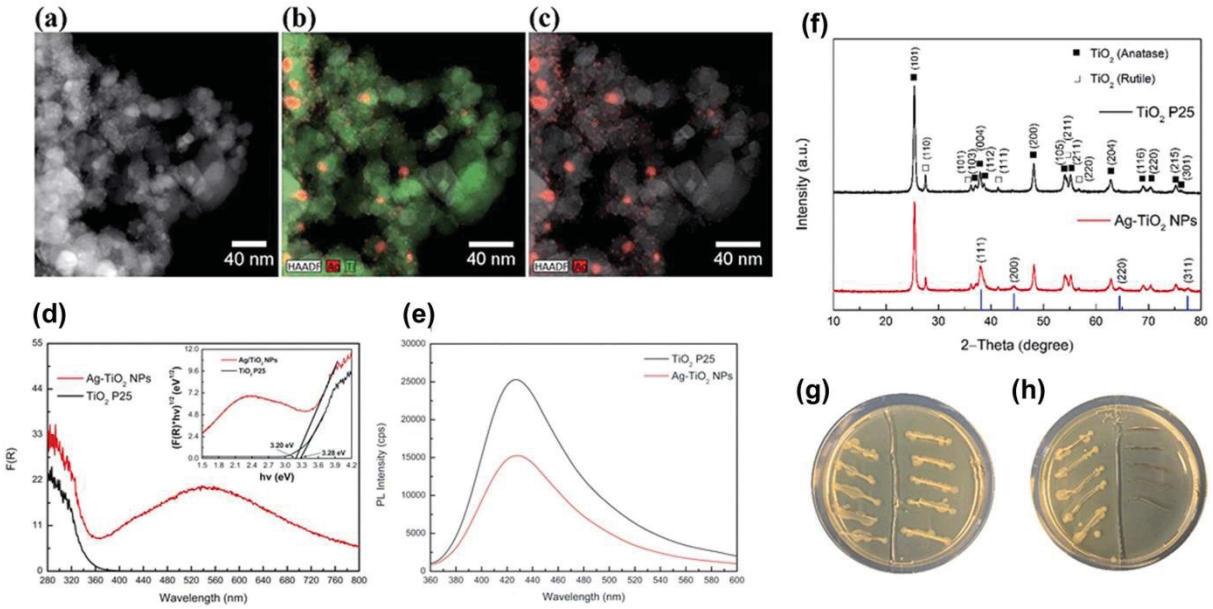


**Fig. 12.** (a) HRTEM image of Ag/$TiO_2$; (b) EDS map of Ag/$TiO_2$ with Ag in red and Ti in green atomic distribution; (c) EDS map of Ag/$TiO_2$ with Ag atomic distribution (red). (d) UV-Vis absorption spectra of $TiO_2$ P25 and Ag/$TiO_2$ NPs (e). Powder XRD patterns of $TiO_2$ P25 and Ag/$TiO_2$ NPs (f). The inhibitory bacteria growth potential of $TiO_2$ (g) and Ag–$TiO_2$ NPs (h) against *E. coli*: (g) *E. coli* broth on the left part of the agar plate, $TiO_2$ P25 and *E. coli* broth on the right part of the agar plate; (h) *E. coli* broth on the left part of the agar plate, Ag/$TiO_2$ NPs and *E. coli* broth on the right part of the agar plate [96].

The Ag/$TiO_2$ core-shell was employed for the nonphotochemical catalytic hydrolysis of the organothiophosphate pesticide methyl parathion (MeP) under mild and ambient conditions. From the transmittance electron micrograph (TEM) images, Ag NPs have an average size of 20 nm and a spherical core-shell NPs are observed. XRD showed for Ag/$TiO_2$ at 200 °C peaks with Ag reflections and no peak corresponding to $TiO_2$, confirming an amorphous layer. At 600 °C, the peaks are narrower and crystalline for Ag/$TiO_2$, while at 1000 °C, a stronger peak for anatase is observed. Scanning electron microscopy (SEM) indicates that the

freeze-drying method resulted in the formation of agglomerates with irregular surfaces. These agglomerates were observed to contain $TiO_2$ with intertwined crystalline domains, with a size five times larger than that of the agglomerates observed in the $Ag/TiO_2$ sample. The material displays the presence of mesopores. The formation of p-nitrophenolate anion (PNP) was observed for up to five cycles. However, the conversion exhibited a notable decline in performance compared to the initial cycle. The initial rate of hydrolysis may be attributed to the pH of the reaction mixture, with p-nitrophenolate (PNP) being the sole degradation product. The catalytic activity of $Ag/TiO_2$ was found to be related to the higher acidity that is mediated by the presence of Ag NPs. The hydrolysis mechanism may occur by coordination of electron-rich $P_2O_5$ to Lewis acid sites on the surface of the material, by nucleophilic attack of the OH ion on the P atom and loss of the leaving group and generation of the hydrolysis product (**Figure 13**) [292].

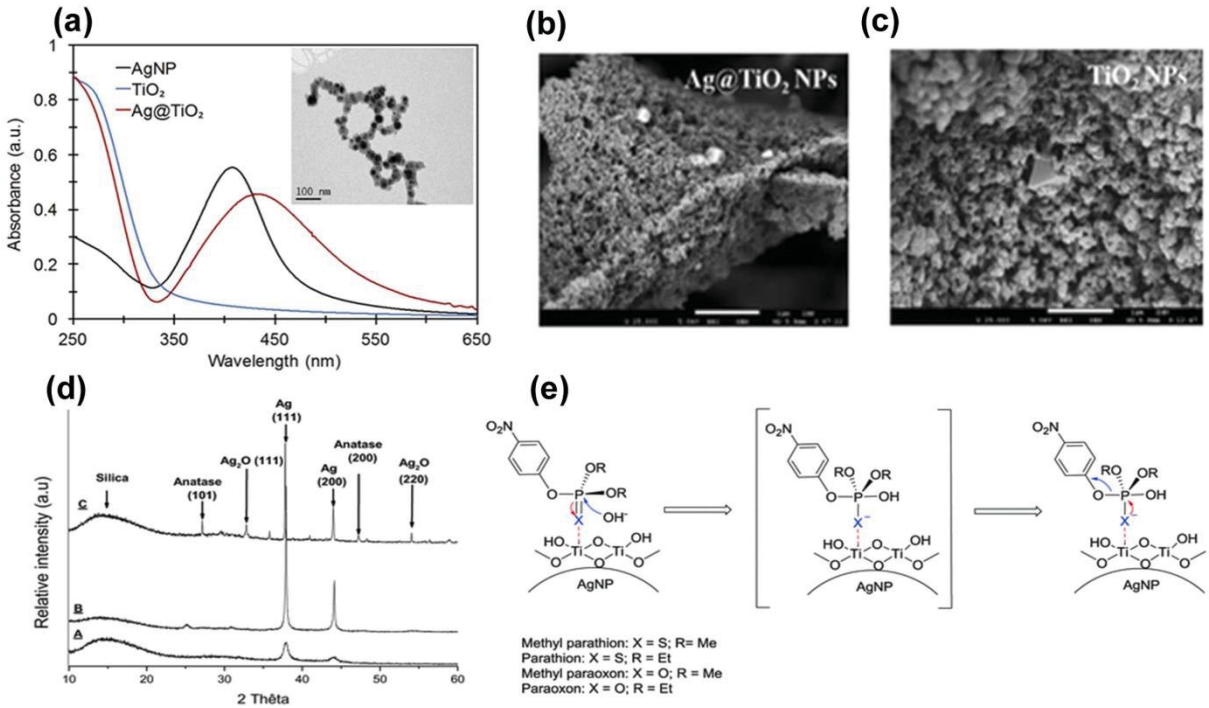


**Fig. 13.** (a) UV-Vis absorption spectra of Ag, $TiO_2$, and $Ag/TiO_2$ NPs and TEM image of $Ag/TiO_2$ (inset). SEM micrographs of $Ag/TiO_2$ (b) and $TiO_2$ (c) particles. (d) X-ray diffraction patterns of $Ag/TiO_2$ after heating at (A) 200 °C, (B) 650 °C, and (C) 1000 °C. (e) Proposed mechanism for organophosphate hydrolysis on $Ag/TiO_2$ [292].

$Ag/TiO_2$ was synthesized via formaldehyde-assisted photodeposition (PD) and microwave (MW), and its photocatalytic performance was evaluated using pollutants. The XRD analysis revealed that the $Ag/TiO_2$ sample exhibited an anatase phase of $TiO_2$, and no Ag was detected. The calculated crystallite sizes of $TiO_2$, 1.5 wt% $Ag/TiO_2$ - PD, and 1.5 wt% $Ag/TiO_2$ - MW were 21.9 nm, 22.7 nm, and 23.2 nm, respectively. The smallest band gap was observed for 1 wt% $Ag/TiO_2$ - MW, with a value of 2.47 eV [39].

Scanning electron microscopy with energy dispersive X-ray spectroscopy (SEM-EDX) revealed the presence of spherical particles exhibiting a degree of agglomeration. However, no discernible difference was observed in the morphology and shape of $Ag/TiO_2$ - PD and $Ag/TiO_2$ - MW. This indicates that the synthesis did not affect the morphology and texture of the materials. Energy-dispersive X-ray spectroscopy (EDX) identified the presence of silver (Ag) in the materials, with different amounts of this metal: 0.1 wt% Ag and 0.07 wt% Ag for 0.5 wt% $Ag/TiO_2$ - PD and 0.5 wt% $Ag/TiO_2$ – MW, respectively. The 0.5 wt% $Ag/TiO_2$ - PD demonstrated a markedly elevated photocatalytic efficacy in comparison to the rhodamine B dye. Consequently, the degradation efficiency was 99%, and the pseudo-first-order rate constant was 0.14432 $min^{-1}$, with the influence of Ag, the wt% of Ag, and the synthesis route under observation. The composite synthesized with 1.0 wt% $Ag/TiO_2$ - MW exhibited the most favorable performance, demonstrating 99% photodegradation and pseudo first order rate constants of 0.13759 $min^{-1}$ by microwave and formaldehyde. The 0.5 wt% $Ag/TiO_2$ and 1.0 wt% $Ag/TiO_2$ composites demonstrated photocatalytic degradation of naproxen sodium within 10 min, with a degradation rate of approximately 80% for the $Ag/TiO_2$ - PD catalyst. Additionally, the composites exhibited photocatalytic degradation of flurbiprofen within 60 min, demonstrating their potential for the degradation of pharmaceuticals. The degradation of the pesticides atrazine (48%) and pyrimethanil (56%) was less pronounced than that of the pharmaceuticals using $Ag/TiO_2$ - PD. The 0.5 wt% $Ag/TiO_2$ - PD composite exhibited a distinctive performance in the photodegradation of pollutants, as evidenced by the results presented in reference [39].

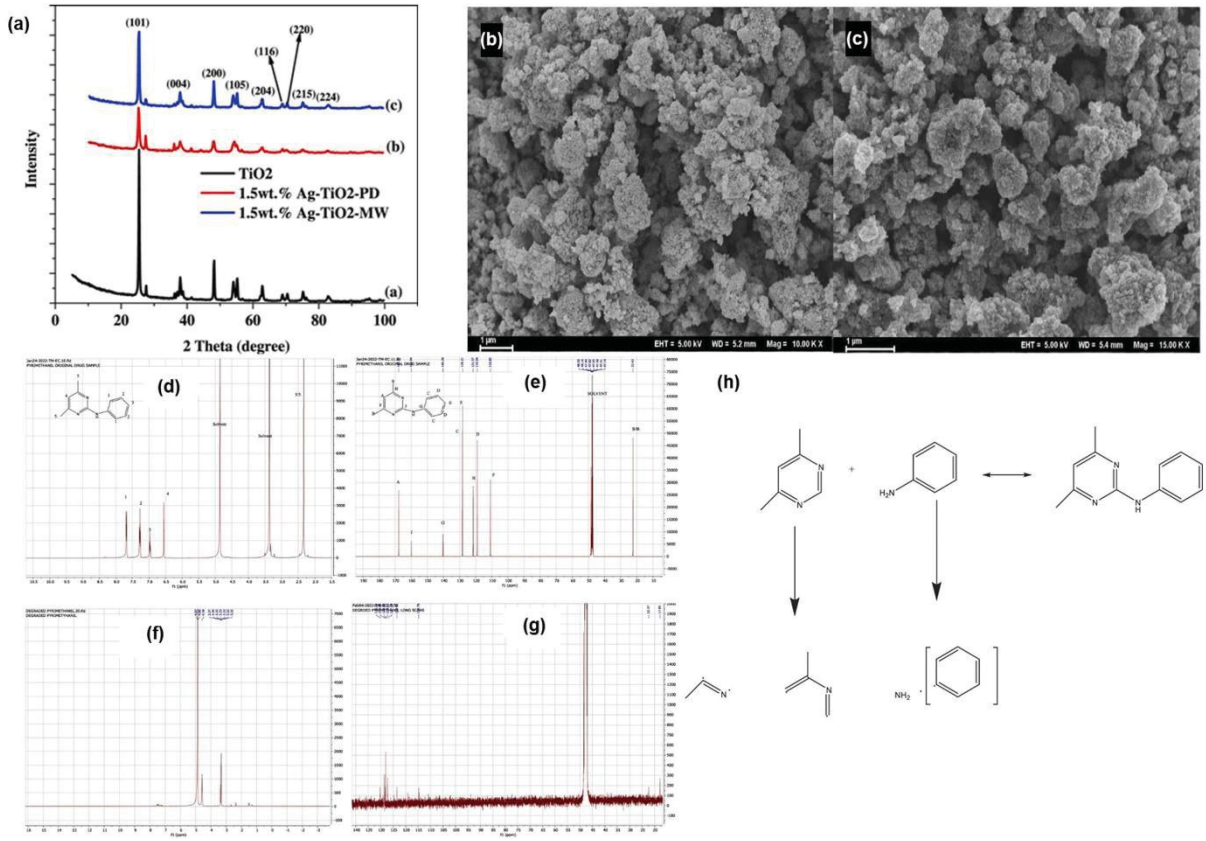


**Fig. 14.** (a) XRD pattern of pure $TiO_2$, 1.5 % $Ag/TiO_2$ - PD and 1.5 % $Ag/TiO_2$ - MW. SEM image of (b) $Ag/TiO_2$ - PD and (c) $Ag/TiO_2$ - MW. (d) 1 H NMR of pure pyrimethanil, (e) 13 C NMR of pure pyrimethanil, (f) 1 H NMR of photodegraded pyrimethanil, (g) 13 C NMR of photodegraded pyrimethanil. (h) Possible fragments obtained from the photodegradation of pyrimethanil by Ag-$TiO_2$ [39].

The photodegraded pyrimethanil was subjected to nuclear magnetic resonance (NMR) analysis with the objective of elucidating the degradation mechanism and identifying the degradation byproducts. Pyrimethanil has six aromatic protons ($p^+$) in the two aromatic rings, six aliphatic $p^+$ in the methyl carbons, and one acidic $p^+$ that was disappearing, possibly due to exchange with deuterium. Two analogous methyl protons were identified. The insecticide in question features aromatic rings with methyl radicals meta linked to the pyrimidine ring. As illustrated in **Figure 14** (d) - (g), a shift in the aromatic region is evident, indicating the disintegration of pyrimethanil. Pyrimethanil is an alkaloid comprising 12 carbon atoms, 10 of which exhibit $sp^2$ hybridization, and 2 exhibiting $sp^3$ hybridization, resulting in a formula of $C_{12}H_{13}N_3$. An aromatic fragment is present

in the degradation mechanism (Figure 14 (h)), which occurs due to the high stability of benzamine, or the positively charged benzene or benzyl radical [39].

The behavioral relationship of $Ag/TiO_2$ with bacterial cells, as well as its antibacterial action, is influenced by its structure, Ag concentration and size [288, 289]. $Ag/TiO_2$ particles with diameters smaller than 10 nm have a more effective antibacterial action than larger sizes, because with a decrease in diameter, the surface contact area with the bacteria increases, thus increasing the antibacterial action of this photocatalyst [293 - 295].

Summarizing the benefits of adding Ag NPs to $TiO_2$: (1) they increase visible light absorption through LSPR and Raman scattering effects [257]; (2) facilitate charge separation by forming Schottky barriers at the $Ag/TiO_2$ interface, reducing $e^-/h^+$ recombination [31, 291]; (3) Ag can inject $e^-$ into adsorbed molecules through the conduction band of $TiO_2$, enhancing charge transfer processes [296]; (4) they suppress anatase - rutile phase transformation [294 - 297]; (5) improve the bactericidal performance of $TiO_2$; (6) they increase oxygen vacancies in the $TiO_2$ matrix [31]; (7) in UV light, Ag serves as an electron acceptor, trapping photogenerated electrons in $TiO_2$ [259]; and (8) assist in the formation of singlet oxygen and hydroxyl radicals, increasing photocatalytic activity [298]. These advantages make Ag a superior choice for $TiO_2$ doping compared to other metals such as Mn, which can inhibit photodegradation due to shadowing effects and facilitated recombination [299].

**Table 2.** Applications of $Ag/TiO_2$ in the degradation of emerging pollutants and their results.

| Catalyst/ Synthesis | Contaminant / Concentration | Degradation Reaction conditions | Results | Reference |
|---|---|---|---|---|
| $Ag/TiO_2$ Nanowires/ Hydrothermal | Rhodamine B/ 3.5 mg/L | Xe Lamp (350 W)/60 min | - Photo discoloration was 100% after 45 min;<br>- Ag improved the absorption of $TiO_2$ nanowires in the visible;<br>- Bandgap of 2.85 eV. | [126] |
| Cassava stem charcoal with $Ag/TiO_2$ (AT/CSAC) and $Ag/TiO_2$/Green synthesis involving sol-gel | Bright green/15 mg/L | Sunlight /60 min | - Crystalline size: 12.37 nm;<br>- AT/CSAC makes a redshift from the absorption edge;<br>- AT/CSAC has a gap of 2.81 eV and a surface area of 238.5 $m^2/g$;<br>- Photobleaching of brilliant green was 98%. | [300] |
| $Ag/TiO_2$ and granules of C from cellulose/Green Synthesis involving supercritical sol-gel and One-Pot | Ceftriaxone sodium/25 mg/L | Xe lamp (500 W)/270 min | - Photocatalytic degradation of 91.9%;<br>- Efficacy reduced to 17.9% after 5 cycles. | [301] |
| $Ag/TiO_2$-Fe and Bentonite Clay/Green Synthesis involving sonication and immersion coating | Ciprofloxacin/25 mg/ L | Solar radiation (940 $Wm^{-2}$)/60 min/pH 3.5 | - Degradation of 94.4% and changed to 81.6% after 30 recyclings;<br>- Reduction of process costs;<br>- Formation of inorganic anions and cations in ciprofloxacin fragmentation. | [302] |
| $Ag/TiO_2$/ Core-shell | Sewage sludge | Anaerobic digestion | - Removal of 91.9% hydrogen sulfide gas;<br>- 3-fold increase in biomethane production;<br>- Degraded organic matter. | [303] |
| $Ag/C-TiO_2$/ Impregnation | Phenol and 4-nitrophenol/10 mg/L | Xe lamp (simulated | - Photocatalyst exhibits 100% removal of phenolic pollutants; | [234] |

| | | | | |
|---|---|---|---|---|
| | | sunlight 300 W)/60 min | - Photocatalyst has good stability and recyclability for degradation/reduction of 4-nitrophenol;<br>- Inorganic ions and pH have little influence on the removal of phenolic compounds. | |
| $TiO_2$ doped with Ag-Zn/Green synthesis | Methylene Blue (MB) and Methyl Orange (MO)/ 0.2 mg/L (Photocatalysis) and 0.004 to 0.025 mmol $L^{-1}$ MO and 0.02 to 0.1 mg/mL MO/Catalysis | Direct sunlight (Photocatalysis) / Reducing agent in catalysis was $NaBH_4$ (1.8 mmol $L^{-1}$) | - Photocatalyst has cubic and tetragonal geometry and size of 5.66 nm;<br>- Extract of *Nicotiana Tabacum* leaves acted as a reducing and stabilizing agent;<br>- MB catalytic discoloration occurred within 8 min;<br>- The photodiscoloration of the MO was 45% and for the MB the photobleaching increases with the amount of catalyst. | [304] |
| Ag-doped $TiO_2$ nanotubes/ Anodizing and electrochemical deposition | MB e MO/2 mg/L | - UV light (365 nm and 0.6 mW $cm^{-2}$), halogen lamp (150 W) with a UV cut filter/300 mins | - Size of homogeneously distributed NPs: 3 to 5 nm;<br>- Surface plasma resonance Ag deposition process was stronger, better homogeneous distribution, finer NPs and absorption in the entire visible light region;<br>- UV degradation of MB was 94% and MO was 89%;<br>- In visible light, the degradation was 35% for MB. | [305] |
| $TiO_2$ NPs doped with Ag and Fe/ Sol-gel | MB/5 ppm | Visible light/240 mins | - Spherical NPs from 10 to 22 nm;<br>- Zone of inhibition: 19.1 and 19.3 mm for *S. aureus* and *E. coli*, respectively;<br>- Band gap of 2.91 eV the synergistic effect of Ag and Fe narrowed the gap of $TiO_2$ NPs;<br>- MB degradation was 80%;<br>- Surface plasmon resonance induced by Ag on the $TiO_2$ surface blocked the photoexcited electrons and delayed the recombination rate of the $e^-/h^+$ pair. | [306] |

| | | | | |
|---|---|---|---|---|
| $Ag/TiO_2$ Nanofibers/ Electrospinning | Phenol/5.62 mg/L | Visible light fluorescent lamp (18 W; 400−500 nm)/ pH 7,87/ 600 mins | - Phenol degradation: 92.9%;<br>- Nanofibers with nanometric diameter and micrometric length. | [307] |
| Films $Ag_xO$/ $Ag/TiO_2$/ Sputtering | Chloroform and butadione/10 g $m^{-3}$ | Visible light fluorescent lamp (24 W/400–720 nm)/400 mins | - Removal of 98% of chloroform;<br>- Kinetics of photocatalytic degradation of butadione is faster than chloroform;<br>- Reuse of films, demonstrates sustainable use of materials;<br>- Almost complete inactivation of *E. coli* in 360 mins of visible light. | [308] |
| $Ag/TiO_2$ NPs / Green Synthesis involving hydrothermal (*Leucas Aspera* aqueous extract) | Picric acid (2,4,6-trinitrophenol) | High pressure Hg lamp (15W/ 545 nm)/150 mins | - Presence of $TiO_2$ in the anatase phase and spherical shape;<br>- Size of $Ag/TiO_2$ NPs of 5 nm;<br>- *L. aspera* aqueous extract acts as a reducing and capping agent;<br>- $Ag/TiO_2$ NPs (0.010 mol $L^{-1}$) had the best performance in picric acid photodegradation in 60 mins. | [309] |
| Ag/ZnO and $Ag/TiO_2$/ Photodeposition | Levofloxacin/ 25 mg/L | Visible lamp (500 W) and UV (400 W)/150 mins | - The doping with Ag in the photocatalysts contributed to the activation of the surface under visible light and prevented the rearrangement of $e^-/h^+$;<br>- Removal of levofloxacin for Ag/ZnO and $Ag/TiO_2$: 99 and 91% (UV); and 56 and 49% (visible light), respectively;<br>- Total removal of organic carbon for Ag/ZnO and $Ag/TiO_2$: 97 and 84% (UV), respectively;<br>- Degradation rate reduces by 6% after 3 cycles. | [310] |

| | | | | |
|---|---|---|---|---|
| $Ag/TiO_2$ and PANI nanocomposite (carbonaceous material) ($Ag/TiO_2$/PANI)/ Photoreduction and oxidative polymerization of aniline | Bisphenol A /5 mg/L | Hg lamp - UV (400 W) and halogen lamp - visible light (500 W)/pH 6.5/120 mins | - Band gap of 3.0 eV;<br>- After 4 cycles, 90% was removed;<br>- Removal of bisphenol (visible light): 82.5% - $Ag/TiO_2$ and 99.7% - $Ag/TiO_2$/PANI;<br>- Bisphenol degradation (UV): 99.4% in 60 mins for $Ag/TiO_2$ and 99.5% in 55 min for $Ag/TiO_2$/PANI;<br>- $Ag/TiO_2$/PANI (UV and visible light) had a removal of 99.8% in 110 mins. | [311] |
| Nanocomposite $Ag/TiO_2$, graphene and N/ Hydrothermal and thermal | Sulfamethoxazole/150 a 500 µg/L | Sunlight and visible light (12 white LEDs 8 W/420 – 800 nm)/ 60 mins (sunlight) | - Band gap of 2.5 eV;<br>- Extension of the photocatalytic capacity to the visible light range;<br>- 90% degradation of the antibiotic in sunlight;<br>- 83% efficiency of antibiotic removal in visible light. | [312] |
| $TiO_2$ and $Ag/TiO_2$/ Sol-gel | Amlodipine besylate/10 mg/L | UV light (250–265 nm)/100 mins | - Photodegradation of 100% amlodipine besylate ($Ag/TiO_2$);<br>- Ag influences the transformation of the rutile phase to $TiO_2$ anatase. | [313] |
| $Ag/TiO_2$/ Photodeposition | Tetrabromodiphenyl ether (BDE-47) with surfactant Triton X-100 (TX-100)/100 mL of BDE-47-TX-100 solution | Hg lamp high pressure - UV (100 W)/30 min vacuum and 100 mins continuous air pump | - BDE-47 degradation rates: 0.858 $min^{-1}$;<br>- $Ag/TiO_2$ decomposes BDE-47 into low bromine diphenyl ethers;<br>- $Ag/TiO_2$ NP is irregular aspherical;<br>- $Ag/TiO_2$ had good photostability and could be reused for 3 cycles;<br>-TX-100 provides modified hydrophobic surface and large surface area to retain BDE-47. | [314] |
| $Ag/TiO_2$-$SiO_2$/Sol-gel, hydrothermal and wet chemical | Penicillin | Visible light and UV/240 mins and 80 mins (UV) | - Increases the spectrum to the visible, optimizes photon adsorption and reduces the band gap; | [315] |

| | | | | |
|---|---|---|---|---|
| | | | - Degradation of almost all penicillin, with apparent decomposition rate: 0.740 $h^{-1}$ (Visible Light);<br>- Degradation time decreased to 15 mins (UV);<br>- Ag/$TiO_2$-$SiO_2$ has good stability after 7 cycles. | |
| Chiral Ag/$TiO_2$ nanosheets/ Photoreduction | 17α-ethinyl estradiol/5 mg/L | Xe lamp (300 W - visible light - 400 nm)/60 mins | - Size of Ag NPs: 12 - 14 nm;<br>- The photocatalyst retains the photocatalytic action for up to 5 cycles;<br>- More than 80% of the hormone was photodegraded;<br>- Decrease of 17% in total organic carbon;<br>- The pseudo-first order rate constant for the photodegradation of the hormone by Ag/$TiO_2$ increased 20.1 times compared to that of $TiO_2$. | [316] |
| Ag/$TiO_2$/Sol-hydrothermal | 4-mercaptobenzoic acid and ciprofloxacin/ $1x10^{-4}$ mol/L | High pressure Hg lamp (375 W, 365 nm - UV)/100 mins | - Ciprofloxacin was almost entirely degraded within 60 mins;<br>- Maintain high performance after 5 cycles. | [317] |
| Ag/$TiO_2$/ $MgC_3N_4$/ Photodeposition | Amoxicillin/5 ppm | Xe Lamp (300 W, 420 nm visible light)/60 mins | - Photocatalyst particles are mesoporous;<br>- Electron transfer and inhibition of $e^-/h^+$ rearrangement was potentiated;<br>- 99% of amoxicillin was degraded;<br>- After 4 cycles Ag/$TiO_2$/$MgC_3N_4$ had high stability. | [318] |
| $Ag_2O$/$TiO_2$/ Precipitation | Iopromide/30 mg/L | Low pressure Hg lamp (UV–C/254 nm/ 12.5 W) and Xe lamp (75 W UV–A/ visible light/ 380–800 nm)/300 mins | - Total organic carbon removal of 65% (200 min);<br>- Mineralization of iopromide up to 86% (UV-C);<br>- Stability of the photocatalyst was 3 cycles (UV-A/visible light). | [319] |

| | | | | |
|---|---|---|---|---|
| Ag/H/$TiO_2$ /Sol-gel | Nitrobenzene (NB), metronidazole (MTZ) and MB/61,5 mg/L (NB), 15 mg/L (MTZ), 25 mg/L (MB) | High pressure Hg vapor lamp (125 W, 435,8 nm, 56 $Wm^{-2}$)/120 mins | - NB, MTZ and MB degradation efficiency: 95.5%, 96.5% and 96.7%, respectively;<br>- Average particle size: 17.7 nm;<br>- Specific surface area:103.2 $m^2 g^{-1}$;<br>- 10% reduction in NB and MTZ degradation efficiency after 6 cycles. | [320] |
| Au/Ag–Ag/$TiO_2$/ Immobilization by sun and phase inversion | Diazinon/30 mg/L | Visible lamp (250 W/390-800 nm)/50 mins | - Degradation rate: 90.3%;<br>- After 5 cycles there was no decline in catalyst activity and selectivity. | [321] |

List of abbreviations: Ag/$TiO_2$- Silver and titanium dioxide, AT/CSAC-Cassava stem charcoal with Ag/$TiO_2$, Ag/$TiO_2$-Fe – Silver, titanium dioxide and iron, Ag/C-$TiO_2$ Silver, carbon and titanium dioxide, MB - Methylene Blue, MO - Methyl Orange, UV- ultraviolet, NPs-nanoparticles, $Ag_xO$ - Silver oxide, Zn – zinc, Ag/ZnO- Silver and oxide zinc, N- nitrogen, Ag/$TiO_2$/PANI – Silver, titanium dioxide and PANI nanocomposite (carbonaceous material), $SiO_2$ – silicon dioxide, Xe- xenon, Hg - mercury, $MgC_3N_4$ - magnesium with carbon nitride NB - Nitrobenzene, MTZ- metronidazole Au/Ag–$TiO_2$ – Gold, silver and titanium dioxide.

The assessment of potential nanotoxicity of catalysts requires a multifaceted approach [322]. The assessment should begin with the thorough characterization of the physical, chemical, and structural properties of the nanomaterial [319, 320]. In vitro studies using cell viability assays and in vivo models can provide insight into the toxicological effects on vascularization, cardiac morphology, and functionality [323 - 325]. Biodistribution in living tissues, blood, and organ effects should be studied. Biochemical, cellular, and immunological processes should be studied to understand the initial effects on physiological functions and chemical defense mechanisms [323].

Ag and $TiO_2$ NPs can penetrate cells and induce oxidative stress, with Ag NPs generally exhibiting greater cytotoxicity than $TiO_2$ NPs [326]. In plants, Ag NPs cause decreased root elongation, reduced chlorophyll content, and reduced fruit production [327]. Ag NPs at low concentrations (<0.5 mg/L) can stimulate human cell proliferation [328], but higher doses (>1.0 mg/L) induce cytotoxicity, causing cellular morphological changes, mitochondrial dysfunction, oxidative stress, and

DNA damage [324, 325]. In aquatic environments, $TiO_2$ NPs can negatively affect the feeding, reproduction, and immunity of organisms [329, 330].

$TiO_2$ coatings with low Ag concentrations (0.3 Ag) showed no toxicity to human fetal osteoblasts, maintaining antibacterial properties, while higher concentrations (3.0 Ag) were cytotoxic [331]. $TiO_2$ NPs showed no significant toxicity in retinal cells at concentrations up to 1.30 µg/mL and demonstrated antiangiogenic effects at 130 ng/mL. However, higher concentrations may induce cytotoxicity [332]. $TiO_2$ NPs at concentrations above 60 µg/mL increased oxidative stress and damaged cellular organelles in mouse fibroblast cells [333].

$Ag/TiO_2$ NPs showed higher toxicity in zebrafish compared to $TiO_2$ NPs, causing increased oxidative stress, histologic lesions, and apoptosis [334]. $Ag/TiO_2$ NPs exhibited lower toxicity in glycerol and water suspension, with CC50 values of 50 and 3.9–58.5 µg/mL for Madin-Darby bovine kidney and Madin-Darby canine kidney cells, respectively [335]. To ensure the safe application of Ag NPs, further research is needed to understand their molecular mechanisms of action, absorption, migration, and biotransformation in plants and ecosystems [336]. In soil microecosystems, $TiO_2$ NPs alone (70 µg/L) were non-toxic, and when combined with aged Ag NPs (20 µg/L), they attenuated the negative effects of Ag on soil microorganisms, plants, and earthworms [337]. $Ag/TiO_2$ NPs can be used safely at appropriate concentrations, and complex interactions between NPs and biological systems are observed, highlighting the need for further research to understand their ecological impacts and potential applications.

Recent advances in synthesis techniques offer promising solutions for large-scale production of $Ag/TiO_2$ materials with improved photocatalytic performance for environmental applications. However, the large-scale application of photocatalytic particles has some problems such as efficient deposition on solid supports, optimal reactor design for high mass transfer, and photon absorption [338]. Scalable synthesis methods for $TiO_2$-based mesoporous photocatalysts are being developed, focusing on high reaction yield, reliable scale-up, and control over morphological and structural features. These advances in synthesis techniques offer promising solutions for large-scale production of $Ag/TiO_2$ materials with enhanced photocatalytic performance for environmental applications such as water treatment and air purification [339]. Despite these efforts, significant challenges remain in developing practical relevant materials and

systems for large-scale environmental remediation and energy applications [334, 336].

$Ag/TiO_2$ effectively degrades organic pollutants, including dyes and pesticides, under solar irradiation [340, 341]. Furthermore, they demonstrate efficacy in disinfecting water contaminated with bacteria [342]. The use of solar energy as the main driver makes this technology economically viable for developing countries [343]. In addition, financing and policy are very important in promoting the deployment of low-carbon technologies, with a focus on overcoming barriers in developing countries [344]. Thus, future research must to focus on improving material efficiency, scalability and practical applicability to overcome these challenges and realize the full potential of $Ag/TiO_2$ for large-scale environmental and energy solutions.

## 8. Conclusion

The bibliographic analysis of the articles classified 267 by InOrdinatio, considering their impact factor, year of publication, citations, and year of publication. These articles described the advances in the synthesis of $Ag/TiO_2$ photocatalysts and influence the photocatalytic efficiency, with degradation rates reaching 80-100% for organic dyes, hormones, pharmaceuticals, pesticides and other emerging pollutants. These materials also exhibit good regeneration capabilities, maintaining high degradation efficiency over multiple cycles. This photocatalyst has better physical, textural, and chemical characteristics than pure $TiO_2$, making it more effective in the degradation of emerging pollutants. The doping of $TiO_2$ with Ag is advantageous, as it increases the photocatalytic activity, decreases the rearrangement of the photoproduced charges, and shifts the photoresponse to the visible light spectrum. The Ag NPs trap the e-excited on the surface of the $Ag/TiO_2$, acting as electron acceptors, which favor the $e^-/h^+$ segregation, suppress the rearrangement, and produce more active ROS, thus causing greater photocatalytic activities. The synergistic impact of ROS and Ag ions showed greater antibacterial activities of $Ag/TiO_2$. Synthesis techniques and reaction factors considerably affect photocatalytic degradation and bacterial inhibition. Thus, requiring rigor and precision to choose the reaction parameters, as well as the development of new studies to optimize industrial applications. A full

cost analysis of $Ag/TiO_2$ will be considered to determine the feasibility for pilot and large-scale experimentation. These nanocomposites offer a promising solution to address the growing concern about emerging pollutants.

## Reference


[1] F.I. Khan, A. Kr. Ghoshal, Removal of Volatile Organic Compounds from polluted air, J. Loss Prev. Process Ind. 13 (2000) 527–545. https://doi.org/10.1016/S0950-4230(00)00007-3.

[2] A. Vaseashta, M. Vaclavikova, S. Vaseashta, G. Gallios, P. Roy, O. Pummakarnchana, Nanostructures in environmental pollution detection, monitoring, and remediation, Sci. Technol. Adv. Mater. 8 (2007) 47–59. https://doi.org/10.1016/J.STAM.2006.11.003.

[3] I. Ojea-Jiménez, X. López, J. Arbiol, V. Puntes, Citrate-Coated Gold Nanoparticles As Smart Scavengers for Mercury(II) Removal from Polluted Waters, ACS Nano 6 (2012) 2253–2260. https://doi.org/10.1021/nn204313a.

[4] P. Biswas, M.M. Hasan, D. Dey, A.C. dos Santos Costa, S.A. Polash, S. Bibi, N. Ferdous, M.A. Kaium, M.H. Rahman, F.K. Jeet, S. Papadakos, K. Islam, M.S. Uddin, Candidate antiviral drugs for COVID-19 and their environmental implications: a comprehensive analysis, Environ. Sci. Pollut. Res. 28 (2021) 59570–59593. https://doi.org/10.1007/s11356-021-16096-3.

[5] X. He, H. Deng, H. min Hwang, The current application of nanotechnology in food and agriculture, J. Food Drug Anal. 27 (2019) 1–21. https://doi.org/10.1016/J.JFDA.2018.12.002.

[6] V. Homem, L. Santos, Degradation and removal methods of antibiotics from aqueous matrices – A review, J. Environ. Manage. 92 (2011) 2304–2347. https://doi.org/10.1016/J.JENVMAN.2011.05.023.

[7] N.M. Vieno, H. Härkki, T. Tuhkanen, L. Kronberg, Occurrence of Pharmaceuticals in River Water and Their Elimination in a Pilot-Scale Drinking Water Treatment Plant, Environ. Sci. Technol. 41 (2007) 5077–5084. https://doi.org/10.1021/es062720x.

[8] P.M. Rajaitha, S. Hajra, M. Sahu, K. Mistewicz, B. Toroń, R. Abolhassani, S. Panda, Y.K. Mishra, H.J. Kim, Unraveling highly efficient nanomaterial photocatalyst for pollutant removal: a comprehensive review and future progress, Mater. Today Chem. 23 (2022) 100692. https://doi.org/10.1016/j.mtchem.2021.100692.

[9] N.O. Eddy, R.A. Ukpe, R. Garg, R. Garg, A. Odiongenyi, P. Ameh, I. Nyambi Akpet, Enhancing water purification efficiency through adsorption and photocatalysis: models, applications, and challenges, Int. J. Environ. Anal. Chem. (2023) 1–18. https://doi.org/10.1080/03067319.2023.2295934.

[10] R. Wei, P. Wang, G. Zhang, N. Wang, T. Zheng, Microwave-responsive catalysts for wastewater treatment: A review, Chem. Eng. J. 382 (2020) 122781. https://doi.org/10.1016/J.CEJ.2019.122781.

[11] Y. Wang, H. Li, J. Xu, J. Yu, J. Wang, H. Jiang, C. Li, X. Zhang, N. Liu, High-performance carbon@ metal oxide nanocomposites derived metal–organic framework-perovskite hybrid boosted microwave-induced catalytic degradation of norfloxacin: Performance, degradation pathway and mechanism, Sep. Purif. Technol. 330 (2024) 125399.

https://doi.org/10.1016/j.seppur.2023.125399.
[12] V.I. Parvulescu, F. Epron, H. Garcia, P. Granger, Recent Progress and Prospects in Catalytic Water Treatment, Chem. Rev. 122 (2022) 2981–3121. https://doi.org/10.1021/acs.chemrev.1c00527.
[13] P.G. Jessop, T. Ikariya, R. Noyori, Homogeneous Hydrogenation of Carbon Dioxide, Chem. Rev. 95 (1995) 259–272. https://doi.org/10.1021/cr00034a001.
[14] M.A.I. Molla, A.Z. Ahmed, S. Kaneco, Reaction mechanism for photocatalytic degradation of organic pollutants, Nanostructured Photocatal. From Fundam. to Pract. Appl. (2021) 63–84. https://doi.org/10.1016/B978-0-12-823007-7.00011-0.
[15] A. Fujishima, K. Honda, Electrochemical Photolysis of Water at a Semiconductor Electrode, Nature 238 (1972) 37–38. https://doi.org/10.1038/238037a0.
[16] S. Nallusamy, S. Asaithambi, S. Pandiaraj, M. Rahaman, V. Elangovan, N. Eswaramoorthy, C. Nandagopal, Cerium-modified $TiO_2$/g-$C_3N_4$ nanocomposites with synergistic effect on enhancing visible-light photocatalytic activity employing cationic dyes, Colloids Surfaces A Physicochem. Eng. Asp. 685 (2024) 133175. https://doi.org/10.1016/J.COLSURFA.2024.133175.
[17] D. Bahnemann, Photocatalytic Detoxification of Polluted Waters, in: 1999: pp. 285–351. https://doi.org/10.1007/978-3-540-69044-3_11.
[18] Sonu, V. Dutta, S. Sharma, P. Raizada, A. Hosseini-Bandegharaei, V. Kumar Gupta, P. Singh, Review on augmentation in photocatalytic activity of $CoFe_2O_4$ via heterojunction formation for photocatalysis of organic pollutants in water, J. Saudi Chem. Soc. 23 (2019) 1119–1136. https://doi.org/10.1016/j.jscs.2019.07.003.
[19] K.P. Gopinath, N.V. Madhav, A. Krishnan, R. Malolan, G. Rangarajan, Present applications of titanium dioxide for the photocatalytic removal of pollutants from water: A review, J. Environ. Manage. 270 (2020) 110906. https://doi.org/10.1016/j.jenvman.2020.110906.
[20] J. Chen, C. Poon, Photocatalytic construction and building materials: From fundamentals to applications, Build. Environ. 44 (2009) 1899–1906. https://doi.org/10.1016/j.buildenv.2009.01.002.
[21] C.B. Anucha, I. Altin, E. Bacaksiz, V.N. Stathopoulos, Titanium dioxide ($TiO_2$)-based photocatalyst materials activity enhancement for contaminants of emerging concern (CECs) degradation: In the light of modification strategies, Chem. Eng. J. Adv. 10 (2022) 100262. https://doi.org/10.1016/j.ceja.2022.100262.
[22] H. Wang, L. Zhang, Z. Chen, J. Hu, S. Li, Z. Wang, J. Liu, X. Wang, Semiconductor heterojunction photocatalysts: design, construction, and photocatalytic performances, Chem. Soc. Rev. 43 (2014) 5234. https://doi.org/10.1039/C4CS00126E.
[23] J. Chen, X. Zhang, X. Shi, F. Bi, Y. Yang, Y. Wang, Synergistic effects of octahedral $TiO_2$-MIL-101(Cr) with two heterojunctions for enhancing visible-light photocatalytic degradation of liquid tetracycline and gaseous toluene, J. Colloid Interface Sci. 579 (2020) 37–49. https://doi.org/10.1016/j.jcis.2020.06.042.
[24] F. Zivic, N. Grujovic, S. Mitrovic, I.U. Ahad, D. Brabazon, Characteristics and Applications of Silver Nanoparticles, in: Commer. Nanotechnologies–A Case

Study Approach, Springer International Publishing, Cham, 2018: pp. 227–273. https://doi.org/10.1007/978-3-319-56979-6_10.
[25] S. Seyedmonir, Characterization of supported silver catalysts I. Adsorption of $O_2$, $H_2$, $N_2O$, and the $H_2$-titration of adsorbed oxygen on well-dispersed Ag on $TiO_2$, J. Catal. 87 (1984) 424–436. https://doi.org/10.1016/0021-9517(84)90202-1.
[26] L. Wang, J. Ali, C. Zhang, G. Mailhot, G. Pan, Simultaneously enhanced photocatalytic and antibacterial activities of $TiO_2$/Ag composite nanofibers for wastewater purification, J. Environ. Chem. Eng. 8 (2020) 102104. https://doi.org/10.1016/j.jece.2017.12.057.
[27] M.M. Viana, Study of thin films and particulate materials of $TiO_2$ and Ag/$TiO_2$ produced by the sol-gel process., Universidade Federal de Minas Gerais, 2011. http://hdl.handle.net/1843/SFSA-8H6URU (accessed March 21, 2023).
[28] X.H. Yang, H.T. Fu, X.C. Wang, J.L. Yang, X.C. Jiang, A.B. Yu, Synthesis of silver-titanium dioxide nanocomposites for antimicrobial applications, J. Nanoparticle Res. 16 (2014) 2526. https://doi.org/10.1007/s11051-014-2526-8.
[29] A. Kumar, G. Sharma, M. Naushad, T. Ahamad, R.C. Veses, F.J. Stadler, Highly visible active $Ag_2CrO_4$/Ag/$BiFeO_3$@RGO nano-junction for photoreduction of $CO_2$ and photocatalytic removal of ciprofloxacin and bromate ions: The triggering effect of Ag and RGO, Chem. Eng. J. 370 (2019) 148–165. https://doi.org/10.1016/J.CEJ.2019.03.196.
[30] R. Saravanan, D. Manoj, J. Qin, M. Naushad, F. Gracia, A.F. Lee, M.M. Khan, M.A. Gracia-Pinilla, Mechanothermal synthesis of Ag/$TiO_2$ for photocatalytic methyl orange degradation and hydrogen production, Process Saf. Environ. Prot. 120 (2018) 339–347. https://doi.org/10.1016/j.psep.2018.09.015.
[31] H. Chakhtouna, H. Benzeid, N. Zari, A. el kacem Qaiss, R. Bouhfid, Recent progress on Ag/$TiO_2$ photocatalysts: photocatalytic and bactericidal behaviors, Environ. Sci. Pollut. Res. 28 (2021) 44638–44666. https://doi.org/10.1007/s11356-021-14996-y.
[32] D. Hariharan, P. Thangamuniyandi, A. Jegatha Christy, R. Vasantharaja, P. Selvakumar, S. Sagadevan, A. Pugazhendhi, L.C. Nehru, Enhanced photocatalysis and anticancer activity of green hydrothermal synthesized Ag@$TiO_2$ nanoparticles, J. Photochem. Photobiol. B Biol. 202 (2020) 111636. https://doi.org/10.1016/j.jphotobiol.2019.111636.
[33] C. Hu, T. Peng, X. Hu, Y. Nie, X. Zhou, J. Qu, H. He, Plasmon-Induced Photodegradation of Toxic Pollutants with Ag−AgI/$Al_2O_3$ under Visible-Light Irradiation, J. Am. Chem. Soc. 132 (2010) 857–862. https://doi.org/10.1021/ja907792d.
[34] D. Komaraiah, E. Radha, J. Sivakumar, M. V. Ramana Reddy, R. Sayanna, Photoluminescence and photocatalytic activity of spin coated $Ag^+$ doped anatase $TiO_2$ thin films, Opt. Mater. (Amst). 108 (2020) 110401. https://doi.org/10.1016/J.OPTMAT.2020.110401.
[35] R. Naidu, V.A. Arias Espana, Y. Liu, J. Jit, Emerging contaminants in the environment: Risk-based analysis for better management, Chemosphere 154 (2016) 350–357. https://doi.org/10.1016/J.CHEMOSPHERE.2016.03.068.
[36] Z. Cao, S. Zhu, H. Qu, D. Qi, U. Ziener, L. Yang, Y. Yan, H. Yang,

Preparation of visible-light nano-photocatalysts through decoration of $TiO_2$ by silver nanoparticles in inverse miniemulsions, J. Colloid Interface Sci. 435 (2014) 51–58. https://doi.org/10.1016/j.jcis.2014.08.021.
[37] R.N. Pagani, B. Pedroso, C.B. dos Santos, C.T. Picinin, J.L. Kovaleski, Methodi Ordinatio 2.0: revisited under statistical estimation, and presenting FInder and RankIn, Qual. Quant. (2022). https://doi.org/10.1007/s11135-022-01562-y.
[38] M. Hernández-Contreras, J.C. Cruz, M.P. Gurrola, B. Pamplona Solis, R.E. Vega-Azamar, Application of nanosilica in the construction industry: A bibliometric analysis using Methodi Ordinatio, MethodsX 12 (2024) 102642. https://doi.org/10.1016/J.MEX.2024.102642.
[39] E. Nyankson, N. Yeboah, S.O. Jnr, S. Onaja, T. Mensah, J.K. Efavi, The effect of synthesis route on the photocatalytic performance of Ag-$TiO_2$ using rhodamine b dyes, pesticides, and pharmaceutical waste as model pollutants, Mater. Res. Express 9 (2022) 094001. https://doi.org/10.1088/2053-1591/ac871f.
[40] S.-Y. Lee, R. Aris, The Distribution of Active ingredients in Supported Catalysts Prepared by Impregnation, Catal. Rev. 27 (1985) 207–340. https://doi.org/10.1080/01614948508064737.
[41] T. Deblonde, C. Cossu-Leguille, P. Hartemann, Emerging pollutants in wastewater: A review of the literature, Int. J. Hyg. Environ. Health 214 (2011) 442–448. https://doi.org/10.1016/J.IJHEH.2011.08.002.
[42] Q. Zhang, Y. Zhang, K. Xiao, Z. Meng, W. Tong, H. Huang, Q. An, Plasmonic gold particle generation in layer-by-layer 2D titania films as an effective immobilization strategy of composite photocatalytsts for hydrogen generation, Chem. Eng. J. 358 (2019) 389–397. https://doi.org/10.1016/j.cej.2018.10.052.
[43] K.C. Machado, M.T. Grassi, C. Vidal, I.C. Pescara, W.F. Jardim, A.N. Fernandes, F.F. Sodré, F. V. Almeida, J.S. Santana, M.C. Canela, C.R.O. Nunes, K.M. Bichinho, F.J.R. Severo, A preliminary nationwide survey of the presence of emerging contaminants in drinking and source waters in Brazil, Sci. Total Environ. 572 (2016) 138–146. https://doi.org/10.1016/J.SCITOTENV.2016.07.210.
[44] J. Xia, Y. Gao, G. Yu, Tetracycline removal from aqueous solution using zirconium-based metal-organic frameworks (Zr-MOFs) with different pore size and topology: Adsorption isotherm, kinetic and mechanism studies, J. Colloid Interface Sci. 590 (2021) 495–505. https://doi.org/10.1016/j.jcis.2021.01.046.
[45] D. Jacobo-Marín, G. Santacruz de León, Contaminantes emergentes en el agua: Regulación en México, principio precautorio y perspectiva comparada, Rev. Derecho Ambient. 15 (2021) 51. https://doi.org/10.5354/0719-4633.2021.57414.
[46] J. Wilkinson, P.S. Hooda, J. Barker, S. Barton, J. Swinden, Occurrence, fate and transformation of emerging contaminants in water: An overarching review of the field, Environ. Pollut. 231 (2017) 954–970. https://doi.org/10.1016/J.ENVPOL.2017.08.032.
[47] J.P.R. Sorensen, D.J. Lapworth, D.C.W. Nkhuwa, M.E. Stuart, D.C. Gooddy, R.A. Bell, M. Chirwa, J. Kabika, M. Liemisa, M. Chibesa, S. Pedley, Emerging contaminants in urban groundwater sources in Africa, Water Res. 72 (2015) 51–63. https://doi.org/10.1016/J.WATRES.2014.08.002.

[48] R.P. Schwarzenbach, B.I. Escher, K. Fenner, T.B. Hofstetter, C.A. Johnson, U. von Gunten, B. Wehrli, The Challenge of Micropollutants in Aquatic Systems, Science (80). 313 (2006) 1072–1077. https://doi.org/10.1126/science.1127291.
[49] L.-J. Bao, K.A. Maruya, S.A. Snyder, E.Y. Zeng, China's water pollution by persistent organic pollutants, Environ. Pollut. 163 (2012) 100–108. https://doi.org/10.1016/j.envpol.2011.12.022.
[50] O.A.H. Jones, N. Voulvoulis, J.N. Lester, Potential Ecological and Human Health Risks Associated With the Presence of Pharmaceutically Active Compounds in the Aquatic Environment, Crit. Rev. Toxicol. 34 (2004) 335–350. https://doi.org/10.1080/10408440490464697.
[51] Y. Zhou, J. Lu, Y. Zhou, Y. Liu, Recent advances for dyes removal using novel adsorbents: A review, Environ. Pollut. 252 (2019) 352–365. https://doi.org/10.1016/J.ENVPOL.2019.05.072.
[52] M.R.D. Khaki, M.S. Shafeeyan, A.A.A. Raman, W.M.A.W. Daud, Application of doped photocatalysts for organic pollutant degradation - A review, J. Environ. Manage. 198 (2017) 78–94. https://doi.org/10.1016/J.JENVMAN.2017.04.099.
[53] Q. Bu, B. Wang, J. Huang, S. Deng, G. Yu, Pharmaceuticals and personal care products in the aquatic environment in China: A review, J. Hazard. Mater. 262 (2013) 189–211. https://doi.org/10.1016/j.jhazmat.2013.08.040.
[54] T.P. Van Boeckel, C. Brower, M. Gilbert, B.T. Grenfell, S.A. Levin, T.P. Robinson, A. Teillant, R. Laxminarayan, Global trends in antimicrobial use in food animals, Proc. Natl. Acad. Sci. 112 (2015) 5649–5654. https://doi.org/10.1073/pnas.1503141112.
[55] V. Thi Quyen, H. Jae Kim, J. Kim, L. Thi Thu Ha, P. Thi Huong, D. My Thanh, N. Minh Viet, P. Quang Thang, Synthesizing S-doped graphitic carbon nitride for improvement photodegradation of tetracycline under solar light, Sol. Energy 214 (2021) 288–293. https://doi.org/10.1016/j.solener.2020.12.016.
[56] J. Hazarika, M. Ganguly, G. Borgohain, S. Sarma, P. Bhuyan, R. Mahanta, Disruption of androgen receptor signaling by chlorpyrifos (CPF) and its environmental degradation products: a structural insight, J. Biomol. Struct. Dyn. 40 (2022) 6027–6038. https://doi.org/10.1080/07391102.2021.1875885.
[57] H. Chart, VTEC enteropathogenicity, J. Appl. Microbiol. 88 (2000) 12S-23S. https://doi.org/10.1111/j.1365-2672.2000.tb05328.x.
[58] C.C. Fowler, J.E. Galán, Decoding a Salmonella Typhi Regulatory Network that Controls Typhoid Toxin Expression within Human Cells, Cell Host Microbe 23 (2018) 65-76.e6. https://doi.org/10.1016/j.chom.2017.12.001.
[59] F. Rivera-Chávez, J.J. Mekalanos, Cholera toxin promotes pathogen acquisition of host-derived nutrients, Nature 572 (2019) 244–248. https://doi.org/10.1038/s41586-019-1453-3.
[60] A.M. Taiwo, A review of environmental and health effects of organochlorine pesticide residues in Africa, Chemosphere 220 (2019) 1126–1140. https://doi.org/10.1016/J.CHEMOSPHERE.2019.01.001.
[61] P. Sane, S. Chaudhari, P. Nemade, S. Sontakke, Photocatalytic reduction of chromium (VI) using combustion synthesized $TiO_2$, J. Environ. Chem. Eng. 6 (2018) 68–73. https://doi.org/10.1016/j.jece.2017.11.060.
[62] P.B. Tchounwou, C.G.P.A.K.S.D.J. Yedjou, Molecular, clinical and environmental toxicology: v.2: Clinical toxicology, Choice Rev. Online 47

(2010) 47-5683-47–5683. https://doi.org/10.5860/CHOICE.47-5683.
[63] N. Shaheen, N.M. Irfan, I.N. Khan, S. Islam, M.S. Islam, M.K. Ahmed, Presence of heavy metals in fruits and vegetables: Health risk implications in Bangladesh, Chemosphere 152 (2016) 431–438. https://doi.org/10.1016/j.chemosphere.2016.02.060.
[64] Y. Zhang, Z.-R. Tang, X. Fu, Y.-J. Xu, Nanocomposite of Ag–AgBr–$TiO_2$ as a photoactive and durable catalyst for degradation of volatile organic compounds in the gas phase, Appl. Catal. B Environ. 106 (2011) 445–452. https://doi.org/10.1016/j.apcatb.2011.06.002.
[65] A. Khan, S. Khan, M.A. Khan, Z. Qamar, M. Waqas, The uptake and bioaccumulation of heavy metals by food plants, their effects on plants nutrients, and associated health risk: a review, Environ. Sci. Pollut. Res. 22 (2015) 13772–13799. https://doi.org/10.1007/s11356-015-4881-0.
[66] T. Rasheed, M. Bilal, F. Nabeel, M. Adeel, H.M.N. Iqbal, Environmentally-related contaminants of high concern: Potential sources and analytical modalities for detection, quantification, and treatment, Environ. Int. 122 (2019) 52–66. https://doi.org/10.1016/J.ENVINT.2018.11.038.
[67] O.M. Rodriguez-Narvaez, J.M. Peralta-Hernandez, A. Goonetilleke, E.R. Bandala, Treatment technologies for emerging contaminants in water: A review, Chem. Eng. J. 323 (2017) 361–380. https://doi.org/10.1016/J.CEJ.2017.04.106.
[68] R.R. Solís, J. Bedia, J.J. Rodríguez, C. Belver, A review on alkaline earth metal titanates for applications in photocatalytic water purification, Chem. Eng. J. 409 (2021) 128110. https://doi.org/10.1016/j.cej.2020.128110.
[69] C. Adams, Y. Wang, K. Loftin, M. Meyer, Removal of Antibiotics from Surface and Distilled Water in Conventional Water Treatment Processes, J. Environ. Eng. 128 (2002) 253–260. https://doi.org/10.1061/(ASCE)0733-9372(2002)128:3(253).
[70] V. Muelas-Ramos, M.J. Sampaio, C.G. Silva, J. Bedia, J.J. Rodriguez, J.L. Faria, C. Belver, Degradation of diclofenac in water under LED irradiation using combined g-$C_3N_4$/$NH_2$-MIL-125 photocatalysts, J. Hazard. Mater. 416 (2021) 126199. https://doi.org/10.1016/j.jhazmat.2021.126199.
[71] X. Zhong, K.-X. Zhang, D. Wu, X.-Y. Ye, W. Huang, B.-X. Zhou, Enhanced photocatalytic degradation of levofloxacin by Fe-doped BiOCl nanosheets under LED light irradiation, Chem. Eng. J. 383 (2020) 123148. https://doi.org/10.1016/j.cej.2019.123148.
[72] N. Parmar, J.K. Srivastava, Process optimization and kinetics study for photocatalytic ciprofloxacin degradation using $TiO_2$ nanoparticle: A comparative study of Artificial Neural Network and Surface Response Methodology, J. Indian Chem. Soc. 99 (2022) 100584. https://doi.org/10.1016/J.JICS.2022.100584.
[73] H.H. Shaarawy, H.S. Hussein, N.H. Hussien, G.A. Al Bazedi, S.I. Hawash, Green production of titanium dioxide nanometric particles through electrolytic anodic dissolution of titanium metal, Environ. Sci. Pollut. Res. 30 (2022) 24043–24061. https://doi.org/10.1007/s11356-022-23766-3.
[74] P. Saravanan, K. Pakshirajan, P. Saha, Degradation of phenol by $TiO_2$-based heterogeneousphotocatalysts in presence of sunlight, J. Hydro-Environment Res. 3 (2009) 45–50. https://doi.org/10.1016/J.JHER.2009.04.001.
[75] N. Bhargava, N. Bahadur, A. Kansal, Techno-economic assessment of

integrated photochemical AOPs for sustainable treatment of textile and dyeing wastewater, J. Water Process Eng. 56 (2023) 104302. https://doi.org/10.1016/j.jwpe.2023.104302.
[76] N.R. Mirza, R. Huang, E. Du, M. Peng, Z. Pan, H. Ding, G. Shan, L. Ling, Z. Xie, A review of the textile wastewater treatment technologies with special focus on advanced oxidation processes (AOPs), membrane separation and integrated AOP-membrane processes, Desalin. Water Treat. 206 (2020) 83–107. https://doi.org/10.5004/dwt.2020.26363.
[77] Y. Zhang, K. Shaad, D. Vollmer, C. Ma, Treatment of Textile Wastewater Using Advanced Oxidation Processes—A Critical Review, Water 13 (2021) 3515. https://doi.org/10.3390/w13243515.
[78] T. An, H. Yang, W. Song, G. Li, H. Luo, W.J. Cooper, Mechanistic Considerations for the Advanced Oxidation Treatment of Fluoroquinolone Pharmaceutical Compounds using $TiO_2$ Heterogeneous Catalysis, J. Phys. Chem. A 114 (2010) 2569–2575. https://doi.org/10.1021/jp911349y.
[79] J. Diaz-Angulo, J. Lara-Ramos, M. Mueses, A. Hernández-Ramírez, G. Li Puma, F. Machuca-Martínez, Enhancement of the oxidative removal of diclofenac and of the $TiO_2$ rate of photon absorption in dye-sensitized solar pilot scale CPC photocatalytic reactors, Chem. Eng. J. 381 (2020) 122520. https://doi.org/10.1016/j.cej.2019.122520.
[80] E. Lipczynska-Kochany, Humic substances, their microbial interactions and effects on biological transformations of organic pollutants in water and soil: A review, Chemosphere 202 (2018) 420–437. https://doi.org/10.1016/j.chemosphere.2018.03.104.
[81] H. Wang, X. Li, X. Zhao, C. Li, X. Song, P. Zhang, P. Huo, A review on heterogeneous photocatalysis for environmental remediation: From semiconductors to modification strategies, Chinese J. Catal. 43 (2022) 178–214. https://doi.org/10.1016/S1872-2067(21)63910-4.
[82] H.S. Bae, M.A. Mahadik, Y.S. Seo, W.S. Chae, H.S. Chung, H.I. Ryu, M. Cho, P.J. Shea, S.H. Choi, J.S. Jang, Palladium metal oxide/hydroxide clustered cobalt oxide co-loading on acid treated $TiO_2$ nanorods for degradation of organic pollutants and Salmonella typhimurium inactivation under simulated solar light, Chem. Eng. J. 408 (2021) 127260. https://doi.org/10.1016/J.CEJ.2020.127260.
[83] R. Kumar Patnaik, N. Divya, A brief review on the synthesis of $TiO_2$ thin films and its application in dye degradation, Mater. Today Proc. 72 (2023) 2749–2756. https://doi.org/10.1016/J.MATPR.2022.10.064.
[84] Y.-M. Chu, H.M.A. Javed, M. Awais, M.I. Khan, S. Shafqat, F.S. Khan, M.S. Mustafa, D. Ahmed, S.U. Khan, R.M.A. Khalil, Photocatalytic Pretreatment of Commercial Lignin Using $TiO_2$-ZnO Nanocomposite-Derived Advanced Oxidation Processes for Methane Production Synergy in Lab Scale Continuous Reactors, Catalysts 11 (2021) 54. https://doi.org/10.3390/catal11010054.
[85] R. Molinari, C. Limonti, C. Lavorato, A. Siciliano, P. Argurio, Upgrade of a slurry photocatalytic membrane reactor based on a vertical filter and an external membrane and testing in the photodegradation of a model pollutant in water, Chem. Eng. J. 451 (2023) 138577. https://doi.org/10.1016/J.CEJ.2022.138577.
[86] Z. Yang, C. Chen, B. Li, Y. Zheng, X. Liu, J. Shen, Y. Zhang, S. Wu, A core–shell 2D-$MoS_2$@MOF heterostructure for rapid therapy of bacteria-infected

wounds by enhanced photocatalysis, Chem. Eng. J. 451 (2023) 139127. https://doi.org/10.1016/J.CEJ.2022.139127.
[87] T. Zadi, M. Azizi, N. Nasrallah, A. Bouzaza, R. Maachi, D. Wolbert, S. Rtimi, A.A. Assadi, Indoor air treatment of refrigerated food chambers with synergetic association between cold plasma and photocatalysis: Process performance and photocatalytic poisoning, Chem. Eng. J. 382 (2020) 122951. https://doi.org/10.1016/J.CEJ.2019.122951.
[88] V.K. Gupta, R. Jain, A. Mittal, T.A. Saleh, A. Nayak, S. Agarwal, S. Sikarwar, Photo-catalytic degradation of toxic dye amaranth on $TiO_2$/UV in aqueous suspensions, Mater. Sci. Eng. C 32 (2012) 12–17. https://doi.org/10.1016/J.MSEC.2011.08.018.
[89] M. Nasr, C. Eid, R. Habchi, P. Miele, M. Bechelany, Recent Progress on Titanium Dioxide Nanomaterials for Photocatalytic Applications, ChemSusChem 11 (2018) 3023–3047. https://doi.org/10.1002/cssc.201800874.
[90] W.S. Koe, J.W. Lee, W.C. Chong, Y.L. Pang, L.C. Sim, An overview of photocatalytic degradation: photocatalysts, mechanisms, and development of photocatalytic membrane, Environ. Sci. Pollut. Res. 27 (2020) 2522–2565. https://doi.org/10.1007/s11356-019-07193-5.
[91] Lalliansanga, D. Tiwari, A. Tiwari, A. Shukla, M.J. Shim, S.-M. Lee, Facile synthesis and characterization of Ag(NP)/$TiO_2$ nanocomposite: Photocatalytic efficiency of catalyst for oxidative removal of Alizarin Yellow, Catal. Today 388–389 (2022) 125–133. https://doi.org/10.1016/j.cattod.2020.09.010.
[92] A. Tiwari, A. Shukla, Lalliansanga, D. Tiwari, S.-M. Lee, Au-nanoparticle/nanopillars $TiO_2$ meso-porous thin films in the degradation of tetracycline using UV-A light, J. Ind. Eng. Chem. 69 (2019) 141–152. https://doi.org/10.1016/j.jiec.2018.09.027.
[93] C. Zarzzeka, J. Goldoni, F. Marafon, W.G. Sganzerla, T. Forster-Carneiro, M.D. Bagatini, L.M.S. Colpini, Use of titanium dioxide nanoparticles for cancertreatment: A comprehensive review and bibliometric analysis, Biocatal. Agric. Biotechnol. 50 (2023) 102710. https://doi.org/10.1016/j.bcab.2023.102710.
[94] C. Nutescu Duduman, C. Gómez de Castro, G.A. Apostolescu, G. Ciobanu, D. Lutic, L. Favier, M. Harja, Enhancing the $TiO_2$-Ag Photocatalytic Efficiency by Acetone in the Dye Removal from Wastewater, Water 14 (2022) 2711. https://doi.org/10.3390/w14172711.
[95] M. Catanho, G.R.P. Malpass, A. de J. Motheo, Avaliação dos tratamentos eletroquímico e fotoeletroquímico na degradação de corantes têxteis, Quim. Nova 29 (2006) 983–989. https://doi.org/10.1590/S0100-40422006000500018.
[96] J. Wang, L. Svoboda, Z. Němečková, M. Sgarzi, J. Henych, N. Licciardello, G. Cuniberti, Enhanced visible-light photodegradation of fluoroquinolone-based antibiotics and *E. coli* growth inhibition using Ag–$TiO_2$ nanoparticles, RSC Adv. 11 (2021) 13980–13991. https://doi.org/10.1039/D0RA10403E.
[97] S. Bae, S. Kim, S. Lee, W. Choi, Dye decolorization test for the activity assessment of visible light photocatalysts: Realities and limitations, Catal. Today 224 (2014) 21–28. https://doi.org/10.1016/j.cattod.2013.12.019.
[98] F.M. Pesci, G. Wang, D.R. Klug, Y. Li, A.J. Cowan, Efficient Suppression of Electron–Hole Recombination in Oxygen-Deficient Hydrogen-Treated $TiO_2$

Nanowires for Photoelectrochemical Water Splitting, J. Phys. Chem. C 117 (2013) 25837–25844. https://doi.org/10.1021/jp4099914.
[99] A. Ghaffarian Khorram, N. Fallah, Comparison of electrocoagulation and photocatalytic process for treatment of industrial dyeing wastewater: Energy consumption analysis, Environ. Prog. Sustain. Energy 39 (2020). https://doi.org/10.1002/ep.13288.
[100] M. Behnajady, H. Eskandarloo, M. Shokri, Influence of the chemical structure of organic pollutants on photocatalytic activity of $TiO_2$ nanoparticles: kinetic analysis and evaluation of electrical energy per order (EEO), Chem. Environ. Sci. Mater. Sci. (2011).
[101] S.G. Poulopoulos, A. Yerkinova, G. Ulykbanova, V.J. Inglezakis, Photocatalytic treatment of organic pollutants in a synthetic wastewater using UV light and combinations of $TiO_2$, $H_2O_2$ and Fe(III), PLoS One 14 (2019) e0216745. https://doi.org/10.1371/journal.pone.0216745.
[102] E. Mousset, W.H. Loh, W.S. Lim, L. Jarry, Z. Wang, O. Lefebvre, Cost comparison of advanced oxidation processes for wastewater treatment using accumulated oxygen-equivalent criteria, Water Res. 200 (2021) 117234. https://doi.org/10.1016/j.watres.2021.117234.
[103] C. Köhler, S. Venditti, E. Igos, K. Klepiszewski, E. Benetto, A. Cornelissen, Elimination of pharmaceutical residues in biologically pre-treated hospital wastewater using advanced UV irradiation technology: A comparative assessment, J. Hazard. Mater. 239–240 (2012) 70–77. https://doi.org/10.1016/j.jhazmat.2012.06.006.
[104] R.C. Asha, M.A. Vishnuganth, N. Remya, N. Selvaraju, M. Kumar, Livestock Wastewater Treatment in Batch and Continuous Photocatalytic Systems: Performance and Economic Analyses, Water, Air, Soil Pollut. 226 (2015) 132. https://doi.org/10.1007/s11270-015-2396-4.
[105] R. Tanveer, A. Yasar, A.-B. Tabinda, A. Ikhlaq, H. Nissar, A.-S. Nizami, Comparison of ozonation, Fenton, and photo-Fenton processes for the treatment of textile dye-bath effluents integrated with electrocoagulation, J. Water Process Eng. 46 (2022) 102547. https://doi.org/10.1016/j.jwpe.2021.102547.
[106] P. Asaithambi, R. Govindarajan, M. Busier Yesuf, P. Selvakumar, E. Alemayehu, Enhanced treatment of landfill leachate wastewater using sono(US)-ozone($O_3$)–electrocoagulation(EC) process: role of process parameters on color, COD and electrical energy consumption, Process Saf. Environ. Prot. 142 (2020) 212–218. https://doi.org/10.1016/j.psep.2020.06.024.
[107] M. Krichevskaya, D. Klauson, E. Portjanskaja, S. Preis, The Cost Evaluation of Advanced Oxidation Processes in Laboratory and Pilot-Scale Experiments, Ozone Sci. Eng. 33 (2011) 211–223. https://doi.org/10.1080/01919512.2011.554141.
[108] S. Verbruggen, T. Tytgat, S. Passel, J. Martens, S. Lenaerts, Cost-effectiveness analysis to assess commercial $TiO_2$ photocatalysts for acetaldehyde degradation in air, Chem. Pap. 68 (2014). https://doi.org/10.2478/s11696-014-0557-3.
[109] H. Yang, K. Dai, J. Zhang, G. Dawson, Inorganic-organic hybrid photocatalysts: Syntheses, mechanisms, and applications, Chinese J. Catal. 43 (2022) 2111–2140. https://doi.org/10.1016/S1872-2067(22)64096-8.
[110] E.C. Silva, J.A. Bonacin, R.R. Passos, L.A. Pocrifka, The effect of an

external magnetic field on the photocatalytic activity of $CoFe_2O_4$ particles anchored in carbon cloth, J. Photochem. Photobiol. A Chem. 416 (2021) 113317. https://doi.org/10.1016/J.JPHOTOCHEM.2021.113317.
[111] M.S.N. Zahraei, R. Fazaeli, H. Aliyan, D. Richeson, Photocatalytic degradation abilities of binary core-shell $SiO_2$@m$ZrO_2$/$TiO_2$ nanocomposites: Characterization, kinetic and thermodynamic study of metoclopramide (MCP) eradication for water purification, Mater. Res. Bull. 157 (2023) 112029. https://doi.org/10.1016/J.MATERRESBULL.2022.112029.
[112] J. Li, Q. Wu, J. Wu, Synthesis of nanoparticles via solvothermal and hydrothermal methods. In: Handbook of Nanoparticles, in: M. Aliofkhazraei (Ed.), Springer International Publishing, Cham, 2015. https://doi.org/10.1007/978-3-319-13188-7.
[113] J. Varghese, CuS–ZnS decorated graphene nanocomposites: Synthesis and photocatalytic properties, J. Phys. Chem. Solids 156 (2021) 109911. https://doi.org/10.1016/J.JPCS.2020.109911.
[114] R.E. Krebs, The history and use of our earth's chemical elements: a reference guide, Greenwood Publishing Group, 2006.
[115] E. Pulido Melián, O. González Díaz, A. Ortega Méndez, C.R. López, M. Nereida Suárez, J.M. Doña Rodríguez, J.A. Navío, D. Fernández Hevia, J. Pérez Peña, Efficient and affordable hydrogen production by water photo-splitting using $TiO_2$-based photocatalysts, Int. J. Hydrogen Energy 38 (2013) 2144–2155. https://doi.org/10.1016/j.ijhydene.2012.12.005.
[116] J.S. Jang, H.G. Kim, J.S. Lee, Heterojunction semiconductors: A strategy to develop efficient photocatalytic materials for visible light water splitting, Catal. Today 185 (2012) 270–277. https://doi.org/10.1016/j.cattod.2011.07.008.
[117] D. Hou, Q. Mao, Y. Ren, K.H. Luo, Atomic insights into mechanisms of carbon coating on titania nanoparticle during flame synthesis, Carbon N. Y. 201 (2023) 189–199. https://doi.org/10.1016/J.CARBON.2022.09.002.
[118] N.'A. Razali, S.A. Othman Sol-gel technique in study of titanium dioxide ($TiO_2$) photocatalytic activity- a short review Mater. Today Proc., 66 (2022), pp. 4077-4083, 10.1016/j.matpr.2022.07.150
[119] T.L.R. Hewer, Síntese e modificação superficial do $TiO_2$ visando aumentar a eficiência do processo de fotocatálise heterogênea no tratamento de compostos fenólicos, Universidade de São Paulo, 2005. https://doi.org/10.11606/D.46.2005.tde-28022007-174000.
[120] D. Spasiano, R. Marotta, S. Malato, P. Fernandez-Ibañez, I. Di Somma, Solar photocatalysis: Materials, reactors, some commercial, and pre-industrialized applications. A comprehensive approach, Appl. Catal. B Environ. 170–171 (2015) 90–123. https://doi.org/10.1016/J.APCATB.2014.12.050.
[121] M.-I. Mendoza-Diaz, J. Cure, M.D. Rouhani, K. Tan, S.-G. Patnaik, D. Pech, M. Quevedo-Lopez, T. Hungria, C. Rossi, A. Estève, On the UV–Visible Light Synergetic Mechanisms in Au/$TiO_2$ Hybrid Model Nanostructures Achieving Photoreduction of Water, J. Phys. Chem. C 124 (2020) 25421–25430. https://doi.org/10.1021/acs.jpcc.0c08381.
[122] J. Li, Z. Jin, Y. Zhang, D. Liu, A. Ma, Y. Sun, X. Li, Q. Cai, J. Gui, Ag-induced anatase-rutile $TiO_2$−x heterojunction facilitating the photogenerated carrier separation in visible-light irradiation, J. Alloys Compd. 909 (2022) 164815.

https://doi.org/10.1016/J.JALLCOM.2022.164815.
[123] J.M. Herrmann, C. Guillard, P. Pichat, Heterogeneous photocatalysis : an emerging technology for water treatment, Catal. Today 17 (1993) 7–20. https://doi.org/10.1016/0920-5861(93)80003-J.
[124] M.R. Hoffmann, S.T. Martin, W. Choi, D.W. Bahnemann, Environmental Applications of Semiconductor Photocatalysis, Chem. Rev. 95 (1995) 69–96. https://doi.org/10.1021/cr00033a004.
[125] W. Tu, W. Guo, J. Hu, H. He, H. Li, Z. Li, W. Luo, Y. Zhou, Z. Zou, State-of-the-art advancements of crystal facet-exposed photocatalysts beyond $TiO_2$: Design and dependent performance for solar energy conversion and environment applications, Mater. Today 33 (2020) 75–86. https://doi.org/10.1016/J.MATTOD.2019.09.003.
[126] B. Sun, Q. Li, M. Zheng, G. Su, S. Lin, M. Wu, C. Li, Q. Wang, Y. Tao, L. Dai, Y. Qin, B. Meng, Recent advances in the removal of persistent organic pollutants (POPs) using multifunctional materials:a review, Environ. Pollut. 265 (2020) 114908. https://doi.org/10.1016/J.ENVPOL.2020.114908.
[127] K.H. Ng, Adoption of $TiO_2$-photocatalysis for palm oil mill effluent (POME) treatment: Strengths, weaknesses, opportunities, threats (SWOT) and its practicality against traditional treatment in Malaysia, Chemosphere 270 (2021) 129378. https://doi.org/10.1016/J.CHEMOSPHERE.2020.129378.
[128] G. Ozin, Accelerated optochemical engineering solutions to $CO_2$ photocatalysis for a sustainable future, Matter 5 (2022) 2594–2614. https://doi.org/10.1016/j.matt.2022.07.033.
[129] B. Yahia, S. Faouzi, C. Ahmed, S. lounis, T. Mohamed, A new hybrid process for Amoxicillin elimination by combination of adsorption and photocatalysis on (CuO/AC) under solar irradiation, J. Mol. Struct. 1261 (2022) 132769. https://doi.org/10.1016/J.MOLSTRUC.2022.132769.
[130] J. Carbajo, A. Tolosana-Moranchel, J.A. Casas, M. Faraldos, A. Bahamonde, Analysis of photoefficiency in $TiO_2$ aqueous suspensions: Effect of titania hydrodynamic particle size and catalyst loading on their optical properties, Appl. Catal. B Environ. 221 (2018) 1–8. https://doi.org/10.1016/J.APCATB.2017.08.032.
[131] D. Chen, Y. Cheng, N. Zhou, P. Chen, Y. Wang, K. Li, S. Huo, P. Cheng, P. Peng, R. Zhang, L. Wang, H. Liu, Y. Liu, R. Ruan, Photocatalytic degradation of organic pollutants using $TiO_2$-based photocatalysts: A review, J. Clean. Prod. 268 (2020) 121725. https://doi.org/10.1016/j.jclepro.2020.121725.
[132] S. Lakshmi, R. Renganathan, S. Fujita, Study on $TiO_2$-mediated photocatalytic degradation of methylene blue, J. Photochem. Photobiol. A Chem. 88 (1995) 163–167. https://doi.org/10.1016/1010-6030(94)04030-6.
[133] M. Tobajas, C. Belver, J.J. Rodriguez, Degradation of emerging pollutants in water under solar irradiation using novel $TiO_2$-ZnO/clay nanoarchitectures, Chem. Eng. J. 309 (2017) 596–606. https://doi.org/10.1016/j.cej.2016.10.002.
[134] M. Chaki Borrás, R. Sluyter, P.J. Barker, K. Konstantinov, S. Bakand, $Y_2O_3$ decorated $TiO_2$ nanoparticles: Enhanced UV attenuation and suppressed photocatalytic activity with promise for cosmetic and sunscreen applications, J. Photochem. Photobiol. B Biol. 207 (2020) 111883. https://doi.org/10.1016/J.JPHOTOBIOL.2020.111883.
[135] S. Qourzal, M. Tamimi, A. Assabbane, Y. Ait-Ichou, Photocatalytic degradation and adsorption of 2-naphthol on suspended $TiO_2$ surface in a

dynamic reactor, J. Colloid Interface Sci. 286 (2005) 621–626. https://doi.org/10.1016/J.JCIS.2005.01.046.
[136] J.A. Khan, M. Sayed, S. Khan, N.S. Shah, D.D. Dionysiou, G. Boczkaj, Advanced oxidation processes for the treatment of contaminants of emerging concern, Contam. Emerg. Concern Water Wastewater Adv. Treat. Process. (2020) 299–365. https://doi.org/10.1016/B978-0-12-813561-7.00009-2.
[137] Q. Chen, L. Chen, J. Qi, Y. Tong, Y. Lv, C. Xu, J. Ni, W. Liu, Photocatalytic degradation of amoxicillin by carbon quantum dots modified $K_2Ti_6O_{13}$ nanotubes: Effect of light wavelength, Chinese Chem. Lett. 30 (2019) 1214–1218. https://doi.org/10.1016/J.CCLET.2019.03.002.
[138] G. Pansamut, T. Charinpanitkul, P. Biswas, A. Suriyawong, Removal of Humic Acid by Photocatalytic Process: Effect of Light Intensity, Eng. J. 17 (2013) 25–32. https://doi.org/10.4186/ej.2013.17.3.25.
[139] Y. Meng, X. Huang, Y. Wu, X. Wang, Y. Qian, Kinetic study and modeling on photocatalytic degradation of para-chlorobenzoate at different light intensities, Environ. Pollut. 117 (2002) 307–313. https://doi.org/10.1016/S0269-7491(01)00184-1.
[140] F. Chen, X. Yang, Q. Wu, Photocatalytic Oxidation of *Escherischia coli*, *Aspergillus niger*, and Formaldehyde under Different Ultraviolet Irradiation Conditions, Environ. Sci. Technol. 43 (2009) 4606–4611. https://doi.org/10.1021/es900505h.
[141] J.M. Doña, C. Garriga, J. Araña, J. Pérez, G. Colon, M. Macías, J.A. Navio, The effect of dosage on the photocatalytic degradation of organic pollutants, Res. Chem. Intermed. 33 (2007) 351–358. https://doi.org/10.1163/156856707779238676.
[142] S. Upadhya, D.F. Ollis, A Simple Kinetic Model for the Simultaneous Concentration and Intensity Dependencies of TCE Photocatalyzed Destruction, J. Adv. Oxid. Technol. 3 (1998). https://doi.org/10.1515/jaots-1998-0214.
[143] I. Poulios, I. Tsachpinis, Photodegradation of the textile dye Reactive Black 5 in the presence of semiconducting oxides, J. Chem. Technol. Biotechnol. 74 (1999) 349–357. https://doi.org/10.1002/(SICI)1097-4660(199904)74:4<349::AID-JCTB5>3.0.CO;2-7.
[144] S. Dai, L. Xiao, Q. Li, G. Hao, Y. Hu, W. Jiang, 0D/1D $Co_3O_4$ quantum dots/surface hydroxylated g-$C_3N_4$ nanofibers heterojunction with enhanced photocatalytic removal of pharmaceuticals and personal care products, Sep. Purif. Technol. 297 (2022) 121481. https://doi.org/10.1016/J.SEPPUR.2022.121481.
[145] T. Sauer, Photocatalytic degradation of dye and textile effluent., UFSC, 2002.
[146] J. He, A. Kumar, M. Khan, I.M.C. Lo, Critical review of photocatalytic disinfection of bacteria: from noble metals- and carbon nanomaterials-$TiO_2$ composites to challenges of water characteristics and strategic solutions, Sci. Total Environ. 758 (2021) 143953. https://doi.org/10.1016/j.scitotenv.2020.143953.
[147] L. Yuan, D. Huang, W. Guo, Q. Yang, J. Yu, $TiO_2$/montmorillonite nanocomposite for removal of organic pollutant, Appl. Clay Sci. 53 (2011) 272–278. https://doi.org/10.1016/J.CLAY.2011.03.013.
[148] M.R. Prairie, L.R. Evans, B.M. Stange, S.L. Martinez, An investigation of

titanium dioxide photocatalysis for the treatment of water contaminated with metals and organic chemicals, Environ. Sci. Technol. 27 (1993) 1776–1782. https://doi.org/10.1021/es00046a003.
[149] W. Zhang, Y. Li, Y. Su, K. Mao, Q. Wang, Effect of water composition on $TiO_2$ photocatalytic removal of endocrine disrupting compounds (EDCs) and estrogenic activity from secondary effluent, J. Hazard. Mater. 215–216 (2012) 252–258. https://doi.org/10.1016/j.jhazmat.2012.02.060.
[150] A. Katz, A. McDonagh, L. Tijing, H.K. Shon, Fouling and Inactivation of Titanium Dioxide-Based Photocatalytic Systems, Crit. Rev. Environ. Sci. Technol. 45 (2015) 1880–1915. https://doi.org/10.1080/10643389.2014.1000763.
[151] P.R. Gogate, A.B. Pandit, A review of imperative technologies for wastewater treatment II: hybrid methods, Adv. Environ. Res. 8 (2004) 553–597. https://doi.org/10.1016/S1093-0191(03)00031-5.
[152] B. Liu, H. Wu, I.P. Parkin, New Insights into the Fundamental Principle of Semiconductor Photocatalysis, ACS Omega 5 (2020) 14847–14856. https://doi.org/10.1021/acsomega.0c02145.
[153] M.A. Fox, M.T. Dulay, Heterogeneous photocatalysis, Chem. Rev. 93 (1993) 341–357. https://doi.org/10.1021/cr00017a016.
[154] J. Goniakowski, C. Noguera, Theoretical investigation of hydroxylated oxide surfaces, Surf. Sci. 330 (1995) 337–349. https://doi.org/10.1016/0039-6028(95)00348-7.
[155] Y. Du, W. Li, Y. Bai, Z. Huangfu, W. Wang, R. Chai, C. Chen, X. Yang, Q. Feng, Facile synthesis of $TiO_2/Ag_3PO_4$ composites with co-exposed high-energy facets for efficient photodegradation of rhodamine B solution under visible light irradiation, RSC Adv. 10 (2020) 24555–24569. https://doi.org/10.1039/D0RA04183A.
[156] M. Salazar-Villanueva, L.R. Morales-Juárez, O. Flores Sánchez, A. Cruz-López, A. Tovar-Corona, O. Vázquez-Cuchillo, Enhanced photocatalytic water splitting hydrogen production on $TiO_2$ nanospheres: A theoretical-experimental approach, J. Photochem. Photobiol. A Chem. 434 (2023) 114212. https://doi.org/10.1016/J.JPHOTOCHEM.2022.114212.
[157] P.V. Govardhana Reddy, B. Rajendra Prasad Reddy, M. Venkata Krishna Reddy, K. Raghava Reddy, N.P. Shetti, T.A. Saleh, T.M. Aminabhavi, A review on multicomponent reactions catalysed by zero-dimensional/one-dimensional titanium dioxide ($TiO_2$) nanomaterials: Promising green methodologies in organic chemistry, J. Environ. Manage. 279 (2021) 111603. https://doi.org/10.1016/J.JENVMAN.2020.111603.
[158] P. Kalita, P. Jyoti Boruah, R. Ruchel Khanikar, H. Bailung, Plasma–induced rapid crystallization and surface engraving of amorphous $TiO_x(OH)_y$ to enhance adsorption and photocatalytic activity, J. Photochem. Photobiol. A Chem. 434 (2023) 114251. https://doi.org/10.1016/J.JPHOTOCHEM.2022.114251.
[159] M. Zalfani, B. van der Schueren, M. Mahdouani, R. Bourguiga, W.B. Yu, M. Wu, O. Deparis, Y. Li, B.L. Su, ZnO quantum dots decorated 3DOM $TiO_2$ nanocomposites: Symbiose of quantum size effects and photonic structure for highly enhanced photocatalytic degradation of organic pollutants, Appl. Catal. B Environ. 199 (2016) 187–198. https://doi.org/10.1016/J.APCATB.2016.06.016.
[160] S.I. Mogal, V.G. Gandhi, M. Mishra, S. Tripathi, T. Shripathi, P.A. Joshi, D.O.

Shah, Single-Step Synthesis of Silver-Doped Titanium Dioxide: Influence of Silver on Structural, Textural, and Photocatalytic Properties, Ind. Eng. Chem. Res. 53 (2014) 5749–5758. https://doi.org/10.1021/ie404230q.
[161] X. Li, L. Wang, X. Lu, Preparation of silver-modified $TiO_2$ via microwave-assisted method and its photocatalytic activity for toluene degradation, J. Hazard. Mater. 177 (2010) 639–647. https://doi.org/10.1016/j.jhazmat.2009.12.080.
[162] N.Z. Hafizah, J. M. Juoi, M.R. Zulkifli, M.A. Musa, Effect of Silver Content on the Crystalline Phase and Microstructure of $TiO_2$ Coating Deposited on Unglazed Ceramics Tile, Int. J. Automot. Mech. Eng. 17 (2020) 8179–8185. https://doi.org/10.15282/ijame.17.3.2020.11.0615.
[163] J.A. Rengifo-Herrera, C. Pulgarin, Why five decades of massive research on heterogeneous photocatalysis, especially on $TiO_2$, has not yet driven to water disinfection and detoxification applications? Critical review of drawbacks and challenges, Chem. Eng. J. 477 (2023) 146875. https://doi.org/10.1016/j.cej.2023.146875.
[164] M.G. Alalm, R. Djellabi, D. Meroni, C. Pirola, C.L. Bianchi, D.C. Boffito, Toward Scaling-Up Photocatalytic Process for Multiphase Environmental Applications, Catalysts 11 (2021) 562. https://doi.org/10.3390/catal11050562.
[165] Y. Ding, L. Zeng, X. Xiao, T. Chen, Y. Pan, Multifunctional Magnetic Nanoagents for Bioimaging and Therapy, ACS Appl. Bio Mater. 4 (2021) 1066–1076. https://doi.org/10.1021/acsabm.0c01099.
[166] C.H. Nguyen, C.-C. Fu, R.-S. Juang, Degradation of methylene blue and methyl orange by palladium-doped $TiO_2$ photocatalysis for water reuse: Efficiency and degradation pathways, J. Clean. Prod. 202 (2018) 413–427. https://doi.org/10.1016/j.jclepro.2018.08.110.
[167] M.R. Panigrahi, M. Devi, Variation of Optical and Electrical Properties of Zr Doped $TiO_2$ Thin Films with Different Annealing Temperatures, J. Phys. Conf. Ser. 1172 (2019) 012046. https://doi.org/10.1088/1742-6596/1172/1/012046.
[168] J. Schneider, M. Matsuoka, M. Takeuchi, J. Zhang, Y. Horiuchi, M. Anpo, D.W. Bahnemann, Understanding $TiO_2$ Photocatalysis: Mechanisms and Materials, Chem. Rev. 114 (2014) 9919–9986. https://doi.org/10.1021/cr5001892.
[169] M.R. Al-Mamun, S. Kader, M.S. Islam, M.Z.H. Khan, Photocatalytic activity improvement and application of UV-$TiO_2$ photocatalysis in textile wastewater treatment: A review, J. Environ. Chem. Eng. 7 (2019) 103248. https://doi.org/10.1016/j.jece.2019.103248.
[170] P.S. Basavarajappa, S.B. Patil, N. Ganganagappa, K.R. Reddy, A. V. Raghu, C.V. Reddy, Recent progress in metal-doped $TiO_2$, non-metal doped/codoped $TiO_2$ and $TiO_2$ nanostructured hybrids for enhanced photocatalysis, Int. J. Hydrogen Energy 45 (2020) 7764–7778. https://doi.org/10.1016/j.ijhydene.2019.07.241.
[171] R. Daghrir, P. Drogui, D. Robert, Modified $TiO_2$ For Environmental Photocatalytic Applications: A Review, Ind. Eng. Chem. Res. 52 (2013) 3581–3599. https://doi.org/10.1021/ie303468t.
[172] S. Oros-Ruiz, R. Zanella, B. Prado, Photocatalytic degradation of trimethoprim by metallic nanoparticles supported on $TiO_2$-P25, J. Hazard. Mater. 263 (2013) 28–35. https://doi.org/10.1016/j.jhazmat.2013.04.010.

[173] T. Aguilar, J. Navas, R. Alcántara, C. Fernández-Lorenzo, J.J. Gallardo, G. Blanco, J. Martín-Calleja, A route for the synthesis of Cu-doped $TiO_2$ nanoparticles with a very low band gap, Chem. Phys. Lett. 571 (2013) 49–53. https://doi.org/10.1016/j.cplett.2013.04.007.
[174] Z. Wang, L. Shi, F. Wu, S. Yuan, Y. Zhao, M. Zhang, The sol–gel template synthesis of porous $TiO_2$ for a high performance humidity sensor, Nanotechnology 22 (2011) 275502. https://doi.org/10.1088/0957-4484/22/27/275502.
[175] C. Liao, Y. Li, S.C. Tjong, Visible-Light Active Titanium Dioxide Nanomaterials with Bactericidal Properties, Nanomaterials 10 (2020) 124. https://doi.org/10.3390/nano10010124.
[176] C.M. Teh, A.R. Mohamed, Roles of titanium dioxide and ion-doped titanium dioxide on photocatalytic degradation of organic pollutants (phenolic compounds and dyes) in aqueous solutions: A review, J. Alloys Compd. 509 (2011) 1648–1660. https://doi.org/10.1016/j.jallcom.2010.10.181.
[177] S. Abbad, K. Guergouri, S. Gazaout, S. Djebabra, A. Zertal, R. Barille, M. Zaabat, Effect of silver doping on the photocatalytic activity of $TiO_2$ nanopowders synthesized by the sol-gel route, J. Environ. Chem. Eng. 8 (2020) 103718. https://doi.org/10.1016/j.jece.2020.103718.
[178] S.-Y. Ryu, J.W. Chung, S.-Y. Kwak, Dependence of photocatalytic and antimicrobial activity of electrospun polymeric nanofiber composites on the positioning of Ag–$TiO_2$ nanoparticles, Compos. Sci. Technol. 117 (2015) 9–17. https://doi.org/10.1016/j.compscitech.2015.05.014.
[179] B. Koozegar Kaleji, M. Gorgani, Comparison of sol-gel and hydrothermal synthesis methods on the structural, optical and photocatalytic properties of Nb/Ag codoped $TiO_2$ mesoporous nanoparticles, Int. J. Environ. Anal. Chem. 102 (2022) 3357–3372. https://doi.org/10.1080/03067319.2020.1767096.
[180] R.T. Yunarti, L.C.C. Dimonti, D. Angelia, A. Buhori, A. Umar, A.A. Dwiatmoko, J.-M. Ha, Comparison study of the effects of different synthesis methods towards $Ag_2O/TiO_2$ nanowires' morphology and catalytic activity on the 4-nitrophenol reduction reaction, Nano-Struct. & Nano-Objects 36 (2023) 101042. https://doi.org/10.1016/j.nanoso.2023.101042.
[181] D. Jiang, K. Kusdianto, M. Kubo, M. Shimada, Effect of Ag loading content on morphology and photocatalytic activity of Ag-$TiO_2$ nanoparticulate films prepared via simultaneous plasma-enhanced chemical and physical vapor deposition, Mater. Res. Express 7 (2020) 116406. https://doi.org/10.1088/2053-1591/abc720.
[182] S.-J. Lee, A. Gavriilidis, Supported Au Catalysts for Low-Temperature CO Oxidation Prepared by Impregnation, J. Catal. 206 (2002) 305–313. https://doi.org/10.1006/jcat.2001.3500.
[183] J. Girardon, E. Quinet, A. Gribovalconstant, P. Chernavskii, L. Gengembre, A. Khodakov, Cobalt dispersion, reducibility, and surface sites in promoted silica-supported Fischer–Tropsch catalysts, J. Catal. 248 (2007) 143–157. https://doi.org/10.1016/j.jcat.2007.03.002.
[184] X. Hao, S. Barnes, J.R. Regalbuto, A fundamental study of Pt impregnation of carbon: Adsorption equilibrium and particle synthesis, J. Catal. 279 (2011) 48–65. https://doi.org/10.1016/j.jcat.2010.12.021.
[185] R. M. Kulkarni, R. S. Malladi, M. S. Hanagadakar, Ag-$TiO_2$ nanoparticles for photocatalytic degradation of sparfloxacin, Adv. Mater. Proc. 3 (2021) 526–529. https://doi.org/10.5185/amp.2018/7018.

[186] G. Suriati, M. Mariatti, A. Azizan, Synthesis of silver nanoparticles by chemical reduction method: effect of reducing agent and surfactant concentration, Int. J. Automot. Mech. Eng. 10 (2014) 1920–1927. https://doi.org/10.15282/ijame.10.2014.9.0160.
[187] N. Zhou, V. López-Puente, Q. Wang, L. Polavarapu, I. Pastoriza-Santos, Q.-H. Xu, Plasmon-enhanced light harvesting: applications in enhanced photocatalysis, photodynamic therapy and photovoltaics, RSC Adv. 5 (2015) 29076–29097. https://doi.org/10.1039/C5RA01819F.
[188] Z. Shan, J. Wu, F. Xu, F.-Q. Huang, H. Ding, Highly Effective Silver/Semiconductor Photocatalytic Composites Prepared by a Silver Mirror Reaction, J. Phys. Chem. C 112 (2008) 15423–15428. https://doi.org/10.1021/jp804482k.
[189] J. Li, J. Xu, W.-L. Dai, K. Fan, Dependence of Ag Deposition Methods on the Photocatalytic Activity and Surface State of $TiO_2$ with Twistlike Helix Structure, J. Phys. Chem. C 113 (2009) 8343–8349. https://doi.org/10.1021/jp8114012.
[190] K. Do Kim, D.N. Han, J.B. Lee, H.T. Kim, Formation and characterization of Ag-deposited $TiO_2$ nanoparticles by chemical reduction method, Scr. Mater. 54 (2006) 143–146. https://doi.org/10.1016/j.scriptamat.2005.09.054.
[191] A. Feinle, M.S. Elsaesser, N. Hüsing, Sol–gel synthesis of monolithic materials with hierarchical porosity, Chem. Soc. Rev. 45 (2016) 3377–3399. https://doi.org/10.1039/C5CS00710K.
[192] C. Prasad, Q. Liu, H. Tang, G. Yuvaraja, J. Long, A. Rammohan, G. V. Zyryanov, An overview of graphene oxide supported semiconductors based photocatalysts: Properties, synthesis and photocatalytic applications, J. Mol. Liq. 297 (2020) 111826. https://doi.org/10.1016/j.molliq.2019.111826.
[193] P. Periyat, P.A. Saeed, S.G. Ullattil, Anatase titania nanorods by pseudo-inorganic templating, Mater. Sci. Semicond. Process. 31 (2015) 658–665. https://doi.org/10.1016/j.mssp.2014.12.040.
[194] M. Sharma, M. Pathak, P.N. Kapoor, The Sol-Gel Method: Pathway to Ultrapure and Homogeneous Mixed Metal Oxide Nanoparticles, Asian J. Chem. 30 (2018) 1405–1412. https://doi.org/10.14233/ajchem.2018.20845.
[195] C. Prasad, X. Yang, Q. Liu, H. Tang, A. Rammohan, S. Zulfiqar, G. V. Zyryanov, S. Shah, Recent advances in MXenes supported semiconductors based photocatalysts: Properties, synthesis and photocatalytic applications, J. Ind. Eng. Chem. 85 (2020) 1–33. https://doi.org/10.1016/j.jiec.2019.12.003.
[196] Pant, Park, Park, Recent Advances in $TiO_2$ Films Prepared by Sol-gel Methods for Photocatalytic Degradation of Organic Pollutants and Antibacterial Activities, Coatings 9 (2019) 613. https://doi.org/10.3390/coatings9100613.
[197] O. V. Kharissova, B.I. Kharisov, C.M. Oliva González, Y.P. Méndez, I. López, Greener synthesis of chemical compounds and materials, R. Soc. Open Sci. 6 (2019) 191378. https://doi.org/10.1098/rsos.191378.
[198] H. Bel Hadjltaief, M.E. Galvez, M. Ben Zina, P. Da Costa, $TiO_2$/clay as a heterogeneous catalyst in photocatalytic/photochemical oxidation of anionic reactive blue 19, Arab. J. Chem. 12 (2019) 1454–1462. https://doi.org/10.1016/j.arabjc.2014.11.006.
[199] A. Nazir, A. Akbar, H.B. Baghdadi, S. ur Rehman, E. Al-Abbad, M. Fatima, M. Iqbal, N. Tamam, N. Alwadai, M. Abbas, Zinc oxide nanoparticles

fabrication using *Eriobotrya japonica* leaves extract: Photocatalytic performance and antibacterial activity evaluation, Arab. J. Chem. 14 (2021) 103251. https://doi.org/10.1016/J.ARABJC.2021.103251.
[200] C.H. Nguyen, R.-S. Juang, Efficient removal of methylene blue dye by a hybrid adsorption–photocatalysis process using reduced graphene oxide/titanate nanotube composites for water reuse, J. Ind. Eng. Chem. 76 (2019) 296–309. https://doi.org/10.1016/j.jiec.2019.03.054.
[201] S.P. Ghawade, K.N. Pande, S.J. Dhoble, A.D. Deshmukh, Tuning the properties of ZnS semiconductor by the addition of graphene, in: Nanoscale Compd. Semicond. Their Optoelectron. Appl., Elsevier, 2022: pp. 351–381. https://doi.org/10.1016/B978-0-12-824062-5.00005-1.
[202] G. Huang, C.-H. Lu, H.-H. Yang, Magnetic Nanomaterials for Magnetic Bioanalysis, in: Nov. Nanomater. Biomed. Environ. Energy Appl., Elsevier, 2019: pp. 89–109. https://doi.org/10.1016/B978-0-12-814497-8.00003-5.
[203] W.-X. Liu, J. Ma, X.-G. Qu, W.-B. Cao, Hydrothermal synthesis of (Fe, N) co-doped $TiO_2$ powders and their photocatalytic properties under visible light irradiation, Res. Chem. Intermed. 35 (2009) 321–328. https://doi.org/10.1007/s11164-009-0025-9.
[204] T. Parangi, M.K. Mishra, Titania Nanoparticles as Modified Photocatalysts: A Review on Design and Development, Comments Inorg. Chem. 39 (2019) 90–126. https://doi.org/10.1080/02603594.2019.1592751.
[205] A.B. Uluşan, A. Tataroğlu, Frequency-Dependent Dielectric Parameters of Au/$TiO_2$/n-Si (MIS) Structure, Silicon 10 (2018) 2071–2077. https://doi.org/10.1007/s12633-017-9722-y.
[206] A. Mezni, N. Ben Saber, M.M. Ibrahim, N. Hamdaoui, A. Alrooqi, A. Mlayah, T. altalhi, Photocatalytic activity of hybrid gold-titania nanocomposites, Mater. Chem. Phys. 221 (2019) 118–124. https://doi.org/10.1016/j.matchemphys.2018.09.035.
[207] R. Zanella, L. Delannoy, C. Louis, Mechanism of deposition of gold precursors onto $TiO_2$ during the preparation by cation adsorption and deposition–precipitation with NaOH and urea, Appl. Catal. A Gen. 291 (2005) 62–72. https://doi.org/10.1016/j.apcata.2005.02.045.
[208] D. Zhang, C. Zhang, P. Zhou, Preparation of porous nano-calcium titanate microspheres and its adsorption behavior for heavy metal ion in water, J. Hazard. Mater. 186 (2011) 971–977. https://doi.org/10.1016/j.jhazmat.2010.11.096.
[209] J. Yu, G. Dai, B. Huang, Fabrication and Characterization of Visible-Light-Driven Plasmonic Photocatalyst Ag/AgCl/$TiO_2$ Nanotube Arrays, J. Phys. Chem. C 113 (2009) 16394–16401. https://doi.org/10.1021/jp905247j.
[210] H. Cheng, B. Huang, P. Wang, Z. Wang, Z. Lou, J. Wang, X. Qin, X. Zhang, Y. Dai, In situ ion exchange synthesis of the novel Ag/AgBr/BiOBr hybrid with highly efficient decontamination of pollutants, Chem. Commun. 47 (2011) 7054. https://doi.org/10.1039/c1cc11525a.
[211] X. Zhou, G. Liu, J. Yu, W. Fan, Surface plasmon resonance-mediated photocatalysis by noble metal-based composites under visible light, J. Mater. Chem. 22 (2012) 21337. https://doi.org/10.1039/c2jm31902k.
[212] K. Wenderich, G. Mul, Methods, Mechanism, and Applications of Photodeposition in Photocatalysis: A Review, Chem. Rev. 116 (2016) 14587–14619. https://doi.org/10.1021/acs.chemrev.6b00327.
[213] J. Prakash, P. Kumar, R.A. Harris, C. Swart, J.H. Neethling, A.J. van Vuuren,

H.C. Swart, Synthesis, characterization and multifunctional properties of plasmonic Ag–$TiO_2$ nanocomposites, Nanotechnology 27 (2016) 355707. https://doi.org/10.1088/0957-4484/27/35/355707.
[214] S. Anandan, P. Sathish Kumar, N. Pugazhenthiran, J. Madhavan, P. Maruthamuthu, Effect of loaded silver nanoparticles on $TiO_2$ for photocatalytic degradation of Acid Red 88, Sol. Energy Mater. Sol. Cells 92 (2008) 929–937. https://doi.org/10.1016/j.solmat.2008.02.020.
[215] E. Pipelzadeh, A.A. Babaluo, M. Haghighi, A. Tavakoli, M.V. Derakhshan, A.K. Behnami, Silver doping on $TiO_2$ nanoparticles using a sacrificial acid and its photocatalytic performance under medium pressure mercury UV lamp, Chem. Eng. J. 155 (2009) 660–665. https://doi.org/10.1016/j.cej.2009.08.023.
[216] Ion Exchange, in: Pract. Waste Water Treat., Wiley, 2019: pp. 403–407. https://doi.org/10.1002/9781119527114.ch18.
[217] A. Ali, M. Sadia, M. Azeem, M.Z. Ahmad, M. Umar, Z. Ul Abbas, Ion Exchange Resins and their Applications in Water Treatment and Pollutants Removal from Environment: A Review, Futur. Biotechnol. (2023) 12–19. https://doi.org/10.54393/fbt.v3i03.51.
[218] Q. Yang, M. Hu, J. Guo, Z. Ge, J. Feng, Synthesis and enhanced photocatalytic performance of Ag/AgCl/$TiO_2$ nanocomposites prepared by ion exchange method, J. Mater. 4 (2018) 402–411. https://doi.org/10.1016/j.jmat.2018.06.002.
[219] Z. Liu, M. Haddad, S. Sauvé, B. Barbeau, Alleviating the burden of ion exchange brine in water treatment: From operational strategies to brine management, Water Res. 205 (2021) 117728. https://doi.org/10.1016/j.watres.2021.117728.
[220] B. Paull, R. Michalski, Ion Exchange: Ion Chromatography Principles and Applications, in: Ref. Modul. Chem. Mol. Sci. Chem. Eng., Elsevier, 2018. https://doi.org/10.1016/B978-0-12-409547-2.14502-0.
[221] N. Torkian, A. Bahrami, A. Hosseini-Abari, M.M. Momeni, M. Abdolkarimi-Mahabadi, A. Bayat, P. Hajipour, H. Amini Rourani, M.S. Abbasi, S. Torkian, Y. Wen, M. Yazdan Mehr, A. Hojjati-Najafabadi, Synthesis and characterization of Ag-ion-exchanged zeolite/$TiO_2$ nanocomposites for antibacterial applications and photocatalytic degradation of antibiotics, Environ. Res. 207 (2022) 112157. https://doi.org/10.1016/j.envres.2021.112157.
[222] H. Zhang, G. Chen, Potent Antibacterial Activities of Ag/$TiO_2$ Nanocomposite Powders Synthesized by a One-Pot Sol−Gel Method, Environ. Sci. Technol. 43 (2009) 2905–2910. https://doi.org/10.1021/es803450f.
[223] A. Mills, N. Elliott, I.P. Parkin, S.A. O'Neill, R.J. Clark, Novel $TiO_2$ CVD films for semiconductor photocatalysis, J. Photochem. Photobiol. A Chem. 151 (2002) 171–179. https://doi.org/10.1016/S1010-6030(02)00190-9.
[224] S. Ahmadi, N. Asim, M.A. Alghoul, F.Y. Hammadi, K. Saeedfar, N.A. Ludin, S.H. Zaidi, K. Sopian, The Role of Physical Techniques on the Preparation of Photoanodes for Dye Sensitized Solar Cells, Int. J. Photoenergy 2014 (2014) 1–19. https://doi.org/10.1155/2014/198734.
[225] A.V. Rane, K. Kanny, V.K. Abitha, S. Thomas, Methods for Synthesis of Nanoparticles and Fabrication of Nanocomposites, in: Synth. Inorg. Nanomater., Elsevier, 2018: pp. 121–139. https://doi.org/10.1016/B978-0-08-101975-7.00005-1.

[226] M.C. Joseph, C. Tsotsos, M.A. Baker, P.J. Kench, C. Rebholz, A. Matthews, A. Leyland, Characterisation and tribological evaluation of nitrogen-containing molybdenum–copper PVD metallic nanocomposite films, Surf. Coatings Technol. 190 (2005) 345–356. https://doi.org/10.1016/j.surfcoat.2004.04.074.
[227] G.S. Falk, M. Borlaf, M.J. López-Muñoz, J.C. Fariñas, J.B. Rodrigues Neto, R. Moreno, Microwave-assisted synthesis of $TiO_2$ nanoparticles: photocatalytic activity of powders and thin films, J. Nanoparticle Res. 20 (2018) 23. https://doi.org/10.1007/s11051-018-4140-7.
[228] A. Kubiak, Z. Bielan, M. Kubacka, E. Gabała, A. Zgoła-Grześkowiak, M. Janczarek, M. Zalas, A. Zielińska-Jurek, K. Siwińska-Ciesielczyk, T. Jesionowski, Microwave-assisted synthesis of a $TiO_2$-CuO heterojunction with enhanced photocatalytic activity against tetracycline, Appl. Surf. Sci. 520 (2020) 146344. https://doi.org/10.1016/j.apsusc.2020.146344.
[229] S. Phromma, T. Wutikhun, P. Kasamechonchung, S. Sattayaporn, T. Eksangsri, C. Sapcharoenkun, Effects of Ag modified $TiO_2$ on local structure investigated by XAFS and photocatalytic activity under visible light, Mater. Res. Bull. 148 (2022) 111668. https://doi.org/10.1016/J.MATERRESBULL.2021.111668.
[230] J. Zhuang, C. He, K. Wang, K. Teng, Z. Ma, S. Zhang, L. Lu, X. Li, Y. Zhang, Q. An, Nanoscopically-optimized carrier transportation and utilization in immobilized AuNP-$TiO_2$ composite HER photocatalysts, Appl. Surf. Sci. 537 (2021) 148055. https://doi.org/10.1016/J.APSUSC.2020.148055.
[231] O.K. Mmelesi, N. Masunga, A. Kuvarega, T.T. Nkambule, B.B. Mamba, K.K. Kefeni, Cobalt ferrite nanoparticles and nanocomposites: Photocatalytic, antimicrobial activity and toxicity in water treatment, Mater. Sci. Semicond. Process. 123 (2021) 105523. https://doi.org/10.1016/J.MSSP.2020.105523.
[232] O. Carp, Photoinduced reactivity of titanium dioxide, Prog. Solid State Chem. 32 (2004) 33–177. https://doi.org/10.1016/j.progsolidstchem.2004.08.001.
[233] M. Peñas-Garzón, A. Gómez-Avilés, J. Álvarez-Conde, J. Bedia, E.M. García-Frutos, C. Belver, Azaindole grafted titanium dioxide for the photodegradation of pharmaceuticals under solar irradiation, J. Colloid Interface Sci. 629 (2023) 593–603. https://doi.org/10.1016/J.JCIS.2022.09.005.
[234] X. Zhang, Z. Zhu, R. Rao, J. Chen, X. Han, S. Jiang, Y. Yang, Y. Wang, L. Wang, Highly efficient visible-light-driven photocatalytic degradation of gaseous toluene by rutile-anatase $TiO_2$@MIL-101 composite with two heterojunctions, J. Environ. Sci. (2022). https://doi.org/10.1016/J.JES.2022.03.014.
[235] A. Rostami-Vartooni, M. Nasrollahzadeh, M. Alizadeh, Green synthesis of seashell supported silver nanoparticles using Bunium persicum seeds extract: Application of the particles for catalytic reduction of organic dyes, J. Colloid Interface Sci. 470 (2016) 268–275. https://doi.org/10.1016/j.jcis.2016.02.060.
[236] J. Prakash, B.S. Kaith, S. Sun, S. Bellucci, H.C. Swart, Recent Progress on Novel Ag–$TiO_2$ Nanocomposites for Antibacterial Applications, in: 2019: pp. 121–143. https://doi.org/10.1007/978-3-030-16534-5_7.
[237] S. Rengaraj, X.Z. Li, Enhanced photocatalytic activity of $TiO_2$ by doping with Ag for degradation of 2,4,6-trichlorophenol in aqueous suspension, J. Mol. Catal. A Chem. 243 (2006) 60–67.

https://doi.org/10.1016/j.molcata.2005.08.010.
[238] Z. Duan, Y. Huang, D. Zhang, S. Chen, Electrospinning Fabricating Au/$TiO_2$ Network-like Nanofibers as Visible Light Activated Photocatalyst, Sci. Rep. 9 (2019) 8008. https://doi.org/10.1038/s41598-019-44422-w.
[239] S. Yin, Q. Zhang, F. Saito, T. Sato, Preparation of Visible Light-Activated Titania Photocatalyst by Mechanochemical Method, Chem. Lett. 32 (2003) 358–359. https://doi.org/10.1246/cl.2003.358.
[240] K.H. Leong, B.L. Gan, S. Ibrahim, P. Saravanan, Synthesis of surface plasmon resonance (SPR) triggered Ag/$TiO_2$ photocatalyst for degradation of endocrine disturbing compounds, Appl. Surf. Sci. 319 (2014) 128–135. https://doi.org/10.1016/j.apsusc.2014.06.153.
[241] Z. Noreen, N.R. Khalid, R. Abbasi, S. Javed, I. Ahmad, H. Bokhari, Visible light sensitive Ag/$TiO_2$/graphene composite as a potential coating material for control of Campylobacter jejuni, Mater. Sci. Eng. C 98 (2019) 125–133. https://doi.org/10.1016/j.msec.2018.12.087.
[242] M.I. Din, R. Khalid, Z. Hussain, Minireview: Silver-Doped Titanium Dioxide and Silver-Doped Zinc Oxide Photocatalysts, Anal. Lett. 51 (2018) 892–907. https://doi.org/10.1080/00032719.2017.1363770.
[243] P. Ribao, J. Corredor, M.J. Rivero, I. Ortiz, Role of reactive oxygen species on the activity of noble metal-doped $TiO_2$ photocatalysts, J. Hazard. Mater. 372 (2019) 45–51. https://doi.org/10.1016/j.jhazmat.2018.05.026.
[244] H.-Y. Ma, L. Zhao, L.-H. Guo, H. Zhang, F.-J. Chen, W.-C. Yu, Roles of reactive oxygen species (ROS) in the photocatalytic degradation of pentachlorophenol and its main toxic intermediates by $TiO_2$/UV, J. Hazard. Mater. 369 (2019) 719–726. https://doi.org/10.1016/j.jhazmat.2019.02.080.
[245] P. Eskandari, E. Amarloo, H. Zangeneh, M. Rezakazemi, M.R. Zamani, T.M. Aminabhavi, Photocatalytic activity of visible-light-driven L-Proline-$TiO_2$/BiOBr nanostructured materials for dyes degradation: The role of generated reactive species, J. Environ. Manage. 326 (2023) 116691. https://doi.org/10.1016/j.jenvman.2022.116691.
[246] J. Shen, Z.-J. Li, Z.-F. Hang, S.-F. Xu, Q.-Q. Liu, H. Tang, X.-W. Zhao, Insights into the Effect of Reactive Oxygen Species Regulation on Photocatalytic Performance via Construction of a Metal-Semiconductor Heterojunction, J. Nanosci. Nanotechnol. 20 (2020) 3478–3485. https://doi.org/10.1166/jnn.2020.17405.
[247] J. Kim, N. Hasan, K.D. Tran, H.T.M. Truong, S. Kim, Degradation of organic compounds in the dark using pre-illuminated Ag/$TiO_2$ as a reusable Fenton-like material, Environ. Technol. Innov. 32 (2023) 103323. https://doi.org/10.1016/j.eti.2023.103323.
[248] A. Furube, S. Hashimoto, Insight into plasmonic hot-electron transfer and plasmon molecular drive: new dimensions in energy conversion and nanofabrication, NPG Asia Mater. 9 (2017) e454–e454. https://doi.org/10.1038/am.2017.191.
[249] T. Tatsuma, H. Nishi, T. Ishida, Plasmon-induced charge separation: chemistry and wide applications, Chem. Sci. 8 (2017) 3325–3337. https://doi.org/10.1039/C7SC00031F.
[250] A. Meng, L. Zhang, B. Cheng, J. Yu, Dual Cocatalysts in $TiO_2$ Photocatalysis, Adv. Mater. (2019) 1807660. https://doi.org/10.1002/adma.201807660.
[251] D. Wang, S.C. Pillai, S.-H. Ho, J. Zeng, Y. Li, D.D. Dionysiou, Plasmonic-based nanomaterials for environmental remediation, Appl. Catal. B Environ.

237 (2018) 721–741. https://doi.org/10.1016/j.apcatb.2018.05.094.
[252] S. Lal, S. Link, N.J. Halas, Nano-optics from sensing to waveguiding, Nat. Photonics 1 (2007) 641–648. https://doi.org/10.1038/nphoton.2007.223.
[253] S. Kunwar, P. Pandey, J. Lee, Enhanced Localized Surface Plasmon Resonance of Fully Alloyed AgAuPdPt, AgAuPt, AuPt, AgPt, and Pt Nanocrystals: Systematical Investigation on the Morphological and LSPR Properties of Mono **-,** Bi-, Tri-, and Quad-Metallic Nanoparticles, ACS Omega 4 (2019) 17340–17351. https://doi.org/10.1021/acsomega.9b02066.
[254] S.-H. Jeong, H. Choi, J.Y. Kim, T.-W. Lee, Silver-Based Nanoparticles for Surface Plasmon Resonance in Organic Optoelectronics, Part. Part. Syst. Charact. 32 (2015) 164–175. https://doi.org/10.1002/ppsc.201400117.
[255] A.J. Haes, C.L. Haynes, A.D. McFarland, G.C. Schatz, R.P. Van Duyne, S. Zou, Plasmonic Materials for Surface-Enhanced Sensing and Spectroscopy, MRS Bull. 30 (2005) 368–375. https://doi.org/10.1557/mrs2005.100.
[256] L.M. Santos, W.A. Machado, M.D. França, K.A. Borges, R.M. Paniago, A.O.T. Patrocinio, A.E.H. Machado, Structural characterization of Ag-doped $TiO_2$ with enhanced photocatalytic activity, RSC Adv. 5 (2015) 103752–103759. https://doi.org/10.1039/C5RA22647C.
[257] S.H. Hwang, D.H. Shin, J. Yun, C. Kim, M. Choi, J. Jang, $SiO_2$/$TiO_2$ Hollow Nanoparticles Decorated with Ag Nanoparticles: Enhanced Visible Light Absorption and Improved Light Scattering in Dye-Sensitized Solar Cells, Chem. – A Eur. J. 20 (2014) 4439–4446. https://doi.org/10.1002/chem.201304522.
[258] H. Li, W. Lu, J. Tian, Y. Luo, A.M. Asiri, A.O. Al-Youbi, X. Sun, Synthesis and Study of Plasmon-Induced Carrier Behavior at Ag/$TiO_2$ Nanowires, Chem. – A Eur. J. 18 (2012) 8508–8514. https://doi.org/10.1002/chem.201103523.
[259] Y. He, P. Basnet, S.E.H. Murph, Y. Zhao, Ag Nanoparticle Embedded $TiO_2$ Composite Nanorod Arrays Fabricated by Oblique Angle Deposition: Toward Plasmonic Photocatalysis, ACS Appl. Mater. Interfaces 5 (2013) 11818–11827. https://doi.org/10.1021/am4035015.
[260] H. Zhang, G. Wang, D. Chen, X. Lv, J. Li, Tuning Photoelectrochemical Performances of Ag−$TiO_2$ Nanocomposites via Reduction/Oxidation of Ag, Chem. Mater. 20 (2008) 6543–6549. https://doi.org/10.1021/cm801796q.
[261] R.S. Varma, N. Thorat, R. Fernandes, D.C. Kothari, N. Patel, A. Miotello, Dependence of photocatalysis on charge carrier separation in Ag-doped and decorated $TiO_2$ nanocomposites, Catal. Sci. Technol. 6 (2016) 8428–8440. https://doi.org/10.1039/C6CY01605G.
[262] M.-Z. Ge, C.-Y. Cao, S.-H. Li, Y.-X. Tang, L.-N. Wang, N. Qi, J.-Y. Huang, K.-Q. Zhang, S.S. Al-Deyab, Y.-K. Lai, In situ plasmonic Ag nanoparticle anchored $TiO_2$ nanotube arrays as visible-light-driven photocatalysts for enhanced water splitting, Nanoscale 8 (2016) 5226–5234. https://doi.org/10.1039/C5NR08341A.
[263] V. V. Torbina, A.A. Vodyankin, S. Ten, G. V. Mamontov, M.A. Salaev, V.I. Sobolev, O. V. Vodyankina, Ag-Based Catalysts in Heterogeneous Selective Oxidation of Alcohols: A Review, Catalysts 8 (2018) 447. https://doi.org/10.3390/catal8100447.
[264] J. He, J. Cheng, I.M.C. Lo, Green photocatalytic disinfection of real sewage: efficiency evaluation and toxicity assessment of eco-friendly $TiO_2$-based magnetic photocatalyst under solar light, Water Res. 190 (2021) 116705.

https://doi.org/10.1016/J.WATRES.2020.116705.
[265] Z. Xiong, J. Ma, W.J. Ng, T.D. Waite, X.S. Zhao, Silver-modified mesoporous TiO2 photocatalyst for water purification, Water Res. 45 (2011) 2095–2103. https://doi.org/10.1016/j.watres.2010.12.019.
[266] S.N.A. Sulaiman, M. Zaky Noh, N. Nadia Adnan, N. Bidin, S.N. Ab Razak, Effects of photocatalytic activity of metal and non-metal doped $TiO_2$ for Hydrogen production enhancement - A Review, J. Phys. Conf. Ser. 1027 (2018) 012006. https://doi.org/10.1088/1742-6596/1027/1/012006.
[267] T.H.M. Wint, M.F. Smith, N. Chanlek, F. Chen, T.Z. Oo, P. Songsiriritthigul, Physical Origin of Diminishing Photocatalytic Efficiency for Recycled $TiO_2$ Nanotubes and Ag-Loaded $TiO_2$ Nanotubes in Organic Aqueous Solution, Catalysts 10 (2020) 737. https://doi.org/10.3390/catal10070737.
[268] N. Mohaghegh, B. Eshaghi, E. Rahimi, M.R. Gholami, $Ag_2CO_3$ sensitized $TiO_2$ nanoparticles prepared in ionic liquid medium: A new $Ag_2CO_3/TiO_2$/RTIL heterostructure with highly efficient photocatalytic activity, J. Mol. Catal. A Chem. 406 (2015) 152–158. https://doi.org/10.1016/j.molcata.2015.06.004.
[269] R. Ravi, A. Kumar Golder, Efficient recovery of $TiO_2$ and Pt-doped $TiO_2$ photocatalysts in wastewater treatment using a pilot-scale cross-flow ultrafiltration membrane system, Sep. Purif. Technol. 339 (2024) 126710. https://doi.org/10.1016/j.seppur.2024.126710.
[270] N. Coffman, D. Meeroff, F. Bloetscher, Photocatalytic oxidation of landfill leachate using UV/$TiO_2$ with catalyst recovery, Int. J. Eng. Technol. Manag. Res. 7 (2020) 21–34. https://doi.org/10.29121/ijetmr.v7.i8.2020.735.
[271] C. Su, L. Liu, M. Zhang, Y. Zhang, C. Shao, Fabrication of Ag/$TiO_2$ nanoheterostructures with visible light photocatalytic function via a solvothermal approach, CrystEngComm 14 (2012) 3989. https://doi.org/10.1039/c2ce25161b.
[272] N. Ali, H. Zaman, M. Bilal, A.-H.A. Shah, M.S. Nazir, H.M.N. Iqbal, Environmental perspectives of interfacially active and magnetically recoverable composite materials – A review, Sci. Total Environ. 670 (2019) 523–538. https://doi.org/10.1016/j.scitotenv.2019.03.209.
[273] T. Leshuk, A.B. Holmes, D. Ranatunga, P.Z. Chen, Y. Jiang, F. Gu, Magnetic flocculation for nanoparticle separation and catalyst recycling, Environ. Sci. Nano 5 (2018) 509–519. https://doi.org/10.1039/C7EN00827A.
[274] Y. Zhang, J. Chen, H. Tang, Y. Xiao, S. Qiu, S. Li, S. Cao, Hierarchically-structured $SiO_2$-Ag@$TiO_2$ hollow spheres with excellent photocatalytic activity and recyclability, J. Hazard. Mater. 354 (2018) 17–26. https://doi.org/10.1016/j.jhazmat.2018.04.047.
[275] G.E. Schaumann, A. Philippe, M. Bundschuh, G. Metreveli, S. Klitzke, D. Rakcheev, A. Grün, S.K. Kumahor, M. Kühn, T. Baumann, F. Lang, W. Manz, R. Schulz, H.-J. Vogel, Understanding the fate and biological effects of Ag- and $TiO_2$-nanoparticles in the environment: The quest for advanced analytics and interdisciplinary concepts, Sci. Total Environ. 535 (2015) 3–19. https://doi.org/10.1016/j.scitotenv.2014.10.035.
[276] Z.S. Mahdi, A.M. Aljeboree, F.A. Rasen, N.A.A. Salman, A.F. Alkaim, Synthesis, Characterization, and Regeneration of Ag/$TiO_2$ Nanoparticles: Photocatalytic Removal of Mixed Dye Pollutants, in: Raise-2023, MDPI, Basel Switzerland, 2024: p. 216. https://doi.org/10.3390/engproc2023059216.

[277] A.R. Donovan, C.D. Adams, Y. Ma, C. Stephan, T. Eichholz, H. Shi, Single particle ICP-MS characterization of titanium dioxide, silver, and gold nanoparticles during drinking water treatment, Chemosphere 144 (2016) 148–153. https://doi.org/10.1016/j.chemosphere.2015.07.081.
[278] V.S. Sousa, M. Ribau Teixeira, Conventional water treatment improvement through enhanced conventional and hybrid membrane processes to remove Ag, CuO and $TiO_2$ nanoparticles mixture in surface waters, Sep. Purif. Technol. 248 (2020) 117047. https://doi.org/10.1016/j.seppur.2020.117047.
[279] P. Kirkegaard, S.F. Hansen, M. Rygaard, Potential exposure and treatment efficiency of nanoparticles in water supplies based on wastewater reclamation, Environ. Sci. Nano 2 (2015) 191–202. https://doi.org/10.1039/C4EN00192C.
[280] B. Deng, S. Fu, Y. Zhang, Y. Wang, D. Ma, S. Dong, Simultaneous pollutant degradation and power generation in visible-light responsive photocatalytic fuel cell with an Ag-$TiO_2$ loaded photoanode, Nano-Struct. & Nano-Obj. 15 (2018) 167–172. https://doi.org/10.1016/j.nanoso.2017.09.011.
[281] A. Carmalin Sophia, E.C. Lima, N. Allaudeen, S. Rajan, Application of graphene based materials for adsorption of pharmaceutical traces from water and wastewater- a review, Desalin. Water Treat. (2016) 1–14. https://doi.org/10.1080/19443994.2016.1172989.
[282] R. Oblak, M. Kete, U.L. Štangar, M. Tasbihi, Alternative support materials for titania photocatalyst towards degradation of organic pollutants, J. Water Process Eng. 23 (2018) 142–150. https://doi.org/10.1016/j.jwpe.2018.03.015.
[283] J.F. Gomes, A. Lopes, M. Gmurek, R.M. Quinta-Ferreira, R.C. Martins, Study of the influence of the matrix characteristics over the photocatalytic ozonation of parabens using Ag-$TiO_2$, Sci. Total Environ. 646 (2019) 1468–1477. https://doi.org/10.1016/j.scitotenv.2018.07.430.
[284] E.T. Wahyuni, R. Roto, M. PrameSwari, $TiO_2$/Ag-nanoparticle as a Photocatalyst for Dyes Degradation, in: Rhodes, 2017.
[285] S.P. Onkani, P.N. Diagboya, F.M. Mtunzi, M.J. Klink, B.I. Olu-Owolabi, V. Pakade, Comparative study of the photocatalytic degradation of 2–chlorophenol under UV irradiation using pristine and Ag-doped species of $TiO_2$, ZnO and ZnS photocatalysts, J. Environ. Manage. 260 (2020) 110145. https://doi.org/10.1016/j.jenvman.2020.110145.
[286] S.K. Kansal, P. Kundu, S. Sood, R. Lamba, A. Umar, S.K. Mehta, Photocatalytic degradation of the antibiotic levofloxacin using highly crystalline $TiO_2$ nanoparticles, New J. Chem. 38 (2014) 3220–3226. https://doi.org/10.1039/C3NJ01619F.
[287] N. Kaneva, A. Bojinova, K. Papazova, Enhanced Removal of Organic Dyes Using Co-Catalytic Ag-Modified ZnO and $TiO_2$ Sol-Gel Photocatalysts, Catalysts 13 (2023) 245. https://doi.org/10.3390/catal13020245.
[288] R. Frankowski, A. Zgoła-Grześkowiak, T. Grześkowiak, E. Stanisz, J. Werner, J. Płatkiewicz, Photocatalytic Treatment of Emerging Contaminants with Ag-Modified Titania—Is There a Risk Arising from the Degradation Products?, Processes 10 (2022) 2523. https://doi.org/10.3390/pr10122523.
[289] H. Palza, Antimicrobial Polymers with Metal Nanoparticles, Int. J. Mol. Sci. 16 (2015) 2099–2116. https://doi.org/10.3390/ijms16012099.
[290] J. Li, B. Xie, K. Xia, Y. Li, J. Han, C. Zhao, Enhanced Antibacterial Activity of Silver Doped Titanium Dioxide-Chitosan Composites under Visible Light,

Materials (Basel). 11 (2018) 1403. https://doi.org/10.3390/ma11081403.
[291] Z. Habib, S.J. Khan, N.M. Ahmad, H.M.A. Shahzad, Y. Jamal, I. Hashmi, Antibacterial behaviour of surface modified composite polyamide nanofiltration (NF) membrane by immobilizing Ag-doped $TiO_2$ nanoparticles, Environ. Technol. 41 (2020) 3657–3669. https://doi.org/10.1080/09593330.2019.1617355.
[292] S. Talebzadeh, F. Forato, B. Bujoli, S.A. Trammell, S. Grolleau, H. Pal, C. Queffélec, D.A. Knight, Non-photochemical catalytic hydrolysis of methyl parathion using core–shell Ag@$TiO_2$ nanoparticles, RSC Adv. 8 (2018) 42346–42352. https://doi.org/10.1039/C8RA09553A.
[293] J. Bahadur, S. Agrawal, V. Panwar, A. Parveen, K. Pal, Antibacterial properties of silver doped $TiO_2$ nanoparticles synthesized via sol-gel technique, Macromol. Res. 24 (2016) 488–493. https://doi.org/10.1007/s13233-016-4066-9.
[294] M.A. Muflikhun, A.Y. Chua, G.N.C. Santos, Structures, Morphological Control, and Antibacterial Performance of Ag/$TiO_2$ Micro-Nanocomposite Materials, Adv. Mater. Sci. Eng. 2019 (2019) 1–12. https://doi.org/10.1155/2019/9821535.
[295] P. Dong, F. Yang, X. Cheng, Z. Huang, X. Nie, Y. Xiao, X. Zhang, Plasmon enhanced photocatalytic and antimicrobial activities of Ag-$TiO_2$ nanocomposites under visible light irradiation prepared by DBD cold plasma treatment, Mater. Sci. Eng. C 96 (2019) 197–204. https://doi.org/10.1016/j.msec.2018.11.005.
[296] L. Yang, X. Jiang, W. Ruan, J. Yang, B. Zhao, W. Xu, J.R. Lombardi, Charge-Transfer-Induced Surface-Enhanced Raman Scattering on Ag−$TiO_2$ Nanocomposites, J. Phys. Chem. C 113 (2009) 16226–16231. https://doi.org/10.1021/jp903600r.
[297] E. AlArfaj, Investigation of Ag-$TiO_2$ nanostructures photocatalytic properties prepared by modified dip coating method, Philos. Mag. 96 (2016) 1386–1398. https://doi.org/10.1080/14786435.2016.1163432.
[298] C.A. Castro, P. Osorio, A. Sienkiewicz, C. Pulgarin, A. Centeno, S.A. Giraldo, Photocatalytic production of $^1O_2$ and OH mediated by silver oxidation during the photoinactivation of *Escherichia coli* with $TiO_2$, J. Hazard. Mater. 211–212 (2012) 172–181. https://doi.org/10.1016/j.jhazmat.2011.08.076.
[299] Jessica, M. Ibadurrohman, Slamet, Effect of Ag and Mn doping for methylene blue photodegradation performance, IOP Conf. Ser. Mater. Sci. Eng. 1011 (2021) 012043. https://doi.org/10.1088/1757-899X/1011/1/012043.
[300] K. Sathishkumar, K. Sowmiya, L. Arul Pragasan, R. Rajagopal, R. Sathya, S. Ragupathy, M. Krishnakumar, V.R. Minnam Reddy, Enhanced photocatalytic degradation of organic pollutants by Ag–$TiO_2$ loaded cassava stem activated carbon under sunlight irradiation, Chemosphere 302 (2022) 134844. https://doi.org/10.1016/j.chemosphere.2022.134844.
[301] J. Yang, X. Luo, Ag-doped $TiO_2$ immobilized cellulose-derived carbon beads: One-Pot preparation, photocatalytic degradation performance and mechanism of ceftriaxone sodium, Appl. Surf. Sci. 542 (2021) 148724. https://doi.org/10.1016/j.apsusc.2020.148724.
[302] N. Kaur, A. Verma, I. Thakur, S. Basu, In-situ dual effect of Ag-Fe-$TiO_2$ composite for the photocatalytic degradation of Ciprofloxacin in aqueous

solution, Chemosphere 276 (2021) 130180. https://doi.org/10.1016/j.chemosphere.2021.130180.
[303] G.K. Hassan, W.H. Mahmoud, A. Al-sayed, S.H. Ismail, A.A. El-Sherif, S.M. Abd El Wahab, Multi-functional of $TiO_2$@Ag core–shell nanostructure to prevent hydrogen sulfide formation during anaerobic digestion of sewage sludge with boosting of bio-$CH_4$ production, Fuel 333 (2023) 126608. https://doi.org/10.1016/j.fuel.2022.126608.
[304] F. Ali, G. Moin-ud-Din, M. Iqbal, A. Nazir, I. Altaf, N. Alwadai, U.H. Siddiqua, U. Younas, A. Ali, A. Kausar, N. Ahmad, Ag and Zn doped $TiO_2$ nano-catalyst synthesis via a facile green route and their catalytic activity for the remediation of dyes, J. Mater. Res. Technol. 23 (2023) 3626–3637. https://doi.org/10.1016/J.JMRT.2023.02.011.
[305] E. Montakhab, F. Rashchi, S. Sheibani, Enhanced photocatalytic activity of $TiO_2$ nanotubes decorated with Ag nanoparticles by simultaneous electrochemical deposition and reduction processes, Appl. Surf. Sci. 615 (2023) 156332. https://doi.org/10.1016/j.apsusc.2023.156332.
[306] G.K. Sukhadeve, H. Bandewar, S.Y. Janbandhu, J.R. Jayaramaiah, R.S. Gedam, Photocatalytic hydrogen production, dye degradation, and antimicrobial activity by Ag-Fe co-doped $TiO_2$ nanoparticles, J. Mol. Liq. 369 (2023) 120948. https://doi.org/10.1016/j.molliq.2022.120948.
[307] M. Norouzi, A. Fazeli, O. Tavakoli, Phenol contaminated water treatment by photocatalytic degradation on electrospun Ag/$TiO_2$ nanofibers: Optimization by the response surface method, J. Water Process Eng. 37 (2020) 101489. https://doi.org/10.1016/j.jwpe.2020.101489.
[308] M. Abidi, W. Abou Saoud, A. Bouzaza, A. Hajjaji, B. Bessais, D. Wolbert, A.A. Assadi, S. Rtimi, Dynamics of VOCs degradation and bacterial inactivation at the interface of $Ag_xO$/Ag/$TiO_2$ prepared by HiPIMS under indoor light, J. Photochem. Photobiol. A Chem. 435 (2023) 114321. https://doi.org/10.1016/j.jphotochem.2022.114321.
[309] K. Nagaraj, P. Thankamuniyandi, S. Kamalesu, S. Lokhandwala, N.M. Parekh, S. Sakthinathan, T.-W. Chiu, C. Karuppiah, Green synthesis, characterization and efficient photocatalytic study of hydrothermal-assisted Ag@$TiO_2$ nanocomposites, Inorg. Chem. Commun. 148 (2023) 110362. https://doi.org/10.1016/j.inoche.2022.110362.
[310] F. Jandaghian, A. Ebrahimian Pirbazari, O. Tavakoli, N. Asasian-Kolur, S. Sharifian, Comparison of the performance of Ag-deposited ZnO and $TiO_2$ nanoparticles in levofloxacin degradation under UV/visible radiation, J. Hazard. Mater. Adv. 9 (2023) 100240. https://doi.org/10.1016/j.hazadv.2023.100240.
[311] S. Sambaza, A. Maity, K. Pillay, Enhanced degradation of BPA in water by PANI supported Ag/$TiO_2$ nanocomposite under UV and visible light, J. Environ. Chem. Eng. 7 (2019) 102880. https://doi.org/10.1016/j.jece.2019.102880.
[312] A. Urda, T. Radu, C. Socaci, V. Floare-Avram, D. Cosma, M.C. Rosu, M. Coros, S. Pruneanu, F. Pogacean, Evaluation of N-doped graphene role in the visible-light driven photodegradation of sulfamethoxazole by a $TiO_2$-silver-graphene composite, J. Photochem. Photobiol. A Chem. 425 (2022) 113701. https://doi.org/10.1016/j.jphotochem.2021.113701.
[313] S. Rabhi, H. Belkacemi, M. Bououdina, A. Kerrami, L. Ait Brahem, E. Sakher, Effect of Ag doping of $TiO_2$ nanoparticles on anatase-rutile phase

transformation and excellent photodegradation of amlodipine besylate, Mater. Lett. 236 (2019) 640–643. https://doi.org/10.1016/J.MATLET.2018.11.006.
[314] K. Huang, H. Liu, J. He, Y. He, X. Tao, H. Yin, Z. Dang, G. Lu, Application of Ag/$TiO_2$ in photocatalytic degradation of 2,2′,4,4′-tetrabromodiphenyl ether in simulated washing waste containing Triton X-100, J. Environ. Chem. Eng. 9 (2021) 105077. https://doi.org/10.1016/j.jece.2021.105077.
[315] L. Zhu, M.J.C. Opulencia, D.O. Bokov, I.I. Krasnyuk, C.-H. Su, H.C. Nguyen, A. Mohamed, M.H. Zare, M. Zwawi, M. Algarni, Synthesis of Ag-coated on a wrinkled $SiO_2$@$TiO_2$ architectural photocatalyst: New method of wrinkled shell for use of semiconductors in the visible light range and penicillin antibiotic degradation, Alexandria Eng. J. 61 (2022) 9315–9334. https://doi.org/10.1016/j.aej.2022.03.009.
[316] C. Zhang, Y. Li, D. Wang, W. Zhang, Q. Wang, Y. Wang, P. Wang, Ag@helical chiral $TiO_2$ nanofibers for visible light photocatalytic degradation of 17α-ethinylestradiol, Environ. Sci. Pollut. Res. 22 (2015) 10444–10451. https://doi.org/10.1007/s11356-015-4251-y.
[317] L. Yang, Q. Sang, J. Du, M. Yang, X. Li, Y. Shen, X. Han, X. Jiang, B. Zhao, A Ag synchronously deposited and doped $TiO_2$ hybrid as an ultrasensitive SERS substrate: a multifunctional platform for SERS detection and photocatalytic degradation, Phys. Chem. Chem. Phys. 20 (2018) 15149–15157. https://doi.org/10.1039/C8CP01680A.
[318] B. Gao, J. Wang, M. Dou, C. Xu, X. Huang, Enhanced photocatalytic removal of amoxicillin with Ag/$TiO_2$/mesoporous g-$C_3N_4$ under visible light: property and mechanistic studies, Environ. Sci. Pollut. Res. 27 (2020) 7025–7039. https://doi.org/10.1007/s11356-019-07112-8.
[319] J.C. Durán-Álvarez, V.A. Hernández-Morales, M. Rodríguez-Varela, D. Guerrero-Araque, D. Ramirez-Ortega, F. Castillón, P. Acevedo-Peña, R. Zanella, $Ag_2O$/$TiO_2$ nanostructures for the photocatalytic mineralization of the highly recalcitrant pollutant iopromide in pure and tap water, Catal. Today 341 (2020) 71–81. https://doi.org/10.1016/j.cattod.2019.01.027.
[320] S.S. Boxi, S. Paria, Visible light induced enhanced photocatalytic degradation of organic pollutants in aqueous media using Ag doped hollow $TiO_2$ nanospheres, RSC Adv. 5 (2015) 37657–37668. https://doi.org/10.1039/C5RA03421C.
[321] N. Jalili-Jahani, A. Fatehi, J. Azizi-Saadi, M. Moallem, Enhanced photocatalytic degradation of diazinon by bimetallic Au/Ag-decorated $TiO_2$ nanorods and quadrupole time-of-flight LC-MS/MS assay for detection of by-products, Ceram. Int. 48 (2022) 34415–34427. https://doi.org/10.1016/j.ceramint.2022.08.020.
[322] C. Jiang, J. Jia, S. Zhai, Mechanistic Understanding of Toxicity from Nanocatalysts, Int. J. Mol. Sci. 15 (2014) 13967–13992. https://doi.org/10.3390/ijms150813967.
[323] J. Kardos, K. Jemnitz, I. Jablonkai, A. Bóta, Z. Varga, J. Visy, L. Héja, The Janus Facet of Nanomaterials, Biomed Res. Int. 2015 (2015) 1–10. https://doi.org/10.1155/2015/317184.
[324] M. Joshi, B. Prabhakar, Nanotoxicity Assessment: A Necessity, Nanosci. Nanotechnology-Asia 10 (2020) 248–265. https://doi.org/10.2174/2210681209666190228142315.
[325] G.H. Jang, K.Y. Lee, J. Choi, S.H. Kim, K.H. Lee, Multifaceted toxicity

assessment of catalyst composites in transgenic zebrafish embryos, Environ. Pollut. 216 (2016) 755–763. https://doi.org/10.1016/j.envpol.2016.06.045.
[326] K. Tomankova, J. Horakova, M. Harvanova, L. Malina, J. Soukupova, S. Hradilova, K. Kejlova, J. Malohlava, L. Licman, M. Dvorakova, D. Jirova, H. Kolarova, Cytotoxicity, cell uptake and microscopic analysis of titanium dioxide and silver nanoparticles in vitro, Food Chem. Toxicol. 82 (2015) 106–115. https://doi.org/10.1016/j.fct.2015.03.027.
[327] U. Song, H. Jun, B. Waldman, J. Roh, Y. Kim, J. Yi, E.J. Lee, Functional analyses of nanoparticle toxicity: A comparative study of the effects of $TiO_2$ and Ag on tomatoes (Lycopersicon esculentum), Ecotoxicol. Environ. Saf. 93 (2013) 60–67. https://doi.org/10.1016/j.ecoenv.2013.03.033.
[328] K. Kawata, M. Osawa, S. Okabe, In Vitro Toxicity of Silver Nanoparticles at Noncytotoxic Doses to HepG2 Human Hepatoma Cells, Environ. Sci. Technol. 43 (2009) 6046–6051. https://doi.org/10.1021/es900754q.
[329] S. Behzadi, V. Serpooshan, W. Tao, M.A. Hamaly, M.Y. Alkawareek, E.C. Dreaden, D. Brown, A.M. Alkilany, O.C. Farokhzad, M. Mahmoudi, Cellular uptake of nanoparticles: journey inside the cell, Chem. Soc. Rev. 46 (2017) 4218–4244. https://doi.org/10.1039/C6CS00636A.
[330] Z. Luo, Z. Li, Z. Xie, I.M. Sokolova, L. Song, W.J.G.M. Peijnenburg, M. Hu, Y. Wang, Rethinking Nano-$TiO_2$ Safety: Overview of Toxic Effects in Humans and Aquatic Animals, Small 16 (2020). https://doi.org/10.1002/smll.202002019.
[331] B.S. Necula, J.P.T.M. van Leeuwen, L.E. Fratila-Apachitei, S.A.J. Zaat, I. Apachitei, J. Duszczyk, In vitro cytotoxicity evaluation of porous $TiO_2$–Ag antibacterial coatings for human fetal osteoblasts, Acta Biomater. 8 (2012) 4191–4197. https://doi.org/10.1016/j.actbio.2012.07.005.
[332] D.H. Jo, J.H. Kim, J.G. Son, N.W. Song, Y.-I. Kim, Y.S. Yu, T.G. Lee, J.H. Kim, Anti-angiogenic effect of bare titanium dioxide nanoparticles on pathologic neovascularization without unbearable toxicity, Nanomedicine Nanotechnology, Biol. Med. 10 (2014) e1109–e1117. https://doi.org/10.1016/j.nano.2014.02.007.
[333] C.-Y. Jin, B.-S. Zhu, X.-F. Wang, Q.-H. Lu, Cytotoxicity of Titanium Dioxide Nanoparticles in Mouse Fibroblast Cells, Chem. Res. Toxicol. 21 (2008) 1871–1877. https://doi.org/10.1021/tx800179f.
[334] M. Mahjoubian, A.S. Naeemi, M. Sheykhan, Toxicological effects of $Ag_2O$ and $Ag_2CO_3$ doped $TiO_2$ nanoparticles and pure $TiO_2$ particles on zebrafish (*Danio rerio*), Chemosphere 263 (2021) 128182. https://doi.org/10.1016/j.chemosphere.2020.128182.
[335] M.M. Zahornyi, N.I. Tyschenko, T.F. Lobunets, O.F. Kolomys, V. V. Strelchuk, K.S. Naumenko, L.O. Biliavska, S.D. Zahorodnia, O.M. Lavrynenko, A.I. Ievtushenko, The Ag Influence on the Surface States of $TiO_2$, Optical Activity and Its Cytotoxicity, J. Nano- Electron. Phys. 13 (2021) 06009-1-06009–5. https://doi.org/10.21272/jnep.13(6).06009.
[336] N. Zhang, J. Sun, L. Yin, J. Liu, C. Chen, Silver nanoparticles: From in vitro green synthesis to in vivo biological effects in plants, Adv. Agrochem 2 (2023) 313–323. https://doi.org/10.1016/j.aac.2023.08.004.
[337] J. Liu, P.C. Williams, B.M. Goodson, J. Geisler-Lee, M. Fakharifar, M.E. Gemeinhardt, $TiO_2$ nanoparticles in irrigation water mitigate impacts of aged Ag nanoparticles on soil microorganisms, Arabidopsis thaliana plants, and

Eisenia fetida earthworms, Environ. Res. 172 (2019) 202–215. https://doi.org/10.1016/j.envres.2019.02.010.
[338] Z. Kuspanov, B. Bakbolat, A. Baimenov, A. Issadykov, M. Yeleuov, C. Daulbayev, Photocatalysts for a sustainable future: Innovations in large-scale environmental and energy applications, Sci. Total Environ. 885 (2023) 163914. https://doi.org/10.1016/j.scitotenv.2023.163914.
[339] F. Petronella, A. Truppi, M. Dell'Edera, A. Agostiano, M.L. Curri, R. Comparelli, Scalable Synthesis of Mesoporous $TiO_2$ for Environmental Photocatalytic Applications, Materials (Basel). 12 (2019) 1853. https://doi.org/10.3390/ma12111853.
[340] A.B. Djurišić, Y. He, A.M.C. Ng, Visible-light photocatalysts: Prospects and challenges, APL Mater. 8 (2020). https://doi.org/10.1063/1.5140497.
[341] J.Z.X. Heng, K.Y. Tang, M.D. Regulacio, M. Lin, X.J. Loh, Z. Li, E. Ye, Solar-Powered Photodegradation of Pollutant Dyes Using Silver-Embedded Porous $TiO_2$ Nanofibers, Nanomaterials 11 (2021) 856. https://doi.org/10.3390/nano11040856.
[342] M.F. Haris, A.M. Didit, M. Ibadurrohman, Setiadi, Slamet, Silver Doped $TiO_2$ Photocatalyst for Disinfection of *E. coli* and Microplastic Pollutant Degradation in Water, Asian J. Chem. 33 (2021) 2038–2042. https://doi.org/10.14233/ajchem.2021.23255.
[343] A.T. Cooper, D.Y. Goswami, S. Block, Solar Photochemical Detoxification and Disinfection for Water Treatment in Tropical Developing Countries, J. Adv. Oxid. Technol. 3 (1998). https://doi.org/10.1515/jaots-1998-0207.
[344] Energy Technology Perspectives 2010, OECD, 2009. https://doi.org/10.1787/energy_tech-2010-en.

# CHAPTER III

**Synthesis, characterization and application of silver nanoparticles as antimicrobial agents**


## ABSTRACT

Drug-resistant pathogens can be inactivated by nanomaterials or light-activated materials, such as Ag/$TiO_2$, thus preventing the development of antibiotic-resistant bacteria. Thus, we sought to synthesize silver (Ag)-based catalysts (in concentrations of 2% and 10%) supported on titanium dioxide ($TiO_2$) using the excess solvent impregnation method, characterize them, and evaluate them for bacterial inactivation. The results presented by infrared spectrometry identified titanium bands for the synthesized catalysts, as well as asymmetric vibrations of Ti-Ag-O. X-ray diffraction analysis revealed that these catalysts present peaks of anatase, rutile, Ag and silver oxide. It was observed in the bacterial inactivation test that, under white light (9 W), none of the catalysts were photoactivated. This indicates that the antibacterial action against *Escherichia coli* (NEWP0022) was influenced by the Ag concentration present in the impregnated catalyst at 10%. Similar results were obtained in the dark test. Under black light, the impregnated catalysts were photoactivated against *E. coli* and *Staphylococcus aureus* (NEWP0023) and demonstrated bactericidal activity in 15 minutes. The rapid antibacterial action of these catalysts was demonstrated in the reactive oxygen species detection test. Therefore, the impregnated catalysts present greater antimicrobial efficacy compared to $TiO_2$ and can be applied in disinfection devices.



**Keywords:** Impregnation, Bacteria, Photoactivation, ROS.



Manuscript elaborated and formatted according to the guidelines of scientific publication, submitted to the journal *Chemical Engineering Journal*. Available at: <https://www.sciencedirect.com/journal/chemical-engineering-journal>

## 1. Introdution

The ongoing global pandemic of the novel coronavirus (2019-nCoV) is an illustrative example of a viral infection that has the potential to affect human health and life on a global scale. This highlights the critical need for the development and implementation of effective prevention procedures and strategies to mitigate and contain the rapid transmission of infectious diseases [1–3]. These diseases are caused by bacteria, viruses, and fungi and represent a significant global threat. They can be spread rapidly through contaminated food and water, through the air by means of sneezing, breathing, and coughing, or by contact with untreated wounds [4]. The inactivation of pathogens can be achieved through a variety of physical and chemical methods, including ultraviolet radiation, autoclaving, disinfection with ozone, alcohol, or chlorine [5]. Additionally, antimicrobial and antiviral drugs can be employed for this purpose. However, these methods may prove ineffective against multi-resistant pathogens, thereby posing a significant challenge [6,7].

The inactivation of drug-resistant pathogens can be achieved through the use of nanomaterials or materials that are photoactivated by light. This approach presents a promising solution against these microorganisms [8] without the development of resistant bacteria [9]. Consequently, these materials or semiconductors are employed in photocatalysis, exemplified by $TiO_2$ [10], and demonstrate considerable potential for wastewater purification [11], the degradation of organic pollutants [12], and surface sterilization [13], without the generation of deleterious by-products. This process is based on the capacity to generate reactive oxygen species (ROS) through the irradiation of light sources that emit light at varying wavelengths, most commonly ultraviolet (UV). Furthermore, it is an economically viable and environmentally sustainable solution that exhibits robust oxidizing capabilities and high reaction kinetics [14].

$TiO_2$ offers a number of advantages, including low toxicity, photochemical stability, high photodegradation efficiency, low energy consumption, and cost-effectiveness [10,15,16]. However, this oxide has a relatively wide band gap (3.2 eV), a light spectrum limited to the UV region, and rapid rearrangement of electrons and gaps, which reduces the quantum yield [16–18].

There are numerous techniques for modifying the surface of $TiO_2$ in order to improve its photocatalytic action. These include the addition of organic materials [19], coupling of semiconductors [20], co-doping with metals [12] or non-metals [21], metal ions [22], and doping with anions [23]. The doping of $TiO_2$ with metal ions, such as Ag, broadens the spectrum of $TiO_2$ for visible light, decreases the band gap, and consequently reduces the speed of electron rearrangement [24, 25]. This process also helps to increase the antibacterial properties of $TiO_2$, facilitates the separation of electrons and holes ($e^-/h^+$), and finally, Ag costs significantly less than other metals. $Ag/TiO_2$ has been demonstrated to be effective against pathogenic bacteria that are spread by water and food. Furthermore, it can be used in antimicrobial coatings for the purpose of disinfecting pathogens, thereby preventing their growth and proliferation [25, 26]. The reactive oxygen species (ROS) produced from the photoactivation of $Ag/TiO_2$, such as hydroxyls, can act on the bacterial cell wall, breaking the covalent bonds of peptidoglycan, thus causing disruption of the microorganism's cytoplasmic membrane [27, 28] and DNA [29].

Among the pathogenic representatives are *Staphylococcus aureus* (*S. aureus*), a cocci Gram-positive bacterium, and *Escherichia coli* (*E. coli*), a bacilli Gram-negative bacterium. These bacteria are also involved in water-related [30] outbreaks and have the capacity to survive for an extended period of time in a variety of materials [31]. *E. coli* is a causative agent of diarrhea, with an estimated 80,000 deaths annually [32]. It can also induce hemolytic-uremic syndrome, urinary tract infections, and thrombotic thrombocytopenia [33]. *S. aureus* can develop resistance to multiple drugs through mutation, such as methicillin, and is a leading cause of postoperative infections [34].

This study presents a significant contribution to science by demonstrating the superior bactericidal effects of $Ag/TiO_2$ catalysts, paving the way for the development of new strategies in the control of bacterial infections. Therefore, the aim was to synthesize mixed oxides of $Ag/TiO_2$ (2 and 10% w/w) using the impregnation method and subsequently characterize these catalysts in terms of their physicochemical properties, as well as evaluate their efficacy in inactivating bacteria under bright light, black light and in the absence of light. Thus, providing crucial insights for the advancement of more effective and affordable antibacterial

materials, as well as driving the search for innovative and low-cost solutions to combat bacterial infections, a global public health challenge.

## 2. Material and Methods

### 2.1 Material

Titanium oxide ($TiO_2$, Êxodo Científica) and silver nitrate ($AgNO_3$, Alphatec, Ag precursor) were employed in this study. Both compounds were of analytical grade and did not undergo any additional purification. The water utilized in the synthesis was of Milli-Qplus quality, exhibiting an approximate resistivity of 18 MΩcm.

### 2.2 Impregnation Synthesis of Mixed Oxides

The $Ag/TiO_2$ mixed oxides were synthesized using the classic method of excess solvent impregnation, as described by Castro et al. [35]. The $TiO_2$ was dried in an oven with air circulation for 21 h at 120°C and used as a support for the mixed oxides and as a catalyst. Subsequently, the mixed oxides were prepared in proportions of 2% (0.9638 g) and 10% (5.2477 g) relative to the mass of $TiO_2$ (30 g). The oxide was then dissolved in ultrapure water to form a fine paste, after which $AgNO_3$, which had been previously dissolved in water, was added. The resulting solution was subsequently transferred to a rotary evaporator and maintained at a constant rotation speed of 120 rpm for 17 h at room temperature (25 °C). Subsequently, the excess solvent was removed by vacuum evaporation in the aforementioned equipment, with heating to 80°C. Subsequently, the material was subjected to drying in an oven for 21 h at 120°C and calcination with heating ramp up to 400°C for 5 h (**Figure 1**). The mixed oxides were as follows: The samples were designated as 2AgT/I (2% $Ag/TiO_2$/Impregnation), 10AgT/I (10% $Ag/TiO_2$/Impregnation), and T ($TiO_2$).

**Figure 1** - Illustration of the mixed oxide impregnation synthesis.

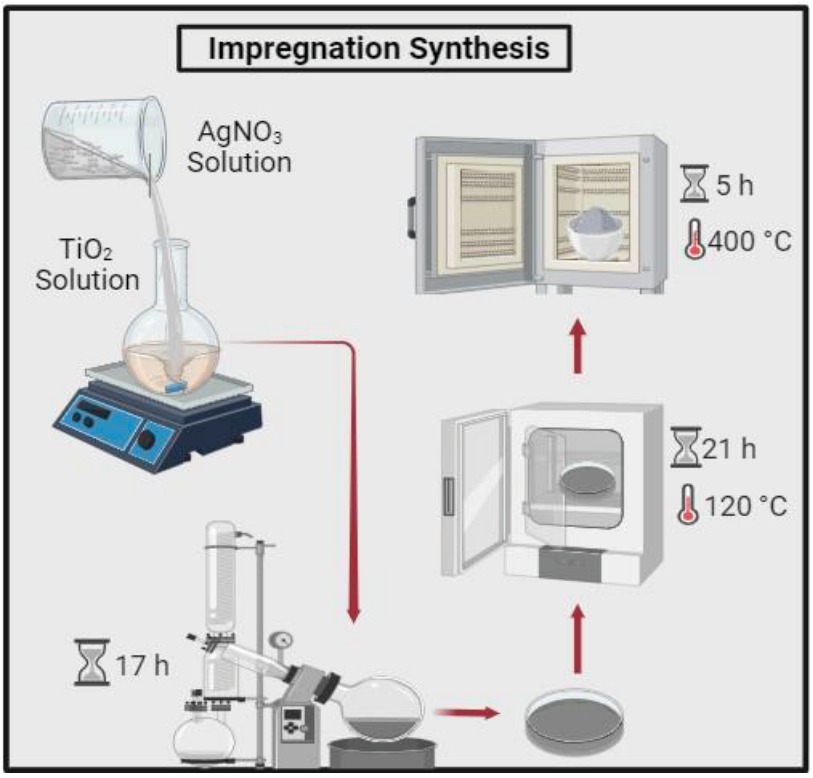


## 2.3 Characterization of the catalysts

Infrared spectra were obtained using pellets of the materials dispersed in KBr, in the 4000-500 $cm^{-1}$ region, employing a Perkin Elmer FT-IR spectrophotometer, model Frontier. The crystalline structure of the catalysts was confirmed through the analysis of the Miniflex 600 X-ray diffraction pattern (XRD), obtained using Rigaku Cu Kα radiation (λ= 0.154 nm).

## 2.4 Antimicrobial activity test

The antimicrobial activity of the catalysts was investigated through the use of Gram-negative *E. coli* (NEWP0022) and Gram-positive *S. aureus* (NEWP0023) bacteria. All materials were previously prepared and sterilized in an autoclave at 121 °C for 15 min, and the tests were conducted under aseptic conditions [36]. We used established protocols, with adaptations [37,38]. A lyophilized disk of the standard strain was introduced into a vial containing 5 mL of nutrient broth and subsequently transferred to a bacteriological incubator for 48 h at 37 °C. After this period, with the aid of a platinum loop, three transfers were made to a new vial

containing 5 mL of nutrient broth and incubated in a bacteriological incubator at 37 °C for 24 h. After this incubation period, the bacterial cultures were serially diluted (1:10 v/v) using saline solution (0.9% NaCl) with the bacterial suspension (solution 1) to $10^5$ CFU $mL^{-1}$. The catalyst solutions T, 2AgT/I and 10AgT/I were previously sonicated for 30 min and a volume of 0.1 mL (equivalent to 0.01 g $mL^{-1}$) of these was added to each well of sterile microplates (six-well microplate). As well, 3.9 mL of saline solution were also added to each well. The start of the reaction was marked by the introduction of 1 mL of the bacterial suspension, prepared in solution 1. Therefore, the final volume in each well corresponded to 5 mL. During the experiment, the microplate was kept under agitation at 350 rpm at 37 °C on a shaking platform to aid in the homogenization of the reaction solution. The microplates containing the final mixture (catalyst, saline solution and bacteria) were then irradiated separately under three different illumination conditions: bright light irradiation (Manplex, 9 W), black light (Luatek, 36 W) and in the absence of light. The distance between the light source and the microplate was 10 cm. Sampling was conducted at 0, 5, 10 and 15 min. At each time point, a sample was collected using a sterile cotton swab and spread on nutrient agar plates, gently over the agar surface in five different directions. Subsequently, the medium was allowed to absorb the inoculum for a period of 15 min. The experiments were conducted in triplicate, and the plates were subsequently incubated in a bacteriological oven at 37 ± 2 °C for 24 h. Control experiments were conducted in the absence of a catalyst. The number of Colony Forming Units (CFU) was counted and subjected to statistical analysis. **Figure 2** describes the results of the catalyst bacteria inactivation experiment.

**Figure 2** – Illustration of the inactivation of bacteria by catalysts.

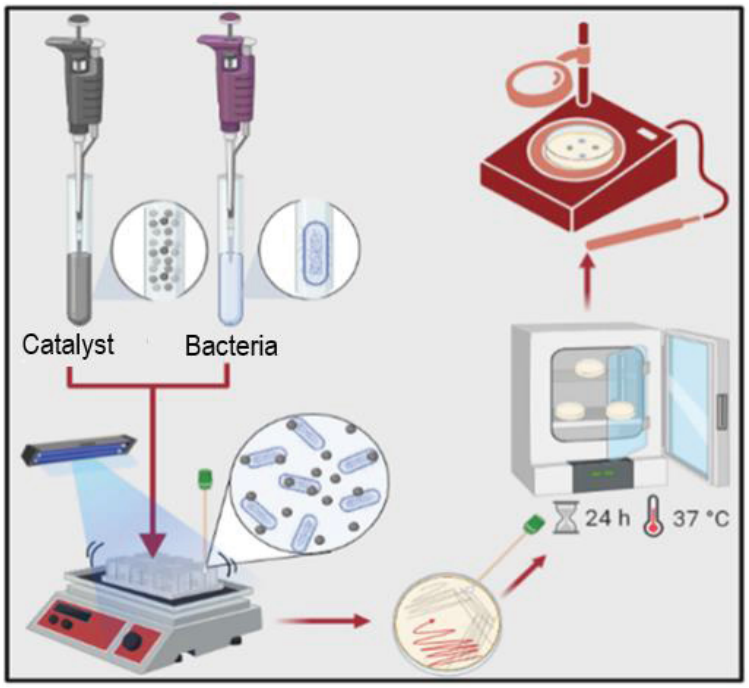


## 2.5 Detection of reactive oxygen species (ROS)

We employed a protocol established [39], with adaptations, to detect ROS in bacterial samples. We followed the same experimental procedure described in item 2.4, differing only in the dilution of the bacteria, being $1x10^3$ CFU $mL^{-1}$ in this one versus $1x10^5$ CFU $mL^{-1}$ in that one. After the reaction times, the collected sample was washed in phosphate-buffered saline (1 $mmol.L^{-1}$) and centrifuged at 3000 rpm for 5 min. Then, the supernatant was discarded and the pellet was incubated for 30 min at 37 ºC in the dark with 1 mL of 2',7'-dichlorofluorescein diacetate ($H_2$DCF-DA) in phosphate-buffered saline. After the time elapsed, the cells were centrifuged at 5000 rpm for 6 min to remove the remaining $H_2$DCF-DA. Then, the cell pellets were suspended in 1 mL of phosphate-buffered saline and mixed with 200 µL of alkaline lysis buffer (1% SDS; 0.2 $mol.L^{-1}$ NaOH) for 10 min at 37 ºC. Finally, the mixture was centrifuged at 5000 rpm for 6 min and the final supernatant product was collected for fluorescence readings (488 nm excitation and 525 nm emission) (Thermo Scientific™ Varioskan™ LUX). The results were expressed as percentage (%) of ROS relative to 0 min (initial time).

## 2.6 Statistical analysis

The statistical analyses were conducted using GraphPad Prism 9.0 software, which is provided to academic users. The Kolmogorov-Smirnov test was employed to assess the normality of the data, and the Grubbs test was utilized to identify and exclude outliers. All experiments were conducted in triplicate, and the differences between groups with respect to the variables under investigation were evaluated using one-way analysis of variance (ANOVA), as appropriate, followed by Tukey's post-hoc test. A p-value of less than 0.05 was considered to indicate a statistically significant difference. The data were presented in graphical form and expressed as mean and standard deviation.

## 3. Results and Discussion

### 3.1 Characterization of the catalysts

As illustrated in **Figure 3**, the FT-IR spectra of the T, 2AgT/I, and 10AgT/I catalysts exhibited distinctive titanium (Ti) bands at 570 $cm^{-1}$, which can be attributed to the bonding of oxygen and titanium (Ti-O-Ti) [38, 39]. Additionally, the shoulder observed at 1638 $cm^{-1}$ is associated with the unfolding modes of water and Ti-OH [40-42]. In the region of 3000 $cm^{-1}$, the band refers to the stretching vibration of the OH group and may be related to the process of water adsorption on the surface of the materials [40, 41]. As a consequence of doping, the 2AgT/I and 10AgT/I catalysts exhibit a slight displacement of the peaks in the range of 660-700 $cm^{-1}$, which is indicative of the asymmetric vibration of Ti-Ag-O [42, 43]. A band at 1370 $cm^{-1}$ is observable in the AgT/I samples' spectrum, which is characteristic of Ag-$TiO_2$ bonds. This confirms the deposition of Ag on the support and corroborates the XRD results [44, 45]. The intensities of the bands of the 2AgT/I and 10AgT/I catalysts were found to be lower than those of the T bands, indicating that the Ag particles had combined with the $TiO_2$ after impregnation [46].

**Figure 3** - FT-IR spectra of the catalysts.

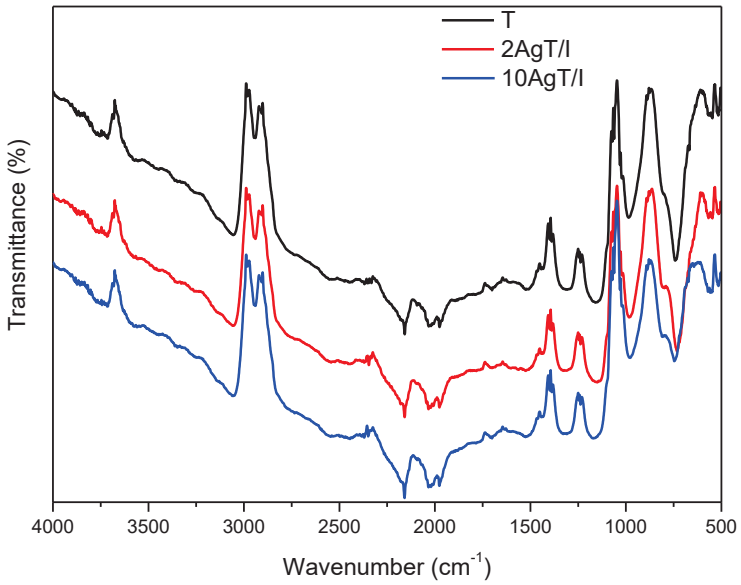


**Figure 4** depicts the X-ray diffraction patterns of the T, 2AgT/I, and 10AgT/I catalysts. The T catalyst exhibits well-defined diffraction peaks, indicative of organized crystalline phases. Two crystalline phases are present: anatase (JCPDS 21-1272), which is more abundant, and rutile (JCPDS 71-0650). The anatase phase exhibits pronounced peaks at 25.4, 37.9, 48.1, 53.9, 55.1, and 62.8 degrees. The rutile phase exhibited 2θ peaks at 27.5, 29.8, and 44.4° [47]. The 2AgT/I catalyst displays a diffraction pattern indicative of the silver oxide (AgO) phase (JCPDS 84-1108) at the 2θ angle of 67.6° [44, 45], thereby substantiating the assertion that the metal was associated with the support. In the case of the 10AgT/I catalyst, characteristic diffraction patterns of metallic silver were observed at angles of 2θ of 35.9, 39.9, and 54.6°. It can be observed that the 2AgT/I and 10AgT/I catalysts exhibit broad peaks, which provide evidence of structural and amorphous disorder [46, 47]. The detection of these Ag peaks in the AgT/I catalysts by XRD serves to confirm that diffusion of the Ag atoms was indeed deposited on the $TiO_2$ support [48, 49].

**Figure 4** - Diffractograms of the catalysts.

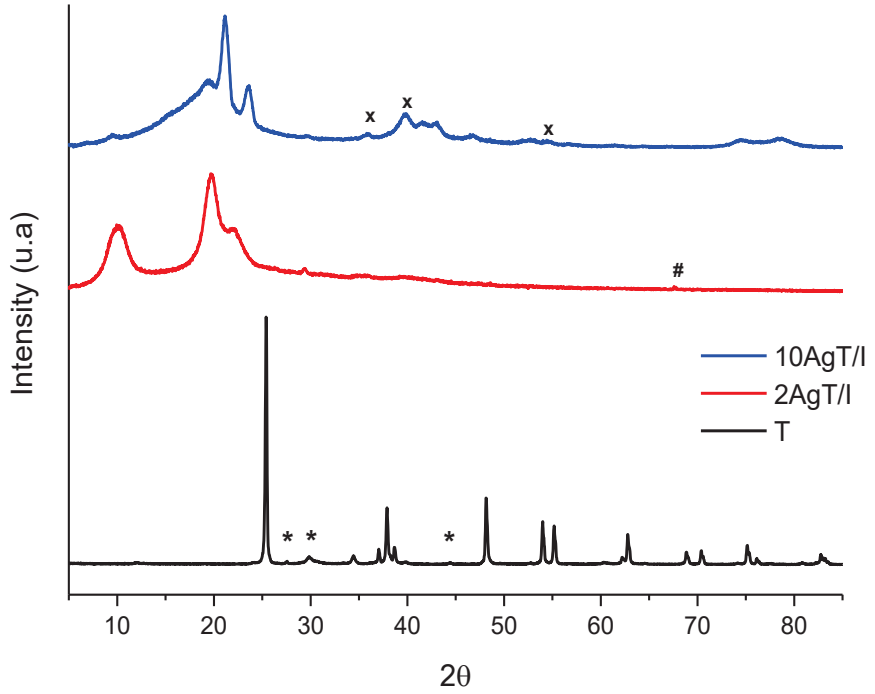


The * symbol denotes the presence of rutile, while the other peaks of the T catalyst represent the anatase phase. The symbol "#" silver oxide, while "x" represents metallic silver.

### 3.2 Antimicrobial activity test

**Figures 5** (A-L) and **6** (A-L) illustrate the impact of visible light sources (termed “clear light”), black light, and the absence of light (referred to as "dark") on the inactivation of *E. coli* and *S. aureus*, respectively. The figures depict the effects of these light sources on controls (A, E, and I), catalysts T (B, F, and J), 2AgT/I (C, G, and K), and 10AgT/I (D, H, and L).

**Figure 5** – Antibacterial activity test (*E. coli*) of T, 2AgT/I and 10AgT/I catalysts photoactivated by clear light (A-D), dark (E-H) and black light (I-L).

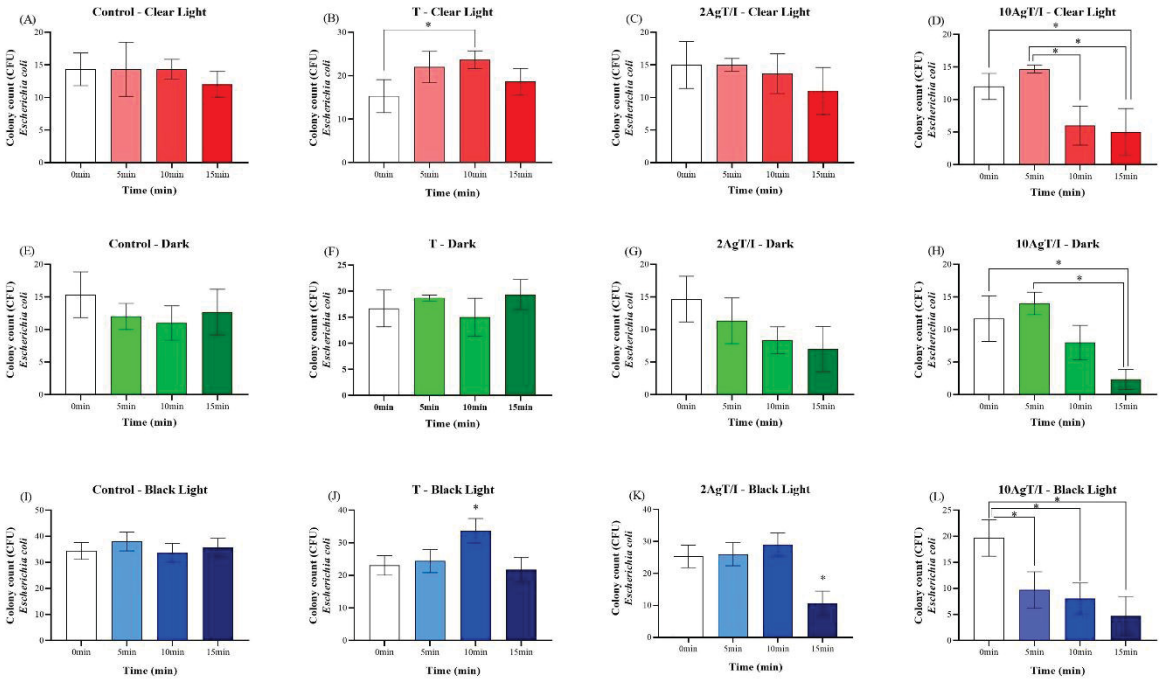


Antibacterial action against *E. coli* of the control (A, E, and I) and the catalysts T (B, F, and J), 2AgT/I (C, G, and K) and 10AgT/I (D, H, and L) in the light test (A-D), dark test (E-H) and black light test (I-L), according to the time variation 0, 5, 10 and 15 min. Asterisks indicate $p<0.05$ (one-way ANOVA, post Tukey test).

**Figure 6** – Antibacterial activity test (*S. aureus*) of T, 2AgT/I and 10AgT/I catalysts photoactivated by clear light (A-D), dark (E-H) and black light (I-L).

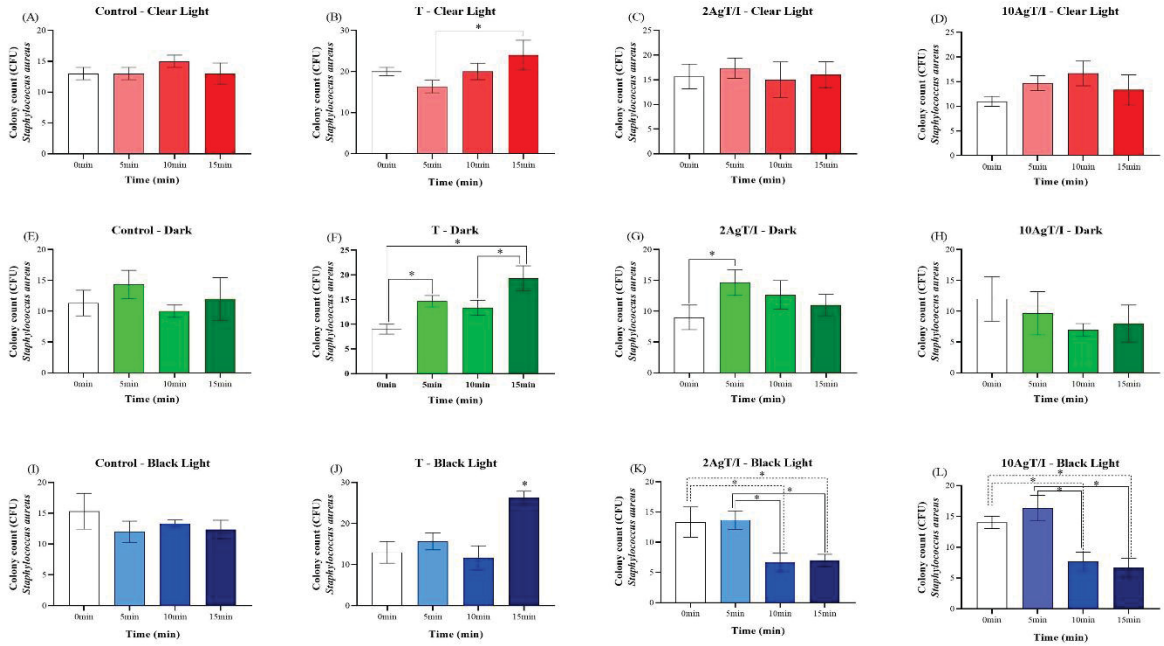

Antibacterial action against *S. aureus* of the control (A, E, and I) and the catalysts T (B, F, and J), 2AgT/I (C, G, and K) and 10AgT/I (D, H, and L) in the clear light test (A-D), dark test (E-H) and black light test (I-L), according to the time variation 0, 5, 10 and 15 min. Asterisks indicate $p<0.05$ (one-way ANOVA, post Tukey test).

It can be observed that catalyst T (Figures 5B, 6B and 6F) had an elevation in the number of bacterial colonies, which can be attributed to two potential factors. The first potential explanation is that viable bacteria are adsorbed onto the surface of the catalyst, resulting in underutilization [50, 51] of the active component due to their large number. The second potential explanation is that the T catalyst did not undergo photoactivation under visible light, as the irradiated energy was below its band gap [52, 53]. It is likely that a combination of these factors was responsible.

As illustrated in Figure 6G, the 2AgT/I catalyst exhibited an increase in the number of colonies over the course of the dark test, with a notable increase observed between time 0 and 5 min. This may indicate that the dose of Ag nanoparticles released by this catalyst was relatively low, and despite adhering to the surface of the cell membrane and wall, accumulated and caused cell death, which may have stimulated the recovery of the microorganisms in the dark. This mechanism facilitates the repair of damage caused by Ag nanoparticles released by this catalyst to the structure of the bacteria, thereby promoting cell regeneration and potentially stimulating growth [49, 50]. The antibacterial efficacy of an Ag-based catalyst is contingent upon the rate of release of Ag ions [54].

The 10AgT/I catalyst (Figure 5D) demonstrated a bactericidal effect under bright light conditions after 10 min. In the dark test, the catalyst (Figure 5H) exhibited a bactericidal effect comparable to that observed in the light test (Figure 5D), with a latency period of 15 min. The antimicrobial activity of the 10AgT/I catalyst may be attributed to the release of Ag nanoparticles. Therefore, the concentration of this metal in the photocatalyst influences its antimicrobial efficacy. The introduction of additional silver into the titanium dioxide matrix results in enhanced bactericidal action, which operates via disparate mechanisms [48, 52]. The initial mechanism involves the adhesion of these nanoparticles to the surface of the cell membrane and wall, which results in the accumulation and leakage of intracellular organelles, ultimately leading to cell death [55, 56]. Consequently, the released Ag can interact with enzymes in the bacterial membranes, thereby disrupting their functionality or entering the cell and damaging the DNA [57, 58].

Subsequently, the formation of spaces within the cell results in the disintegration of the cell walls and the death of the bacteria [59, 60]. Another potential mechanism involves the insertion of Ag nanoparticles into the bacterial cell, resulting in damage to intracellular organelles (e.g., endoplasmic reticulum, mitochondria) and biomolecules (e.g., lipids, DNA, proteins). Moreover, Ag nanoparticles have been demonstrated to induce cell toxicity and oxidative stress through the generation of free radicals. The final mechanism is associated with the modulation of signal transduction pathways [59].

As illustrated in Figures 5J and 6J, the T catalysts exhibited an increase in the number of colonies following irradiation with black light. This suggests that UV irradiation facilitated the photoreparation of the bacteria, thereby promoting cell regeneration [54,55]. This indicates that the applied UV dose was sublethal. This allows for the repair of damage caused by irradiation in microorganisms, such as photoreactivation. Thus occurs when ultraviolet radiation is absorbed by various intracellular organelles, including deoxyribonucleic acid (DNA), at a wavelength of 260 nm. This results in the formation of pyrimidine dimers, which subsequently leads to an increase in bactericidal activity. It is possible that these dimers may not be removed by specific intracellular repair enzymes, which could result in the inhibition or modification of DNA replication and, consequently, in the loss of the bacterial cell's ability to reproduce or mutate. The utilization of a sublethal dose of UV enables microorganisms to repair the damage to their DNA structure [49, 50, 56].

At the 15 min mark (Figures 5I-L and 6I-L), a decline was observed in the number of colonies for catalysts T (Figure 5J), 2AgT/I (Figures 5K and 6K), and 10AgT/I (Figure 6L). Conversely, the 10AgT/I catalyst (Figure 5L) demonstrated bactericidal activity after 5 min. It is plausible that these catalysts were photoactivated by UV radiation, resulting in an enhanced generation of ROS (superoxide radical ($O_2^{-\bullet}$), hydroxyl radical ($OH^\bullet$), hydrogen peroxide ($H_2O_2$), hydroperoxyl radical ($HO_2^\bullet$), and singlet oxygen ($^1O_2$), and consequently exhibited augmented antibacterial activity when compared to the light and dark test (Figures 5A-H and 6A-H) [50]. This surpassed the photorepair of *E. coli* and *S. aureus*. The 2AgT/I (Figures 5K and 6K) and 10AgT/I (Figures 5L and 6L) catalysts exhibited more pronounced photocatalytic effects than the T catalyst (Figures 5J and 6J) [59, 60]. The AgT/I catalysts, particularly 10AgT/I, have been demonstrated to be

effective against both Gram-negative and Gram-positive bacteria. This is attributed to the synergistic effect of Ag and $TiO_2$, which results in a combination of ROS production and Ag release, as well as greater particle stability [61, 62].

The AgT/I catalysts demonstrated a markedly enhanced bactericidal efficacy against *E. coli* (2AgT/I - black light test and 10AgT/I in all the tests illustrated in Figure 5). However, these catalysts demonstrated a reduction in their performance against *S. aureus*. Specifically, 2AgT/I and 10AgT/I exhibited activity only under black light. This suggests that different microorganisms respond in disparate ways to AgT/I catalysts. This phenomenon is primarily attributable to structural differences, particularly the complexity and thickness of the cell wall. This is attributable to the distinct cellular constitution of Gram-positive microorganisms, which are composed of 90% peptidoglycan and 10% teichoic acid, with the reticular structure of the peptides being more compact than that of Gram-negative bacteria [63].

### 3.3 Detection of reactive oxygen species

**Figure 7** (A and B) shows the intracellular ROS generation values of *E. coli* (A) and *S. aureus* (B) for the 10AgT/I catalyst, under black light.

**Figure 7** - The intracellular ROS generation values of *E. coli* (A) and *S. aureus* (B) from the $H_2$DCF-DA ROS detection assay for the 10AgT/I catalyst are presented.

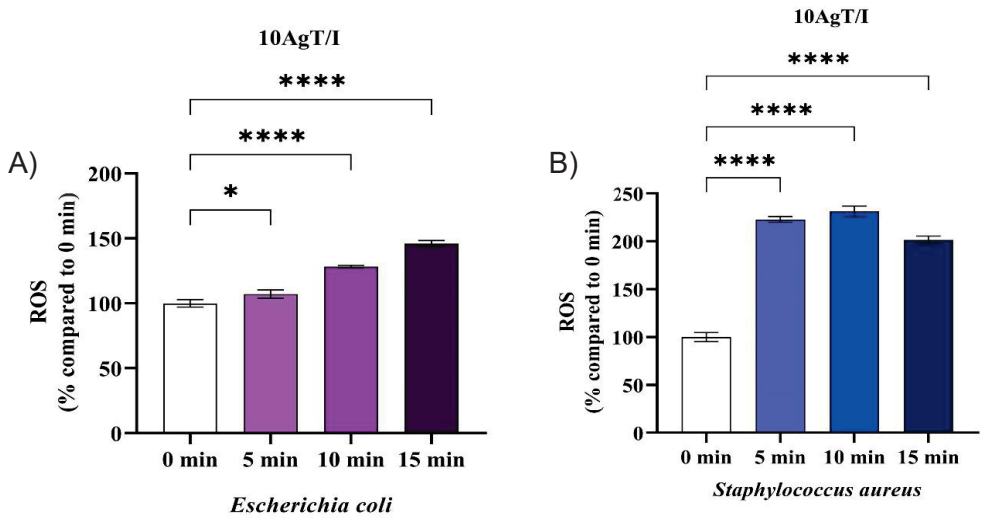


Asterisks indicate * p <0.05; ** p <0.01; *** p< 0.001 and **** p < 0.0001 (one-way ANOVA, with Dunnett's post-hoc test).

The level of reactive oxygen species (ROS), which encompasses $O_2^{-\bullet}$, $HO_2^{\bullet}$, $OH^{\bullet}$, and other species, was quantified through exposure to the 10AgT/I catalyst, which exhibited the most pronounced antibacterial activity among the impregnated catalysts under investigation. An increase in the level of ROS was observed after 5 min for both *E. coli* (Figure 7A) and *S. aureus* (Figure 7B). These findings are consistent with the data presented in Figures 5L and 6L, which demonstrate that ROS were generated through photocatalytic processes. These species accumulate and overwhelm the bacteria's antioxidant defense mechanisms, thereby causing membrane damage and cell death [64].

The bactericidal action of AgT/I catalysts is dependent on oxidative stress and can be linked to a sequence of reactions (**Figure 8**). Firstly, they attract the bacterial surface, thereby destabilizing the cell wall and membrane. This alters the cell's permeability, induces toxicity and oxidative stress through ROS and free radicals, and finally modulates the signal transduction pathways [65]. Consequently, $TiO_2$ is stimulated by UV radiation, whereby the photon energy surpasses the catalyst's bandgap energy, resulting in the production of electron-hole pairs ($e^-/h^+$). The electron-hole pairs generated subsequently react with molecules present in the surrounding environment, including water and oxygen ($O_2$), resulting in the production of hydroxyl ($^{\bullet}OH$) and superoxide ($O_2^{-\bullet}$) radicals. The gaps serve to separate the water molecules into their constituent $OH^-$ and $H^+$ ions. The dissolved oxygen molecules are transformed into the superoxide anion radical ($O_2^{-\bullet}$). This reaction results in the production of $HO_2^-$ radicals, which subsequently collide with $e^-$ to generate hydrogen peroxide anions ($HO_2^-$). Subsequently, they react with $H^+$ ions to produce $H_2O_2$ [66]. Concurrently, the Ag nanoparticles facilitate the capture of electrons, transferring them from the $TiO_2$ conduction band to $O_2^{-\bullet}$, thereby generating superoxide radicals. These nanoparticles facilitate the generation of hydroxyl radicals, which are produced by the reaction of water with the remaining photoproduced gaps in the $TiO_2$ valence band. The photoproduced ROS can penetrate the cell membrane and result in bacterial death [67].

**Figure 8** – Illustration of the mechanism of action of Ag/$TiO_2$ catalysts.

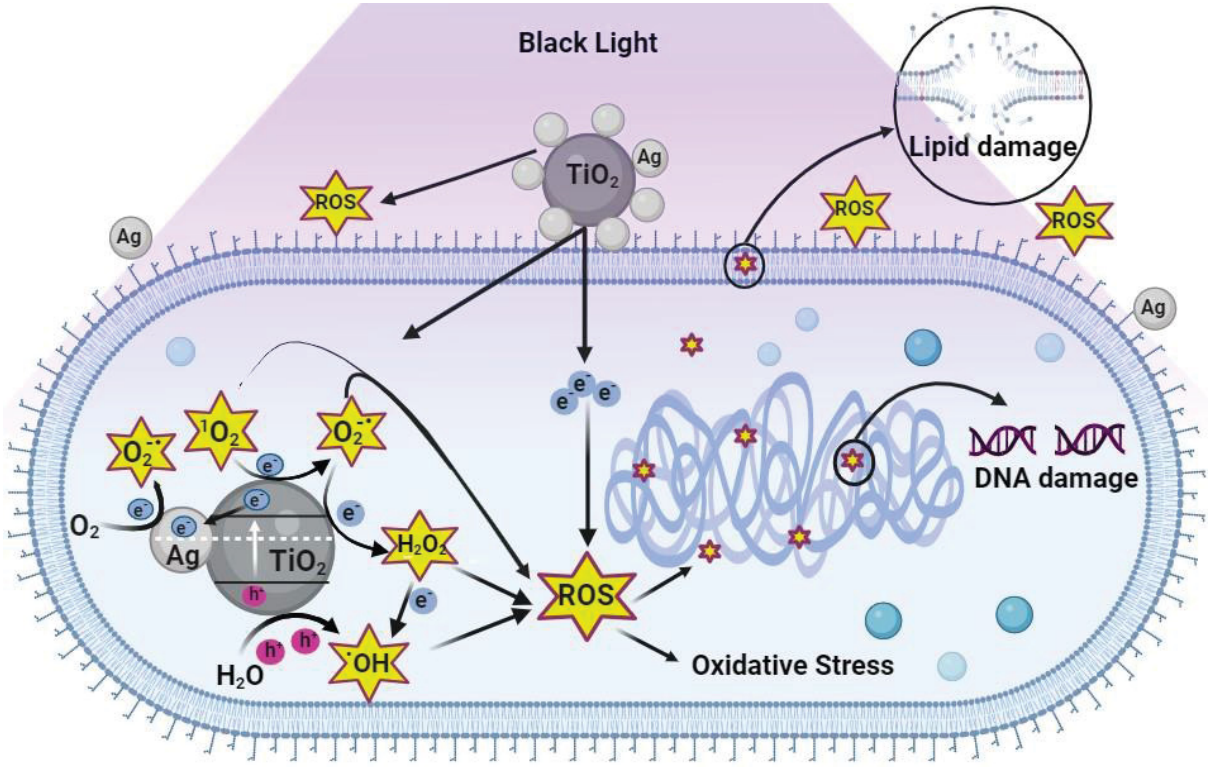


The photoactivated Ag/$TiO_2$ catalyst mediates oxidative stress by exciting electrons ($e^-$) from the valence band to the conduction band, thereby generating $e^-/h^+$ pairs within the bacterial cell. Subsequently, the $e^-/h^+$ pairs migrate to the $TiO_2$ surface, where they engage in oxidation/reduction reactions with $H_2O$ and $O_2$, resulting in the production of reactive oxygen species (ROS). Ag captures the electrons transported from $TiO_2$ and transfers them to $O_2$, thereby producing superoxide radicals ($O_2^{-\bullet}$), hydroxyl radicals ($HO^\bullet$), hydrogen peroxide ($H_2O_2$), and singlet oxygen ($^1O_2$). The ROS and Ag nanoparticles are attracted to the surface of the bacteria, accumulate, and overwhelm the antioxidant defense mechanisms, causing damage to the bacterial membrane, DNA, and, consequently, cell death.

## 4. Conclusion

The impregnation method for synthesizing AgT/I catalysts was simple and effective. The AgT/I catalysts have disorganized crystalline faces. AgT/I catalysts, especially 10AgT/I, are effective against Gram-negative (action in test under bright light, dark and black light) and Gram-positive (action under black light) bacteria due to the synergistic effect of Ag and $TiO_2$. Antibacterial materials with a rapid bactericidal action have been developed, with the possibility of less expensive and broader application in antibacterial therapy. AgT/I catalysts have promising antimicrobial effects, with potential for application in rapid bacterial disinfection devices and use in environments where infection control is crucial.

## References


[1] M. Worobey, J. Pekar, B.B. Larsen, M.I. Nelson, V. Hill, J.B. Joy, A. Rambaut, M.A. Suchard, J.O. Wertheim, P. Lemey, The emergence of SARS-CoV-2 in Europe and North America, Science (80). 370 (2020) 564–570. https://doi.org/10.1126/science.abc8169.

[2] S.M. Imani, L. Ladouceur, T. Marshall, R. Maclachlan, L. Soleymani, T.F. Didar, Antimicrobial Nanomaterials and Coatings: Current Mechanisms and Future Perspectives to Control the Spread of Viruses Including SARS-CoV-2, ACS Nano 14 (2020) 12341–12369. https://doi.org/10.1021/acsnano.0c05937.

[3] C. Yang, S. Krishnamurthy, J. Liu, S. Liu, X. Lu, D.J. Coady, W. Cheng, G. De Libero, A. Singhal, J.L. Hedrick, Y.Y. Yang, Broad-Spectrum Antimicrobial Star Polycarbonates Functionalized with Mannose for Targeting Bacteria Residing inside Immune Cells, Adv. Healthc. Mater. 5 (2016) 1272–1281. https://doi.org/10.1002/adhm.201600070.

[4] D. Rodríguez-Lázaro, N. Cook, F.M. Ruggeri, J. Sellwood, A. Nasser, M.S.J. Nascimento, M. D'Agostino, R. Santos, J.C. Saiz, A. Rzeżutka, A. Bosch, R. Gironés, A. Carducci, M. Muscillo, K. Kovač, M. Diez-Valcarce, A. Vantarakis, C.-H. von Bonsdorff, A.M. de Roda Husman, M. Hernández, W.H.M. van der Poel, Virus hazards from food, water and other contaminated environments, FEMS Microbiol. Rev. 36 (2012) 786–814. https://doi.org/10.1111/j.1574-6976.2011.00306.x.

[5] K. Todar, Todar's online textbook of bacteriology., Department of Bacteriology, University of Wisconsin, Madison., 2006. http://www.textbookofbacteriology.net/. (accessed September 25, 2023).

[6] L. Wang, C. Hu, L. Shao, The antimicrobial activity of nanoparticles: present situation and prospects for the future, Int. J. Nanomedicine Volume 12 (2017) 1227–1249. https://doi.org/10.2147/IJN.S121956.

[7] A.-P. Magiorakos, A. Srinivasan, R.B. Carey, Y. Carmeli, M.E. Falagas, C.G. Giske, S. Harbarth, J.F. Hindler, G. Kahlmeter, B. Olsson-Liljequist, D.L. Paterson, L.B. Rice, J. Stelling, M.J. Struelens, A. Vatopoulos, J.T. Weber, D.L. Monnet, Multidrug-resistant, extensively drug-resistant and pandrug-resistant bacteria: an international expert proposal for interim standard definitions for acquired resistance, Clin. Microbiol. Infect. 18 (2012) 268–281. https://doi.org/10.1111/j.1469-0691.2011.03570.x.

[8] P. Makvandi, C. Wang, E.N. Zare, A. Borzacchiello, L. Niu, F.R. Tay, Metal-Based Nanomaterials in Biomedical Applications: Antimicrobial Activity and Cytotoxicity Aspects, Adv. Funct. Mater. 30 (2020). https://doi.org/10.1002/adfm.201910021.

[9] V.G. Benatto, J.P.A. de Jesus, A.A. de Castro, L.C. Assis, T.C. Ramalho, F.A. La Porta, Prospects of ZnS and ZnO as smart semiconductor materials in light-activated antimicrobial coatings for mitigation of severe acute respiratory syndrome coronavirus-2 infection, Mater. Today Commun. 34 (2023) 105192. https://doi.org/10.1016/j.mtcomm.2022.105192.

[10] M.Z. Ghori, S. Veziroglu, B. Henkel, A. Vahl, O. Polonskyi, T. Strunskus, F. Faupel, O.C. Aktas, A comparative study of photocatalysis on highly active columnar $TiO_2$ nanostructures in-air and in-solution, Sol. Energy Mater. Sol. Cells 178 (2018) 170–178. https://doi.org/10.1016/j.solmat.2018.01.019.

[11] Y. Liu, J. Li, X. Qiu, C. Burda, Novel $TiO_2$ nanocatalysts for wastewater

purification: tapping energy from the sun, Water Sci. Technol. 54 (2006) 47–54. https://doi.org/10.2166/wst.2006.733.
[12] J. Singh, B. Satpati, S. Mohapatra, Structural, Optical and Plasmonic Properties of Ag-$TiO_2$ Hybrid Plasmonic Nanostructures with Enhanced Photocatalytic Activity, Plasmonics 12 (2017) 877–888. https://doi.org/10.1007/s11468-016-0339-6.
[13] S.M. Zacarías, M.L. Satuf, M.C. Vaccari, O.M. Alfano, Photocatalytic inactivation of bacterial spores using $TiO_2$ films with silver deposits, Chem. Eng. J. 266 (2015) 133–140. https://doi.org/10.1016/J.CEJ.2014.12.074.
[14] M. Fioreze, E.P. dos Santos, N. Schmachtenberg, Processos oxidativos avançados: fundamentos e aplicação ambiental, Rev. Eletrônica Em Gestão, Educ. e Tecnol. Ambient. 18 (2014). https://doi.org/10.5902/2236117010662.
[15] M.B. Heo, M. Kwak, K.S. An, H.J. Kim, H.Y. Ryu, S.M. Lee, K.S. Song, I.Y. Kim, J.-H. Kwon, T.G. Lee, Oral toxicity of titanium dioxide P25 at repeated dose 28-day and 90-day in rats, Part. Fibre Toxicol. 17 (2020) 34. https://doi.org/10.1186/s12989-020-00350-6.
[16] K. Chalastara, F. Guo, S. Elouatik, G.P. Demopoulos, Tunable Composition Aqueous-Synthesized Mixed-Phase $TiO_2$ Nanocrystals for Photo-Assisted Water Decontamination: Comparison of Anatase, Brookite and Rutile Photocatalysts, Catalysts 10 (2020) 407. https://doi.org/10.3390/catal10040407.
[17] S. Chandra, P. Jagdale, I. Medha, A. Tiwari, M. Bartoli, A. Nino, F. Olivito, Biochar-Supported $TiO_2$-Based Nanocomposites for the Photocatalytic Degradation of Sulfamethoxazole in Water—A Review, Toxics 9 (2021) 313. https://doi.org/10.3390/toxics9110313.
[18] C. Zarzzeka, J. Goldoni, F. Marafon, W.G. Sganzerla, T. Forster-Carneiro, M.D. Bagatini, L.M.S. Colpini, Use of titanium dioxide nanoparticles for cancertreatment: A comprehensive review and bibliometric analysis, Biocatal. Agric. Biotechnol. 50 (2023) 102710. https://doi.org/10.1016/j.bcab.2023.102710.
[19] S. Goulart, L.J. Jaramillo Nieves, A.G. Dal Bó, A.M. Bernardin, Sensitization of $TiO_2$ nanoparticles with natural dyes extracts for photocatalytic activity under visible light, Dye. Pigment. 182 (2020) 108654. https://doi.org/10.1016/j.dyepig.2020.108654.
[20] J. Singh, S.A. Khan, J. Shah, R.K. Kotnala, S. Mohapatra, Nanostructured $TiO_2$ thin films prepared by RF magnetron sputtering for photocatalytic applications, Appl. Surf. Sci. 422 (2017) 953–961. https://doi.org/10.1016/j.apsusc.2017.06.068.
[21] P.S. Basavarajappa, S.B. Patil, N. Ganganagappa, K.R. Reddy, A. V. Raghu, C.V. Reddy, Recent progress in metal-doped $TiO_2$, non-metal doped/codoped $TiO_2$ and $TiO_2$ nanostructured hybrids for enhanced photocatalysis, Int. J. Hydrogen Energy 45 (2020) 7764–7778. https://doi.org/10.1016/j.ijhydene.2019.07.241.
[22] H. Zhang, D. Yu, W. Wang, P. Gao, L. Zhang, S. Zhong, B. Liu, Recyclable and highly efficient photocatalytic fabric of Fe(III)@$BiVO_4$/cotton via thiol-ene click reaction with visible-light response in water, Adv. Powder Technol. 30 (2019) 3182–3192. https://doi.org/10.1016/j.apt.2019.09.027.
[23] M.A. Mohamed, W.N. W. Salleh, J. Jaafar, A.F. Ismail, M.A. Mutalib, N.A.A. Sani, S.E.A. M. Asri, C.S. Ong, Physicochemical characteristic of

regenerated cellulose/N-doped $TiO_2$ nanocomposite membrane fabricated from recycled newspaper with photocatalytic activity under UV and visible light irradiation, Chem. Eng. J. 284 (2016) 202–215. https://doi.org/10.1016/j.cej.2015.08.128.
[24] L. Rizzello, P.P. Pompa, Nanosilver-based antibacterial drugs and devices: Mechanisms, methodological drawbacks, and guidelines, Chem. Soc. Rev. 43 (2014) 1501–1518. https://doi.org/10.1039/C3CS60218D.
[25] A. Kumar, P. Choudhary, A. Kumar, P.H.C. Camargo, V. Krishnan, Recent Advances in Plasmonic Photocatalysis Based on $TiO_2$ and Noble Metal Nanoparticles for Energy Conversion, Environmental Remediation, and Organic Synthesis, Small 18 (2022). https://doi.org/10.1002/smll.202101638.
[26] J. Gamage, Z. Zhang, Applications of Photocatalytic Disinfection, Int. J. Photoenergy 2010 (2010) 1–11. https://doi.org/10.1155/2010/764870.
[27] K.S. Butler, B.J. Casey, G.V.M. Garborcauskas, B.J. Dair, R.K. Elespuru, Assessment of titanium dioxide nanoparticle effects in bacteria: Association, uptake, mutagenicity, co-mutagenicity and DNA repair inhibition, Mutat. Res. Toxicol. Environ. Mutagen. 768 (2014) 14–22. https://doi.org/10.1016/j.mrgentox.2014.04.008.
[28] L. Ge, G. Na, S. Zhang, K. Li, P. Zhang, H. Ren, Z. Yao, New insights into the aquatic photochemistry of fluoroquinolone antibiotics: Direct photodegradation, hydroxyl-radical oxidation, and antibacterial activity changes, Sci. Total Environ. 527–528 (2015) 12–17. https://doi.org/10.1016/j.scitotenv.2015.04.099.
[29] A.T. Dharmaraja, Role of Reactive Oxygen Species (ROS) in Therapeutics and Drug Resistance in Cancer and Bacteria, J. Med. Chem. 60 (2017) 3221–3240. https://doi.org/10.1021/acs.jmedchem.6b01243.
[30] M.C. Hlavsa, B.L. Cikesh, V.A. Roberts, A.M. Kahler, M. Vigar, E.D. Hilborn, T.J. Wade, D.M. Roellig, J.L. Murphy, L. Xiao, K.M. Yates, J.M. Kunz, M.J. Arduino, S.C. Reddy, K.E. Fullerton, L.A. Cooley, M.J. Beach, V.R. Hill, J.S. Yoder, Outbreaks associated with treated recreational water — United States, 2000–2014, Am. J. Transplant. 18 (2018) 1815–1819. https://doi.org/10.1111/ajt.14956.
[31] F. Pérez-Rodríguez, G.D. Posada-Izquierdo, A. Valero, R.M. García-Gimeno, G. Zurera, Modelling survival kinetics of *Staphylococcus aureus* and *Escherichia coli* O157:H7 on stainless steel surfaces soiled with different substrates under static conditions of temperature and relative humidity, Food Microbiol. 33 (2013) 197–204. https://doi.org/10.1016/J.FM.2012.09.017.
[32] N. López-Vinent, A. Cruz-Alcalde, G. Moussavi, I. del Castillo Gonzalez, A. Hernandez Lehmann, J. Giménez, S. Giannakis, Improving ferrate disinfection and decontamination performance at neutral pH by activating peroxymonosulfate under solar light, Chem. Eng. J. 450 (2022) 137904. https://doi.org/10.1016/j.cej.2022.137904.
[33] E.A. Zottola, L.B. Smith, The microbiology of foodborne disease outbreaks: an update[1], J. Food Saf. 11 (1990) 13–29. https://doi.org/10.1111/j.1745-4565.1990.tb00035.x.
[34] A.-M. Aziz, The role of healthcare strategies in controlling antibiotic resistance, Br. J. Nurs. 22 (2013) 1066–1074. https://doi.org/10.12968/bjon.2013.22.18.1066.
[35] L.E.N. Castro, A.H. Meira, L.N.B. Almeida, G. Gonçalves Lenzi, L.M.S.

Colpini, Experimental design and optimization of textile dye photodiscoloration using Zn/$TiO_2$ catalysts, Desalin. WATER Treat. 266 (2022) 173–185. https://doi.org/10.5004/dwt.2022.28599.
[36] N. Silva, V.C.A.. Junqueira, N.F.A. Silveira, M.H. Taniwaki, R.A.R. Gomes, M.M. Okazaki, Manual of methods for microbiological analysis of food and water., 5ª ed., Blucher, São Paulo, 2018.
[37] A.C. de S. Cordeiro, S.G.F. Leite, M. Dezotti, Inativação por oxidação fotocatalítica de *Escherichia coli* e *Pseudomonas sp*., Quim. Nova 27 (2004) 689–694. https://doi.org/10.1590/S0100-40422004000500002.
[38] T. Tsai, H. Chang, K. Chang, Y. Liu, C. Tseng, A comparative study of the bactericidal effect of photocatalytic oxidation by $TiO_2$ on antibiotic-resistant and antibiotic-sensitive bacteria, J. Chem. Technol. Biotechnol. 85 (2010) 1642–1653. https://doi.org/10.1002/jctb.2476.
[39] S. Liao, Y. Zhang, X. Pan, F. Zhu, C. Jiang, Q. Liu, Z. Cheng, G. Dai, G. Wu, L. Wang, L. Chen, Antibacterial activity and mechanism of silver nanoparticles against multidrug-resistant em *Pseudomonas aeruginosa*, Int. J. Nanomedicine 14 (2019) 1469–1487. https://doi.org/10.2147/IJN.S191340.
[40] E.H. Alsharaeh, T. Bora, A. Soliman, F. Ahmed, G. Bharath, M.G. Ghoniem, K.M. Abu-Salah, J. Dutta, Sol-Gel-Assisted Microwave-Derived Synthesis of Anatase Ag/$TiO_2$/GO Nanohybrids toward Efficient Visible Light Phenol Degradation, Catalysts 7 (2017) 133. https://doi.org/10.3390/catal7050133.
[41] M. Safaei, M. Taran, Optimal conditions for producing bactericidal sodium hyaluronate-$TiO_2$ bionanocomposite and its characterization, Int. J. Biol. Macromol. 104 (2017) 449–456. https://doi.org/10.1016/J.IJBIOMAC.2017.06.016.
[42] A. León, P. Reuquen, C. Garín, R. Segura, P. Vargas, P. Zapata, P. Orihuela, FTIR and Raman Characterization of $TiO_2$ Nanoparticles Coated with Polyethylene Glycol as Carrier for 2-Methoxyestradiol, Appl. Sci. 7 (2017) 49. https://doi.org/10.3390/app7010049.
[43] H. Yang, K. Dai, J. Zhang, G. Dawson, Inorganic-organic hybrid photocatalysts: Syntheses, mechanisms, and applications, Chinese J. Catal. 43 (2022) 2111–2140. https://doi.org/10.1016/S1872-2067(22)64096-8.
[44] D. Gogoi, A. Namdeo, A.K. Golder, N.R. Peela, Ag-doped $TiO_2$ photocatalysts with effective charge transfer for highly efficient hydrogen production through water splitting, Int. J. Hydrogen Energy 45 (2020) 2729–2744. https://doi.org/10.1016/J.IJHYDENE.2019.11.127.
[45] R.D. Desiati, M. Taspika, E. Sugiarti, Effect of calcination temperature on the antibacterial activity of $TiO_2$/Ag nanocomposite, Mater. Res. Express 6 (2019) 095059. https://doi.org/10.1088/2053-1591/ab155c.
[46] M.B. Poudel, A.A. Kim, Silver nanoparticles decorated $TiO_2$ nanoflakes for antibacterial properties, Inorg. Chem. Commun. 152 (2023) 110675. https://doi.org/10.1016/J.INOCHE.2023.110675.
[47] JCPDS, JCPDS—International Center for Diffraction Data, PCPDFWIN, 2013.
[48] K.A. Razak, D.S.C. Halin, A. Azani, M.M.A.B. Abdullah, M.A.A.M. Salleh, N. Mahmed, V. Chobpattana, L. Kaczmarek, A.V. Sandu, S. Garus, Microstructural Study on Ag/$TiO_2$ Thin Film, Acta Phys. Pol. A 142 (2022) 70–73. https://doi.org/10.12693/APhysPolA.142.70.
[49] R.S. André, C.A. Zamperini, E.G. Mima, V.M. Longo, A.R. Albuquerque, J.R.

Sambrano, A.L. Machado, C.E. Vergani, A.C. Hernandes, J.A. Varela, E. Longo, Antimicrobial activity of $TiO_2$:Ag nanocrystalline heterostructures: Experimental and theoretical insights, Chem. Phys. 459 (2015) 87–95. https://doi.org/10.1016/J.CHEMPHYS.2015.07.020.

[50] H. Sharma, R. Singhal, V. V. Siva Kumar, K. Asokan, Structural, optical and electronic properties of Ag–$TiO_2$ nanocomposite thin film, Appl. Phys. A 122 (2016) 1010. https://doi.org/10.1007/s00339-016-0552-3.

[51] A.A. Mosquera, J.L. Endrino, J.M. Albella, XANES observations of the inhibition and promotion of anatase and rutile phases in silver containing films, J. Anal. At. Spectrom. 29 (2014) 736. https://doi.org/10.1039/c3ja50354b.

[52] O.M. JUNIOR, Inactivation of bacteria in the gas phase by heterogeneous photocatalysis: effect of metal addition., Paulista State University, 2008. https://repositorio.unesp.br/bitstream/handle/11449/97853/modestojunior_o_me_araiq.pdf;jsessionid=9D40A96A3698F51A8C28A5FAB432C63F?sequence=1 (accessed December 19, 2023).

[53] A.A. Ashkarran, S.M. Aghigh, M. Kavianipour, N.J. Farahani, Visible light photo-and bioactivity of Ag/$TiO_2$ nanocomposite with various silver contents, Curr. Appl. Phys. 11 (2011) 1048–1055. https://doi.org/10.1016/J.CAP.2011.01.042.

[54] Y.Y. Chan, E.G. Killick, The effect of salinity, light and temperature in a disposal environment on the recovery of *E.coli* following exposure to ultraviolet radiation, Water Res. 29 (1995) 1373–1377. https://doi.org/10.1016/0043-1354(94)00226-W.

[55] K. Tosa, T. Hirata, Photoreactivation of enterohemorrhagic *Escherichia coli* following UV disinfection, Water Res. 33 (1999) 361–366. https://doi.org/10.1016/S0043-1354(98)00226-7.

[56] C. Liu, L. Geng, Y. Yu, Y. Zhang, B. Zhao, Q. Zhao, Mechanisms of the enhanced antibacterial effect of Ag-$TiO_2$ coatings, Biofouling 34 (2018) 190–199. https://doi.org/10.1080/08927014.2017.1423287.

[57] P. Dong, F. Yang, X. Cheng, Z. Huang, X. Nie, Y. Xiao, X. Zhang, Plasmon enhanced photocatalytic and antimicrobial activities of Ag-$TiO_2$ nanocomposites under visible light irradiation prepared by DBD cold plasma treatment, Mater. Sci. Eng. C 96 (2019) 197–204. https://doi.org/10.1016/j.msec.2018.11.005.

[58] H. Chakhtouna, H. Benzeid, N. Zari, A. el kacem Qaiss, R. Bouhfid, Recent progress on Ag/$TiO_2$ photocatalysts: photocatalytic and bactericidal behaviors, Environ. Sci. Pollut. Res. 28 (2021) 44638–44666. https://doi.org/10.1007/s11356-021-14996-y.

[59] J. Tian, K.K.Y. Wong, C. Ho, C. Lok, W. Yu, C. Che, J. Chiu, P.K.H. Tam, Topical Delivery of Silver Nanoparticles Promotes Wound Healing, ChemMedChem 2 (2007) 129–136. https://doi.org/10.1002/cmdc.200600171.

[60] K. Zawadzka, A. Kisielewska, I. PiwońskI, K. Kądzioła, A. Felczak, S. Różalska, N. Wrońska, K. Lisowska, Mechanisms of antibacterial activity and stability of silver nanoparticles grown on magnetron sputtered $TiO_2$ coatings, Bull. Mater. Sci. 39 (2016) 57–68. https://doi.org/10.1007/s12034-015-1137-z.

[61] M. Dahl, Y. Liu, Y. Yin, Composite Titanium Dioxide Nanomaterials, Chem. Rev. 114 (2014) 9853–9889. https://doi.org/10.1021/cr400634p.

[62] K. Gupta, R.P. Singh, A. Pandey, A. Pandey, Photocatalytic antibacterial performance of $TiO_2$ and Ag-doped $TiO_2$ against *S. aureus* . *P. aeruginosa* and *E. coli*, Beilstein J. Nanotechnol. 4 (2013) 345–351. https://doi.org/10.3762/bjnano.4.40.

[63] Q. Zhao, M. Wang, H. Yang, D. Shi, Y. Wang, Preparation, characterization and the antimicrobial properties of metal ion-doped $TiO_2$ nano-powders, Ceram. Int. 44 (2018) 5145–5154. https://doi.org/10.1016/j.ceramint.2017.12.117.

[64] S.-S. Yong, J.-I. Lee, D.-H. Kang, $TiO_2$-based photocatalyst Generated Reactive Oxygen Species cause cell membrane disruption of *Staphylococcus aureus* and *Escherichia coli* O157:H7, Food Microbiol. 109 (2023) 104119. https://doi.org/10.1016/j.fm.2022.104119.

[65] S. Zhang, X. Liang, G.M. Gadd, Q. Zhao, Advanced titanium dioxide-polytetrafluorethylene ($TiO_2$-PTFE) nanocomposite coatings on stainless steel surfaces with antibacterial and anti-corrosion properties, Appl. Surf. Sci. 490 (2019) 231–241. https://doi.org/10.1016/J.APSUSC.2019.06.070.

[66] N. Zhou, V. López-Puente, Q. Wang, L. Polavarapu, I. Pastoriza-Santos, Q.-H. Xu, Plasmon-enhanced light harvesting: applications in enhanced photocatalysis, photodynamic therapy and photovoltaics, RSC Adv. 5 (2015) 29076–29097. https://doi.org/10.1039/C5RA01819F.

[67] M.I. Din, R. Khalid, Z. Hussain, Minireview: Silver-Doped Titanium Dioxide and Silver-Doped Zinc Oxide Photocatalysts, Anal. Lett. 51 (2018) 892–907. https://doi.org/10.1080/00032719.2017.1363770.

# CHAPTER IV

## Ag/$TiO_2$ photocatalysts: A promising tool in combating bacterial resistance


### ABSTRACT

Infectious diseases are a global health problem, driving the search for new antimicrobial therapies. The photoactivation of materials is emerging as a promising strategy, as it allows pathogens to be inactivated without the selection of resistant strains. The identification and development of new drugs or photoactive agents represents an active field of research, with the aim of offering more effective therapeutic options for the control of bacterial infections. This study synthesized silver-based catalysts (Ag) (2% and 10% w/w%) supported on titanium dioxide ($TiO_2$) by the sol-gel method (2AgT/SG and 10AgT/SG). The AgT/SG catalysts characterized by infrared spectrometry showed characteristic titanium bands and the asymmetric vibration of Ti-Ag-O. X-ray diffraction identified that these catalysts have well-defined anatase peaks representing organized crystalline phases. The differential scanning calorimetry data shows smaller endothermic peaks for the AgT/SG catalysts, indicating a low melting point. Thermogravimetric analysis showed minimal loss of mass for the catalysts. Similar results were observed for the 10AgT/SG catalyst under clear light (9 W) and in the dark, with the antibacterial action against *Escherichia coli* being strongly influenced by the concentration of Ag. Black light photoactivated all the catalysts against *Escherichia coli* and *Staphylococcus aureus*. The AgT/SG catalysts stood out due to their rapid bactericidal action, within 10 minutes, as demonstrated by the reactive oxygen species detection test. These results show that AgT/SG catalysts have enhanced antimicrobial effects compared to $TiO_2$, with possible applications in disinfection devices.



**Keywords:** Sol-gel, Bacteria, Photoactivation, Reactive oxygen species



Manuscript elaborated and formatted according to the guidelines of scientific publication, submitted to the Microbiological Research. Available at: <https://www.sciencedirect.com/journal/microbiological-research>

## 1 Introdution

The occurrence of pathogenic bacteria has become a worldwide problem thanks to numerous infectious diseases, which can cause acute and chronic effects on human health. This is exacerbated by the increased consumption of antibiotics and the resistance of microorganisms to these drugs, thus causing worldwide concern and challenging public health (Graham, 1999). The production of antibiotics is around 100,000 to 200,000 tons per year, totaling more than one billion tons generated since 1940 (Serwecińska, 2020). It was estimated that in 2019, 4.95 million deaths were related to bacterial resistance to antibiotics, with 1.27 million deaths specified by antimicrobial resistance (World Health Organization, 2022). The high use of antibiotics consequently increases the production of waste after consumption, as between 40 and 90% of the antibiotics administered are eliminated from the human body in their active form, contaminating the environment and generating irreversible environmental problems (Duong et al., 2021).

Antibiotic resistance for *Escherichia coli* (*E. coli*) and *Staphylococcus aureus* (*S. aureus*) is related to prolonged hospital stays, with specific resistance influenced by duration in different ways for each microorganism (Frickmann et al., 2019). These pathogens are responsible for numerous urinary tract infections and bacteremia (Poolman and Anderson, 2018).

Researchers are seeking new approaches to combat infection, such as developing new drugs and compounds, as well as improving hygiene and sanitation measures (Prakash et al., 2019). In addition, the World Health Organization (WHO) encourages the research, development and deployment of new bacteriostatic agents or biocides. Therefore, nanomaterials are used as emerging candidates for antimicrobial agents thanks to their low to reasonable toxicity, moderate cost and effective inhibition mechanism against bacterial resistance (World Health Organization, 2001), making them suitable for antibacterial and biomedical applications.

Promising nanomaterials include noble metal nanoparticles (NPs) such as silver (Ag), which have adaptable optoelectronic characteristics in terms of particle size, high surface energy and reduced imperfections (Khanna et al., 2007). Ag has intrinsic characteristics such as high surface area for catalytic reactions, localized

surface plasmon resonance (LSPR) effect and enhanced stability. The LSPR of Ag increases light absorption, scattering and enhancement of the local electromagnetic field in photocatalysis (Ahmed et al., 2021). Ag, whether in elemental form or in suspension, acts against bacteria, fungi and some viruses without adverse effects on human health and has been used in medical devices (Patil et al., 2018). This metal has an antibacterial effect, generally attributed to the release of $Ag^{+}$, which follows various biochemical pathways, such as adherence to and disruption of the bacterial cell membrane and oxidative stress through the generation of extra or intracellular reactive oxygen species (ROS) (Ferdous and Nemmar, 2020; Roy et al., 2019). The limitations of Ag NPs are their easy aggregation at low concentrations, thus influencing their stability, and at high concentrations they increase cytotoxicity and make it difficult to recover them from reactions (Patil et al., 2018). Ag nanoparticles showed reduced toxicity compared to $Ag^{+}$ in human hepatoma cells, despite similar cellular uptake, both forms of Ag can induce oxidative stress, apoptosis and necrosis in human monocytes (Vrček et al., 2016).

To overcome the limitations of Ag NPs, supports such as polymers, silica and metal oxides are used (Patil et al., 2018). Among these supports, titanium dioxide ($TiO_2$) stands out, thanks to its attractive combination of physicochemical characteristics, low cost, low toxicity, chemical stability, biocompatibility and photocatalytic efficiency (M. Patil et al., 2017). However, this oxide has some limitations, such as a wide band gap (3.00 - 3.2 eV) and an absorption spectrum limited to the UV range. These limitations can be overcome by doping with Ag, due to changes in its physical, chemical and photoelectric properties (Etacheri et al., 2015; Wu et al., 2013; Zarzzeka et al., 2023) and by expanding its photocatalytic efficiency towards the visible spectrum (Ali et al., 2018). Ag doping influences the crystalline phases of $TiO_2$ showing more anatase phase (Halin et al., 2018), increases photocatalytic activity and influences crystallization processes (Golim et al., 2019) and reduces electron-lacuna recombination. Thus, the association of Ag and $TiO_2$ enhances the individual characteristics and forms $Ag/TiO_2$ which exhibits optimized photocatalytic and antibacterial properties attributed to the synergistic effects of Ag and $TiO_2$ NPs (Prakash et al., 2019). These oxides demonstrate potent antibacterial activity against Gram-positive and Gram-negative species under visible and UV light irradiation, with complete inhibition achieved at low

concentrations (Deshmukh et al., 2018) in light and dark conditions, surpassing the efficacy of Ag or $TiO_2$ alone (Li et al., 2011).

Various methods, such as photodeposition (Dinh et al., 2011), current deposition (Lai et al., 2010), impregnation, chemical deposition, photodeposition (Li et al., 2009), spin coating, sol-gel (Al Amin and Kowser, 2024) and others have been developed to adapt Ag/$TiO_2$ materials to improve their photocatalytic and antibacterial performance. Most of the methods used in the synthesis of Ag/$TiO_2$ have reports of mixed phases, extensive and complicated protocols in the design of the catalyst or limited scope for antibacterial research, as well as catalysts with Ag aggregation and non-uniformity, which causes a decrease in the antibacterial activity of the material (Deshmukh et al., 2018). Therefore, the sol-gel method offers a versatile route for obtaining materials with high purity, homogeneity and control over the morphology and size of the particles (Borrego Pérez et al., 2023; Uboncholakate et al., 2012). It also makes it possible to control the size and distribution of Ag NPs on $TiO_2$ surfaces, significantly influencing their antibacterial efficacy, with smaller Ag agglomerates (< 5 nm) demonstrating excellent bactericidal performance. These modifications aim to further increase the photocatalytic activity, stability and bactericidal action of Ag/$TiO_2$ for various environmental applications, including wastewater treatment, antimicrobial coatings and biomedical (Zhang and Chen, 2009).

In search of new strategies to develop and improve the future production of agents to control bacterial diseases, this research seeks to present the superior bactericidal actions of Ag/$TiO_2$ oxides. It is hoped that this study will provide new insights into the development of antibacterial agents with a cheaper and broader application alternative in antibacterial therapy. The aim was to synthesize Ag/$TiO_2$ oxides (2 and 10% w/w) using the sol-gel method, and to characterize their physicochemical properties in terms of their bacterial inactivation action under light, black light and absence of light.

## 2 Material and Methods

### 2.1 Material

Titanium (IV) isopropoxide (≥ 97%, Aldrich®), silver nitrate ($AgNO_3$, Alphatec), nitric acid (Sigma-Aldrich®, ≥ 65%), ethyl alcohol P.A. (Dinâmica) were

used. The water used in the method was Milli-Qplus with an approximate resistivity of 18 MΩcm.

Studies of the antimicrobial action of the catalysts were carried out on the bacteria *Escherichia coli* (NEWP0022) and *Staphylococcus aureus* (NEWP0023).

## 2.2 Sol-gel synthesis

To obtain the mixed oxides synthesized by the sol-gel route, there was an adaptation of the methodology (Castro et al., 2020), where the $TiO_2$ oxide synthesized via sol-gel, called T/SG, was prepared using a molar ratio of $n_{water}$: $n_{alcoxide}$: $n_{acid}$ = 2.4:1:0.08. Two solutions were prepared: the first (A) consisted of titanium (IV) isopropoxide dissolved in ethanol under a nitrogen atmosphere and the second (B) consisted of $HNO_3$ (65%), double-distilled water, silver nitrate and ethanol. The two solutions were homogenized separately under vigorous magnetic stirring for 10 min. Solution B was then added to solution A using a funnel for 1 min under a nitrogen atmosphere. A clear, firm gel formed in approximately 15 seconds. This gel was aged overnight and then washed with a mixture of water and acetone (1:1) in order to remove residues of the reagents and by-products. The gel was washed three times a day for four days. Finally, the product was dried in a rotary evaporator and then in a vacuum oven at 80 °C for 24 h. The pure oxide obtained was calcined at 400 °C for 5 h, with a heating ramp.

The 2% Ag/$TiO_2$/Sol-gel and 10% Ag/$TiO_2$/Sol-gel catalysts will be represented as: 2AgT/SG and 10AgT/SG and followed practically the same synthesis as $TiO_2$. The differences were the addition of the Ag precursor salt added in proportions of Ag varying between 2% and 10% by mass, 0.9638 g and 5.2477 g respectively, and the absence of the water:acetone washing step. The drying and calcination stage was the same as that used for $TiO_2$. **Figure 1** shows the sol-gel process of the mixed oxides.

**Figure 1** – Sol-gel synthesis

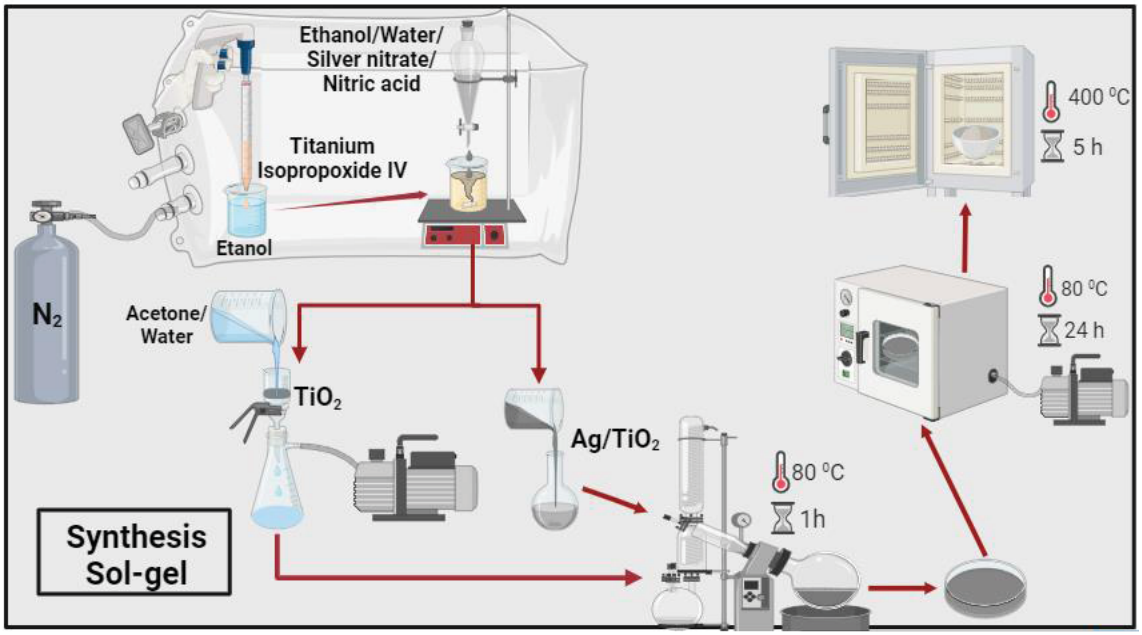


## 2.3 Characterization of the catalysts

The spectra in the infrared region (FT-IR) were analyzed from pellets of the materials dispersed in KBr, covering the 4000 to 500 $cm^{-1}$ range, using a Perkin Elmer FT-IR spectrophotometer, model Frontier. Confirmation of the crystal structure of the catalysts was obtained from X-ray diffraction (XRD) patterns using Rigaku's Miniflex 600, with Cu kα radiation (λ= 0.154 nm). An exploratory differential calorimeter (DSC) (model Q20, TA instruments) was used with a temperature of up to 550 °C and a cooling aid to check for structural changes, crystallization, phase changes and melting. Thermogravimetric analysis (TGA) was carried out on a simultaneous thermal analyzer (PerkinElmer, model STA6000, Akron, Ohio, USA) which involved heating the samples (10 mg) at a rate of 20 ºC $min^{-1}$ between 50 and 900 ºC in an $N_2$ environment (99.997% pure) at a flow rate of 20 mL $min^{-1}$.

## 2.4 Antimicrobial activity test

The antimicrobial activity of the catalysts was investigated through the use of Gram-negative *E. coli* (NEWP0022) and Gram-positive *S. aureus* (NEWP0023) bacteria. All materials were previously prepared and sterilized in an autoclave at 121 °C for 15 min, and the tests were conducted under aseptic conditions (Silva et

al., 2018). We used established protocols, with adaptations (Cordeiro et al., 2004; Tsai et al., 2010). A lyophilized disk of the standard strain was introduced into a vial containing 5 mL of nutrient broth and subsequently transferred to a bacteriological incubator for 48 h at 37 °C. After this period, with the aid of a platinum loop, three transfers were made to a new vial containing 5 mL of nutrient broth and incubated in a bacteriological incubator at 37 °C for 24 h. After this incubation period, the bacterial cultures were serially diluted (1:10 v/v) using saline solution (0.9% NaCl) with the bacterial suspension (solution 1) to $10^5$ CFU $mL^{-1}$. The catalyst solutions T, 2AgT/I and 10AgT/I were previously sonicated for 30 min and a volume of 0.1 mL (equivalent to 0.01 g $mL^{-1}$) of these was added to each well of sterile microplates (six-well microplate). As well, 3.9 mL of saline solution were also added to each well. The start of the reaction was marked by the introduction of 1 mL of the bacterial suspension, prepared in solution 1. Therefore, the final volume in each well corresponded to 5 mL. During the experiment, the microplate was kept under agitation at 350 rpm at 37 °C on a shaking platform to aid in the homogenization of the reaction solution. The microplates containing the final mixture (catalyst, saline solution and bacteria) were then irradiated separately under three different illumination conditions: bright light irradiation (Manplex, 9 W), black light (Luatek, 36 W) and in the absence of light. The distance between the light source and the microplate was 10 cm. Sampling was conducted at 0, 5, 10 and 15 min. At each time point, a sample was collected using a sterile cotton swab and spread on nutrient agar plates, gently over the agar surface in five different directions. Subsequently, the medium was allowed to absorb the inoculum for a period of 15 min. The experiments were conducted in triplicate, and the plates were subsequently incubated in a bacteriological oven at 37 ± 2 °C for 24 h. Control experiments were conducted in the absence of a catalyst. The number of Colony Forming Units (CFU) was counted and subjected to statistical analysis.

### 2.5 Detection of reactive oxygen species (ROS)

We used a protocol with modifications to identify ROS in bacterial samples (Liao et al., 2019). We followed the same experimental procedure described in item 2.4, differing only in the dilution of the bacteria, being $1x10^3$ CFU $mL^{-1}$ in this

one versus $1x10^5$ CFU $mL^{-1}$ in that one. After the reaction times, the collected sample was washed in phosphate-buffered saline (1 $mmol.L^{-1}$) and centrifuged at 3000 rpm for 5 min. Then, the supernatant was discarded and the pellet was incubated for 30 min at 37 ºC in the dark with 1 mL of 2',7'-dichlorofluorescein diacetate ($H_2$DCF-DA) in phosphate-buffered saline. After the time elapsed, the cells were centrifuged at 5000 rpm for 6 min to remove the remaining $H_2$DCF-DA. Then, the cell pellets were suspended in 1 mL of phosphate-buffered saline and mixed with 200 µL of alkaline lysis buffer (1% SDS; 0.2 $mol.L^{-1}$ NaOH) for 10 min at 37 ºC. Finally, the mixture was centrifuged at 5000 rpm for 6 min and the final supernatant product was collected for fluorescence readings (488 nm excitation and 525 nm emission) (Thermo Scientific™ Varioskan™ LUX). The results were expressed as percentage (%) of ROS relative to 0 min (initial time).

### 2.6 Statistical analysis

The test version for academics of GraphPad Prism 9.0 was used to verify the statistical analyses. The Kolmogorov-Smirnov test was used to analyze normality, and the Grubbs test was used to eliminate outliers. Each experiment was carried out in triplicate and the differences between the groups in relation to the research variables were assessed by one-way analysis of variance (ANOVA) - according to the number of variables analyzed in the test. Tukey's post-test was then applied. Oscillations with a p-value $< 0.05$ were considered statistically significant. The results were presented in graphs and shown as mean and standard deviation.

## 3 Results and Discussion

### 3.1 Characterization of the catalysts

The FT-IR spectra of the T/SG, 2AgT/SG and 10AgT/SG catalysts are shown in **Figure 2**. These catalysts showed characteristic Ti bands between 500-740 $cm^{-1}$ which were correlated to the binding of oxygen and titanium (Ti-O-Ti). It can be seen that this band on the T/SG catalyst was narrower and widened on the AgT/SG catalysts, indicating that the Ti-O-Ti stretching vibration had become stronger

(Alsharaeh et al., 2017; Noviagel et al., 2024; Safaei and Taran, 2017). The absorption band for the 2AgT/SG and 10AgT/SG catalysts at 3400-3500 $cm^{-1}$ correlated with the stretching of the free -OH group, which is related to the increase in the number of H bonds between $TiO_2$ and the OH group (Noviagel et al., 2024). In addition, the band at 1610 $cm^{-1}$ refers to C-O stretching (Eleftheriadou et al., 2020), and can also be attributed to the stretching and bending vibration of the OH group (Sathishkumar et al., 2022). There is a weak band for the 10AgT/SG catalyst at 1344 $cm^{-1}$ which indicates the formation of a bond between the $Ag^{+}$ ion and the $TiO_2$ lattice, confirming the deposition of silver on the support (Desiati et al., 2019). Thanks to the addition of Ag to the AgT/SG catalysts, there is a slight shift in the bands around 650-700 $cm^{-1}$, correlated to the asymmetric vibration of Ti-Ag-O (Gogoi et al., 2020). It can be seen that the band intensities of the AgT/SG catalysts are lower than those of the T/SG catalyst, indicating that the Ag particles have bonded to the $TiO_2$ after sol-gel synthesis (Poudel and Kim, 2023).

**Figure 2** - FT-IR spectra of the catalysts

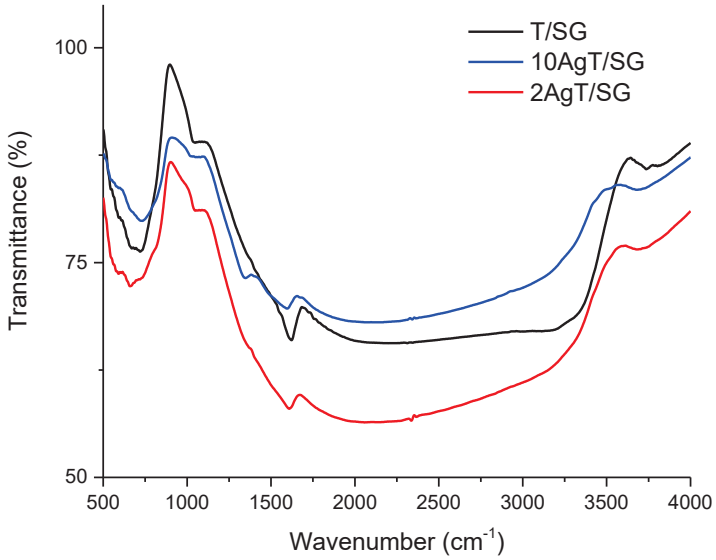


**Figure 3** shows the diffractograms of the T/SG, 2AgT/SG and 10AgT/SG catalysts. The T/SG catalyst has delineated diffraction peaks representing organized crystalline phases, containing the tetragonal anatase phase (JCPDS 84-1286) with the most intense peaks at 25.4, 38, 48.1, 54, 55.3 and 62.7º (Poudel et al., 2022; JCPDS, 2013). The XRD patterns showed no peaks associated with brookite or rutile and no peaks of metallic Ag or Ag oxides (Borrego Pérez et al.,

2023; Gang et al., 2022). It was observed that the addition of Ag did not affect the crystal structure of $TiO_2$, remaining in the anatase phase (Cotolan et al., 2016), so this may be due to the presence of highly dispersed Ag nanoagglomerates in the material (Zhang and Chen, 2009).

**Figure 3** - Catalyst diffractograms

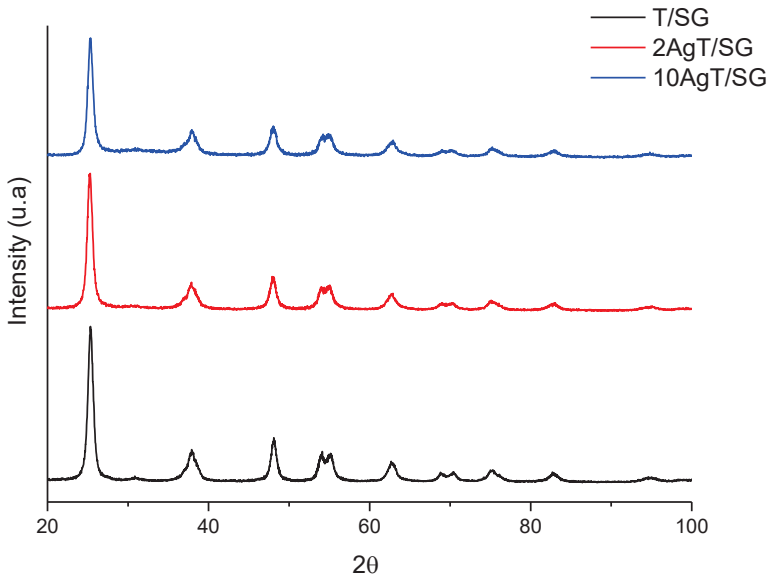


All peaks present in the catalysts are anatase phase

DSC thermal analyses, shown in **Figure 4**, were carried out to investigate the thermal properties of the T/SG, 2AgT/SG and 10AgT/SG catalysts. Smaller endothermic peaks were observed in the 2AgT/SG and 10AgT/SG catalysts (61.2 and 62.5 °C, respectively), indicating a lower melting point compared to the T/SG catalyst (71.6 °C). These endothermic peaks were attributed to the elimination of water adsorbed on the surface of the catalyst particles, and the peak amplitude shows that the dehydration of the materials was rapid. As for the lower melting point of AgT/SG catalysts compared to T/SG, this is because Ag has strong thermal conductivity, due to the free electrons found in its network. In contrast, materials such as $TiO_2$ do not have free electrons, making them non-conductive, so Ag slightly reduces the melting point (García-Serrano et al., 2009; Ramírez-Cedillo et al., 2019).

The first exothermic peak observed in the catalysts occurs at 130 °C (AgT/SG) and 160 °C (T/SG) and can be attributed to the crystallization of amorphous $TiO_2$ into the anatase phase, indicating that the particles of this oxide

crystallized at lower temperatures and completed the crystallization process. There are shifts in the peaks to lower temperatures in the AgT/SG catalysts compared to the T/SG catalyst, which may be associated with Ag doping and the vacuum atmosphere. The second exothermic peak, at around 273 (T/SG), 301 (10AgT/SG) and 307 °C (2AgT/SG), corresponds to the temperature associated with the elimination of organic components, associated with the combustion process. This combustion is not a simple desorption process, but also involves the chemical species decomposition (García-Serrano et al., 2009).

**Figure 4 –** DSC curve of catalysts

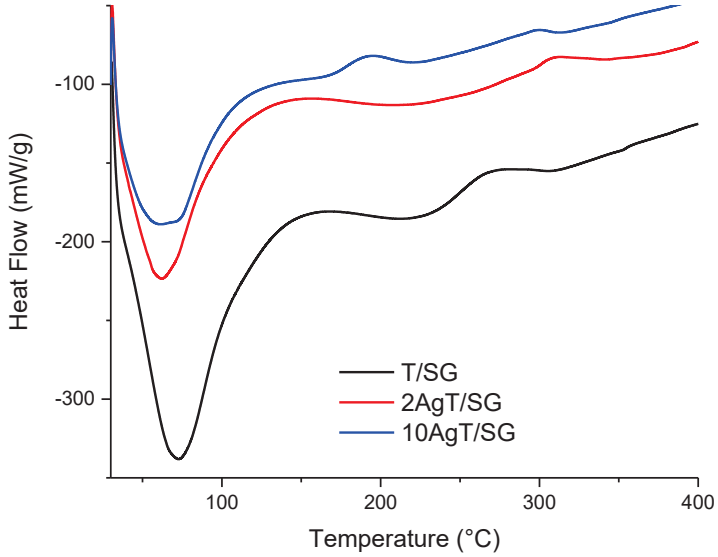


The TGA curves for the T/SG, 2AgT/SG and 10AgT/SG catalysts are shown in **Figure 5**. There is a decrease in mass with temperature for all the catalysts. The initial loss of mass and the endothermic process arround 200 °C can be attributed to the evaporation of water adsorbed on the surface of the material. It should be noted that all the catalysts showed a loss of mass up to 900 °C, probably due to the presence of traces of organic impurities/residues (Chelli et al., 2018; Ren et al., 2022). The 10AgT/SG catalyst had an exothermic reduction near 600-800 °C correlated to the organization of the system that will induce the generation of the anatase structure. This reduction above 600 °C occurred at higher temperatures compared to the T/SG catalyst, because the Ag ion added to the $TiO_2$ structure tends to cause greater destructuring, thus requiring greater energy for the organization of the system (Sullivan and Cole, 1959; Viana et al., 2010).

**Figure 5**- Thermogravimetric analysis of catalysts

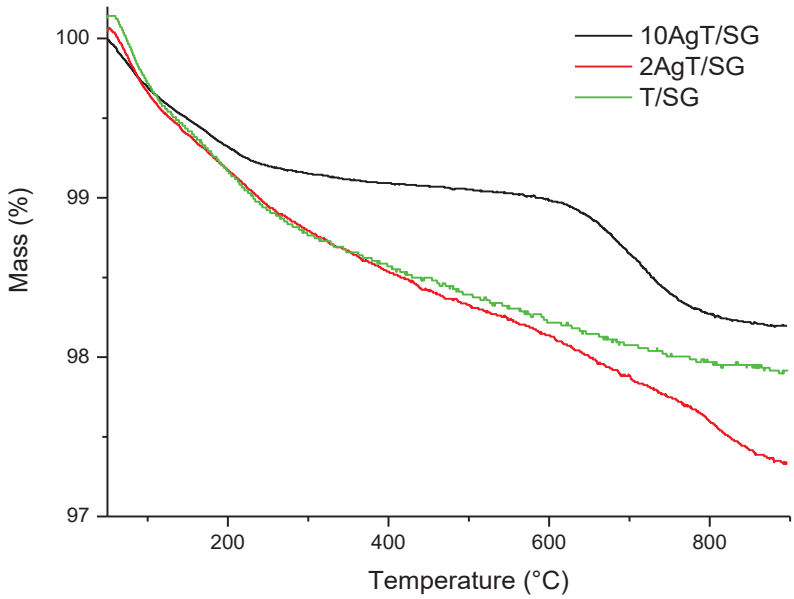


### 3.2 Antimicrobial activity test

**Figure 6** (A-L) and **Figure 7** (A-L) show the effects of visible light sources (called clear light), black light and no light (called dark) for: controls (A, E and I) and the catalysts T/SG (B, F and J), 2AgT/SG (C, G and K) and 10AgT/SG (D, H and L) on the inactivation of *E. coli* and *S. aureus*, respectively.

Under bright light, the 10AgT/SG catalyst (Figures 6D and 7D) showed bactericidal action after 15 min. In the dark test, this catalyst (Figure 6H) had a bactericidal action from the 5 min, indicating that the Ag NPs were responsible for the antimicrobial effect in the dark. The antibacterial efficiency of an Ag-based catalyst depends on the rate of release of Ag ions (Liu et al., 2018). Thus, this bactericidal action can be caused by the Ag NPs released by the 10AgT/SG catalyst, so the amount of this metal in the catalyst influences its antimicrobial action, because when more Ag is added to the $TiO_2$ matrix, the bactericidal action increases, acting by various mechanisms (Ashkarran et al., 2011; Dong et al., 2019). Ag can adhere to the surface of the cell membrane and wall where it accumulates and causes leakage from the intracellular organelles and death (Chakhtouna et al., 2021). In addition, the released Ag can bind to enzymes in the bacterial membranes, thus deregulating their functionality, or penetrate the cell, damaging the DNA (Ashkarran et al., 2011; Dong et al., 2019; Tian et al., 2007).

Subsequently, spaces are created in the bacterial cell, causing the wall to break down and cell death (Zawadzka et al., 2016). Another mechanism is the intracellular penetration of Ag NPs into the bacteria, causing damage to intracellular organelles such as the endoplasmic reticulum and mitochondria, as well as biomolecules such as lipids, DNA and others. This metal can also incite cellular toxicity and oxidative stress due to the generation of ROS, and the final mechanism is the modulation of signal transduction pathways (Tian et al., 2007).

At 10 min (Figures 6I-L and 7L), there was a decline in the number of colonies for the T/SG (Figure 6J), 2AgT/SG (Figures 6K) and 10AgT/SG (Figures 6L and 7L) catalysts. On the other hand, the T/SG (Figure 7J) and 2AgT/SG (Figure 7K) catalysts showed a bactericidal effect against *S. aureus* after 15 min. The catalysts were photoactivated by UV, causing a greater production of radicals: superoxide ($O_2^{-\bullet}$), hydroxyl ($HO^{\bullet}$), hydrogen peroxide ($H_2O_2$), hydroperoxyl ($HO_2^{\bullet}$) and singlet oxygen ($^1O_2$), thus the ROS increase the antibacterial action (Junior, 2008). The 10AgT/I catalyst (Figures 6D, 6H, 6L, 7D and 7L) has a more pronounced photocatalytic effect than the T/SG catalyst against Gram-negative and positive bacteria, due to the synergistic action of Ag and $TiO_2$, thus combining the generation of ROS and the release of Ag (Dahl et al., 2014; Gupta et al., 2013). The bactericidal activity of the AgT/SG catalysts was higher than that of the T/SG catalyst. It was also higher as the Ag content increased, as can be seen in Figure 7K and 7L.

The AgT/SG catalysts had a more pronounced bactericidal action against *E. coli* (10AgT/SG in Figure 6). However, these catalysts showed reduced performance against *S. aureus*, as 2AgT/SG only acted under black light (Figure 7K) and 10AgT/SG had no bactericidal action in the dark. In other words, the different bacteria responded in different ways to the AgT/SG catalysts, thanks to the different complexity and thickness of their cell walls. Therefore, the cell wall constitution of Gram-positive strains is 90% peptidoglycan and the rest is made up of teichoic acid with a denser peptide reticular constitution than Gram-negative strains (Zhang and Chen, 2009; Zhao et al., 2018).

**Figure 6** – Antibacterial activity test (*E. coli*) of T/SG, 2AgT/SG and 10AgT/SG catalysts photoactivated by clear light (A-D), dark (E-H) and black light (I-L).

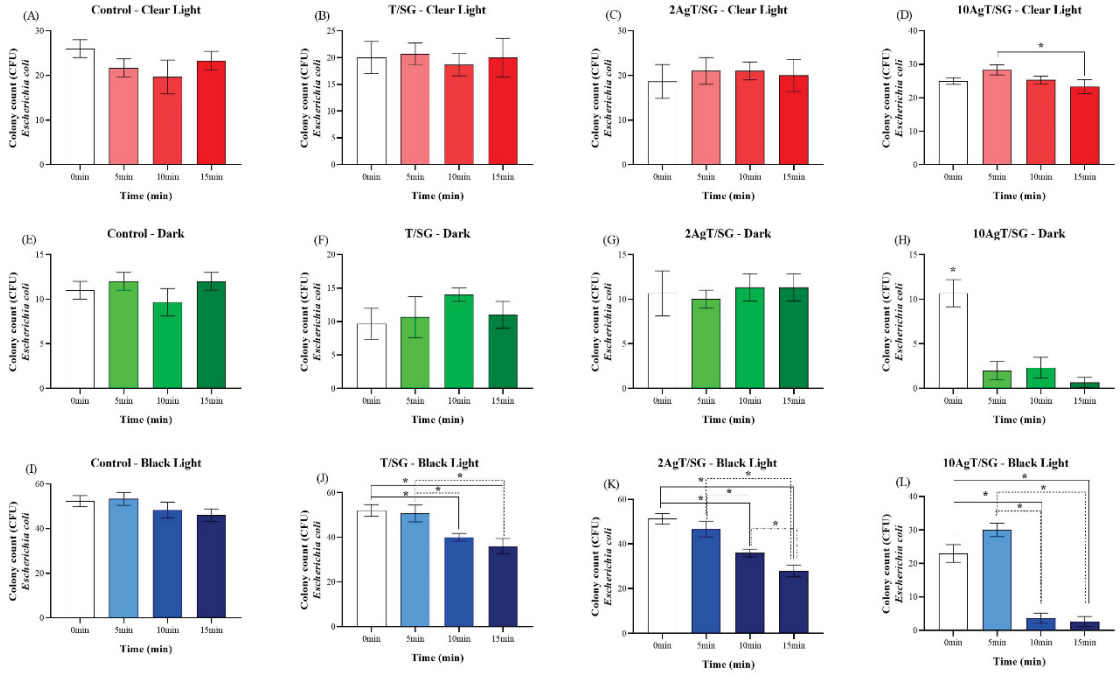


Antibacterial action against *E. coli* of the control (A, E and I) and of the catalysts T/SG (B, F and J), 2AgT/SG (C, G and K) and 10AgT/SG (D, H and L) in the clear light (A-D), dark (E-H) and black light (I-L) tests, according to the time variation 0, 5, 10 and 15 min. Asterisks indicate $p<0.05$ (one-way ANOVA, post-Tukey test).

**Figure 7** – Antibacterial activity test (*S. aureus*) of the catalysts T/SG, 2AgT/SG and 10AgT/SG photoactivated by clear light (A-D), dark (E-H) and black light (I-L).

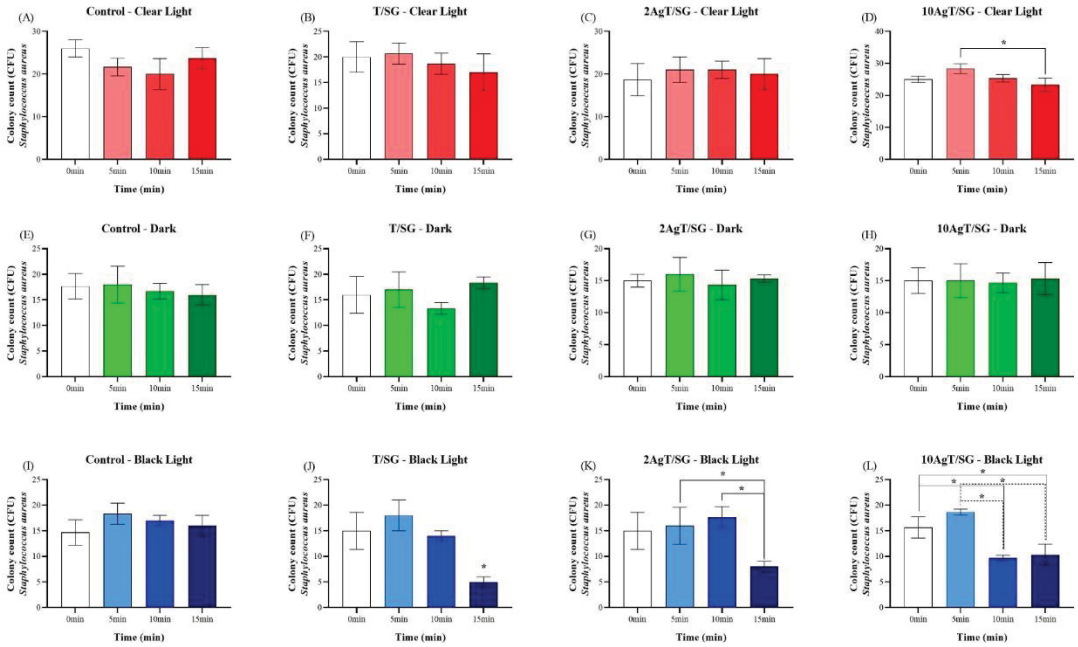


Antibacterial action against *S. aureus* of the control (A, E and I) and the catalysts T/SG (B, F and J), 2AgT/SG (C, G and K) and 10AgT/SG (D, H and L) in the clear light (A-D), dark (E-H) and black light (I-L) tests, according to the time variation 0, 5, 10 and 15 min. Asterisks indicate $p<0.05$ (one-way ANOVA, post-Tukey test).

### 3.3 Detection of reactive oxygen species

**Figure 8** (A-C) and **Figure 9** (A-C) demonstrate the values of intracellular ROS generation of *E. coli* and *S. aureus*, respectively, for the catalysts T/SG (A), 2AgT/SG (B) and 10AgT/SG (C), under black light.

**Figure 8** - Intracellular ROS generation values of *E. coli* from the ROS detection assay by $H_2$DCF-DA for the catalysts T/SG (A), 2AgT/SG (B) and 10AgT/SG (C).

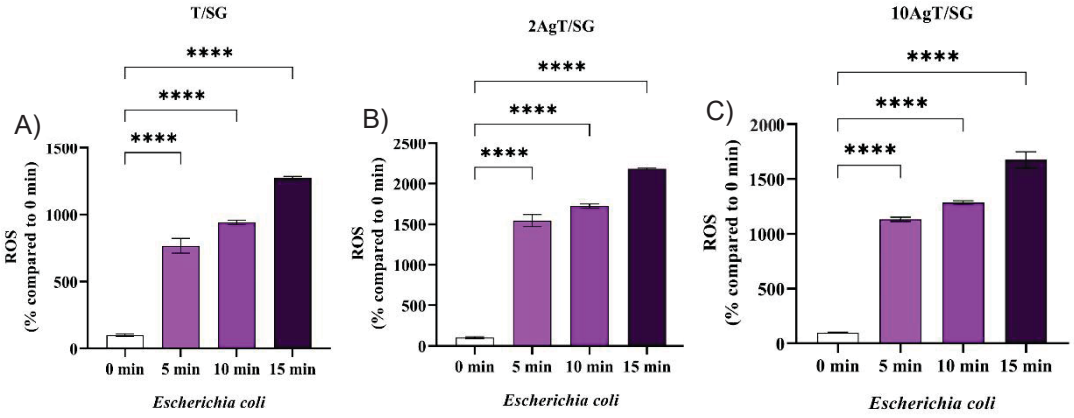


Asterisks indicate * p <0.05; ** p <0.01; *** p< 0.001 e **** p < 0.0001 (One-way ANOVA, with Dunnett's post-hoc test).

**Figura 9** - Intracellular ROS generation values of *S. aureus* from the ROS detection assay by $H_2$DCF-DA for the catalysts T/SG (A), 2AgT/SG (B) and 10AgT/SG (C).

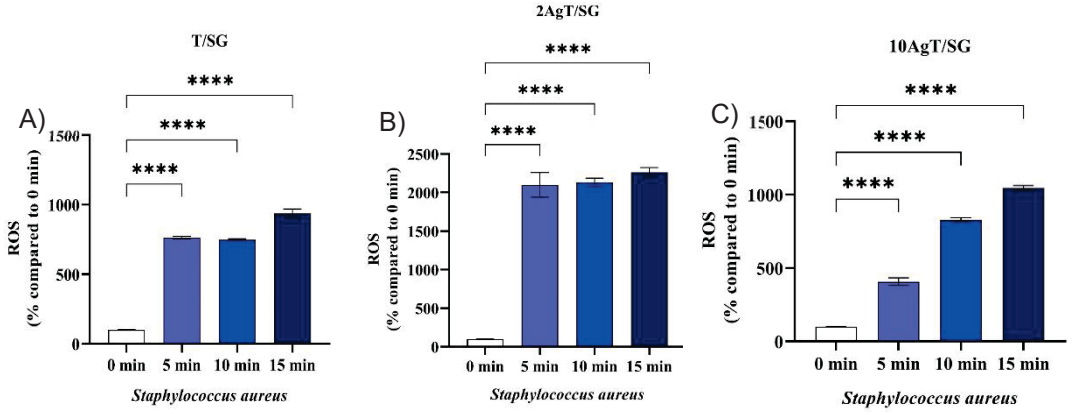


Asterisks indicate * p <0.05; ** p <0.01; *** p< 0.001 e **** p < 0.0001 (One-way ANOVA, with Dunnett's post-hoc test).

An increase in the level of ROS can be seen after 5 min for *E. coli* (Figures 8A - C) and *S. aureus* (Figures 9A - C), corroborating the data presented in Figures 6J-L and 7J-L and confirming that the ROS generated come from the photocatalytic effects. These species accumulate in the bacterial membrane, overloading the bacterial antioxidant defense system and causing membrane damage and death (Yong et al., 2023). The greatest production of ROS was observed for the 2AgT/SG catalyst in the deaths of *E. coli* and *S. aureus* (Figure 8B and 9B). It should also be noted that the number of reactive species for *S. aureus* was higher when

compared to the other strains, thus demonstrating that the diversity of microorganisms, such as the complexity and thickness of the cell wall, interferes with the response of the catalyst (Zhang and Chen, 2009).

It can be seen that the mechanism of bactericidal action of catalysts is dependent on ROS and may be linked to a sequence of reactions. ROS are attracted to the bacterial surface and interact, thus compromising the integrity of the membrane and cell wall, altering permeability and inducing oxidative stress via ROS and free radicals, culminating in the modulation of signal transduction pathways (Zhang et al., 2019). Catalysts are excited by UV (**Figure 10**) generating electron ($e^-$) and gap ($h^+$) pairs found in the conduction band and valence band, respectively. These $e^-/h^+$ pairs react with intramolecular molecules such as water and oxygen ($O_2$), thus generating $^{\bullet}OH$ e $O_2^{-\bullet}$ radicals. The $h^+$ reacts with water, separating it into $OH^-$ and $H^+$, and dissolved $O_2$ molecules change into $O_2^{-\bullet}$. This radical acts with $H^+$ to generate $HO_2^{\bullet}$ radicals, which collide with $e^-$ to produce $HO_2^-$. Finally, these radicals react with $H^+$ ions to produce $H_2O_2$ (Zhou et al., 2015). At the same time, Ag NPs capture $e^-$, transporting them from the conduction band of $TiO_2$ and then to $O_2^{-\bullet}$, generating superoxide radicals. Ag helps in the generation of $^{\bullet}OH$ radicals produced from $H_2O$ with the remaining photoproduced $h^+$ present in the $TiO_2$ valence band. These photoproduced ROS adhere to and penetrate the membrane, thus killing the bacteria (Din et al., 2018).

**Figure 10** – Illustration of the mechanism of action of AgT/SG catalysts and representations of Gram-negative and Gram-positive bacterial membranes.

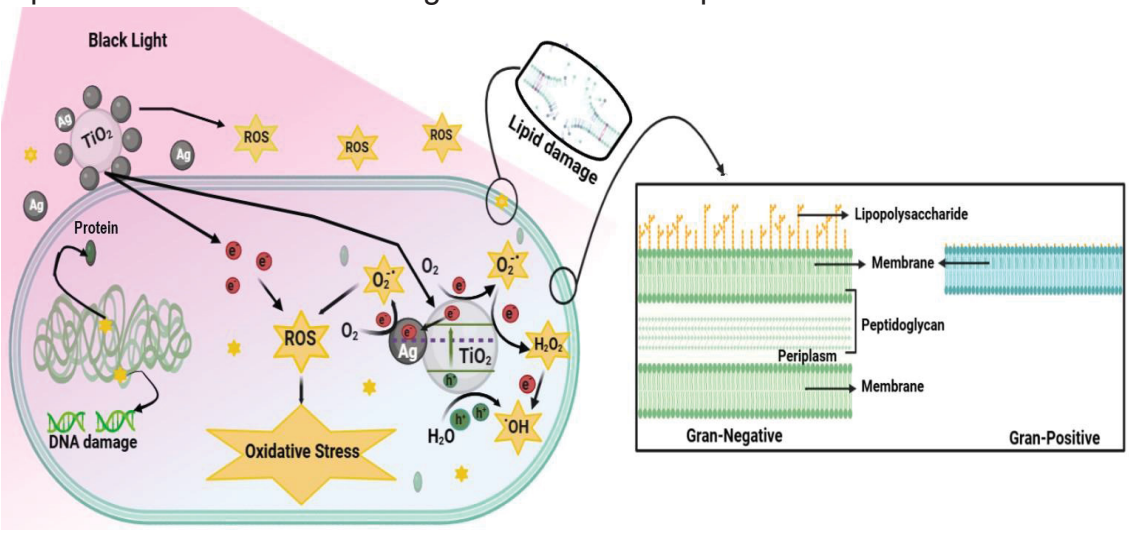


UV light irradiation on the AgT/SG catalyst promotes the excitation of $e^-$, generating $e^-/h^+$ pairs. These pairs migrate to the catalyst surface and react with water and oxygen molecules, forming

hydroxyl radicals ($HO^{\bullet}$), superoxide ($O_2^{-\bullet}$) and hydrogen peroxide ($H_2O_2$) and singlet oxygen ($^1O_2$). Silver (Ag) nanoparticles amplify the production of $O_2^{-\bullet}$ radicals by capturing electrons from $TiO_2$. These highly toxic reactive species penetrate bacterial cells, oxidizing biomolecules such as lipids, proteins and DNA, and triggering an oxidative stress process that culminates in cell death.

## 4 Conclusion

The sol-gel method used to synthesize Ag/$TiO_2$ catalysts was simple and effective. AgT/SG catalysts have crystalline phases with little mass loss during synthesis. The 10AgT/SG catalyst showed the best bactericidal action and high photocatalytic efficiency under UV irradiation, visible light and in the absence of light. The AgT/SG catalysts were more effective than pure $TiO_2$ against Gram-negative and -positive bacteria, due to the synergistic effect of Ag and $TiO_2$. Antibacterial oxides with rapid bactericidal action were produced, thus enabling less expensive and broader applications in antibacterial therapy, with potential use in bacterial disinfection devices and in places that need to control infections.

## References


Ahmed, F., Kanoun, M.B., Awada, C., Jonin, C., Brevet, P.-F., 2021. An Experimental and Theoretical Study on the Effect of Silver Nanoparticles Concentration on the Structural, Morphological, Optical, and Electronic Properties of $TiO_2$ Nanocrystals. Crystals 11, 1488. https://doi.org/10.3390/cryst11121488

Al Amin, S.M., Kowser, M.A., 2024. Influence of Ag doping on structural, morphological, and optical characteristics of sol-gel spin-coated $TiO_2$ thin films. Heliyon 10, e37558. https://doi.org/10.1016/j.heliyon.2024.e37558

Ali, T., Ahmed, A., Alam, U., Uddin, I., Tripathi, P., Muneer, M., 2018. Enhanced photocatalytic and antibacterial activities of Ag-doped $TiO_2$ nanoparticles under visible light. Mater. Chem. Phys. 212, 325–335. https://doi.org/10.1016/j.matchemphys.2018.03.052

Alsharaeh, E.H., Bora, T., Soliman, A., Ahmed, F., Bharath, G., Ghoniem, M.G., Abu-Salah, K.M., Dutta, J., 2017. Sol-Gel-Assisted Microwave-Derived Synthesis of Anatase Ag/$TiO_2$/GO Nanohybrids toward Efficient Visible Light Phenol Degradation. Catalysts 7, 133. https://doi.org/10.3390/catal7050133

Ashkarran, A.A., Aghigh, S.M., Kavianipour, M., Farahani, N.J., 2011. Visible light photo-and bioactivity of Ag/$TiO_2$ nanocomposite with various silver contents. Curr. Appl. Phys. 11, 1048–1055. https://doi.org/10.1016/J.CAP.2011.01.042

Borrego Pérez, J.A., Morales, E.R., Paraguay Delgado, F., Meza Avendaño, C.A., Alonso Guzman, E.M., Mathews, N.R., 2023. Ag nanoparticle dispersed $TiO_2$ thin films by single step sol gel process: Evaluation of the physical properties and photocatalytic degradation. Vacuum 215, 112276. https://doi.org/10.1016/j.vacuum.2023.112276

Castro, L.E.N. de, Meurer, E.C., Alves, H.J., Santos, M.A.R. dos, Vasques, E. de C., Colpini, L.M.S., 2020. Photocatalytic Degradation of Textile dye Orange-

122 Via Electrospray Mass Spectrometry. Brazilian Arch. Biol. Technol. 63. https://doi.org/10.1590/1678-4324-2020180573
Chakhtouna, H., Benzeid, H., Zari, N., Qaiss, A. el kacem, Bouhfid, R., 2021. Recent progress on Ag/$TiO_2$ photocatalysts: photocatalytic and bactericidal behaviors. Environ. Sci. Pollut. Res. 28, 44638–44666. https://doi.org/10.1007/s11356-021-14996-y
Chelli, V.R., Chakraborty, S., Golder, A.K., 2018. Ag-doping on $TiO_2$ using plant-based glycosidic compounds for high photonic efficiency degradative oxidation under visible light. J. Mol. Liq. 271, 380–388. https://doi.org/10.1016/j.molliq.2018.08.140
Cordeiro, A.C. de S., Leite, S.G.F., Dezotti, M., 2004. Inativação por oxidação fotocatalítica de *Escherichia coli* e *Pseudomonas sp*. Quim. Nova 27, 689–694. https://doi.org/10.1590/S0100-40422004000500002
Cotolan, N., Rak, M., Bele, M., Cör, A., Muresan, L.M., Milošev, I., 2016. Sol-gel synthesis, characterization and properties of $TiO_2$ and Ag-$TiO_2$ coatings on titanium substrate. Surf. Coatings Technol. 307, 790–799. https://doi.org/10.1016/j.surfcoat.2016.09.082
Dahl, M., Liu, Y., Yin, Y., 2014. Composite Titanium Dioxide Nanomaterials. Chem. Rev. 114, 9853–9889. https://doi.org/10.1021/cr400634p
Deshmukh, S.P., Mullani, S.B., Koli, V.B., Patil, S.M., Kasabe, P.J., Dandge, P.B., Pawar, S.A., Delekar, S.D., 2018. Ag Nanoparticles Connected to the Surface of $TiO_2$ Electrostatically for Antibacterial Photoinactivation Studies. Photochem. Photobiol. 94, 1249–1262. https://doi.org/10.1111/php.12983
Desiati, R.D., Taspika, M., Sugiarti, E., 2019. Effect of calcination temperature on the antibacterial activity of $TiO_2$/Ag nanocomposite. Mater. Res. Express 6, 095059. https://doi.org/10.1088/2053-1591/ab155c
Din, M.I., Khalid, R., Hussain, Z., 2018. Minireview: Silver-Doped Titanium Dioxide and Silver-Doped Zinc Oxide Photocatalysts. Anal. Lett. 51, 892–907. https://doi.org/10.1080/00032719.2017.1363770
Dinh, C.-T., Nguyen, T.-D., Kleitz, F., Do, T.-O., 2011. A New Route to Size and Population Control of Silver Clusters on Colloidal $TiO_2$ Nanocrystals. ACS Appl. Mater. Interfaces 3, 2228–2234. https://doi.org/10.1021/am200480b
Dong, P., Yang, F., Cheng, X., Huang, Z., Nie, X., Xiao, Y., Zhang, X., 2019. Plasmon enhanced photocatalytic and antimicrobial activities of Ag-$TiO_2$ nanocomposites under visible light irradiation prepared by DBD cold plasma treatment. Mater. Sci. Eng. C 96, 197–204. https://doi.org/10.1016/j.msec.2018.11.005
Duong, H.A., Phung, T.V., Nguyen, T.N., Phan Thi, L.-A., Pham, H.V., 2021. Occurrence, Distribution, and Ecological Risk Assessment of Antibiotics in Selected Urban Lakes of Hanoi, Vietnam. J. Anal. Methods Chem. 2021, 1–13. https://doi.org/10.1155/2021/6631797
Eleftheriadou, M. N., Ofrydopoulou, A., Papageorgiou, M., Lambropoulou, D., 2020. Development of Novel Polymer Supported Nanocomposite GO/$TiO_2$ Films, Based on poly(L-lactic acid) for Photocatalytic Applications. Appl. Sci. 10, 2368. https://doi.org/10.3390/app10072368
Etacheri, V., Di Valentin, C., Schneider, J., Bahnemann, D., Pillai, S.C., 2015. Visible-light activation of $TiO_2$ photocatalysts: Advances in theory and experiments. J. Photochem. Photobiol. C Photochem. Rev. 25, 1–29. https://doi.org/10.1016/j.jphotochemrev.2015.08.003
Ferdous, Z., Nemmar, A., 2020. Health Impact of Silver Nanoparticles: A Review

of the Biodistribution and Toxicity Following Various Routes of Exposure. Int. J. Mol. Sci. 21, 2375. https://doi.org/10.3390/ijms21072375
Frickmann, H., Hahn, A., Berlec, S., Ulrich, J., Jansson, M., Schwarz, N.G., Warnke, P., Podbielski, A., 2019. On the etiological relevance of *Escherichia coli* and *Staphylococcus aureus* in superficial and deep infections – a hypothesis-forming, retrospective assessment. Eur. J. Microbiol. Immunol. 9, 124–130. https://doi.org/10.1556/1886.2019.00021
Gang, R., Xia, Y., Xu, L., Zhang, L., Ju, S., Wang, Z., Koppala, S., 2022. Size controlled Ag decorated $TiO_2$ plasmonic photocatalysts for tetracycline degradation under visible light. Surfaces and Interfaces 31, 102018. https://doi.org/10.1016/j.surfin.2022.102018
García-Serrano, J., Gómez-Hernández, E., Ocampo-Fernández, M., Pal, U., 2009. Effect of Ag doping on the crystallization and phase transition of $TiO_2$ nanoparticles. Curr. Appl. Phys. 9, 1097–1105. https://doi.org/10.1016/j.cap.2008.12.008
Gogoi, D., Namdeo, A., Golder, A.K., Peela, N.R., 2020. Ag-doped $TiO_2$ photocatalysts with effective charge transfer for highly efficient hydrogen production through water splitting. Int. J. Hydrogen Energy 45, 2729–2744. https://doi.org/10.1016/J.IJHYDENE.2019.11.127
Golim, O.P., Desiati, R.D., Muslimin, A.N., Sugiarti, E., 2019. Morphological evolution of sol-gel synthesized Ag-$TiO_2$ nanocomposite. J. Phys. Conf. Ser. 1191, 012049. https://doi.org/10.1088/1742-6596/1191/1/012049
Graham, N., 1999. Guidelines for Drinking-Water Quality, 2nd edition, Addendum to Volume 1 – Recommendations, World Health Organisation, Geneva, 1998, 36 pages. Urban Water 1, 183. https://doi.org/10.1016/S1462-0758(00)00006-6
Gupta, K., Singh, R.P., Pandey, Ashutosh, Pandey, Anjana, 2013. Photocatalytic antibacterial performance of $TiO_2$ and Ag-doped $TiO_2$ against *S. aureus* . *P. aeruginosa* and *E. coli*. Beilstein J. Nanotechnol. 4, 345–351. https://doi.org/10.3762/bjnano.4.40
Halin, D.S.C., Mahmed, N., Mohd Salleh, M.A.A., Mohd Sakeri, A.N., Abdul Razak, K., 2018. Synthesis and Characterization of Ag/$TiO_2$; Thin Film via Sol-Gel Method. Solid State Phenom. 273, 140–145. https://doi.org/10.4028/www.scientific.net/SSP.273.140
JCPDS, 2013. JCPDS—International Center for Diffraction Data, PCPDFWIN. ed.
Junior, O.M., 2008. Inactivation of bacteria in the gas phase by heterogeneous photocatalysis: effect of metal addition. Paulista State University, Araraquara, SP.
Khanna, P.K., Singh, N., Kulkarni, D., Deshmukh, S., Charan, S., Adhyapak, P.V., 2007. Water based simple synthesis of re-dispersible silver nano-particles. Mater. Lett. 61, 3366–3370. https://doi.org/10.1016/j.matlet.2006.11.064
Lai, Y., Zhuang, H., Xie, K., Gong, D., Tang, Y., Sun, L., Lin, C., Chen, Z., 2010. Fabrication of uniform Ag/$TiO_2$ nanotube array structures with enhanced photoelectrochemical performance. New J. Chem. 34, 1335. https://doi.org/10.1039/b9nj00780f
Li, J., Xu, J., Dai, W.-L., Fan, K., 2009. Dependence of Ag Deposition Methods on the Photocatalytic Activity and Surface State of $TiO_2$ with Twistlike Helix Structure. J. Phys. Chem. C 113, 8343–8349. https://doi.org/10.1021/jp8114012
Li, M., Noriega-Trevino, M.E., Nino-Martinez, N., Marambio-Jones, C., Wang, J.,

Damoiseaux, R., Ruiz, F., Hoek, E.M. V., 2011. Synergistic Bactericidal Activity of Ag-$TiO_2$ Nanoparticles in Both Light and Dark Conditions. Environ. Sci. Technol. 45, 8989–8995. https://doi.org/10.1021/es201675m

Liao, S., Zhang, Y., Pan, X., Zhu, F., Jiang, C., Liu, Q., Cheng, Z., Dai, G., Wu, G., Wang, L., Chen, L., 2019. Antibacterial activity and mechanism of silver nanoparticles against multidrug-resistant *Pseudomonas aeruginosa*. Int. J. Nanomedicine Volume 14, 1469–1487. https://doi.org/10.2147/IJN.S191340

Liu, C., Geng, L., Yu, Y., Zhang, Y., Zhao, B., Zhao, Q., 2018. Mechanisms of the enhanced antibacterial effect of Ag-$TiO_2$ coatings. Biofouling 34, 190–199. https://doi.org/10.1080/08927014.2017.1423287

Noviagel, I., Heryanto, H., Putri, S.E., Rauf, I., Tahir, D., 2024. Tapioca-starch-based bionanocomposites with fructose and titanium dioxide for food packaging and fertilization applications. Int. J. Biol. Macromol. 273, 132803. https://doi.org/10.1016/j.ijbiomac.2024.132803

Patil, S.M, P. Deshmukh, S., G. Dhodamani, A., V. More, K., D. Delekar, S., 2017. Different Strategies for Modification of Titanium Dioxide as Heterogeneous Cata lyst in Chemical Transformations. Curr. Org. Chem. 21, 821–833. https://doi.org/10.2174/1385272820666161013151816

Patil, S.M., Dhodamani, A.G., Vanalakar, S.A., Deshmukh, S.P., Delekar, S.D., 2018. Multi-applicative tetragonal $TiO_2$/$SnO_2$ nanocomposites for photocatalysis and gas sensing. J. Phys. Chem. Solids 115, 127–136. https://doi.org/10.1016/j.jpcs.2017.12.020

Poolman, J.T., Anderson, A.S., 2018. *Escherichia coli* and *Staphylococcus aureus*: leading bacterial pathogens of healthcare associated infections and bacteremia in older-age populations. Expert Rev. Vaccines 17, 607–618. https://doi.org/10.1080/14760584.2018.1488590

Poudel, M., Chandra Lohani, P., Kim, A.A., 2022. Synthesis of silver nanoparticles decorated tungsten oxide nanorods as high-performance supercapacitor electrode. Chem. Phys. Lett. 804, 139884. https://doi.org/10.1016/J.CPLETT.2022.139884

Poudel, M.B., Kim, A.A., 2023. Silver nanoparticles decorated $TiO_2$ nanoflakes for antibacterial properties. Inorg. Chem. Commun. 152, 110675. https://doi.org/10.1016/J.INOCHE.2023.110675

Prakash, J., Kaith, B.S., Sun, S., Bellucci, S., Swart, H.C., 2019. Recent Progress on Novel Ag–$TiO_2$ Nanocomposites for Antibacterial Applications. pp. 121–143. https://doi.org/10.1007/978-3-030-16534-5_7

Ramírez-Cedillo, E., Ortega-Lara, W., Rocha-Pizaña, M.R., Gutierrez-Uribe, J.A., Elías-Zúñiga, A., Rodríguez, C.A., 2019. Electrospun Polycaprolactone Fibrous Membranes Containing Ag, $TiO_2$ and $Na_2Ti_6O_{13}$ Particles for Potential Use in Bone Regeneration. Membranes (Basel). 9, 12. https://doi.org/10.3390/membranes9010012

Ren, Y., Xing, S., Wang, J., Liang, Y., Zhao, D., Wang, H., Wang, N., Jiang, W., Wu, S., Liu, S., Liu, C., Ding, W., Zhang, Z., Pang, J., Dong, C., 2022. Weak-light-driven Ag–$TiO_2$ photocatalyst and bactericide prepared by coprecipitation with effective Ag doping and deposition. Opt. Mater. (Amst). 124, 111993. https://doi.org/10.1016/j.optmat.2022.111993

Roy, A., Bulut, O., Some, S., Mandal, A.K., Yilmaz, M.D., 2019. Green synthesis of silver nanoparticles: biomolecule-nanoparticle organizations targeting antimicrobial activity. RSC Adv. 9, 2673–2702. https://doi.org/10.1039/C8RA08982E

Safaei, M., Taran, M., 2017. Optimal conditions for producing bactericidal sodium hyaluronate-$TiO_2$ bionanocomposite and its characterization. Int. J. Biol. Macromol. 104, 449–456. https://doi.org/10.1016/J.IJBIOMAC.2017.06.016

Sathishkumar, K., Sowmiya, K., Arul Pragasan, L., Rajagopal, R., Sathya, R., Ragupathy, S., Krishnakumar, M., Minnam Reddy, V.R., 2022. Enhanced photocatalytic degradation of organic pollutants by Ag–$TiO_2$ loaded cassava stem activated carbon under sunlight irradiation. Chemosphere 302, 134844. https://doi.org/10.1016/j.chemosphere.2022.134844

Serwecińska, L., 2020. Antimicrobials and Antibiotic-Resistant Bacteria: A Risk to the Environment and to Public Health. Water 12, 3313. https://doi.org/10.3390/w12123313

Silva, N., Junqueira, V.C.A.., Silveira, N.F.A., Taniwaki, M.H., Gomes, R.A.R., Okazaki, M.M., 2018. Manual de métodos de análise microbiológica de alimentos e água., 5ª ed. ed. Blucher, São Paulo.

Sullivan, W.F., Cole, S.S., 1959. Thermal Chemistry of Colloidal Titanium Dioxide. J. Am. Ceram. Soc. 42, 127–133. https://doi.org/10.1111/j.1151-2916.1959.tb14079.x

Tian, J., Wong, K.K.Y., Ho, C., Lok, C., Yu, W., Che, C., Chiu, J., Tam, P.K.H., 2007. Topical Delivery of Silver Nanoparticles Promotes Wound Healing. ChemMedChem 2, 129–136. https://doi.org/10.1002/cmdc.200600171

Tsai, T., Chang, H., Chang, K., Liu, Y., Tseng, C., 2010. A comparative study of the bactericidal effect of photocatalytic oxidation by $TiO_2$ on antibiotic-resistant and antibiotic-sensitive bacteria. J. Chem. Technol. Biotechnol. 85, 1642–1653. https://doi.org/10.1002/jctb.2476

Uboncholakate, K., Sikong, L., Saito, F., 2012. Photocatalytic disinfection of P.aeruginosa bacterial Ag-doped $TiO_2$ film. Procedia Eng. 32, 656–662. https://doi.org/10.1016/j.proeng.2012.01.1323

Viana, M.M., Soares, V.F., Mohallem, N.D.S., 2010. Synthesis and characterization of $TiO_2$ nanoparticles. Ceram. Int. 36, 2047–2053. https://doi.org/10.1016/j.ceramint.2010.04.006

Vrček, I.V., Žuntar, I., Petlevski, R., Pavičić, I., Dutour Sikirić, M., Ćurlin, M., Goessler, W., 2016. Comparison of *in vitro* toxicity of silver ions and silver nanoparticles on human hepatoma cells. Environ. Toxicol. 31, 679–692. https://doi.org/10.1002/tox.22081

World Health Organization, 2001. The World Health Report 2001: Mental health: new understanding, new hope.

World Health Organization (WHO), 2022. Global Antimicrobial Resistance and Use Surveillance System (GLASS) report 2022 .

Wu, X., Yin, S., Dong, Q., Liu, B., Wang, Y., Sekino, T., Lee, S.W., Sato, T., 2013. UV, visible and near-infrared lights induced $NO_x$ destruction activity of (Yb,Er)-$NaYF_4$/C-$TiO_2$ composite. Sci. Rep. 3, 2918. https://doi.org/10.1038/srep02918

Yong, S.-S., Lee, J.-I., Kang, D.-H., 2023. $TiO_2$-based photocatalyst Generated Reactive Oxygen Species cause cell membrane disruption of Staphylococcus aureus and *Escherichia coli* O157:H7. Food Microbiol. 109, 104119. https://doi.org/10.1016/j.fm.2022.104119

Zarzzeka, C., Goldoni, J., Marafon, F., Sganzerla, W.G., Forster-Carneiro, T., Bagatini, M.D., Colpini, L.M.S., 2023. Use of titanium dioxide nanoparticles for cancertreatment: A comprehensive review and bibliometric analysis. Biocatal. Agric. Biotechnol. 50, 102710. https://doi.org/10.1016/j.bcab.2023.102710

Zawadzka, K., Kisielewska, A., Piwoński, I., Kądzioła, K., Felczak, A., Różalska, S., Wrońska, N., Lisowska, K., 2016. Mechanisms of antibacterial activity and stability of silver nanoparticles grown on magnetron sputtered $TiO_2$ coatings. Bull. Mater. Sci. 39, 57–68. https://doi.org/10.1007/s12034-015-1137-z

Zhang, H., Chen, G., 2009. Potent Antibacterial Activities of $Ag/TiO_2$ Nanocomposite Powders Synthesized by a One-Pot Sol−Gel Method. Environ. Sci. Technol. 43, 2905–2910. https://doi.org/10.1021/es803450f

Zhang, S., Liang, X., Gadd, G.M., Zhao, Q., 2019. Advanced titanium dioxide-polytetrafluorethylene ($TiO_2$-PTFE) nanocomposite coatings on stainless steel surfaces with antibacterial and anti-corrosion properties. Appl. Surf. Sci. 490, 231–241. https://doi.org/10.1016/J.APSUSC.2019.06.070

Zhao, Q., Wang, M., Yang, H., Shi, D., Wang, Y., 2018. Preparation, characterization and the antimicrobial properties of metal ion-doped $TiO_2$ nano-powders. Ceram. Int. 44, 5145–5154. https://doi.org/10.1016/j.ceramint.2017.12.117

Zhou, N., López-Puente, V., Wang, Q., Polavarapu, L., Pastoriza-Santos, I., Xu, Q.-H., 2015. Plasmon-enhanced light harvesting: applications in enhanced photocatalysis, photodynamic therapy and photovoltaics. RSC Adv. 5, 29076–29097. https://doi.org/10.1039/C5RA01819F

# CHAPTER V

## Green synthesis of $Ag/TiO_2$ nanoparticles: properties and antibacterial potential for environmental applications


### ABSTRACT

The spread of bacteria resistant to multiple drugs has required the development of new strategies for treating infections. Light-activated materials are emerging as a promising alternative, as they can inactivate bacteria by generating reactive oxygen species, without inducing resistance. Based on this search for new materials, silver (Ag) catalysts (2% and 10%) supported on titanium dioxide ($TiO_2$) were synthesized via modified sol-gel synthesis using tapioca as a gelling agent. The $Ag/TiO_2$ catalysts (2AgT/V and 10AgT/V) characterized by spectra in the infrared region showed characteristic titanium bands, asymmetric Ti-Ag-O vibration and $Ag\text{-}TiO_2$ bonding, confirming the deposition of silver on the support. X-ray diffraction identified delineated peaks characteristic of metallic Ag and anatase for the AgT/V catalysts, representing organized crystalline phases. White light (9 W) did not induce photoactivation in any of the catalysts tested, as the antibacterial activity observed for the 10AgT/V catalyst under dark conditions against *Escherichia coli* suggests an antimicrobial effect intrinsic to Ag. Photoactivation of the AgT/V catalysts under black light resulted in significant bacterial inactivation. The production of reactive oxygen species, proven in the detection test, induced by ultraviolet radiation and together with the intrinsic antimicrobial action of Ag, explains the high efficiency of these catalysts. These results demonstrate the potential of AgT/V catalysts for the development of antimicrobial coatings for surfaces, contributing to the prevention and control of infections in various environments.



Keywords: Tapioca, Bacteria, Photoactivation, ROS.



Manuscript elaborated and formatted according to the guidelines of scientific publication, submitted to the journal Archives of Microbiology. Available at: <https://link.springer.com/journal/283>

## 1 Introdution

Photocatalysis is an oxidation technique with potential in the degradation of organic pollutants, water treatment and the inactivation of microorganisms, and is environmentally friendly and safe. It occurs when a semiconductor, such as titanium dioxide ($TiO_2$), is illuminated by a photon causing the excitation of electrons ($e^-$) belonging to the valence band, which move to the conduction band where they couple with gaps ($h^+$), forming electron-lacuna pairs ($e^-/h^+$). Through redox processes, $e^-$ and $h^+$ generate powerful reactive oxygen species (ROS) on the surface of the semiconductor, which subsequently degrade impurities into carbon dioxide and water, and can also eliminate bacteria (Pathak et al. 2019; Ahmad et al. 2020). Examples of pathogens include *Staphylococcus aureus*, a Gram-positive bacterium, and *Escherichia coli*, a Gram-negative pathogen. These bacteria are transmitted through food, water and air (Hlavsa et al. 2018), survive on various surfaces for long periods (Pérez-Rodríguez et al. 2013; Nag et al. 2021).

$TiO_2$ is a semiconductor that stands out in water purification systems, sterilization and self-cleaning coatings, thanks to its photoelectrochemical, photoinduced, superhydrophilic characteristics and does not produce harmful by-products (Ochiai and Fujishima 2012; Zacarías et al. 2015). However, this oxide has some limitations, such as the wide band energy range, the wavelength region restricted to the ultraviolet, the low quantum efficiency and the fast recombination rate of the $e^-/h^+$ pairs (Chandra et al. 2021; Rajaram et al. 2023). Doping with a transition metal, such as Ag, improves the aforementioned limitations of $TiO_2$, as the metal acts as an e- capture trap, alters the absorption of visible light, optimizes plasmon resonance and increases the photocatalytic action (Rabhi et al. 2019; Rajaram et al. 2023). In addition, the antimicrobial characteristics of $TiO_2$ are improved with Ag doping, thanks to the high surface-to-volume ratio, wide therapeutic range, greater stability and remarkable antibacterial activities (Poudel et al. 2022; Yin et al. 2023).

The antibacterial efficiency of $Ag/TiO_2$ is high, because during the exposure time both $TiO_2$ and $Ag^+$ ions are released, resulting in the interruption of the metabolic activity of the bacterial cell membrane. $Ag^+$ ions facilitate binding affinity to the surfaces of bacterial membranes, which are negatively charged (Padmavathi et al. 2022; Poudel and Kim 2023). Furthermore, Ag nanoparticles on the surface

of cells trigger structural rearrangement of the membrane, thus favoring the entry of ROS into the bacteria, causing DNA damage. Nanomaterials containing Ag can act as multifunctional agents, exerting antibacterial and photodegradation properties, as is the case with $Ag/TiO_2$. They can act on more than one problem, such as organic pollutants and pathogens, making the use of these catalysts more efficient and promising (Saleem et al. 2024).

The sol-gel method has aroused interest due to its simplicity, reproducibility and mild conditions (Ong et al. 2018). To improve this method, a variety of complexing agents have been used to reduce production costs (Gomes et al. 2018). For example, low-cost commercial starch, such as tapioca, is used in the synthesis of particles via the modified sol-gel route, which represents a breakthrough in the synthesis of semiconductors and is also considered green synthesis. This technique is less expensive, generates environmentally sustainable by-products and reduces the toxicity of the synthesized material. It also uses microorganisms, vitamins, enzymes, amino acids, plant extracts or plants during synthesis (Parveen et al. 2016; Gheisari et al. 2024).

Among plants, Manihot esculenta or cassava contains a high carbohydrate content, around 38%, making it a valuable resource in green synthesis (USDA 2019). It also has secondary metabolites, including antioxidant compounds such as terpenes and beta-carotene, as well as other biomolecules, ensuring particle stability and minimizing agglomeration (Rengga et al. 2017; Zakiyyah et al. 2024). Tapioca, made from cassava starch, is a natural polymer that is abundant in nature, renewable, biodegradable and easily stored. It has a uniform constitution with a low-order crystalline structure, which contains an incomplete bond between two glucose molecules, which provides affinity with metal ions (Almeida et al. 2020; Primo et al. 2022). The use of tapioca as a chelating agent in the synthesis of oxides has enormous potential, as it makes production more accessible, simple, economical, cheap and uses low temperatures, as well as increasing the flexibility and strength of composite materials (Khorrami et al. 2015; Tian et al. 2016).

This study aims to synthesize mixed $Ag/TiO_2$ oxides (2 and 10% w/w% Ag) using tapioca in the modified sol-gel process. As well as evaluating their physicochemical characterizations and their antibacterial activity, under light, black light and absence of light.

## 2 Material and Methods

### 2.1 Material

Titanium dioxide ($TiO_2$, Êxodo Científica) and silver nitrate ($AgNO_3$, Alphatec) were used, both analytical grade and without any additional purification. The water used in the synthesis was of Milli-Qplus quality with an approximate resistivity of 18 MΩcm.

The antimicrobial activity of the catalysts was studied using the bacteria *Escherichia coli* (NEWP0022) and *Staphylococcus aureus* (NEWP0023).

### 2.2 Modified sol-gel synthesis/Green synthesis

To obtain mixed oxides synthesized by the modified sol-gel route, known as green synthesis and using tapioca as a gelling agent, adaptations were made to the methodologies (Ferreira et al. 2016; Almeida et al. 2020). To use $TiO_2$ as a support in the preparation of mixed oxides, it was dried in an oven for 21 h at 120 $^oC$. 5 g of tapioca was weighed and mixed with 150 mL of water (solution A) and kept stirring. A previously prepared solution of $TiO_2$ and $AgNO_3$ (solution B) in 50 mL of water was slowly added to this solution A. The mixture was then heated at 80 $^oC$ for 1 hour to form a viscous, homogeneous solution. The final solution was placed in an oven for 24 h at 100 $^oC$ and then calcined, with a heating ramp, at 400 $^oC$ for 5 h. In order to study the effect of Ag concentration on the properties of the materials, the mixed oxides described were obtained containing proportions of Ag varying between 2% and 10% by mass, 0.9638 g and 5.2477 g, respectively. The $TiO_2$ catalysts, 2% Ag/$TiO_2$/Green synthesis and 10% Ag/$TiO_2$/Green synthesis are represented as: 2AgT/V and 10AgT/V. **Figure 1** shows the modified sol-gel/green synthesis process of the mixed oxides.

**Figure 1** – Modified Sol-Gel Synthesis/Green Synthesis of Mixed Oxides.

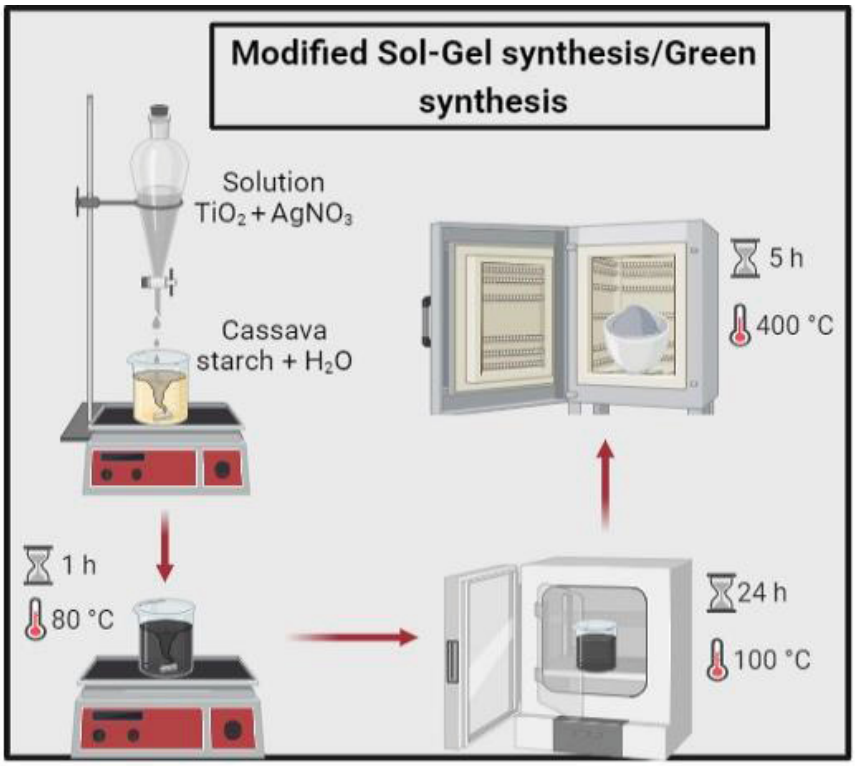


## 2.3 Characterization of the catalysts

Spectra in the infrared region were analyzed from pellets of the materials dispersed in KBr, covering the 4000 to 500 $cm^{-1}$ range, using a Perkin Elmer FT-IR spectrophotometer, model Frontier. Confirmation of the crystal structure of the catalysts was obtained from X-ray diffraction (XRD) patterns using Rigaku's Miniflex 600, with Cu kα radiation (λ= 0.154 nm).

## 2.4 Antimicrobial activity test

The antimicrobial activity of the catalysts was investigated through the use of Gram-negative *E. coli* (NEWP0022) and Gram-positive *S. aureus* (NEWP0023) bacteria. All materials were previously prepared and sterilized in an autoclave at 121 °C for 15 min, and the tests were conducted under aseptic conditions (Silva et al., 2018). We used established protocols, with adaptations (Cordeiro et al., 2004; Tsai et al., 2010). A lyophilized disk of the standard strain was introduced into a vial containing 5 mL of nutrient broth and subsequently transferred to a bacteriological incubator for 48 h at 37 °C. After this period, with the aid of a

platinum loop, three transfers were made to a new vial containing 5 mL of nutrient broth and incubated in a bacteriological incubator at 37 °C for 24 h. After this incubation period, the bacterial cultures were serially diluted (1:10 v/v) using saline solution (0.9% NaCl) with the bacterial suspension (solution 1) to $10^5$ CFU $mL^{-1}$. The catalyst solutions T, 2AgT/I and 10AgT/I were previously sonicated for 30 min and a volume of 0.1 mL (equivalent to 0.01 g $mL^{-1}$) of these was added to each well of sterile microplates (six-well microplate). As well, 3.9 mL of saline solution were also added to each well. The start of the reaction was marked by the introduction of 1 mL of the bacterial suspension, prepared in solution 1. Therefore, the final volume in each well corresponded to 5 mL. During the experiment, the microplate was kept under agitation at 350 rpm at 37 °C on a shaking platform to aid in the homogenization of the reaction solution. The microplates containing the final mixture (catalyst, saline solution and bacteria) were then irradiated separately under three different illumination conditions: bright light irradiation (Manplex, 9 W), black light (Luatek, 36 W) and in the absence of light. The distance between the light source and the microplate was 10 cm. Sampling was conducted at 0, 5, 10 and 15 min. At each time point, a sample was collected using a sterile cotton swab and spread on nutrient agar plates, gently over the agar surface in five different directions. Subsequently, the medium was allowed to absorb the inoculum for a period of 15 min. The experiments were conducted in triplicate, and the plates were subsequently incubated in a bacteriological oven at 37 ± 2 °C for 24 h. Control experiments were conducted in the absence of a catalyst. The number of Colony Forming Units (CFU) was counted and subjected to statistical analysis.

### 2.5 Detection of reactive oxygen species (ROS)

A protocol with modifications to identify ROS in bacterial samples was used (Liao et al. 2019). We followed the same experimental procedure described in item 2.4, differing only in the dilution of the bacteria, being $1x10^3$ CFU $mL^{-1}$ in this one versus $1x10^5$ CFU $mL^{-1}$ in that one. After the reaction times, the collected sample was washed in phosphate-buffered saline (1 $mmol.L^{-1}$) and centrifuged at 3000 rpm for 5 min. Then, the supernatant was discarded and the pellet was incubated for 30 min at 37 ºC in the dark with 1 mL of 2',7'-dichlorofluorescein diacetate ($H_2$DCF-DA) in phosphate-buffered saline. After the time elapsed, the cells were

centrifuged at 5000 rpm for 6 min to remove the remaining $H_2$DCF-DA. Then, the cell pellets were suspended in 1 mL of phosphate-buffered saline and mixed with 200 µL of alkaline lysis buffer (1% SDS; 0.2 mol.$L^{-1}$ NaOH) for 10 min at 37 ºC. Finally, the mixture was centrifuged at 5000 rpm for 6 min and the final supernatant product was collected for fluorescence readings (488 nm excitation and 525 nm emission) (Thermo Scientific™ Varioskan™ LUX). The results were expressed as percentage (%) of ROS relative to 0 min (initial time).

### 2.6 Statistical analysis

GraphPad Prism 9.0, test version for academics, was used to perform the statistical analyses. Normality was analyzed by Kolmogorov-Smirnov, while the Grubbs test excluded outliers. Each experiment was carried out in triplicate and the differences between the groups in relation to the study variables were verified by one-way analysis of variance (ANOVA) according to the number of variables analyzed in the trial. Tukey's post-test was then applied. Variations with a p-value $< 0.05$ were considered statistically significant. The data was shown graphically and represented as mean and standard deviation.

## 3 Results and Discussion

### 3.1 Characterization of the catalysts

The FT-IR spectra of the T, 2AgT/V and 10AgT/V catalysts are shown in **Figure 2**. These catalysts show characteristic titanium (Ti) bands between 500-750 $cm^{-1}$ which have been correlated to the oxygen-titanium bond (Ti-O-Ti). Therefore, the band observed at 739 $cm^{-1}$ belonging to the T catalyst intensified and broadened in the AgT/V catalysts, indicating that the Ti-O-Ti stretching vibration became stronger (Alsharaeh et al. 2017; Safaei and Taran 2017; Noviagel et al. 2024). Related to the 3000 $cm^{-1}$ region of the T catalysts is the stretching vibration of the OH group (León et al. 2017; Yang et al. 2022). The absorption band for the 2AgT/V and 10AgT/V catalysts at 3480 $cm^{-1}$ correlated to the stretching of the free -OH group, which was related to the increase in the number of H bonds between $TiO_2$ and the OH group (Noviagel et al. 2024). In

addition, the band at 1626 $cm^{-1}$ belonging to the 2AgT/V and 10AgT/V catalysts refers to C-O stretching (Malesic Eleftheriadou et al. 2020; Yang et al. 2022; Sathishkumar et al. 2022), and can also be attributed to the stretching and bending vibration of the OH group (Sathishkumar et al. 2022). The band present for these catalysts at 1400 $cm^{-1}$ was characteristic of C-C stretching (Kuz and ateş 2020). There is a weak band at 1350 $cm^{-1}$ for the AgT/V catalysts, which is characteristic of the Ag-$TiO_2$ bond (Desiati et al. 2019), confirming the deposition of silver on the support and highlighting the XRD results.

It is estimated that Ag doping and the use of tapioca can improve the surface condition of the samples, generating more OH on the surface (Sathishkumar et al. 2022). Thanks to the addition of Ag to the 2AgT/V and 10AgT/V catalysts, there is a slight shift in the bands around 660-700 $cm^{-1}$, correlated to the asymmetric vibration of Ti-Ag-O (Gogoi et al. 2020). It can be seen that the intensities of the bands of the 2AgT/V and 10AgT/V catalysts are lower compared to those of the T catalyst, thus indicating that the Ag particles bonded to the $TiO_2$ after the green synthesis (Poudel and Kim 2023).

**Figure 2** - FT-IR spectra of the catalysts.

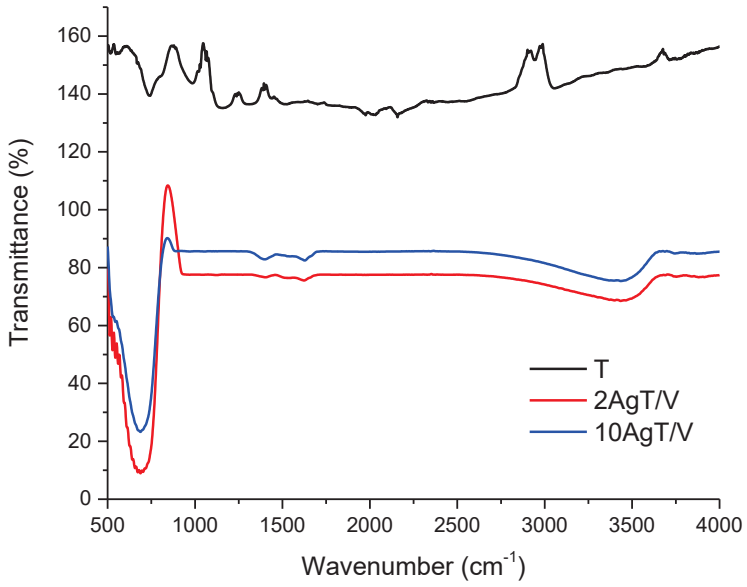

**Figure 3** shows the diffractograms of the T, 2AgT/V and 10AgT/V catalysts. There are diffraction peaks outlined for catalyst T representing organized crystalline phases, containing two phases: anatase (JCPDS 21-1272), which was more abundant, and rutile (JCPDS 71-0650). The anatase phase had intense peaks at 25.4, 37.9, 48.1, 53.9, 55.2 and 62.8º. The rutile phase had peaks at 27.6, 29.8 and 44.4º (JCPDS 2013; Poudel et al. 2022). The 2AgT/V and 10AgT/V catalysts have diffraction patterns characteristic of the cubic Ag phase (JCPDS 87-0717) with a peak at 38.2º and a peak with low intensity in the tetragonal anatase phase at 48.1º (JCPDS 83-2243). The detection of Ag peaks in AgT/V catalysts confirms the diffusion of Ag atoms deposited on the $TiO_2$ support (Mosquera et al. 2014; Sharma et al. 2016).

**Figure 3** - Diffractograms of catalysts

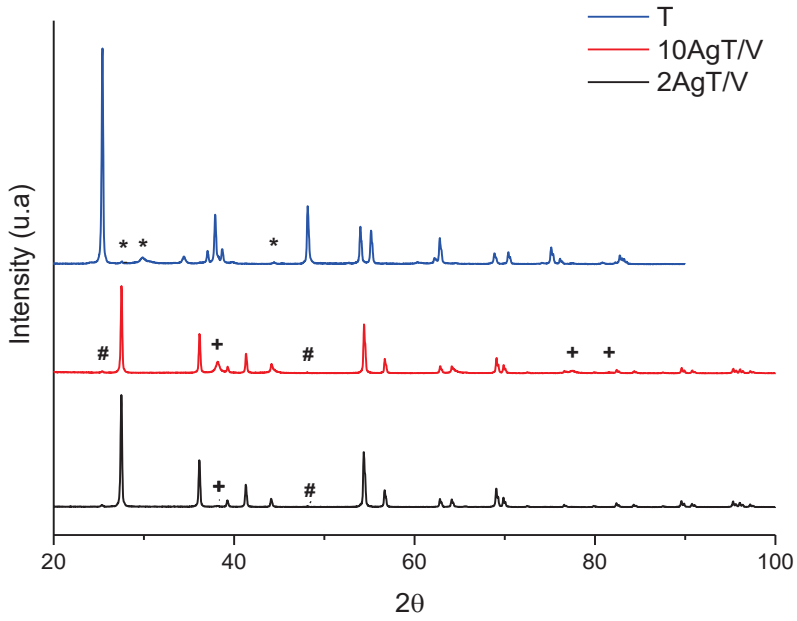


The * identifies rutile while the other peaks of the T catalyst represent the anatase phase. The # identifies the anatase phase and the + stands for metallic Ag. The other peaks present in the AgT/V catalysts are the rutile phase.

### 3.2 Antimicrobial activity test

**Figure 4** (A-I) and **Figure 5** (A-I) show the effects of visible light sources (called clear light), no light (called dark) and black light for: controls (A, D and G)

and the catalysts 2AgT/V (B, E and H) and 10AgT/V (C, F and I) on the inactivation of *E. coli* and *S. aureus*, respectively.

**Figure 4** – Antibacterial activity test (*E. coli*) of 2AgT/V and 10AgT/V catalysts under clear light (A-C), dark (D-F) and black light (G-I).

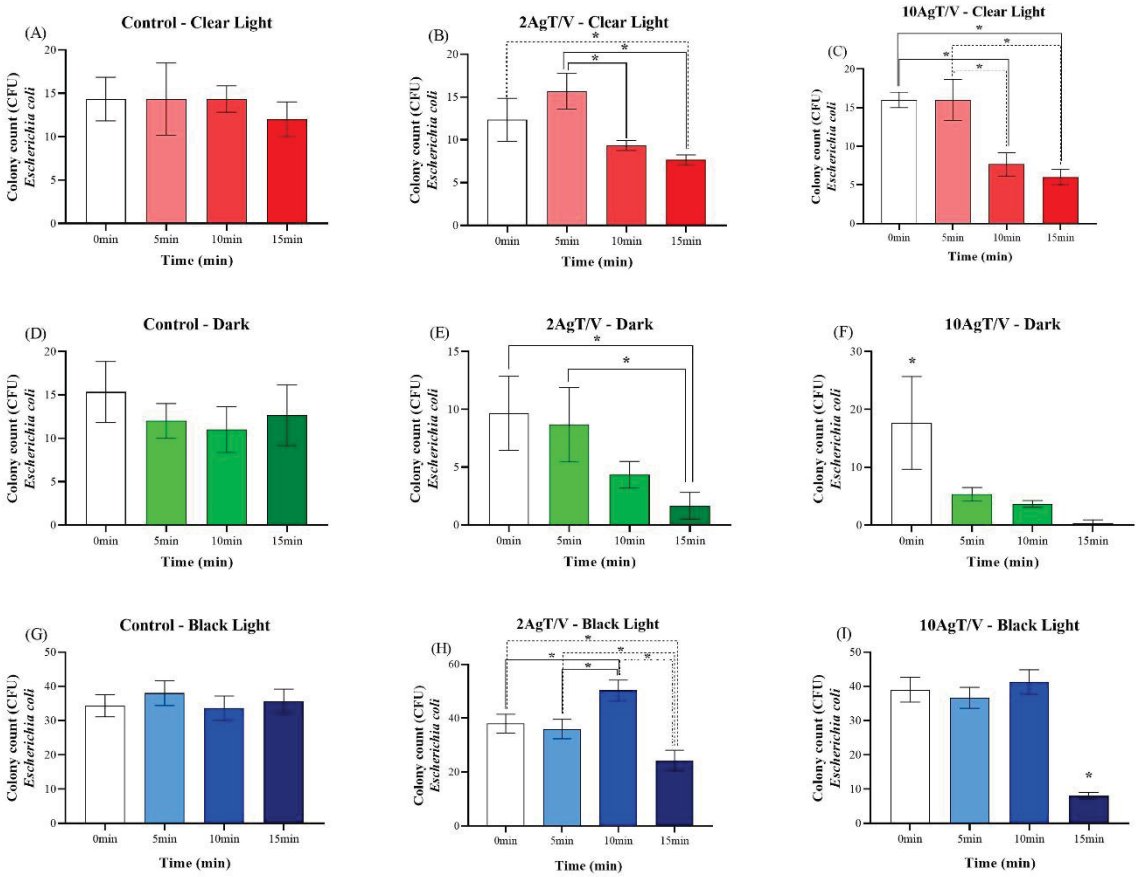


Antibacterial action against *E. coli* of the control (A, D and G) and the catalysts 2AgT/V (B, E and H) and 10AgT/V (C, F and I) in the clear light (A-C), dark (D-F) and black light (G-I) tests. According to time variation 0, 5, 10 and 15 min. Asterisks indicate $p<0.05$ (one-way ANOVA, post Tukey test).

**Figure 5** – Antibacterial activity test (*S. aureus*) of 2AgT/V and 10AgT/V catalysts under clear light (A-C), dark (D-F) and black light (G-I).

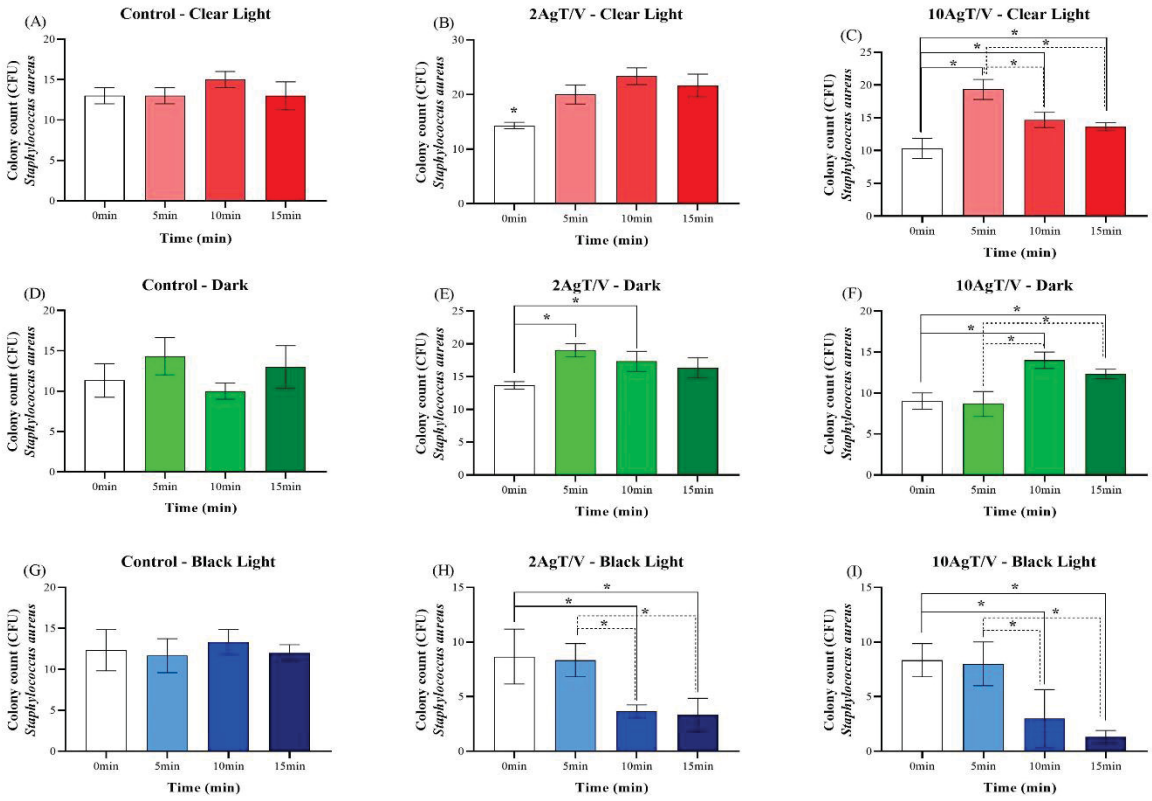


Antibacterial action against *S. aureus* of the control (A, D and G) and the catalysts 2AgT/V (B, E and H) and 10AgT/V (C, F and I) in the clear light (A-C), dark (D-F) and black light (G-I) tests. According to the time variation 0, 5, 10 and 15 min. Asterisks indicate $p<0.05$ (one-way ANOVA, post Tukey test).

The 2AgT/V and 10AgT/V catalysts (Figure 4B and 4C), under white light, showed a bactericidal effect from the 10-minute time point against *E. coli*. In the dark test, the 2AgT/V catalyst (Figure 4E) had a bactericidal effect at 15 min and 10AgT/V (Figure 4F) from 5 min. This microbial inhibition can be related to the Ag nanoparticles released by the AgT/V catalysts, so the amount of this metal in the catalyst affects its antimicrobial action. By introducing more Ag into the $TiO_2$ matrix, the bactericidal action increases and acts by adhesion of these nanoparticles to the surface of the cell membrane and wall, which accumulate and then leakage of the intracellular organelles and death occurs (Ashkarran et al. 2011; Dong et al. 2019; Chakhtouna et al. 2021). Ag nanoparticles can also enter the interior of the bacterial cell, causing damage to intracellular organelles, lipids, DNA and proteins. Ag can also incite cell toxicity and oxidative stress thanks to the generation of ROS (Tian et al. 2007). Thus, the antibacterial effect of these catalysts may come from

the oxidative stress generated by the high concentration of Ag nanoparticles or from the presence of Ag ions on their surface, in addition to the action of ROS (Perkas et al. 2013). These AgT/V catalysts are effective against *E. coli* without photoactivation, due to the release of Ag ions from the $TiO_2$ matrix.

Figure 5C shows the bacterial inhibition of the 10AgT/V catalyst after 10 min, which may be related to the Ag nanoparticles released by the material. This result may be due to the fact that Ag has a powerful contact antibacterial action, and the amount of this metal increases its action. In addition, Ag could cause a decrease in soluble protein expression by suppressing nucleic acid synthesis, inhibiting *S. aureus* (Jiang et al. 2017).

It can be seen that the 2AgT/V catalyst (Figure 4H), when irradiated with black light, indicating that UV favors the photoreparation of bacteria, thus causing bacterial cell regeneration (Chan and Killick 1995; Tosa and Hirata 1999), indicating a sublethal dose of UV, which was overcome by the catalyst after 15 min. The 2AgT/V and 10AgT/V catalysts showed a bactericidal effect after 10 min (Figures 5H and 5I, respectively) and 15 min (Figure 4I). Possibly, these catalysts were photoactivated by UV, thus causing the generation of ROS and pronounced photocatalytic action (Dahl et al. 2014).

The 2AgT/V and 10AgT/V catalysts (Figure 5B, 5C, 5E and 5F), under bright light and in the absence of light, the antibacterial activity was decreased because Gram-negative bacteria have a complex cell membrane structure that makes them resistant to oxidative stress and their cell wall is hydrophobic. In addition, it may be due to the AgT/V catalyst particles being agglomerated, thus decreasing their antibacterial activity thanks to the aggregation of their particles. The size and dispersion of the Ag nanoparticles on the $TiO_2$ interferes with the bactericidal action, with smaller Ag agglomerates (<5 nm) showing superior efficacy, thus affecting the antibacterial efficacy of the AgT/V catalysts (Hajizadeh et al. 2020). Another possibility is that the AgT/V catalysts could cause a mild lesion in the *S. aureus* membrane, altering the membrane's permeability but not causing its decomposition. The lipopolysaccharide membrane of bacteria has negative charges on its surface and the Ag nanoparticles released by the AgT/V catalyst come into contact with this surface, thus modifying its charge and hydrophobicity, affecting cell permeability. However, these modifications do not harm whole cells or induce leakage of macromolecules (Jiang et al. 2017).

The results presented showed that the AgT/V catalysts have antibacterial action, even when there is no light present (against *E. coli*), indicating that the Ag nanoparticles were responsible for the antimicrobial effect in the dark. The greater antibacterial activity of these catalysts under black light is due to the synergistic antibacterial effects of the photocatalytic reaction originating from $TiO_2$ and the Ag nanoparticles. The AgT/V catalysts showed a reduction in their performance against *S. aureus*, as only 10AgT/V had bactericidal action, suggesting that the diversity of microorganisms, such as the complexity and thickness of the cell wall, interfere in the response to the catalysts. The advantage of AgT/V catalysts is that they expand the functions of antibacterial materials to a wider variety of applications. Thus, these catalysts are effective in reducing bacteria and are promising as antibacterial coatings (Zhang and Chen 2009).

### 3.3 Detection of reactive oxygen species

**Figure 6** (A and B) and **Figure 7** (A and B) show the intracellular ROS generation values of *E. coli* and *S. aureus*, respectively, for the 2AgT/V (A) and 10AgT/V (B) catalysts, under black light.

**Figure 6** - *E. coli* intracellular ROS generation values from the $H_2$DCF-DA ROS detection assay for the 2AgT/V (A) and 10AgT/V (B) catalysts.

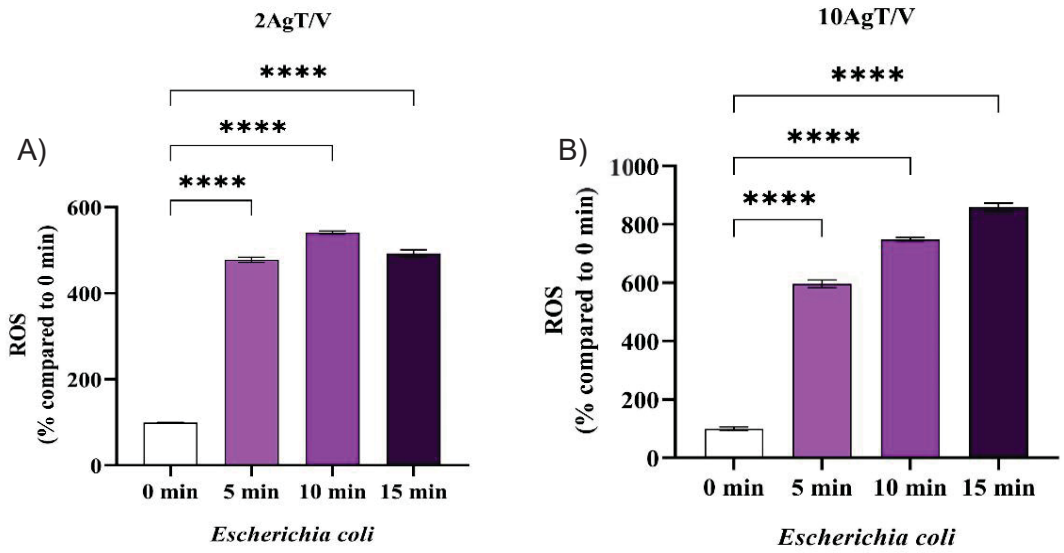


Asterisks indicate * p <0.05; ** p <0.01; *** p< 0.001 and **** p < 0.0001 (one-way ANOVA, with Dunnett's post-hoc test).

**Figure 7**- *S. aureus* intracellular ROS generation values from the $H_2$DCF-DA ROS detection assay for the 2AgT/V (A) and 10AgT/V (B) catalysts.

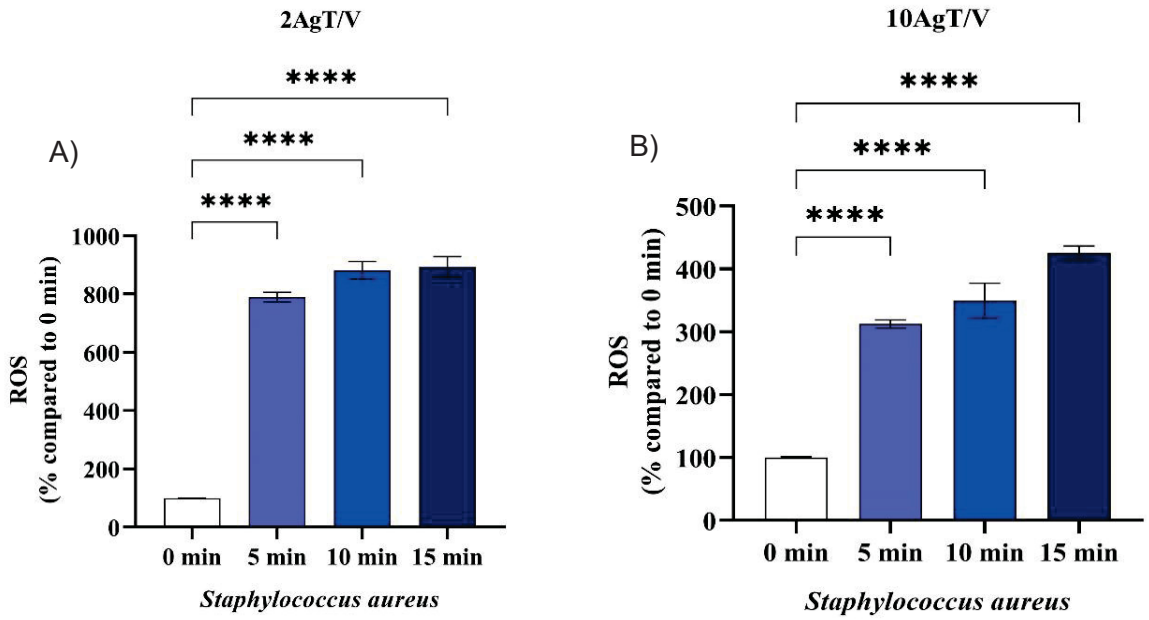


Asterisks indicate * p <0.05; ** p <0.01; *** p< 0.001 and **** p < 0.0001 (one-way ANOVA, with Dunnett's post-hoc test).

The level of ROS was determined using exposure to the 2AgT/V and 10AgT/V catalysts, observing an increase in these levels from the 5 min time point for *E. coli* (Figure 6) and *S. aureus* (Figure 7). These results corroborate the data presented in Figures 4H and I, as well as 5H and I, i.e. the ROS were generated from the photocatalytic effects. These species accumulate and overload the bacteria's antioxidant defense mechanisms, resulting in membrane damage and cell death (Yong et al. 2023). A greater production of ROS was observed for 10AgT/V in the death of *E. coli* (Figure 6B), while 2AgT/V stood out for *S. aureus* (Figure 7A). One possible explanation is the diversity of microorganisms, such as the complexity and thickness of the cell wall, which interferes with the response to catalysts (Zhang and Chen 2009).

AgT/V catalysts have a bactericidal mechanism of action that depends on oxidative stress and may be related to a chain of reactions. ROS are generated during bacterial aerobic metabolism. The constant generation and detoxification of cellular ROS act to control the fine and balanced redox state in normal bacterial cells. However, an imbalance between ROS production and detoxification can arise due to the overproduction of intracellular ROS (**Figure 8**). Initially, they are

attracted to the bacterial surface, disrupting the cell wall and membrane, modifying their permeability, inciting toxicity and oxidative stress due to ROS and free radicals, and ending up modulating signal transduction pathways (Zhang et al. 2019). The photoexcitation of $TiO_2$ by UV light generates $e^-/h^+$ pairs found in the conduction and valence bands, respectively. Therefore, the $e^-$ transferred from $Ag/TiO_2$ to the bacterial intracellular part can affect the $e^-$ transport chain, thus causing the overgeneration of intracellular ROS. These produced $e^-/h^+$ pairs collide with compounds present in the cellular environment, such as water and oxygen ($O_2$), generating $^{\bullet}OH$ and $O_2^{-\bullet}$ radicals. The gaps segregate $H_2O$ into $OH^-$ and $H^+$. The dissolved $O_2$ molecules change into $O_2^{-\bullet}$ which reacts with $H^+$ to generate $HO_2^{\bullet}$. These radicals collide with $e^-$ producing hydrogen peroxide anions ($HO_2^-$). The anions, in turn, react with $H^+$ ions to generate $H_2O_2$ (Zhou et al. 2015). At the same time, the electrons in $TiO_2$'s conduction band are captured by the Ag nanoparticles and transported to $O_2^{-\bullet}$, generating superoxide radicals. This metal also helps to generate $^{\bullet}OH$ radicals produced by the reaction of $H_2O$ with the photoproduced $h^+$, located in the valence band of $TiO_2$. The photogenerated ROS can cross the cell membrane and damage macromolecules such as proteins, DNA and lipids, thus altering biological activity, accelerating mutagenesis and bacterial death. In addition, the $e^-$ donated $Ag/TiO_2$ induces the production of extracellular $O_2^{-\bullet}$ and $H_2O_2$, which can increase the endogenous generation of ROS (Din et al. 2018; Liu et al. 2023).

**Figure 8** – Illustration of the mechanism of action of AgT/V catalysts

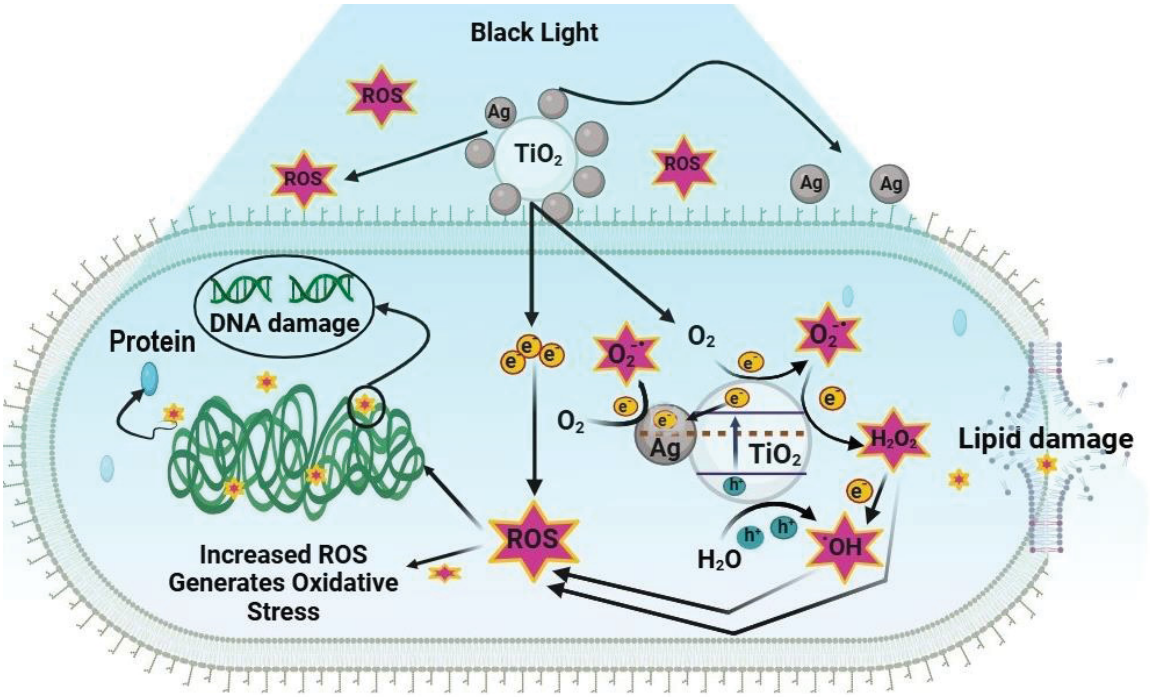


The AgT/V catalyst, when exposed to light, generates electrons ($e^-$) and gaps ($h^+$) which migrate to the surface of the $TiO_2$. Inside the bacterial cell, the $e^-/h^+$ pairs migrate to the surface of the $TiO_2$, where they react with water and molecular oxygen. The silver (Ag) present in the catalyst acts as an efficient e-acceptor, intensifying the production of reactive oxygen species (ROS), such as superoxide radicals ($O_2^{-\bullet}$), hydroxyl radicals ($HO^\bullet$), hydrogen peroxide ($H_2O_2$) and singlet oxygen ($^1O_2$). These highly reactive molecules penetrate the bacteria, damage the DNA and the cell membrane, overloading the antioxidant defense mechanisms and culminating in cell death.

## 4 Conclusions

The synthesis process is simple, which can facilitate its large-scale production and reduce production costs due to the use of tapioca, thus favoring the possible commercial application of these catalysts. In addition, they demonstrate great potential for antibacterial applications, presenting rapid activity, up to 10 min, against bacteria. The combination of the antibacterial action of Ag with the photocatalytic properties of $TiO_2$ results in a promising material for surface decontamination and water purification, demonstrating the great potential of the material. The results obtained indicate that AgT/V catalysts may represent a new generation of antimicrobial materials, with relevant applications in several sectors, such as health, the food industry and the environment.

## References

Ahmad I, Akhtar MS, Ahmed E, Ahmad M (2020) Highly efficient visible light driven

photocatalytic activity of graphene and CNTs based Mg doped ZnO photocatalysts: A comparative study. Sep Purif Technol 245:116892. https://doi.org/10.1016/j.seppur.2020.116892

Almeida WL de, Rodembusch FS, Ferreira NS, Caldas de Sousa V (2020) Eco-friendly and cost-effective synthesis of ZnO nanopowders by Tapioca-assisted sol-gel route. Ceram Int 46:10835–10842. https://doi.org/10.1016/j.ceramint.2020.01.095

Alsharaeh EH, Bora T, Soliman A, et al (2017) Sol-Gel-Assisted Microwave-Derived Synthesis of Anatase Ag/$TiO_2$/GO Nanohybrids toward Efficient Visible Light Phenol Degradation. Catalysts 7:133. https://doi.org/10.3390/catal7050133

Ashkarran AA, Aghigh SM, Kavianipour M, Farahani NJ (2011) Visible light photo- and bioactivity of Ag/$TiO_2$ nanocomposite with various silver contents. Curr Appl Phys 11:1048–1055. https://doi.org/10.1016/J.CAP.2011.01.042

Chakhtouna H, Benzeid H, Zari N, et al (2021) Recent progress on Ag/$TiO_2$ photocatalysts: photocatalytic and bactericidal behaviors. Environ Sci Pollut Res 28:44638–44666. https://doi.org/10.1007/s11356-021-14996-y

Chan YY, Killick EG (1995) The effect of salinity, light and temperature in a disposal environment on the recovery of *E.coli* following exposure to ultraviolet radiation. Water Res 29:1373–1377. https://doi.org/10.1016/0043-1354(94)00226-W

Chandra S, Jagdale P, Medha I, et al (2021) Biochar-Supported $TiO_2$-Based Nanocomposites for the Photocatalytic Degradation of Sulfamethoxazole in Water—A Review. Toxics 9:313. https://doi.org/10.3390/toxics9110313

Cordeiro A C de S, Leite S G F, Dezotti M (2004) Inativação por oxidação fotocatalítica de *Escherichia coli* e *Pseudomonas sp.*, Quim Nova 27: 689–694. https://doi.org/10.1590/S0100-40422004000500002.

Dahl M, Liu Y, Yin Y (2014) Composite Titanium Dioxide Nanomaterials. Chem Rev 114:9853–9889. https://doi.org/10.1021/cr400634p

Desiati RD, Taspika M, Sugiarti E (2019) Effect of calcination temperature on the antibacterial activity of $TiO_2$/Ag nanocomposite. Mater Res Express 6:095059. https://doi.org/10.1088/2053-1591/ab155c

Din MI, Khalid R, Hussain Z (2018) Minireview: Silver-Doped Titanium Dioxide and Silver-Doped Zinc Oxide Photocatalysts. Anal Lett 51:892–907. https://doi.org/10.1080/00032719.2017.1363770

Dong P, Yang F, Cheng X, et al (2019) Plasmon enhanced photocatalytic and antimicrobial activities of Ag-$TiO_2$ nanocomposites under visible light irradiation prepared by DBD cold plasma treatment. Mater Sci Eng C 96:197–204. https://doi.org/10.1016/j.msec.2018.11.005

Ferreira NS, Angélica RS, Marques VB, et al (2016) Cassava-starch-assisted sol–gel synthesis of $CeO_2$ nanoparticles. Mater Lett 165:139–142. https://doi.org/10.1016/J.MATLET.2015.11.107

Gheisari F, Reza Kasaee S, Mohamadian P, et al (2024) Bromelain-loaded silver nanoparticles: Formulation, characterization and biological activity. Inorg Chem Commun 161:112006. https://doi.org/10.1016/J.INOCHE.2023.112006

Gogoi D, Namdeo A, Golder AK, Peela NR (2020) Ag-doped $TiO_2$ photocatalysts with effective charge transfer for highly efficient hydrogen production through water splitting. Int J Hydrogen Energy 45:2729–2744. https://doi.org/10.1016/J.IJHYDENE.2019.11.127

Gomes MA, Brandão-Silva AC, Avila JFM, et al (2018) Particle size effect on

structural and optical properties of $Y_2O_3:Nd^{3+}$ nanoparticles prepared by coconut water-assisted sol-gel route. J Lumin 200:43–49. https://doi.org/10.1016/J.JLUMIN.2018.04.004

Hajizadeh H, Peighambardoust SJ, Peighambardoust SH, Peressini D (2020) Physical, mechanical, and antibacterial characteristics of bio-nanocomposite films loaded with Ag-modified $SiO_2$ and $TiO_2$ nanoparticles. J Food Sci 85:1193–1202. https://doi.org/10.1111/1750-3841.15079

Hlavsa MC, Cikesh BL, Roberts VA, et al (2018) Outbreaks associated with treated recreational water — United States, 2000–2014. Am J Transplant 18:1815–1819. https://doi.org/10.1111/ajt.14956

JCPDS (2013) JCPDS—International Center for Diffraction Data, PCPDFWIN

Jiang X, Lv B, Wang Y, et al (2017) Bactericidal mechanisms and effector targets of $TiO_2$ and Ag-$TiO_2$ against *Staphylococcus aureus*. J Med Microbiol 66:440–446. https://doi.org/10.1099/jmm.0.000457

Khorrami GH, Kompany A, Khorsand Zak A (2015) Structural and optical properties of (K,Na)$NbO_3$ nanoparticles synthesized by a modified sol–gel method using starch media. Adv Powder Technol 26:113–118. https://doi.org/10.1016/J.APT.2014.08.013

Kuz P, ateş M (2020) Starch-Based Bioplastic Materials for Packaging Industry. J Sustain Constr Mater Technol 5:399–406. https://doi.org/10.29187/jscmt.2020.44

León A, Reuquen P, Garín C, et al (2017) FTIR and Raman Characterization of $TiO_2$ Nanoparticles Coated with Polyethylene Glycol as Carrier for 2-Methoxyestradiol. Appl Sci 7:49. https://doi.org/10.3390/app7010049

Liao S, Zhang Y, Pan X, et al (2019) Antibacterial activity and mechanism of silver nanoparticles against multidrug-resistant *Pseudomonas aeruginosa*. Int J Nanomedicine Volume 14:1469–1487. https://doi.org/10.2147/IJN.S191340

Liu Z, Chen Z, Xie H, et al (2023) The effect of electron transfer channel on UV-independent antibacterial activity of $Ag^+$ implanted $TiO_2$. Appl Surf Sci 624:157147. https://doi.org/10.1016/j.apsusc.2023.157147

Malesic Eleftheriadou N, Ofrydopoulou A, Papageorgiou M, Lambropoulou D (2020) Development of Novel Polymer Supported Nanocomposite GO/$TiO_2$ Films, Based on poly(L-lactic acid) for Photocatalytic Applications. Appl Sci 10:2368. https://doi.org/10.3390/app10072368

Mosquera AA, Endrino JL, Albella JM (2014) Xanes observations of the inhibition and promotion of anatase and rutile phases in silver containing films. J Anal At Spectrom 29:736. https://doi.org/10.1039/c3ja50354b

Nag R, Monahan C, Whyte P, et al (2021) Risk assessment of *Escherichia coli* in bioaerosols generated following land application of farmyard slurry. Sci Total Environ 791:148189. https://doi.org/10.1016/J.SCITOTENV.2021.148189

Noviagel I, Heryanto H, Putri SE, et al (2024) Tapioca-starch-based bionanocomposites with fructose and titanium dioxide for food packaging and fertilization applications. Int J Biol Macromol 273:132803. https://doi.org/10.1016/j.ijbiomac.2024.132803

Ochiai T, Fujishima A (2012) Photoelectrochemical properties of $TiO_2$ photocatalyst and its applications for environmental purification. J Photochem Photobiol C Photochem Rev 13:247–262. https://doi.org/10.1016/J.JPHOTOCHEMREV.2012.07.001

Ong CB, Ng LY, Mohammad AW (2018) A review of ZnO nanoparticles as solar photocatalysts: Synthesis, mechanisms and applications. Renew Sustain

Energy Rev 81:536–551. https://doi.org/10.1016/J.RSER.2017.08.020
Padmavathi J, Mani M, Gokulakumar B, et al (2022) A study on the antibacterial activity of silver nanoparticles derived from Corchorus aestuans leaves and their characterization. Chem Phys Lett 805:139952. https://doi.org/10.1016/J.CPLETT.2022.139952
Parveen K, Banse V, Ledwani L (2016) Green synthesis of nanoparticles: Their advantages and disadvantages. p 020048
Pathak N, Caleb OJ, Rauh C, Mahajan P V. (2019) Efficacy of photocatalysis and photolysis systems for the removal of ethylene under different storage conditions. Postharvest Biol Technol 147:68–77. https://doi.org/10.1016/J.POSTHARVBIO.2018.09.006
Pérez-Rodríguez F, Posada-Izquierdo GD, Valero A, et al (2013) Modelling survival kinetics of *Staphylococcus aureus* and *Escherichia coli* O157:H7 on stainless steel surfaces soiled with different substrates under static conditions of temperature and relative humidity. Food Microbiol 33:197–204. https://doi.org/10.1016/J.FM.2012.09.017
Perkas N, Lipovsky A, Amirian G, et al (2013) Biocidal properties of $TiO_2$ powder modified with Ag nanoparticles. J Mater Chem B 1:5309. https://doi.org/10.1039/c2tb00337f
Poudel M, Chandra Lohani P, Kim AA (2022) Synthesis of silver nanoparticles decorated tungsten oxide nanorods as high-performance supercapacitor electrode. Chem Phys Lett 804:139884. https://doi.org/10.1016/J.CPLETT.2022.139884
Poudel MB, Kim AA (2023) Silver nanoparticles decorated $TiO_2$ nanoflakes for antibacterial properties. Inorg Chem Commun 152:110675. https://doi.org/10.1016/J.INOCHE.2023.110675
Primo J de O, Correa J de S, Horsth DFL, et al (2022) Antiviral Properties against SARS-CoV-2 of Nanostructured ZnO Obtained by Green Combustion Synthesis and Coated in Waterborne Acrylic Coatings. Nanomaterials 12:4345. https://doi.org/10.3390/nano12234345
Rabhi S, Belkacemi H, Bououdina M, et al (2019) Effect of Ag doping of $TiO_2$ nanoparticles on anatase-rutile phase transformation and excellent photodegradation of amlodipine besylate. Mater Lett 236:640–643. https://doi.org/10.1016/J.MATLET.2018.11.006
Rajaram P, Jeice AR, Jayakumar K (2023) Review of green synthesized $TiO_2$ nanoparticles for diverse applications. Surfaces and Interfaces 39:102912. https://doi.org/10.1016/j.surfin.2023.102912
Rengga WDP, Yufitasari A, Adi W (2017) Synthesis of silver nanoparticles from silver nitrate solution using green tea extract (*Camelia sinensis*) as bioreductor. J Bahan Alam Terbarukan 6:32–38. https://doi.org/10.15294/jbat.v6i1.6628
Safaei M, Taran M (2017) Optimal conditions for producing bactericidal sodium hyaluronate-$TiO_2$ bionanocomposite and its characterization. Int J Biol Macromol 104:449–456. https://doi.org/10.1016/J.IJBIOMAC.2017.06.016
Saleem A, Iqbal A, Younas U, et al (2024) Antimicrobial attributes and enhanced catalytic potential of PVA stabilized Ag-$NiO_2$ nanocomposite for wastewater treatment. Arab J Chem 17:105545. https://doi.org/10.1016/J.ARABJC.2023.105545
Sathishkumar K, Sowmiya K, Arul Pragasan L, et al (2022) Enhanced photocatalytic degradation of organic pollutants by Ag–$TiO_2$ loaded cassava

stem activated carbon under sunlight irradiation. Chemosphere 302:134844. https://doi.org/10.1016/j.chemosphere.2022.134844

Sharma H, Singhal R, Siva Kumar V V., Asokan K (2016) Structural, optical and electronic properties of Ag–$TiO_2$ nanocomposite thin film. Appl Phys A 122:1010. https://doi.org/10.1007/s00339-016-0552-3

Silva N, Junqueira VCA., Silveira NFA, et al (2018) Manual de métodos de análise microbiológica de alimentos e água., 5ª ed. Blucher, São Paulo

Tian J, Wong KKY, Ho C, et al (2007) Topical Delivery of Silver Nanoparticles Promotes Wound Healing. ChemMedChem 2:129–136. https://doi.org/10.1002/cmdc.200600171

Tian X, Wen J, Wang S, et al (2016) Starch-assisted synthesis and optical properties of ZnS nanoparticles. Mater Res Bull 77:279–283. https://doi.org/10.1016/J.MATERRESBULL.2016.01.046

Tsai, T., Chang, H., Chang, K., Liu, Y., Tseng, C., 2010. A comparative study of the bactericidal effect of photocatalytic oxidation by $TiO_2$ on antibiotic-resistant and antibiotic-sensitive bacteria. J. Chem. Technol. Biotechnol. 85, 1642–1653. https://doi.org/10.1002/jctb.2476

Tosa K, Hirata T (1999) Photoreactivation of enterohemorrhagic *Escherichia coli* following UV disinfection. Water Res 33:361–366. https://doi.org/10.1016/S0043-1354(98)00226-7

Tsai T, Chang H, Chang K, Liu Y, Tseng C (2010) A comparative study of the bactericidal effect of photocatalytic oxidation by $TiO_2$ on antibiotic-resistant and antibiotic-sensitive bacteria, J. Chem. Technol. Biotechnol. 85: 1642–1653. https://doi.org/10.1002/jctb.2476.

USDA (2019) FoodData Central Search Results: Mixed Nuts . In: https://fdc.nal.usda.gov/fdc-app.html#/food-search?query=&type=Foundation

Wang G, Doyle MP (1998) Survival of Enterohemorrhagic *Escherichia coli* O157:H7 in Water. J Food Prot 61:662–667. https://doi.org/10.4315/0362-028X-61.6.662

Yang H, Dai K, Zhang J, Dawson G (2022) Inorganic-organic hybrid photocatalysts: Syntheses, mechanisms, and applications. Chinese J Catal 43:2111–2140. https://doi.org/10.1016/S1872-2067(22)64096-8

Yin J, Lv L, Chu Y, Tan L (2023) Highly antibacterial Cu/Fe/N co-doped $TiO_2$ nanopowder under visible light. Inorg Chem Commun 151:110587. https://doi.org/10.1016/J.INOCHE.2023.110587

Yong S-S, Lee J-I, Kang D-H (2023) $TiO_2$-based photocatalyst Generated Reactive Oxygen Species cause cell membrane disruption of Staphylococcus aureus and *Escherichia coli* O157:H7. Food Microbiol 109:104119. https://doi.org/10.1016/j.fm.2022.104119

Zacarías SM, Satuf ML, Vaccari MC, Alfano OM (2015) Photocatalytic inactivation of bacterial spores using $TiO_2$ films with silver deposits. Chem Eng J 266:133–140. https://doi.org/10.1016/J.CEJ.2014.12.074

Zakiyyah SN, Irkham, Einaga Y, et al (2024) Green Synthesis of Ceria Nanoparticles from Cassava Tubers for Electrochemical Aptasensor Detection of SARS-CoV-2 on a Screen-Printed Carbon Electrode. ACS Appl Bio Mater 7:2488–2498. https://doi.org/10.1021/acsabm.4c00088

Zhang H, Chen G (2009) Potent Antibacterial Activities of Ag/$TiO_2$ Nanocomposite Powders Synthesized by a One-Pot Sol−Gel Method. Environ Sci Technol 43:2905–2910. https://doi.org/10.1021/es803450f

Zhang S, Liang X, Gadd GM, Zhao Q (2019) Advanced titanium dioxide-

polytetrafluorethylene ($TiO_2$-PTFE) nanocomposite coatings on stainless steel surfaces with antibacterial and anti-corrosion properties. Appl Surf Sci 490:231–241. https://doi.org/10.1016/J.APSUSC.2019.06.070

Zhou N, López-Puente V, Wang Q, et al (2015) Plasmon-enhanced light harvesting: applications in enhanced photocatalysis, photodynamic therapy and photovoltaics. RSC Adv 5:29076–29097. https://doi.org/10.1039/C5RA01819F

# CHAPTER VI

## Influence of synthesis method on the photocatalytic performance of Ag/$TiO_2$ for testosterone degradation


### ABSTRACT

Testosterone photodegradation using silver (Ag) doped titanium dioxide ($TiO_2$) catalysts has shown promise for the removal of hormonal contaminants in aquatic environments. The efficiency of this process is linked to the catalyst synthesis method, influencing its structural and morphological properties and catalytic activities. Testosterone photodegradation using Ag/$TiO_2$ represents a relatively new research field, with a limited number of studies. This work evaluated the efficiency of Ag/$TiO_2$ catalysts, containing nominal proportions of Ag (2% and 10%); synthesized by the solvent excess impregnation (AgT/I), modified sol-gel (AgT/V) and sol-gel (AgT/SG) methods. The aim was to characterize and evaluate them for testosterone degradation via photolysis and heterogeneous photocatalysis. Thus, Scanning Electron Microscopy identified agglomerated morphologies as Ag was added to the AgT/I and AgT/V catalysts. Meanwhile, the T ($TiO_2$) and AgT/SG catalysts presented a dense appearance. In the determination of $N_2$ physisorption, it was found that the increase in Ag decreases the surface area of the AgT/I and AgT/V catalysts and the opposite effect occurs for AgT/SG. The band gap of the mesosporous catalysts decreased in relation to T. It was found that the sol-gel method stands out from the other synthesis routes. The photolysis efficiency (82%) was similar to that of heterogeneous photocatalysis using the 2AgT/SG catalyst (79.9%), in the photodegradation of testosterone. The AgT/SG and 10AgT/V catalysts presented greater photocatalytic activities in the photodegradation of testosterone, with a reduction greater than 72%. These catalysts can find applications in water treatment processes, being essential for the development of more efficient and sustainable technologies.



**Keywords:** Impregnation, green synthesis, sol-gel, emerging pollutants.



Manuscript elaborated and formatted according to the guidelines of scientific Desalination publication, submitted to the. Available at: <https://www.sciencedirect.com/journal/desalination >

## 1 Introdution

The growing concern about the presence of emerging pollutants (hormones, antibiotics, cosmetics, and pesticides) in ng/L concentrations in wastewater and their impacts on the health of aquatic ecosystems and humans has driven the search for efficient technologies for their removal [1–4]. Endocrine disruptors have the ability to alter the function of the endocrine system, interfering with metabolism and causing reproductive disorders [5]. These compounds enter waterways through various sources, such as effluents from sewage treatment plants, agricultural runoff, animal excretions, and others [1,6,7]. These pollutants are associated with loss of IQ (intelligence quotient), autism, obesity, diabetes, cancer, and others [8]. According to a 2019 report by the European Parliament, the annual cost of the impacts of exposure to endocrine disrupting chemicals EDCs in the European Union was quantified at 163 billion euros. Research attributed 5% of this value, equivalent to 8.15 billion euros, to reproductive disorders [9]. Testosterone (**Figure 1**), a male sex hormone, can cause hormonal imbalances that affect the production of other hormones and gene expression in aquatic organisms, altering the entire trophic chain, as well as in humans. This hormone can be found in low concentrations in the environment (μg $L^{-1}$ and ng $L^{-1}$) and can negatively interfere with health [1,10,11].

**Figure 1-** Structure and molecular mass of testosterone

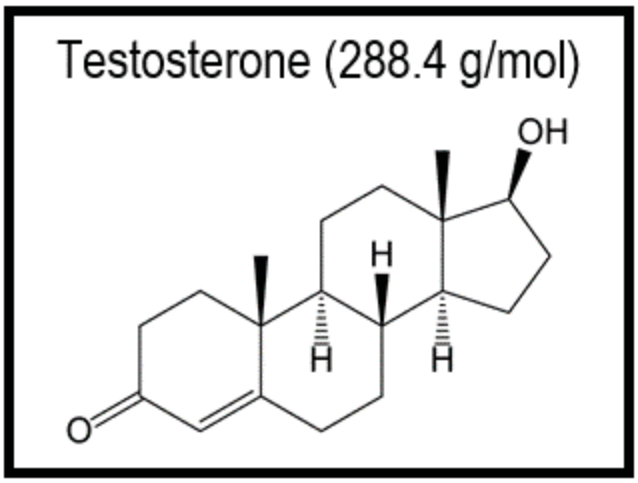


Studies have reported high concentrations of testosterone (up to 214 ng $L^{-1}$) in USA streams, with an average concentration of 116 ng $L^{-1}$ [12], while in

sewage treatment plants, concentrations range from 1 ng $L^{-1}$ to 50 ng $L^{-1}$; for example, 182 ng $L^{-1}$ was found in sewage effluents from Rotorua, North Island, New Zealand [13,14]. Average concentrations found in surface and groundwater were between 1 and 30 ng $L^{-1}$ [15], as in the case of river waters with effluents from a paper mill (Florida, USA), where concentrations ranged from 26.52 ng $L^{-1}$ to 1.362 µg $L^{-1}$, with masculinized mosquitofish being found [16]. In soils, concentrations of up to 260 ng $kg^{-1}$ of testosterone are found, such as in broiler litter [17].

Several approaches have been proposed for wastewater remediation, such as adsorption, nanofiltration, and reverse osmosis membranes, which rely on the phase transfer of pollutants and are not capable of promoting its degradation like heterogeneous photocatalysis and photolysis. This technique breaks down molecules induced by light and plays a significant role in the degradation of hormones in aqueous environments. Heterogeneous photocatalysis uses light to promote redox reactions on the surface of semiconductors, such as titanium dioxide ($TiO_2$), to trigger the production of reactive species (ROS) through the oxidation of water [18,19].

$TiO_2$ is a semiconductor with high chemical stability, photocatalytic activity, high refractive index, low cost, biocompatibility, and low toxicity [20]. However, its response to sunlight is limited to the ultraviolet region and exhibits a wide band gap. To broaden the light absorption spectrum and increase photocatalytic efficiency, this oxide was doped with several elements, such as silver (Ag), to overcome its low quantum performance and ensure efficient segregation of the photogenerated energy in photocatalysis by electron ($e^-$) and hole ($h^+$) pairs [21]. The presence of Ag nanoparticles on the surface of $TiO_2$ can increase the generation of ROS, thus degrading organic compounds [22,23]. The combination of $TiO_2$ and Ag to produce Ag/$TiO_2$ provides a modification to the ceramic and semiconductor matrix of oxides [24,25], as well as generating a narrower band gap and expanding the light capture spectrum due to the plasmonic resonance of the Ag surface [19,26,27].

The photodegradation of testosterone using Ag/$TiO_2$ is a relatively new and specific field of research, with a limited number of studies. However, several studies have demonstrated the effectiveness of Ag/$TiO_2$ photocatalysis for the degradation of other hormones, such as estrogens and progesterone [28–31]. The

relevance of this study lies in the possibility of developing photocatalytic materials, which can be synthesized by different methods, making them more efficient and selective for the removal of hormonal pollutants from effluents, thus contributing to the protection of water resources and human health. Thus, this work aims to: evaluate the efficiency of synthesized Ag/$TiO_2$ mixed oxides containing nominal proportions of silver (2% and 10%) by the methods of solvent excess impregnation, modified sol-gel and sol-gel; characterize and evaluate them in the degradation of testosterone through photolysis and heterogeneous photocatalysis.

## 2 Material and Methods

### 2.1 Material

Titanium dioxide ($TiO_2$, Êxodo Científica), silver nitrate ($AgNO_3$, Alphatec), ethyl alcohol P.A. (Dinâmica) and acetonitrile (Merck Supelco) with HPLC grade, all with analytical grade and without purification, were used. A gel drug (50 mg) containing testosterone (10 mg/g) was used as a detection and quantification standard in the HPLC analysis. The water used in the method was Milli–Qplus with an approximate resistivity of 18 MΩcm.

The testosterone working solution was prepared at a concentration of 20 mg $L^{-1}$, separately, by weighing 2 g of the analyte and dissolving it in 400 mL of acetonitrile and 600 mL of water and storing it at -5 °C for a maximum of 10 days.

### 2.2 Photocatalytic degradation

The catalysts used were synthesized from an adaptation of the methodologies: solvent excess impregnation [32], modified sol-gel (called green synthesis) [33,34] and sol-gel [35]. The abbreviations of the synthesized catalysts are in **Table 1**.

**Table 1** – Abbreviations of synthesized catalysts

| Catalysts | Abbreviations |
|---|---|
| $TiO_2$/Commercial | T |
| 2% Ag/$TiO_2$/Impregnation | 2AgT/I |
| 10% Ag/$TiO_2$/Impregnation | 10AgT/I |

| | |
|---|---|
| 2% Ag/$TiO_2$/Green synthesis | 2AgT/V |
| 10% Ag/$TiO_2$/Green synthesis | 10AgT/V |
| $TiO_2$/Sol-gel | T/SG |
| 2% Ag/$TiO_2$/Sol-gel | 2AgT/SG |
| 10% Ag/$TiO_2$/Sol-gel | 10AgT/SG |

Each photocatalytic experiment was performed by adding 0.5 g $L^{-1}$ of the mentioned catalysts and the testosterone hormone (HT = 20 mg $L^{-1}$) in a batch reactor with a cooling system (20 ± 2 °C) to avoid possible evaporation. The suspension was stirred in the dark for 30 min until reaching HT adsorption equilibrium before illumination. At the end, a centrifugation process was performed to recover the catalyst. The pH of the effluent was not changed, since the objective was to evaluate the degradation under real conditions, where a pH value of 6.6 - 7 is frequently found. The photoreactor (**Figure 2**) consisted of a transparent glass tube where the lamp was located. A 2000 mL borosilicate glass was used to which 1000 mL of an aqueous dissolution of HT was added. The ultraviolet radiation source used was a mercury vapor lamp (Empalux, 250 W, without the glass bulb), fixed in the center of the reactor with a tube. The sample retention time for each treatment was 240 min. Aliquots of 5 mL were removed at intervals of 0, 5, 10, 20, 30 (adsorption and onset of photodegradation), 60, 90, 120, 150, 180, 210 and 240 min of reaction. Then, the samples were filtered through a polyethersulfone membrane with a pore diameter of 0.22 μm and sent for analysis. In order to promote sample homogenization, a magnetic stirrer was used. The reactor was enclosed to prevent damage to the handler during the tests. As for the photolysis test, the same reaction conditions as above were used, but in the absence of a catalyst.

### 2.3 Chromatographic analysis

For the determination and quantification of testosterone hormone in the samples, the high-performance liquid chromatography (HPLC) technique with UV detection SPD-M20A (Photodiode Array Detector - UV) was used; (LCMS model - 2020 Shimadzu). The column used for testosterone analysis was the NST-18 C18 of 5 μm, 250 mm long and 4.6 mm thick. Oven temperature 30 ºC, using the

LabSolution chromatography software. The analyzes were performed with automatic injection of the sample in a volume of 20 µL, under a flow rate of 0.6 mL $min^{-1}$. The mobile phase used consisted of a ratio of acetonitrile (ACN) and ultrapure water (Milli-Q) 70:30 (ACN:$H_2O$). Detection was performed at a wavelength of 242 nm, with a run time of 22 min and a retention time of 9.4 min on the compound column.

**Figura 2** - Photoreactor scheme and quantification of testosterone in HPLC

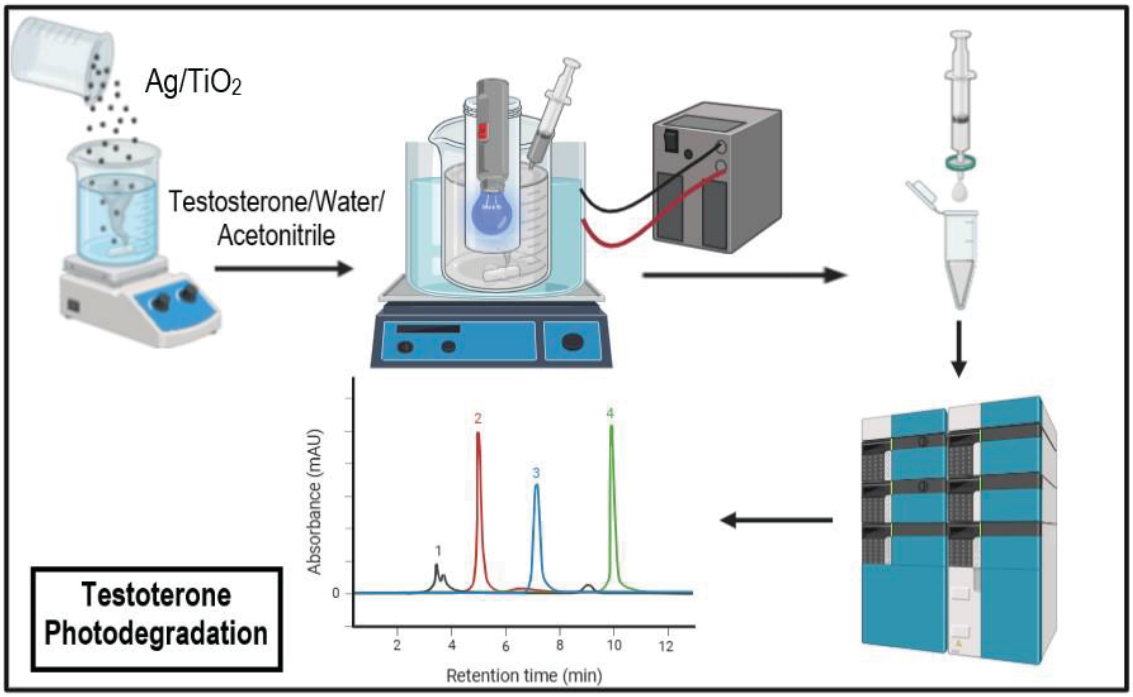


The testosterone concentration was calculated based on the integration of the peak areas of the corresponding chromatogram, and converted into concentration from the calibration curve equation. Solutions at concentrations of 0.1; 0.5; 2.5; 5; 10; 15 and 20 mg $L^{-1}$ were prepared in ultrapure water, starting from the standard stock solution of 20 mg $L^{-1}$. Each point was injected in triplicate into the HPLC, and the means and relative standard deviations were calculated.

## 2.4 Characterization of the catalysts

Scanning electron microscopy (SEM) and energy dispersive X-ray (EDS) images of the catalysts were obtained using a VEGA 3, Tescan model. $N_2$ physisorption performed measurements of specific area, mean pore volume and

mean pore diameter of the materials by Quantachrome Instruments, model NOVA 2000e and the specific area was determined by the Brunauer, Emmett and Teller (B.E.T.) method. Photoacoustic spectroscopy (PAS) in the UV-VIS range was performed using an experimental setup, monochromatic light was obtained from a 225-700 nm (UV-Vis), 800-1600 nm (IVP), and 1600-2550 nm (IVM) lamp (Newport/Oriel; Stanford Research; Brüel&Kjaer; Kimmon Koha; TMC).

## 3 Results and Discussion

### 3.1 Catalyst characterization

The morphological properties of the catalysts T, 2AgT/I, 10AgT/I, 2AgT/V, 10AgT/V, T/SG, 2AgT/SG and 10AgT/SG evaluated through the micrographs, **Figure 3**, demonstrate that the catalyst T (Figure 3A) has a homogeneous shape and size containing rounded particles dispersed on the surface of the material. As the doping with Ag occurs in the oxides 2AgT/I and 10AgT/I (3B and C, respectively), the morphologies are altered, changing to an agglomerate [36,37]. For the 2AgT/V and 10AgT/V catalysts (3D and E, respectively), the morphologies changed to a spongy agglomerate, evidencing the formation of particles with amorphous and polydisperse shapes distributed on the surface [37], which may be due to the aggregation process [36,38]. The surface of the catalysts appears to have no cracks. It can be observed through the microphotographs that the T/SG catalyst (3F) demonstrates a surface structure composed of crystals forming agglomerates. Meanwhile, the AgT/SG catalysts appear to have a more rigid structure than that of the T/SG catalyst, giving the impression of being formed by blocks. Therefore, the AgT/SG catalysts are dense, presenting good distribution [39].

The sol-gel synthesis method proved to be more effective when compared to the solvent excess impregnation and green synthesis methods, which presented agglomerated morphologies, while the AgT/SG catalysts appear to have a more rigid structure.

**Figure 3** – Scanning electron micrographs of catalysts

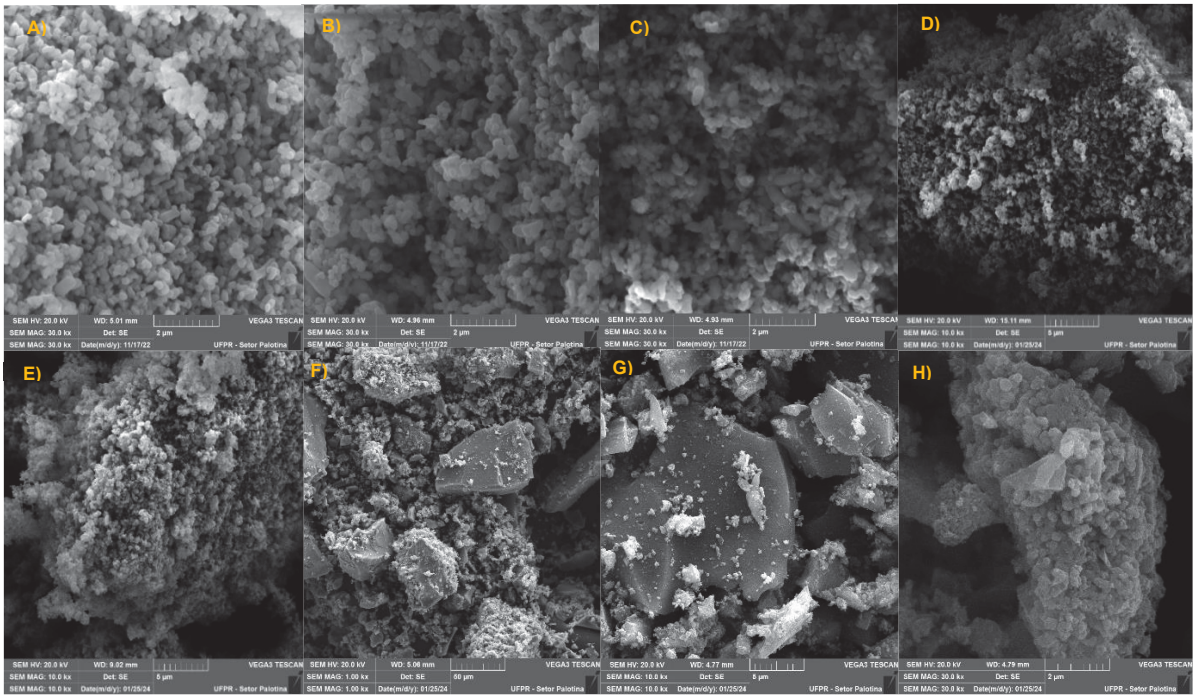


A) T – 30kx; B) 2AgT/I – 30kx; C) 10AgT/I – 30kx; D) 2AgT/V – 1 kx; E) 10AgT/V – 10 kx; F) T/SG – 1 kx; G) 2AgT/SG – 10 kx; H) 10AgT/SG – 30 kx

**Table 2** presents the results obtained for the Ag content in the materials 2AgT/I, 10AgT/I, 2AgT/V, 10AgT/V, 2AgT/SG and 10AgT/SG. It was expected that the catalysts 2AgT/I and 2AgT/V would theoretically present 2% Ag, as well as the catalysts 10AgT/I, 10AgT/V and 10AgT/SG would demonstrate an expected content of 10% Ag. However, the results obtained showed lower Ag percentages than expected during the methods. This difference observed in the amount of Ag present in the catalysts 2AgT (except 2AgT/SG) and 10AgT can be attributed to the dispersion of the metal on the $TiO_2$ surface and the efficiency of metal incorporation during the syntheses. There is a possibility that the irregular distribution of metals in compounds may occur due to limitations in the deposition techniques and control of the morphology of the nanoparticles during the synthesis methods [40]. Furthermore, the interaction between the metal and the support may also influence the effectiveness of the incorporation of the metal on the surface, thus explaining the observed oscillations, and it is also worth noting that the SEM/EDS technique is semiquantitative [41].

The sol-gel synthesis method stands out when compared to the other methods that presented lower doping values than the theoretical ones, while the 2AgT/SG catalyst presented concentrations similar to the theoretical incorporated

value, indicating a more uniform dispersion on the $TiO_2$ surface, maximizing the number of active sites.

**Table 2** – X-ray dispersive energy of catalysts containing Ag

| Catalysts | Ag Percentage (wt%) |
|---|---|
| 2AgT/I | 1.41 |
| 10AgT/I | 5.82 |
| 2AgT/V | 1.55 |
| 10AgT/V | 8.03 |
| 2AgT/SG | 2.12 |
| 10AgT/SG | 9.27 |

**Figure 4** shows the $N_2$ adsorption/desorption isotherms of the catalysts T, 2AgT/I, 10AgT/I, 2AgT/V and 10AgT/V, which are type II according to IUPAC, classifying them as mesoporous materials. The catalysts T/SG, 2AgT/SG and 10AgT/SG are type IV therefore, the isotherms indicated mesoporous structures, formed by denser and rigid-looking particles [42,43]. The formation of mesoporous materials becomes advantageous in photocatalysis, adsorbing more polluting organic compounds, such as testosterone, and degrading them more than non-porous materials [44].

**Figure 4** - $N_2$ adsorption/desorption isotherms of catalysts of impregnated (A), green (B) and sol-gel catalysts

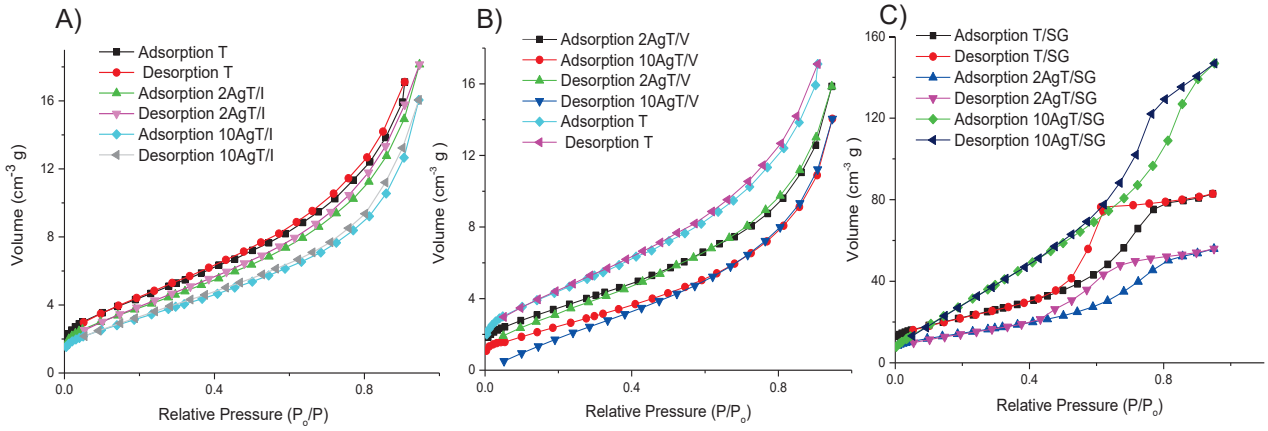

**Table 3** shows the specific area data of the catalysts, as well as the volume and average pore diameter. Table 3 shows a decrease in So and $V_p$ for the T, 2AgT/I, 10AgT/I, 2AgT/V and 10AgT/V catalysts as the Ag doping percentage increases, which can be attributed to strongly agglomerated structures, as verified in the SEM. Ag doping decreases $S_o$ and $V_p$ due to partial pore blockages and structural defects. The low $V_p$ suggests that the particles have low porosity and closed pores [42]. Meanwhile, the $d_p$ increases with the increase in Ag doping, which can be caused by the sintering process and pore union and also helps in the formation of agglomerates, decreasing $S_o$ and $V_p$ [45,46].

For the T/SG, 2AgT/SG and 10AgT/SG catalysts, the result found shows that the catalysts have high specific area values, which is important for the use of catalysts in catalytic activities. Therefore, the addition of Ag favored the increase in the specific area, represented in the 10AgT/SG catalyst. The 2AgT/SG catalyst presented a smaller surface area than the others prepared by the sol-gel method. This one had a hysteresis cycle (Figure 4C) with adsorption and desorption with a smaller pressure range ($P/P_0$) and a less inclined multilayer. This result indicates that the 2AgT/SG catalyst presents a more homogeneous pore distribution when compared to the other synthesized sol-gel catalysts [47].

There is a significant increase in $S_o$ and $V_p$ and a decrease in $d_p$ for these catalysts when compared to the T, AgT/I and AgT/V catalysts. This variation is certainly associated with the synthesis method used. Therefore, modification of the surfaces alters the specific area and porosity of the samples, thus enabling different behaviors. The specific area influences the heterogeneous photocatalysis process, since a larger area tends to present a better photocatalytic response, allowing better use of photons, producing high reaction rates. Other parameters that influence the efficiency of photocatalysis stand out, such as the crystalline phase and activation energy value, which, together with the surface area, act on the generation of $e^-/h^+$ pairs and on the oxidation-reduction processes [48], contributing to greater absorption of photons, in addition to enabling the charge transfer processes, thus assisting in the photodegradation of HT [47].

**Table 3** - Area ($S_o$), average pore volume ($V_p$) and average pore diameter ($d_p$) of the catalysts

| Catalysts | $S_o$ ($m^2/g$) | $V_p$ ($cm^3/g$) | $d_p$ (Å) |
|---|---|---|---|
| T | 16.15 | 0.031 | 37.08 |
| 2AgT/I | 14.13 | 0.028 | 37.78 |
| 10AgT/I | 11.93 | 0.025 | 39.37 |
| 2AgT/V | 12.69 | 0.025 | 36.89 |
| 10AgT/V | 9.22 | 0.021 | 43.67 |
| T/SG | 79.41 | 0.128 | 31.31 |
| 2AgT/SG | 51.92 | 0.086 | 32.28 |
| 10AgT/SG | 116.6 | 0.227 | 32.64 |

**Figure 5** shows the results of the UV-Vis band gaps for the catalysts. The narrowest band gap was for the 10AgT/SG catalyst (2.11 eV), in Figure 5H, which had a modification of the $TiO_2$ network caused by the deposition of Ag. This decrease may be directly correlated to the increase in faults in the $TiO_2$ network, thus causing an increase in the intermediate levels located in the band gap and minimizing the measured optical gap. Or, the decrease in the band gap may be due to the plasmonic effect of Ag on the surface or thanks to the existence of this element on the oxide surface creating new levels in the band gap, probably the junction of these [36,49].

The catalysts 2AgT/I (2.81 eV), 10AgT/I (2.48 eV), 2AgT/V (2.69 eV), 10AgT/V (2.3 eV) and 2AgT/SG (2.7 eV) had smaller band gaps than the catalysts T and T/SG (3.05 eV), which provides a faster transition of the electron from the valence band to the conduction band, with the concomitant production of a gap in the valence band and efficient oxidizing and reducing sites [50]. Therefore, the catalysts indicate that the heterostructure formed with Ag and $TiO_2$ probably facilitated the hybridization between the band gaps of these compounds, increasing the formation of deep states in the gap, thus causing the sharing of electrons between the semiconductor and the metal, highlighting the sol-gel method among the syntheses [36,49]. The T and T/SG catalyst had the typical band gap energy of $TiO_2$ between 3–3.2 eV [51].

**Figure 5** - UV-Vis band gap results for catalysts

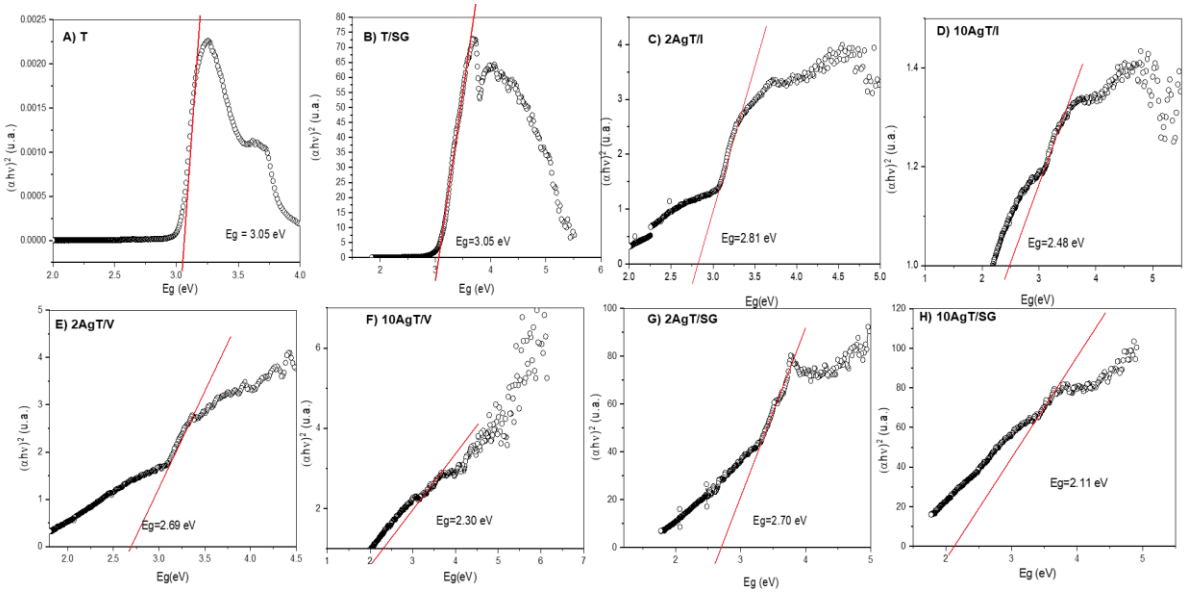


**Table 4** – Comparison between the characterizations of the AgT/I, AgT/V and AgT/SG catalysts

| Characterizations | Solvent Impregnation | Green Synthesis | Sol-Gel |
|---|---|---|---|
| MEV | Agglomerated appearance | Spongy agglomerated appearance | Structures with more rigid appearances |
| EDS | Lower than theoretical value | Lower than theoretical value | Reached the theoretical value |
| PAS | Bang gap smaller than $TiO_2$ | Bang gap smaller than $TiO_2$ | Bang gap smaller than $TiO_2$ |
| Isotermas | Type II | Type II | Type IV |
| $S_o$ | Low | Low | High |
| $V_p$ | Low | Low | High |
| $d_p$ | High | High | Low |

### 3.2 Comparative evaluation of testosterone removal efficiency by photolysis and photocatalysis processes

The experimental tests were conducted in the dark for 30 min until the HT adsorption equilibrium was reached before illumination. According to the results

(**Figure 6**), the photolysis process showed good degradation (82%) of HT [52]. This method occurs from the absorption of photons by the particles, exciting them and triggering several chemical decomposition reactions [53]. Photolysis occurs directly from the interaction of radiation with the molecules, leading to their decomposition [54], or indirectly, where the oxidation of the molecules is caused by radicals generated by photostabilizers [55]. Testosterone contains photoactive groups in its chemical structure, particularly the α, β-unsaturated ketone moiety, which absorbs UV radiation. After UV irradiation, testosterone undergoes several photochemical reactions, including isomerization, enolization, oxidation, and hydration, leading to the formation of multiple photoproducts [52]. Furthermore, the efficiency of photolysis is related to the emission spectrum of the lamp used in the reaction, since the lamp must emit a wavelength in the same absorbance spectrum as the target molecules [56]. HT exhibits absorbance at a wavelength centered at 242 nm, close to that used in photolysis (UV) (λ = 254 nm), indicating its susceptibility to photolysis under UV irradiation. The 254 nm wavelength excites testosterone more efficiently than longer wavelength light [12,52,57]. The ability of photolysis to remove HT is important, and may provide a mechanism to remove its harmful effects from the environment. Furthermore, it can be used in water treatment plants employing UV radiation to disinfect drinking water, helping to eliminate androgenic compounds from the water.

**Figure 6 –** Photolysis and photodegradation of testosterone carried out by the synthesized catalysts

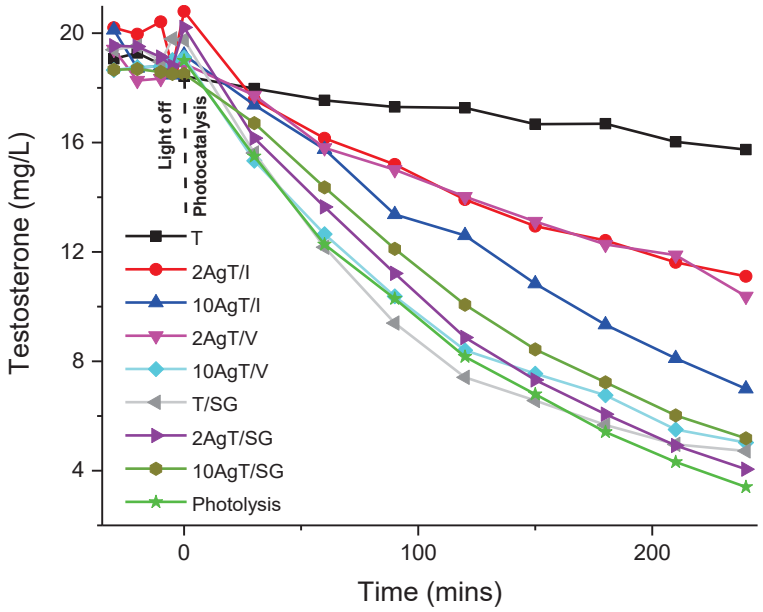


Regarding heterogeneous photocatalysis (Figure 6), in all tests, photocatalytic activity of the catalysts was observed in relation to HT degradation. However, the catalysts: T/SG (76.1%), 10AgT/SG (72%), 10AgT/V (73.7%) and 10AgT/I (63.6%), with emphasis on 2AgT/SG (79.9%), were the most active compared to catalyst T (17.1%). These catalysts exhibit enhanced photocatalytic activities compared to pure $TiO_2$ and the Ag content influenced the porosity and photocatalytic performance, since Ag can accept electrons and increase the density of available reactive sites. Thus, when $Ag/TiO_2$ is exposed to light, energy absorption occurs, promoting the excitation of $e^-$ from the valence band to the conduction band. The formation of $e^-/h^+$ pairs generates active sites on the catalyst surface. The vacancies react with $H_2O$ adsorbed on the catalyst surface, generating hydroxyl radicals ($^{\bullet}OH$). These radicals are extremely reactive and capable of oxidizing a wide variety of organic compounds, including testosterone. The $e^-$ react with adsorbed $O_2$, forming superoxide anions ($O_2^{-\bullet}$) and hydrogen peroxide ($H_2O_2$), which also contribute to the oxidation of testosterone. HT is degraded to form carbon dioxide ($CO_2$), $H_2O$, and other inorganic compounds (**Figure 7**) [28, 58–60].

**Figure 7** - Ag/$TiO_2$ photocatalysts in testosterone degradation

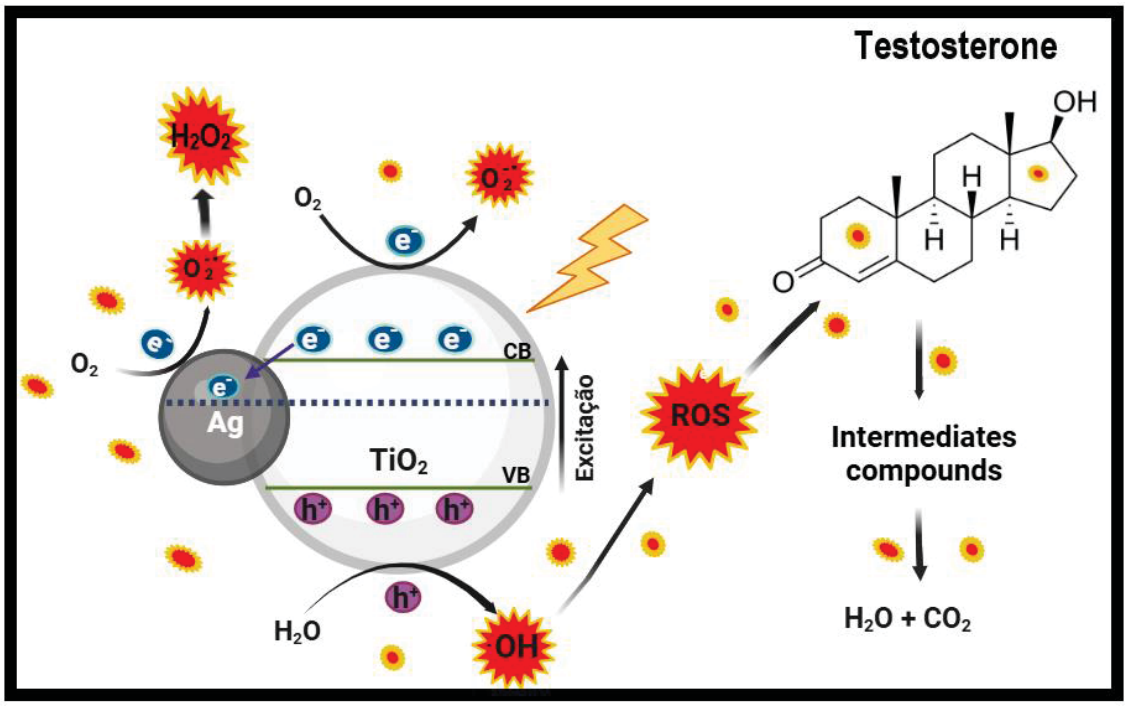


The photoactivation of Ag/$TiO_2$ excites the electron from the valence band (VB) to the conduction band (CB), producing $e^-/h^+$ pairs. These pairs migrate separately to the $TiO_2$ surface and react with $H_2O$ and $O_2$, producing ROS. Ag captures the electrons transported from the BC of $TiO_2$ and transports them to $O_2$, transforming them into superoxide radicals and producing ROS. These react with testosterone, degrading it into $H_2O$ and $CO_2$.

The best catalysts were AgT/SG compared to AgT/I and AgT/V catalysts, since the increase in the area of the catalysts available to absorb radiation was greater and they generated more $e^-/h^+$ pairs, which through a chain of reactions initiated the photodegradation of the hormone. The specific area of the Ag/$TiO_2$ catalysts influences the production of ROS, therefore there is a greater generation of $^{\bullet}OH$ with the increase in the area [61,62]. This radical is the main species responsible for the photodegradation of the hormone, thus increasing its percentage and degradation rate [29]. It is observed that the AgT/I catalysts were less effective, which may be due to agglomeration and low specific surface area. Furthermore, they demonstrated via EDS, a low percentage of Ag, thus affecting the efficiency of charge separation and the generation of ROS, significantly influencing the photocatalytic performance of the catalysts in the photodegradation of HT [59,63]. Since photocatalysis (close to 80%) and photolysis were effective in the photodegradation of HT, it can be inferred that they are valuable processes to

reduce the impact of the persistent and highly active group of this compound present in effluents.

The $e^-$ recombination process was less pronounced in 2AgT/SG, indicating that the ideal Ag doping content in the $TiO_2$ support was 2 w/w%, by the sol-gel method, in which the recombination of the photoinduced $e^-/h^+$ pairs was more effectively inhibited, demonstrating improved photocatalytic efficiency for the photodegradation of HT. It is added that the Ag on the $TiO_2$ surface acts as a trap for the photogenerated $e^-$, thus leading to an increase in the average lifetime of the reactions involved in the generation of ROS. Thus, the sol-gel synthesis provided well-dispersed Ag particles on the $TiO_2$ surfaces resulting in smaller pore sizes, larger specific areas, also improving the absorption of visible light and leading to a superior photocatalytic performance compared to the 2AgT/I and 2AgT/V catalysts [64,65]. Another factor is that Ag has a lower Fermi level than $TiO_2$, so the $e^-$ of the $TiO_2$ conduction band can be transported to the Ag species dispersed on the oxide surface. However, excessive Ag content (> 5 - 6%) can decrease the photocatalytic performance due to the reduction of active sites for electron capture [57,61].

The lowest values of HT degradation during the photocatalytic process were obtained by catalysts T, 2AgT/I (46.6 %) and 2AgT/V (45 %), for 240 min. Testosterone is a more hydrophobic compound, so ACN is used to dissolve it in $H_2O$, but this solvent is an $OH^•$ radical scavenger and can make the oxidation of testosterone photocatalyzed by $TiO_2$ somewhat difficult [66–68]. ACN also directs the photocatalytic reactions. A study demonstrates, using the ultra-high performance liquid chromatography-high-resolution mass spectrometry method, that when using $H_2O$:ACN in the 50:50 ratio, a reaction condition similar to the present work (60:40), the formation of a dehydrogenation compound M−2H (*m/z* 287,20) was favored to the detriment of hydroxylation such as M+O (*m/z* 305,21) and hydroxylation + dehydrogenation with M+O−2H (*m/z* 303,19). However, these three types of products were produced in abundance in the $H_2O$:ACN ratio 99:1. Therefore, at higher concentrations of ACN, the hormones react with the vacancies photoproduced by $TiO_2$, through the oxidation of one and, in succession, by its deprotonation, generating dehydrogenation products. It is also noted that, in $H_2O$:ACN 50:50, the abundance of reaction products increases with the time of exposure to UV and the degradation of HT becomes slower (30 min). Meanwhile, in $H_2O$:ACN 99:1 the degradation of testosterone and the products of

the oxidation reaction becomes faster (12 min) [66]. When investigating the role of ROS in the photodegradation of estrone, 17 β-estradiol and 17 α-ethinylestradiol, the predominant contribution of $HO^{\bullet}$ was observed as an initiator in the degradation process, as well as having a greater influence on the photodegradation. The species $O_2$, $H_2O_2$ e $O_2^{\bullet-}$ have similar relevance for the photodegradation of these hormones [29]. For μg $L^{-1}$ of pollutants, HT is photodegraded through the oxidation of the $HO^{\bullet}$ radical [69].

It is observed that the results of heterogeneous photolysis and photocatalysis (with the 2AgT/SG catalyst) were similar in the photodegradation of testosterone. The efficiency of testosterone photodegradation depends on several factors, including the specific area, the Ag distribution, the particle size and the reaction conditions. As well as the initial concentration of the hormone, the pH, the characteristics of the matrix, the radiation conditions, the reaction temperature [70], and the physicochemical properties of the photocatalyst [44].

The concentration of the hormone influences the efficiency of its removal, and may even mask the release or production of the hormone by means of intermediate compounds originating from the metabolism and biotransformation of this compound. Equilibrium studies with 17α-methyltestosterone (MT) showed that the best removal percentage occurred at low concentrations (μg $L^{-1}$ to ng $L^{-1}$) of this hormone and at room temperature. The removal percentage tended to decrease with increasing initial hormone concentration, since the available adsorption sites on the catalyst surface are occupied by hormone molecules in the solution, thus saturating the available sites [71]. Tests performed with testosterone at a concentration of 1.5–3 mg $L^{-1}$ at pH 3, through photocatalytic oxidation using Fe (III)/UVA, showed removal of 63% of the hormone in 2 reaction hours. Meanwhile, the photocatalytic oxidation of $TiO_2$/UVA presented a HT conversion, in the same reaction time, between 30 and 35%. By adding Fe (III) to the heterogeneous $TiO_2$ photocatalytic system ($TiO_2$/Fe(III)/UVA), the HT conversion increases to values above 90%, this occurs due to the sum of the contributions of the photocatalytic processes to generate hydroxyl free radicals. The heterogeneous processes with ozone ($O_3$/$TiO_2$/Fe (III)/UVA) were the most efficient to eliminate HT. The optimum value of the rate constant of the hydroxyl radical reaction was $1.5 \times 10^{10}$ $M^{-1}$ $s^{-1}$ [69].

Studies indicate that the degradation of 17β-estradiol and 17α-ethinylestradiol is complex, as they are bulky molecules, a parameter similar to that of testosterone [57,72,73]. The results obtained with $Ag/TiO_2$ films in the degradation of these hormones indicate that when the initial concentration is reduced from 1200 to 120 μg $L^{-1}$, the degradation time above 90% decreases from 6.5 to 3.5 h [29]. Another relevant factor is the catalyst load, so when the catalyst load is higher (100 mg/L), the degradation of the hormone increases under visible irradiation. The photocatalytic performance increases with the increase in the catalyst dose, and the degradation kinetics (17β-estradiol and 17α-ethinylestradiol) becomes rapid without the formation of an intermediate. The dose used in this study was 0.5 g/L, which is significantly lower than the catalyst dose (100 mg/L - 5 g/L) used for the degradation of comparable concentrations of various pollutants [57].

It can be inferred that photodegradation was similar between photolysis and photocatalysis of testosterone. These were affected by the choice of experimental conditions, especially the initial concentration of the hormone, catalyst dose and solvent used [66,74].

## 4 Conclusions

The catalysts synthesized via solvent excess impregnation and green synthesis formed agglomerates with a theoretical percentage of Ag below the value. It was observed that the increase in Ag doping caused a decrease in the specific area and average pore volume of the AgT/I and AgT/V catalysts, but the diameter and agglomerated and irregular morphology increased. The T catalyst presented a homogeneous appearance and rounded particles. The AgT/SG catalysts presented more rigid aspects in the materials and similar morphologies. The sol-gel method stands out from the other synthesis routes used in this study, as it allowed more precise control over the composition, morphology and porous structure of the material, presenting larger specific areas and pore volume, with smaller pore diameter. The AgT/I, AgT/V and AgT/SG catalysts are mesosporous, presenting smaller band gaps in relation to the T and T/SG catalysts.

The efficiency of the photolysis process was similar to that of heterogeneous photocatalysis in the photodegradation of testosterone. Furthermore, the

synthesized AgT/SG and 10AgT/V catalysts, with emphasis on 2AgT/SG, showed photocatalytic activity greater than 72% (2AgT/SG>T/SG>10AgT/V>10AgT/SG), in relation to the photodegradation of HT. Materials synthesized by the sol-gel method show great potential for the photodegradation of testosterone, due to their high specific area that provides greater homogeneity in the distribution of Ag particles, thus improving their efficiency in charge transfer and catalytic activity. Therefore, the 2AgT/SG, T/SG, 10AgT/V and 10AgT/SG catalysts can find applications in various water treatment processes, such as wastewater treatment plants to remove hormones such as testosterone, contributing to the protection of aquatic ecosystems, decontamination of contaminated soils, promoting their mineralization; reducing the risk of contamination of groundwater and sewage from pharmaceutical and cosmetic industries, which generate effluents with high concentrations of hormones, thus contributing to the protection of the environment and human health.

## References


[1] A.C. Knag, S. Verhaegen, E. Ropstad, I. Mayer, S. Meier, Effects of polar oil related hydrocarbons on steroidogenesis in vitro in H295R cells, Chemosphere 92 (2013) 106–115. https://doi.org/10.1016/j.chemosphere.2013.02.046.

[2] H. Ramírez-Malule, D.H. Quiñones-Murillo, D. Manotas-Duque, Emerging contaminants as global environmental hazards. A bibliometric analysis, Emerg. Contam. 6 (2020) 179–193. https://doi.org/10.1016/j.emcon.2020.05.001.

[3] J. Wilkinson, P.S. Hooda, J. Barker, S. Barton, J. Swinden, Occurrence, fate and transformation of emerging contaminants in water: An overarching review of the field, Environ. Pollut. 231 (2017) 954–970. https://doi.org/10.1016/J.ENVPOL.2017.08.032.

[4] T. Rasheed, M. Bilal, F. Nabeel, M. Adeel, H.M.N. Iqbal, Environmentally-related contaminants of high concern: Potential sources and analytical modalities for detection, quantification, and treatment, Environ. Int. 122 (2019) 52–66. https://doi.org/10.1016/J.ENVINT.2018.11.038.

[5] X. Wang, S. Wang, R. Qu, J. Ge, Z. Wang, C. Gu, Enhanced Removal of Chlorophene and 17β-estradiol by Mn(III) in a Mixture Solution with Humic Acid: Investigation of Reaction Kinetics and Formation of Co-oligomerization Products, Environ. Sci. Technol. 52 (2018) 13222–13230. https://doi.org/10.1021/acs.est.8b04116.

[6] Y.-L. Chen, C.-H. Wang, F.-C. Yang, W. Ismail, P.-H. Wang, C.-J. Shih, Y.-C. Wu, Y.-R. Chiang, Identification of Comamonas testosteroni as an androgen degrader in sewage, Sci. Rep. 6 (2016) 35386. https://doi.org/10.1038/srep35386.

[7] K. Zhang, Y. Zhao, K. Fent, Occurrence and Ecotoxicological Effects of Free, Conjugated, and Halogenated Steroids Including 17α-Hydroxypregnanolone and Pregnanediol in Swiss Wastewater and Surface Water, Environ. Sci. Technol. 51 (2017) 6498–6506. https://doi.org/10.1021/acs.est.7b01231.
[8] R. Hauser, N.E. Skakkebaek, U. Hass, J. Toppari, A. Juul, A.M. Andersson, A. Kortenkamp, J.J. Heindel, L. Trasande, Male Reproductive Disorders, Diseases, and Costs of Exposure to Endocrine-Disrupting Chemicals in the European Union, J. Clin. Endocrinol. Metab. 100 (2015) 1267–1277. https://doi.org/10.1210/jc.2014-4325.
[9] C.D. Kassotis, L.N. Vandenberg, B.A. Demeneix, M. Porta, R. Slama, L. Trasande, Endocrine-disrupting chemicals: economic, regulatory, and policy implications, Lancet Diabetes Endocrinol. 8 (2020) 719–730. https://doi.org/10.1016/S2213-8587(20)30128-5.
[10] C.J. Houtman, R. ten Broek, A. Brouwer, Steroid hormonal bioactivities, culprit natural and synthetic hormones and other emerging contaminants in waste water measured using bioassays and UPLC-tQ-MS, Sci. Total Environ. 630 (2018) 1492–1501. https://doi.org/10.1016/j.scitotenv.2018.02.273.
[11] M.W. van den Dungen, J.C.W. Rijk, E. Kampman, W.T. Steegenga, A.J. Murk, Steroid hormone related effects of marine persistent organic pollutants in human H295R adrenocortical carcinoma cells, Toxicol. Vitr. 29 (2015) 769–778. https://doi.org/10.1016/j.tiv.2015.03.002.
[12] E. Vulliet, M. Falletta, P. Marote, T. Lomberget, J.-O. Païssé, M.-F. Grenier-Loustalot, Light induced degradation of testosterone in waters, Sci. Total Environ. 408 (2010) 3554–3559. https://doi.org/10.1016/j.scitotenv.2010.05.002.
[13] R.A. Trenholm, B.J. Vanderford, J.C. Holady, D.J. Rexing, S.A. Snyder, Broad range analysis of endocrine disruptors and pharmaceuticals using gas chromatography and liquid chromatography tandem mass spectrometry, Chemosphere 65 (2006) 1990–1998. https://doi.org/10.1016/j.chemosphere.2006.07.004.
[14] E. Bandelj, M.R. Van Den Heuvel, F.D.L. Leusch, N. Shannon, S. Taylor, L.H. McCarthy, Determination of the androgenic potency of whole effluents using mosquitofish and trout bioassays, Aquat. Toxicol. 80 (2006) 237–248. https://doi.org/10.1016/j.aquatox.2006.08.011.
[15] K. Barel-Cohen, L.S. Shore, M. Shemesh, A. Wenzel, J. Mueller, N. Kronfeld-Schor, Monitoring of natural and synthetic hormones in a polluted river, J. Environ. Manage. 78 (2006) 16–23. https://doi.org/10.1016/j.jenvman.2005.04.006.
[16] R. Jenkins, R.A. Angus, H. McNatt, W.M. Howell, J.A. Kemppainen, M. Kirk, E.M. Wilson, Identification of androstenedione in a river containing paper mill effluent, Environ. Toxicol. Chem. 20 (2001) 1325–1331. https://doi.org/10.1002/etc.5620200622.
[17] O. Finlay-Moore, P.G. Hartel, M.L. Cabrera, 17β-Estradiol and Testosterone in Soil and Runoff from Grasslands Amended with Broiler Litter, J. Environ. Qual. 29 (2000) 1604–1611. https://doi.org/10.2134/jeq2000.00472425002900050030x.
[18] K. Ahmad, H.R. Ghatak, S.M. Ahuja, A review on photocatalytic remediation of environmental pollutants and $H_2$ production through water splitting: A sustainable approach, Environ. Technol. Innov. 19 (2020) 100893.

https://doi.org/10.1016/j.eti.2020.100893.
[19] C. Zarzzeka, J. Goldoni, F. Marafon, W.G. Sganzerla, T. Forster-Carneiro, M.D. Bagatini, L.M.S. Colpini, Use of titanium dioxide nanoparticles for cancertreatment: A comprehensive review and bibliometric analysis, Biocatal. Agric. Biotechnol. 50 (2023) 102710. https://doi.org/10.1016/j.bcab.2023.102710.
[20] V.R.A. Ferreira, P.R.M. Santos, C.I.Q. Silva, M.A. Azenha, Latest developments on $TiO_2$-based photocatalysis: a special focus on selectivity and hollowness for enhanced photonic efficiency, Appl. Catal. A Gen. 623 (2021) 118243. https://doi.org/10.1016/j.apcata.2021.118243.
[21] K. Li, C. Teng, S. Wang, Q. Min, Recent Advances in $TiO_2$-Based Heterojunctions for Photocatalytic $CO_2$ Reduction With Water Oxidation: A Review, Front. Chem. 9 (2021). https://doi.org/10.3389/fchem.2021.637501.
[22] C.B. Anucha, I. Altin, E. Bacaksiz, V.N. Stathopoulos, Titanium dioxide ($TiO_2$)-based photocatalyst materials activity enhancement for contaminants of emerging concern (CECs) degradation: In the light of modification strategies, Chem. Eng. J. Adv. 10 (2022) 100262. https://doi.org/10.1016/j.ceja.2022.100262.
[23] C.B. Anucha, I. Altin, E. Bacaksız, T. Kucukomeroglu, M.H. Belay, V.N. Stathopoulos, Enhanced Photocatalytic Activity of $CuWO_4$ Doped $TiO_2$ Photocatalyst Towards Carbamazepine Removal under UV Irradiation, Separations 8 (2021) 25. https://doi.org/10.3390/separations8030025.
[24] M.M. Viana, Estudo de filmes finos e materiais particulados de $TiO_2$ e de Ag/$TiO_2$ produzidos pelo processo sol-gel., Universidade Federal de Minas Gerais, 2011. http://hdl.handle.net/1843/SFSA-8H6URU (accessed March 21, 2023).
[25] X.H. Yang, H.T. Fu, X.C. Wang, J.L. Yang, X.C. Jiang, A.B. Yu, Synthesis of silver-titanium dioxide nanocomposites for antimicrobial applications, J. Nanoparticle Res. 16 (2014) 2526. https://doi.org/10.1007/s11051-014-2526-8.
[26] R. Saravanan, D. Manoj, J. Qin, M. Naushad, F. Gracia, A.F. Lee, M.M. Khan, M.A. Gracia-Pinilla, Mechanothermal synthesis of Ag/$TiO_2$ for photocatalytic methyl orange degradation and hydrogen production, Process Saf. Environ. Prot. 120 (2018) 339–347. https://doi.org/10.1016/j.psep.2018.09.015.
[27] A. Thakur, P. Kumar, S. Bagchi, R.K. Sinha, P. Devi, Green synthesized plasmonic nanostructure decorated $TiO_2$ nanofibers for photoelectrochemical hydrogen production, Sol. Energy 193 (2019) 715–723. https://doi.org/10.1016/j.solener.2019.10.022.
[28] R.N. Padovan, L.S. de Carvalho, P.L. de Souza Bergo, C. Xavier, A. Leitão, Á.J. dos Santos Neto, F.M. Lanças, E.B. Azevedo, Degradation of hormones in tap water by heterogeneous solar $TiO_2$-photocatalysis: Optimization, degradation products identification, and estrogenic activity removal, J. Environ. Chem. Eng. 9 (2021) 106442. https://doi.org/10.1016/j.jece.2021.106442.
[29] K.V. Lima, E.S. Emídio, R.F. Pupo Nogueira, N. do S.L. Vasconcelos, A.B. Araújo, Application of a stable Ag/$TiO_2$ film in the simultaneous photodegradation of hormones, J. Chem. Technol. Biotechnol. 95 (2020) 2656–2663. https://doi.org/10.1002/jctb.6258.
[30] Z. Frontistis, C. Drosou, K. Tyrovola, D. Mantzavinos, D. Fatta-Kassinos, D.

Venieri, N.P. Xekoukoulotakis, Experimental and Modeling Studies of the Degradation of Estrogen Hormones in Aqueous $TiO_2$ Suspensions under Simulated Solar Radiation, Ind. Eng. Chem. Res. 51 (2012) 16552–16563. https://doi.org/10.1021/ie300561b.

[31] M. de Liz, R. de Lima, B. do Amaral, B. Marinho, J. Schneider, N. Nagata, P. Peralta-Zamora, Suspended and Immobilized $TiO_2$ Photocatalytic Degradation of Estrogens: Potential for Application in Wastewater Treatment Processes, J. Braz. Chem. Soc. (2017). https://doi.org/10.21577/0103-5053.20170151.

[32] L.E.N. Castro, A.H. Meira, L.N.B. Almeida, G. Gonçalves Lenzi, L.M.S. Colpini, Experimental design and optimization of textile dye photodiscoloration using $Zn/TiO_2$ catalysts, Desalin. WATER Treat. 266 (2022) 173–185. https://doi.org/10.5004/dwt.2022.28599.

[33] W.L. de Almeida, F.S. Rodembusch, N.S. Ferreira, V. Caldas de Sousa, Eco-friendly and cost-effective synthesis of ZnO nanopowders by Tapioca-assisted sol-gel route, Ceram. Int. 46 (2020) 10835–10842. https://doi.org/10.1016/j.ceramint.2020.01.095.

[34] N.S. Ferreira, R.S. Angélica, V.B. Marques, C.C.O. De Lima, M.S. Silva, Cassava-starch-assisted sol–gel synthesis of $CeO_2$ nanoparticles, Mater. Lett. 165 (2016) 139–142. https://doi.org/10.1016/J.MATLET.2015.11.107.

[35] L.E.N. de Castro, E.C. Meurer, H.J. Alves, M.A.R. dos Santos, E. de C. Vasques, L.M.S. Colpini, Photocatalytic Degradation of Textile dye Orange-122 Via Electrospray Mass Spectrometry, Brazilian Arch. Biol. Technol. 63 (2020). https://doi.org/10.1590/1678-4324-2020180573.

[36] R.S. André, C.A. Zamperini, E.G. Mima, V.M. Longo, A.R. Albuquerque, J.R. Sambrano, A.L. Machado, C.E. Vergani, A.C. Hernandes, J.A. Varela, E. Longo, Antimicrobial activity of $TiO_2$:Ag nanocrystalline heterostructures: Experimental and theoretical insights, Chem. Phys. 459 (2015) 87–95. https://doi.org/10.1016/J.CHEMPHYS.2015.07.020.

[37] M. Cantarella, M. Mangano, M. Zimbone, G. Sfuncia, G. Nicotra, E. Maria Scalisi, M. Violetta Brundo, A. Lucia Pellegrino, F. Giuffrida, V. Privitera, G. Impellizzeri, Green synthesis of photocatalytic $TiO_2$/Ag nanoparticles for an efficient water remediation, J. Photochem. Photobiol. A Chem. 443 (2023) 114838. https://doi.org/10.1016/J.JPHOTOCHEM.2023.114838.

[38] K. Sathishkumar, K. Sowmiya, L. Arul Pragasan, R. Rajagopal, R. Sathya, S. Ragupathy, M. Krishnakumar, V.R. Minnam Reddy, Enhanced photocatalytic degradation of organic pollutants by Ag–$TiO_2$ loaded cassava stem activated carbon under sunlight irradiation, Chemosphere 302 (2022) 134844. https://doi.org/10.1016/j.chemosphere.2022.134844.

[39] S.R. Patil, U.L. Štangar, S. Gross, U. Schubert, Super-Hydrophilic and Photocatalytic Properties of Ag-$TiO_2$ Thin Films Prepared by Sol–Gel Technique, J. Adv. Oxid. Technol. 11 (2008). https://doi.org/10.1515/jaots-2008-0218.

[40] H. Feng, Y. Zhang, J. Liu, D. Liu, Towards Heterogeneous Catalysis: A Review on Recent Advances of Depositing Nanocatalysts in Continuous–Flow Microreactors, Molecules 27 (2022) 8052. https://doi.org/10.3390/molecules27228052.

[41] Y. Pan, X. Shen, L. Yao, A. Bentalib, Z. Peng, Active Sites in Heterogeneous Catalytic Reaction on Metal and Metal Oxide: Theory and Practice, Catalysts 8 (2018) 478. https://doi.org/10.3390/catal8100478.

[42] X. Gao, B. Zhou, R. Yuan, Doping a metal (Ag, Al, Mn, Ni and Zn) on $TiO_2$ nanotubes and its effect on Rhodamine B photocatalytic oxidation, Environ. Eng. Res. 20 (2015) 329–335. https://doi.org/10.4491/eer.2015.062.
[43] M. Thommes, K. Kaneko, A. V. Neimark, J.P. Olivier, F. Rodriguez-Reinoso, J. Rouquerol, K.S.W. Sing, Physisorption of gases, with special reference to the evaluation of surface area and pore size distribution (IUPAC Technical Report), Pure Appl. Chem. 87 (2015) 1051–1069. https://doi.org/10.1515/pac-2014-1117.
[44] J.C. Arévalo-Pérez, D. de la Cruz-Romero, A. Cordero-García, C.E. Lobato-García, A. Aguilar-Elguezabal, J.G. Torres-Torres, Photodegradation of 17 α-methyltestosterone using $TiO_2$-$Gd^{3+}$ and $TiO_2$-$Sm^{3+}$ photocatalysts and simulated solar radiation as an activation source, Chemosphere 249 (2020) 126497. https://doi.org/10.1016/j.chemosphere.2020.126497.
[45] Q. Mu, Y. Li, H. Wang, Q. Zhang, Self-organized $TiO_2$ nanorod arrays on glass substrate for self-cleaning antireflection coatings, J. Colloid Interface Sci. 365 (2012) 308–313. https://doi.org/10.1016/J.JCIS.2011.09.027.
[46] W.L. da Silva, M.A. Lansarin, C.C. Moro, Síntese, caracterização e atividade fotocatalítica de catalisadores nanoestruturados de $TiO_2$ dopados com metais, Quim. Nova 36 (2013) 382–386. https://doi.org/10.1590/S0100-40422013000300006.
[47] L. Santos, Preparation and characterization of catalysts based on titanium oxide doped with silver ions, for use in photocatalysis, Universidade Federal de Uberlândia, 2013. https://doi.org/10.14393/ufu.di.2013.1
[48] C.C. Moro, M.A. Lansarin, M. Bagnara, Nanotubos de $TiO_2$ dopados com nitrogênio: comparação das atividades fotocatalíticas de materiais obtidos através de diferentes técnicas, Quim. Nova 35 (2012) 1560–1565. https://doi.org/10.1590/S0100-40422012000800013.
[49] M. Rycenga, C.M. Cobley, J. Zeng, W. Li, C.H. Moran, Q. Zhang, D. Qin, Y. Xia, Controlling the Synthesis and Assembly of Silver Nanostructures for Plasmonic Applications, Chem. Rev. 111 (2011) 3669–3712. https://doi.org/10.1021/cr100275d.
[50] L.M.S. Colpini, G.G. Lenzi, M.B. Urio, D.M. Kochepka, H.J. Alves, Photodiscoloration of textile reactive dyes on Ni/$TiO_2$ prepared by the impregnation method: Effect of calcination temperature, J. Environ. Chem. Eng. 2 (2014) 2365–2371. https://doi.org/10.1016/J.JECE.2014.01.007.
[51] J. Gomes, J. Lincho, E. Domingues, R. Quinta-Ferreira, R. Martins, N–$TiO_2$ Photocatalysts: A Review of Their Characteristics and Capacity for Emerging Contaminants Removal, Water 11 (2019) 373. https://doi.org/10.3390/w11020373.
[52] L. Méité, B.D. Soro, N.K. Aboua, V. Mambo, K.S. Traoré, P. Mazellier, J. De Laat, Qualitative Determination of Photodegradation Products of Progesterone and Testosterone in Aqueous Solution, Am. J. Anal. Chem. 07 (2016) 22–33. https://doi.org/10.4236/ajac.2016.71003.
[53] W.T. Vieira, M.B. de Farias, M.P. Spaolonzi, M.G.C. da Silva, M.G.A. Vieira, Latest advanced oxidative processes applied for the removal of endocrine disruptors from aqueous media – A critical report, J. Environ. Chem. Eng. 9 (2021) 105748. https://doi.org/10.1016/j.jece.2021.105748.
[54] E.M. Cuerda-Correa, M.F. Alexandre-Franco, C. Fernández-González, Advanced Oxidation Processes for the Removal of Antibiotics from Water. An Overview, Water 12 (2019) 102. https://doi.org/10.3390/w12010102.

[55] S. Dhaka, R. Kumar, M.A. Khan, K.-J. Paeng, M.B. Kurade, S.-J. Kim, B.-H. Jeon, Aqueous phase degradation of methyl paraben using UV-activated persulfate method, Chem. Eng. J. 321 (2017) 11–19. https://doi.org/10.1016/j.cej.2017.03.085.
[56] M. Neamţu, F.H. Frimmel, Degradation of endocrine disrupting bisphenol A by 254nm irradiation in different water matrices and effect on yeast cells, Water Res. 40 (2006) 3745–3750. https://doi.org/10.1016/j.watres.2006.08.019.
[57] N.G. Menon, L. George, S.S. V. Tatiparti, S. Mukherji, Efficacy and reusability of mixed-phase $TiO_2$–ZnO nanocomposites for the removal of estrogenic effects of 17β-Estradiol and 17α-Ethinylestradiol from water, J. Environ. Manage. 288 (2021) 112340. https://doi.org/10.1016/j.jenvman.2021.112340.
[58] K. Mao, Y. Li, H. Zhang, W. Zhang, W. Yan, Photocatalytic Degradation of 17α-Ethinylestradiol and Inactivation of *Escherichia coli* Using Ag-Modified $TiO_2$ Nanotube Arrays, CLEAN – Soil, Air, Water 41 (2013) 455–462. https://doi.org/10.1002/clen.201100698.
[59] C.N. Duduman, J.M.G. de S. y C. de L. Cobos, M. Harja, M.I.B. Perez, C.G. de Castro, D. Lutic, O. Kotova, I. Cretescu, preparation and characterization of nanocomposite material based on $TiO_2$-Ag for environmental applications, Environ. Eng. Manag. J. 17 (2018) 925–936. https://doi.org/10.30638/eemj.2018.093.
[60] D.S.C. Halin, N. Mahmed, M.A.A. Mohd Salleh, A.N. Mohd Sakeri, K. Abdul Razak, Synthesis and Characterization of Ag/$TiO_2$ Thin Film via Sol-Gel Method, Solid State Phenom. 273 (2018) 140–145. https://doi.org/10.4028/www.scientific.net/SSP.273.140.
[61] C. Zarzzeka, J. Goldoni, J. do R. de Paula de Oliveira, G.G. Lenzi, M.D. Bagatini, L.M.S. Colpini, Photocatalytic action of Ag/$TiO_2$ nanoparticles to emerging pollutants degradation: A comprehensive review, Sustain. Chem. Environ. 8 (2024) 100177. https://doi.org/10.1016/j.scenv.2024.100177.
[62] D.P. Macwan, P.N. Dave, S. Chaturvedi, A review on nano-$TiO_2$ sol–gel type syntheses and its applications, J. Mater. Sci. 46 (2011) 3669–3686. https://doi.org/10.1007/s10853-011-5378-y.
[63] V. Sharma, G. Harith, S. Kumar, R. Sharma, K.L. Reddy, A. Bahuguna, V. Krishnan, Amorphous titania matrix impregnated with Ag nanoparticles as a highly efficient visible- and sunlight-active photocatalyst material, Mater. Technol. 32 (2017) 461–471. https://doi.org/10.1080/10667857.2016.1271861.
[64] J. Shen, Z.-J. Li, Z.-F. Hang, S.-F. Xu, Q.-Q. Liu, H. Tang, X.-W. Zhao, Insights into the Effect of Reactive Oxygen Species Regulation on Photocatalytic Performance via Construction of a Metal-Semiconductor Heterojunction, J. Nanosci. Nanotechnol. 20 (2020) 3478–3485. https://doi.org/10.1166/jnn.2020.17405.
[65] K. Balachandran, T. Kalaivani, D. Thangaraju, S. Mageswari, M.S. Viswak Senan, A. Preethi, Fabrication of photoanodes using sol-gel synthesized Ag-doped $TiO_2$ for enhanced DSSC efficiency, Mater. Today Proc. 37 (2021) 515–521. https://doi.org/10.1016/j.matpr.2020.05.485.
[66] M. Ruokolainen, M. Valkonen, T. Sikanen, T. Kotiaho, R. Kostiainen, Imitation of phase I oxidative metabolism of anabolic steroids by titanium dioxide photocatalysis, Eur. J. Pharm. Sci. 65 (2014) 45–55.

https://doi.org/10.1016/j.ejps.2014.08.009.
[67] S. Mitroka, S. Zimmeck, D. Troya, J.M. Tanko, How Solvent Modulates Hydroxyl Radical Reactivity in Hydrogen Atom Abstractions, J. Am. Chem. Soc. 132 (2010) 2907–2913. https://doi.org/10.1021/ja903856t.
[68] F.A.M.G. van Geenen, M.C.R. Franssen, V. Miikkulainen, M. Ritala, H. Zuilhof, R. Kostiainen, M.W.F. Nielen, $TiO_2$ Photocatalyzed Oxidation of Drugs Studied by Laser Ablation Electrospray Ionization Mass Spectrometry, J. Am. Soc. Mass Spectrom. 30 (2019) 639–646. https://doi.org/10.1007/s13361-018-2120-x.
[69] E.M. Rodríguez, G. Fernández, P.M. Alvarez, F.J. Beltrán, $TiO_2$ and Fe (III) photocatalytic ozonation processes of a mixture of emergent contaminants of water, Water Res. 46 (2012) 152–166. https://doi.org/10.1016/j.watres.2011.10.038.
[70] M. Gmurek, M. Olak-Kucharczyk, S. Ledakowicz, Photochemical decomposition of endocrine disrupting compounds – A review, Chem. Eng. J. 310 (2017) 437–456. https://doi.org/10.1016/j.cej.2016.05.014.
[71] A.C. Mendonça, A. de F.A. Venceslau, G.M.D. Ferreira, L.M.A. Pinto, Red-fleshed pitaya peels (*Hylocereus polyrhizus*) as a biosorbent for removal of hormone 17α-methyltestosterone in aqueous medium, J. Porous Mater. 31 (2024) 809–830. https://doi.org/10.1007/s10934-023-01543-y.
[72] Y. Ohko, K. Iuchi, C. Niwa, T. Tatsuma, T. Nakashima, T. Iguchi, Y. Kubota, A. Fujishima, 17β-Estradiol Degradation by $TiO_2$ Photocatalysis as a Means of Reducing Estrogenic Activity, Environ. Sci. Technol. 36 (2002) 4175–4181. https://doi.org/10.1021/es011500a.
[73] R. Wang, X. Ma, T. Liu, Y. Li, L. Song, S.C. Tjong, L. Cao, W. Wang, Q. Yu, Z. Wang, Degradation aspects of endocrine disrupting chemicals: A review on photocatalytic processes and photocatalysts, Appl. Catal. A Gen. 597 (2020) 117547. https://doi.org/10.1016/j.apcata.2020.117547.
[74] R.B. Young, D.E. Latch, D.B. Mawhinney, T.-H. Nguyen, J.C.C. Davis, T. Borch, Direct Photodegradation of Androstenedione and Testosterone in Natural Sunlight: Inhibition by Dissolved Organic Matter and Reduction of Endocrine Disrupting Potential, Environ. Sci. Technol. (2013) 130710075816008. https://doi.org/10.1021/es401689j.

## Final Considerations and Prospective for the Future

AgT/I, AgT/V and AgT/SG catalysts can offer a more sustainable and effective alternative to traditional antibiotics. By combining the antibacterial action of silver with the photocatalytic capacity of titanium dioxide, materials have been obtained that can be used in a variety of applications, such as surface disinfection and wastewater treatment. Ag/$TiO_2$ catalysts enable the creation of self-decontaminating surfaces, significantly reducing the risk of hospital infections. This technology can help reduce the use of aggressive chemical products and preserve the environment.

The sol-gel method stands out from the other synthesis routes used in this study, as it allowed more precise control over the composition, morphology and porous structure of the material. The efficiency of the photolysis process (82%) was similar to that of heterogeneous photocatalysis in the photodegradation of testosterone (79.9%). The catalysts 2AgT/SG, T/SG, 10AgT/V and 10AgT/SG show good efficiency in the photodegradation of emerging pollutants, such as hormones, through the generation of reactive oxygen species. This characteristic makes them promising tools for application in industrial wastewater treatment processes, especially those from the pharmaceutical and cosmetics industries. In addition, they can be used to decontaminate soils, contributing to a more environmentally friendly environment.

This work provides a solid basis for future research, driving the development of innovative solutions for wastewater treatment and the production of cleaning technologies. It is intended to contribute to the mitigation of environmental problems caused by the inappropriate disposal of emerging pollutants. The results obtained open up new perspectives for the development of more sustainable and economically viable wastewater treatment technologies.